Investigating the role of IGF-1R in the cellular response to DNA damage

Submission for the degree of Doctor of Philosophy (DPhil)

Department of Oncology

Wilfride V. Petnga Kamdoum

Balliol College, University of Oxford

Trinity Term 2017





I, Wilfride V. Petnga Kamdoum, declare that this thesis was composed by myself, that the work contained herein is my own except where explicitly stated otherwise in the text, and that this work has not been submitted for any other degree or professional qualification anywhere else.

ABSTRACT

IGF-1R plays an important role in regulating cell proliferation, survival and migration. Its overexpression in a number of cancers has been associated with radio-resistance. Previous studies from our group and others have confirmed that depletion or inhibition of IGF-1R can sensitise cancer cells to ionising radiation. However, the underlying mechanisms remain elusive. Our study aimed to uncover the mechanisms of radio-sensitisation associated with the IGF-1R signalling pathway. This was achieved by investigating changes at the proteome, transcriptome and metabolome levels using siRNA-mediated gene silencing and also IGF-1R mutant isogenic models which we generated from p53 wild-type osteosarcoma U2OS cells using the CRISPR/Cas9 genome editing technique.

We confirmed that suppressing the IGF-1R function through either transient or permanent depletion of the protein enhances U2OS sensitivity to γ-irradiation with average dose enhancement ratios of 3.5 and 3 respectively at 5Gy. Double-strand break induction and resolution were not impaired in IGF1R-deficient cells as determined by γH2AX foci tracking and there was no evidence that the activation of the DNA damage response was compromised in the mutant with evidence of ATM, CHK1 and RPA phosphorylation along with p53 accumulation. Moreover, we did not find defects in cell cycle checkpoint integrity which prompted us to evaluate intrinsic properties associated with IGF-1R deficiency that may affect cell survival following exposure to γ-irradiation.

Transcriptome and metabolome profiling revealed significant differences in genes and metabolites associated with various cellular pathways, particularly the cellular response to stress, intracellular metabolism and, cell motility and migration. The interplay of molecular changes affecting these cellular processes might account for the radio-sensitisation of IGF-1R deficient cells. Future investigations should attempt to explore this possibility given that previous research on this same topic have hinted at the likelihood that the cellular response to ionising radiation is governed by complex multiple factors.

Acknowledgements

For the completion of this thesis, I am thankful to *my ever-present help in time of need*. I am thankful for His advice and constant encouragement, for providing guidance and giving me the strength to make it till the end. HE made it possible to study here at the University of Oxford and provided all I had need for to make it through the DPhil journey.

I would like to thank my entire family, those near and far especially my dad, my mum, and my wonderful siblings for their support throughout the course of my DPhil. I am thankful for their prayers, their words of wisdom and for the joy they bring to my life. They have been and will remain an immense blessing to me.

I would also like to thank the members of the Macaulay group, past and present. I am thankful to my supervisor for her dedication in diligently reviewing this piece of work. I am grateful for the delightful time I spent as a member of the group, for the beautiful friendships that were knitted, for the moments of laughter and for the interesting conversations.

I would like to acknowledge the lovely friends that have prayed, encouraged and brought joy to my heart during the course of my doctorate degree, from the start to the finish line. Many thanks especially to Vanessa Fotso, the Kammogne Family, Sengeziwe Sibeko, Agnes Gwela, Laura Riach and Si Yuen.

Lastly, I am thankful to the Clarendon Fund, the Hakeem Belo-Osagie Scholarship, the Vice-Chancellor Scholarship and Balliol College for financial assistance.

"*Let us not grow weary in well-doing, for in due time we will reap a harvest, if we do not give up*." – Saul of Tarsus

"*Those who sow in tears shall reap with joyful shouting. He who goes to and fro weeping, carrying his bag of seed, shall indeed come again with a shout of joy, bringing his sheaves with him.*" – A wise man

"*Louez l'Éternel, car IL est Bon, car Sa Miséricorde et Sa Bonté durent à toujours!* " – David of Bethlehem

Table of contents

ABSTRACT ..... **III**

ACKNOWLEDGEMENTS ..... **IV**

ABBREVIATIONS ..... **XV**

1 INTRODUCTION **1**

1.1 IGF-1R BIOLOGY: STRUCTURE, ACTIVATION AND SIGNALLING 1

1.1.1. Structure of the IGF-1 receptor *1*

1.1.2. Receptor Activation *3*

1.1.3. IGF-1R downstream signalling pathways *4*

1.2 IGF-1R SIGNALLING IN PHYSIOLOGY AND DISEASE 9

1.2.1. How is the IGF-1R signalling regulated? *9*

1.2.2. IGF-1R signalling and energy metabolism *13*

1.2.3. IGF-1R signalling and Cancer *14*

1.3 IGF-1R TARGETING AND DNA DAMAGE 19

1.3.1. IGF-1R can mediate resistance to radiotherapy *20*

1.3.2. Mechanisms of IGF1R-induced radio-resistance *21*

1.3.3. Approaches to studying the influence of IGF-1R on double-strand break repair *31*

1.4 HYPOTHESIS AND AIMS OF THIS STUDY 37

2. MATERIALS AND METHODS **38**

2.1. CELL LINES 38

2.2. DRUGS AND LIGAND 39

2.3. IONISING RADIATION 40

2.4. WESTERN BLOTTING 40

2.5. GENE SILENCING WITH SHORT INTERFERENCE RNA (SIRNA) 42

2.6. FLOW CYTOMETRY AND CELL CYCLE ANALYSIS 43

2.6.1. Flow cytometry 43

2.6.2. BrdU cell cycle analysis 44

2.7. IMMUNOFLUORESCENCE 44

2.8. FOCI COUNTING 45

2.9. CELL VIABILITY ASSAYS 46

2.10. CLONOGENIC ASSAYS 46

2.11. GENOME EDITING: GRNA DESIGN, SUB-CLONING AND BACTERIAL TRANSFORMATION 47

2.11.1. gRNA design 47

2.11.2. Oligonucleotides ordering and subcloning 47

2.11.3. Bacterial transformation 49

2.12. PLASMID DNA PURIFICATION 50

2.13. GENOMIC DNA ISOLATION 51

2.14. SURVEYOR MUTATION DETECTION ASSAY 51

2.14.1. HEK293T cells transfection 52

2.14.2. Surveyor assay Step one: PCR reaction 53

2.14.3. Surveyor assay Step two: DNA duplex formation 54

2.14.4. Surveyor assay Step three: Digestion of DNA duplexes with surveyor CEL nuclease 55

2.14.5. Surveyor assay Step four: Detection of DNA products 56

2.15. PCR PRODUCT PURIFICATION 56

2.16. TRANSFECTION WITH CRISPR GRNAS 57

2.17. CELL SORTING, CLONAL ISOLATION & EXPANSION AND CLONE SCREENING 57

2.18. RNA EXTRACTION AND TRANSCRIPTOME PROFILING 59

2.18.1. Sample preparation for RNA microarray and Data analysis 60

2.19. REVERSE TRANSCRIPTION, QUANTITATIVE PCR (QPCR) & PRIMERS 60

2.20. METABOLITE EXTRACTION, SAMPLE PREPARATION AND ANALYSIS 63

2.20.1. Metabolite extraction 63

2.20.2. Sample preparation for metabolomics 63

2.20.3. Sample preparation for Amino Acid Analysis 64

2.20.4. Metabolite identification and Statistical evaluation 64

2.21. GRAPHING AND STATISTICAL ANALYSIS 65

2.22. GENERATING HEATMAPS 65

3. IGF-1R IN THE RESPONSE TO TEMOZOLOMIDE-INDUCED DNA DAMAGE 68

3.1. TESTING THE EFFECTS OF IGF-1R COMBINATION WITH TMZ IN MELANOMA AND EWING'S SARCOMA CELL LINES 70

3.1.1. The Effect of IGF-1R inhibition 70

3.1.2. Response to TMZ treatment as a single agent and in combination with IGF-1R inhibition 75

3.2. INVESTIGATING THE MECHANISMS OF CHEMO-SENSITISATION TO TEMOZOLOMIDE IN IGF-1R INHIBITED MELANOMA CELLS 78

3.2.1. Assessing the influence of IGF-1R signalling on HR-mediated double-strand break repair 79

3.2.2. Effects of the combination treatment on the cell cycle 83

3.2.3. Effects of IGF-1R depletion on the cell cycle 86

3.3. DISCUSSION 88

4. GENERATING IGF-1R KNOCKOUT ISOGENIC CELLS 90

4.1. CELL LINE MODEL SELECTION 91

4.2. GUIDE RNA DESIGN AND VALIDATION 94

4.2.1. gRNA design 95

4.2.2. gRNA validation 99

4.3. CHARACTERISATION OF IGF-1R MUTANT U2OS CELLS 104

4.3.1. Screening for IGF-1R knockout cells 105

4.3.2. DNA sequence verification 107

4.4. DISCUSSION 110

5. INVESTIGATING THE ROLE OF IGF-1R IN THE RESPONSE TO DNA DAMAGE INDUCED BY IONISING RADIATION IN U2OS 112

5.1. IGF-1R AND THE DNA DAMAGE RESPONSE TO Γ-IRRADIATION 113

5.1.1. Testing the response to ionising radiation 113

5.1.2. Assessing the activation of the DNA damage response 115

5.1.3. Evaluating γH2AX focus formation and resolution in response to ionising radiation 120

5.1.4. Assessing the cell cycle checkpoint integrity in the IGF-1R mutant 122

5.2. TRANSCRIPT PROFILING OF WILD-TYPE U2OS AND IGF-1R MUTANTS 126

5.2.1. Does deficiency in IGF-1R signalling induce transcriptomic changes? . 126

5.2.2. Deregulated pathways & processes in the IGF-1R mutant #4 129

5.2.3. Deregulated pathways & processes in the IGF-1R mutant #3 131

5.3. METABOLOME PROFILING OF U2OS WILD-TYPE AND MUTANT CELLS 138

5.4. DISCUSSION 145

6. DISCERNING IGF1R-SPECIFIC EFFECTS ON THE RESPONSE TO IONISING RADIATION: COMPARATIVE ANALYSIS BETWEEN IGF-1R MUTANTS AND IGF-1R DEPLETED U2OS CELLS 149

6.1. IGF-1R DEPLETION AND THE RESPONSE TO Γ-IRRADIATION 150

6.1.1. Testing the response to irradiation 150

6.1.2. Assessing the effect of IGF-1R depletion on γH2AX focus formation and resolution following ionising radiation 154

6.2. EFFECTS OF IGF-1R DEPLETION ON GENE EXPRESSION 156

6.2.1. Does IGF-1R depletion induce gene expression changes in U2OS? 157

6.2.2. Deregulated cellular pathways and processes upon IGF-1R knockdown 159

6.2.3. Differentially expressed genes 'in common' between the IGF-1R mutants and depleted cells 164

6.2.4. Validation of some RNA hits by qRT-PCR 165

6.3. PHENOTYPIC CHANGES ASSOCIATED WITH IGF-1R DEPLETION 169

6.3.1. Evaluating the effect of IGF-1R depletion on the cell cycle distribution 169

6.3.2. Assessing the effect of IGF-1R knockdown on cell survival 172

6.4. IGF-1R DEFICIENCY AND THE RESPONSE TO OTHER DNA DAMAGING AGENTS. 175

6.4.1. Assessing the response of IGF-1R mutants to other DNA damaging agents 175

6.4.2. Testing the effects of IGF-1R depletion on the response to cytotoxic drugs 178

6.5. DISCUSSION 181

7. DISCUSSION 184

7.1. IGF-1R SIGNALLING AND DOUBLE-STRAND BREAK REPAIR 184

7.2. LIMITATIONS AND FUTURE WORK RECOMMENDATIONS 184

8. APPENDIX 191

8.1. IMAGEJ MACRO LANGUAGE SCRIPT FOR FOCI COUNTING 191

8.2. RAW DATA FOR FLOW CYTOMETRY 192

8.2.1. Cell cycle changes following drug treatment in CHL-1 192

8.2.2. Cell cycle changes following IGF-1R depletion in CHL-1 193

8.2.3. Assessing checkpoint integrity in response to irradiation 194

8.2.4. Cell cycle changes following IGF-1R depletion in U2OS 195

8.2.5. Apoptotic markers in IGF-1R depleted U2OS cells 196

8.3. STRUCTURAL INFORMATION ON *IGF1R* PROTEIN CODING SPLICE VARIANTS 197

8.4. RESPONSE OF IGF-1R MUTANT CLONES TO IRRADIATION 199

8.4.1. Clonogenic assay with four mutant clones 199

8.4.2. Post-irradiation timecourse in IGF-1R null and wild-type clones 200

8.5. ALL HITS FROM TRANSCRIPTOME ANALYSIS 201

8.5.1. Wild-type vs IGF-1R null 3 201

8.5.2. Wild-type vs IGF-1R null 4 203

8.5.3. Controls vs IGF-1R knockdown 205

8.6. RSTUDIO SCRIPTS FOR GENERATING HEATMAPS 209

8.6.1. Launching the pheatmap package 209

8.6.2. Comparing wild-type vs IGF-1R null4 210

8.6.3. Comparing wild-type vs IGF-1R null3 210

8.6.4. Heatmap with metabolomics data 211

BIBLIOGRAPHY 212

List of Figures

Figure 1-1: **Cartoon representation of the IGF-1 receptor**.....3

Figure 1-2: **Downstream signalling pathways associated with IGF-1R**.....5

Figure 1-3: **Double-strand break repair via Homologous Recombination**.....25

Figure 1-4: **Non-homologous end joining processing of various double-strand break ends**. 27

Figure 1-5: **CRISPR/Cas9-mediated genome editing**.....34

Figure 1-6: **Schematic representation of temozolomide-induced DNA damage.**.....36

Figure 2-1: **Schematic for cloning of the gRNA into pSpCas9(BB)-2A plasmid**. 49

Figure 2-2: **The Surveyor mutation detection technique**.. 52

Figure 3-1: **Effects of IGF-1R inhibition on cell survival in melanoma and Ewing's sarcoma cells**.....71

Figure 3-2: **Effect of the kinase inhibitor drug AZ3801 on IGF-1R activation and AKT signalling in Ewing's sarcoma (A) and melanoma cell lines (B).**.....74

Figure 3-3: **Effects of IGF-1R inhibition (AZ3801) in the response to temozolomide (TMZ) treatment.**.....77

Figure 3-4: **Induction of γH2AX and RAD51 foci upon treatment with TMZ**. 80

Figure 3-5: **Time-course of induction and resolution of TMZ-induced DSBs.**. 83

Figure 3-6: **Effects of the combination treatment on cell cycle distribution in CHL-1 cells**. 85

Figure 3-7: **Effects of IGF-1R depletion on Cell cycle distribution in CHL-1 cells**....87

Figure 4-1: **siRNA-mediated depletion of IGF-1R**.....92

Figure 4-2: **The effect of IGF-1R depletion on the survival of CHL-1, U2OS and TC-32 cell lines**.....94

Figure 4-3: **Graphical representation of three protein-coding *IGF1R* splice variants**. 98

Figure 4-4: **Map showing predicted stop codons as a result of indels**.....99

Figure 4-5: **Efficiency of plasmid transfection in HEK293T cells**.....101

Figure 4-6: **Surveyor Assay - validation of selected gRNAs**.. 104

Figure 4-7: **IGF-1R protein levels in CRISPR-generated mutant clones**. 107

Figure 4-8: **DNA sequence alignment of IGF-1R mutants with wild-type**. 108

Figure 5-1: **Differential response of the IGF-1R knockouts to ionising radiation**....114

Figure 5-2: **DNA damage signalling induced in response to ionising radiation**.....119

Figure 5-3: **Timecourse of induction and resolution of IR-induced γH2AX foci**.....122

Figure 5-4: **Ionising radiation induces late G2-M accumulation in the wild-type and the knockout.**.....125

Figure 5-5: **Comparative diagram of deregulated genes between the IGF-1R knockouts**.....128

Figure 5-6: **Differentially expressed genes in IGF-1R mutant #4**. 130

Figure 5-7: **Overview of deregulated cellular processes in IGF-1R null 3.** 133

Figure 5-8: **Differentially expressed genes in IGF-1R null 3.** 134

Figure 5-9: **Significantly upregulated and downregulated metabolites in IGF-1R mutant #3.**.....140

Figure 5-10: **Overview of downregulated metabolic processes in IGF-1R mutant #3.** 142

Figure 6-1: **IGF-1R depletion leads to reduced proliferation and increased sensitivity to ionising radiation**.....152

Figure 6-2: **Dose enhancement Ratios and radio-sensitivity profile of IGF-1R depleted cells compared to the IGF-1R mutants**.. 153

Figure 6-3: **Induction and Resolution of γH2AX foci upon exposure to ionising radiation**. 155

Figure 6-4: **Levels of *IGF1R* mRNA upon siRNA-mediated depletion**.....157

Figure 6-5: **Comparative diagram of deregulated genes upon siRNA-mediated IGF-1R depletion**. 158

Figure 6-6: **Overview of deregulated cellular processes upon IGF-1R depletion.**....160

Figure 6-7: **Deregulated genes in common between IGF-1R depleted cells and IGF-1R knockout cells**.....165

Figure 6-8: **RNA hits validation by qRT-PCR**.. 168

Figure 6-9: **IGF-1R depletion induces G2 accumulation.** 171

Figure 6-10: **IGF-1R depletion affects cell survival**.....173

Figure 6-11: **IGF-1R depletion induces apoptosis.** 174

Figure 6-12: **chemo-sensitivity profile of IGF-1R mutants**. 177

Figure 6-13: **Chemo-sensitivity profile of IGF-1R depleted U2OS cells**. 179

Figure 6-14: **Comparing the chemo-sensitivity profiles of IGF-1R deficient cells**. ..180

Figure 8-1: **Effect of ionising radiation on cell proliferation in 'full' and 'partial' IGF-1R knockouts**. 199

Figure 8-2: I**onising radiation induces molecular changes in 'full' knockouts and wild-type cells**. 200

List of Tables

Table 2-1: **List of CRISPR guideRNAs**.. 47

Table 2-2: **List of Surveyor primer pairs**. 53

Table 2-3: **List of primer pairs**. 62

Table 2-4**: List of Antibodies** 66

Table 4-1: **BLASTn search results with selected guide oligonucleotides**. 96

Table 4-2: **List of *IGF1R* human transcripts**. 97

Table 5-1: **Transcriptionally deregulated genes in the IGF-1R mutant #4**.....131

Table 5-2: **Transcriptionally deregulated genes associated with extracellular matrix remodelling (ECM) in the IGF-1R mutant #3.** 135

Table 5-3: **Transcriptionally deregulated genes associated with cellular response to stress in the IGF-1R mutant #3.** 136

Table 5-4: **Transcriptionally deregulated genes associated with DNA damage and other cellular processes in the IGF-1R mutant #3.**.....137

Table 5-5: **Transcriptionally deregulated genes associated with intracellular metabolism in the IGF-1R mutant #3.** 138

Table 5-6: **Downregulated metabolites in the IGF-1R mutant #3**.....143

Table 5-7: **Upregulated metabolites in the IGF-1R mutant #3**. 144

Table 6-1: **Transcriptionally deregulated genes associated with the immune/stress response upon IGF-1R depletion**.....161

Table 6-2: **Transcriptionally deregulated genes associated with extracellular matrix reorganisation, cytoskeleton rearrangement and cell adhesion**. 162

Table 6-3: **Transcriptionally deregulated genes associated with metabolism**. 163

Table 6-4: **Transcriptionally deregulated genes associated with IGF-1R signalling**. 163

Abbreviations

4EBP1	Eukaryotic translation initiation factor 4E-binding protein 1
53BP1	p53 binding protein 1
AKR1C3	aldo-keto reductase family 1 member C3
AKT	RAC-alpha serine/threonine-protein kinase
ALDOC	Aldolase C
ATM	Ataxia-telangiectasia mutated
ATR	Ataxia-telangiectasia and Rad3-related
BAD	Bcl2-associated agonist of cell death
BAX	Bcl-2-associated X protein
BLM helicase	Bloom helicase
BRCA1	Breast Cancer Type 1 Susceptibility Protein
BRCA2	Breast Cancer Type 2 Susceptibility Protein
BRCC36	Lys-63-specific deubiquitinase BRCC36
cAMP	cyclic AMP
CBP80	80 kDa nuclear cap-binding protein
c-Cbl	E3 ubiquitin-protein ligase CBL
	Coiled-coil domain-containing protein 98/BRCA1-A complex subunit
CCDC98	Abraxas 1
CDK	Cyclin-dependent kinase
CHK1	Checkpoint kinase 1
CHK2	Checkpoint kinase 2
CREB	Cyclic AMP-responsive element-binding protein
CRISPR	Clustered Regularly Interspaced Short Palindromic Repeats

CtIP	CtBP-interacting protein
DDR	DNA damage response
DHAP	dihydroxyacetone-phosphate
DNA2	DNA replication ATP-dependent helicase/nuclease DNA2
DNA-PK	DNA-dependent protein kinase
DNA-PKcs	DNA-dependent protein kinase catalytic subunit
DSB	double-strand break
dsDNA	double-stranded DNA
DUSP6	Dual specificity protein phosphatase 6
ECM	Extracellular matrix
eEF2K	Eukaryotic elongation factor 2 kinase
EGFR	Epidermal growth factor receptor
Elk1	ETS domain-containing protein Elk-1
EMT	Epithelial-mesenchymal transition
EXO1	Exonuclease 1
FAK	Focal adhesion kinase
FEN1	Flap Structure-Specific Endonuclease 1
FoxO	Forkhead box proteins
G3P	glycerol-3-phosphate
GA3P	glyceraldehyde-3-phosphate
GLUT1	Glucose transporter 1
Grb10	Growth factor receptor-bound protein 10
Grb2	Growth factor receptor-bound protein 2
GSK3β	Glycogen synthase kinase-3 beta
HIF-1	Hypoxia-Inducible Factor-1

HR	Homologous recombination
IGF	Insulin-like growth factor
IGF-1R	Type 1 insulin-like growth factor receptor
IGFBP	Insulin-like growth factor-binding protein
INSR	Insulin Receptor
IR	Ionising Radiation
IRS	Insulin receptor substrate
JCV T-Ag	JC virus T-antigen
JNK	Mitogen-activated protein kinase 8/c-Jun N-terminal kinase
KAP1	KRAB-associated protein 1
MAPK/ERK	Mitogen-activated protein kinase/Extracellular signal-regulated kinase
MDC1	Mediator of DNA damage checkpoint protein 1
MDM2	Mouse Double minute 2 protein
MEK1	Dual specificity mitogen-activated protein kinase kinase 1
MGMT	O-6-Methylguanine-DNA Methyltransferase
MMPs	Matrix metalloproteinases
mTORC1	Mammalian target of rapamycin complex 1
mTORC2	Mammalian target of rapamycin complex 2
NEDD4	Neural precursor cell expressed developmentally down-regulated protein 4
NHEJ	Non-homologous end-joining
NUD14	Nucleoside diphosphate-linked moiety X motif 14
O^6MeG	O-6-methylguanine
PALB2	Partner and localizer of BRCA2
PARP1	Poly [ADP-ribose] polymerase 1
PAXX	Paralog Of XRCC4 And XLF

PDE4	cAMP-specific 3',5'-cyclic phosphodiesterase 4A
PDK1	3-phosphoinositide-dependent protein kinase 1
PFK1/2	Phosphofructokinase ½
PI3K	Phosphoinositide-3-kinase
PIP2	Phosphatidylinositol 4,5-bisphosphate
PIP_3	Phosphatidylinositol (3,4,5)-trisphosphate
PNKP	Polynucleotide Kinase 3'-Phosphatase
PPP	pentose phosphate pathway
PRAS40	Proline-rich AKT1 substrate 1
PTB domain	Phospho-tyrosine binding domain
PTP1B	Protein-tyrosine phosphatase 1B
PUMA	p53 upregulated modulator of apoptosis
RACK1	Receptor of activated protein C kinase 1
RAD51	DNA repair protein RAD51 homolog 1
RAP80	Receptor-associated protein 80
RHEB	Ras homolog enriched in brain
RIF1	Rap1 interacting factor 1
RNF8/RNF168	RING finger protein 8/168
ROS	Reactive oxygen species
RPA	Replication protein A
S6K1	S6 kinase 1
SCID	Severe combined immunodeficiency
Shc	Src homology 2 domain-containing transforming protein C1
SHP1	Protein-tyrosine phosphatase SHP-1
SHP2	Protein-tyrosine phosphatase 2C

SOCS1/2	Suppressor of cytokine signalling 1/2
SOS	Son of sevenless
Sp1	Transcription factor Sp1
SSB	single-strand break
ssDNA	single-stranded DNA
TBC1D4	TBC1 domain family member 4/Akt substrate of 160 kDa
TCA cycle	Tri-carboxylic acid cycle
TDP1	Tyrosyl-DNA phosphodiesterase 1
TGF-β	Transforming growth factor β
TIGAR	TP53-induced glycolysis and apoptosis regulator
TIMP2	Metalloproteinase inhibitor 2
TMZ	Temozolomide
TSC2	Tuberous sclerosis 2 protein
VEGF	Vascular endothelial growth factor
VHL	Von Hippel-Lindau
XLF	XRCC4-like factor
XRCC4	X-Ray Repair Cross-Complementing Protein 4

1. Introduction

1.1 IGF-1R biology: structure, activation and signalling

1.1.1. Structure of the IGF-1 receptor

The type 1 insulin-like growth factor receptor (IGF-1R) is a hetero-tetrameric glycoprotein belonging to the insulin family of tyrosine kinase receptors (Ullrich et al., 1986). Evidence pointing out the existence of IGF-1 receptors came out of studies assessing insulin-like activity in purified rat liver plasma membranes (Megyesi et al., 1975). The IGF-1 receptor is synthesized as a 180-kDa precursor containing a 30-residue signal peptide that undergoes post-transcriptional modifications including glycosylation, dimerization and proteolytic processing to yield a α2β2 tetramer that is then trafficked to the plasma membrane (Ullrich et al., 1986, Jacobs et al., 1983). The receptor is membrane-spanning, containing an extracellular domain harbouring the ligand binding site, a transmembrane domain and a cytosolic domain (Ullrich et al., 1986, Adams et al., 2000).

The extracellular part of the receptor consists of the α-subunit (710 amino acids) and a small portion of the β-subunit (196 amino acids) (Ullrich et al., 1986, Adams et al., 2000). The α-subunit consists mainly of a cysteine-rich region and two L domains (L1 and L2). These arrange themselves in a bi-lobal structure containing a hydrophilic acidic patch for ligand binding (Whittaker et al., 2001, Garrett et al., 1998). Genetic manipulations of the IGF-1 receptor have revealed that the cysteine-rich regions and flanking regions of the two L domains are the key determinants of ligand binding and receptor affinity for its ligands (Mynarcik et al., 1997, Whittaker et al., 2001). For instance, the mutation Phe90Ala in the L1

domain was reported to reduce the receptor's affinity for the IGF-1 ligand by 23-fold (Whittaker et al., 2001).

The intracellular part of the receptor consists solely of the β-subunit and contains the catalytic tyrosine kinase domain flanked by the juxta-membrane and a regulatory C-tail region. The juxta-membrane contains an NPXY motif that serves as a recognition element for receptor internalisation. The deletion of this motif can impair the recruitment of the IGF-1R downstream signalling mediators (Hsu et al., 1994, Prager et al., 1994). The C-terminal region contains residues that serve as binding sites for proteins involved in the regulation of IGF-1R signalling including a tyrosine residue at position 1250 that is reported to be important for ligand-induced receptor-internalisation (O'Connor et al., 2000, Miura and Baserga, 1997). And lastly, the kinase domain harbours the ATP binding site with restricted access due to an inserted A-loop when the receptor is in its inactive form (Hubbard, 1997).

Although the tyrosine kinase domain of the IGF-1R is ~84% homologous to that of the insulin receptor (INSR), the overall level of homology between the two receptors is ~70% due to distinct differences in the C-tail, the ligand-binding domain and the juxta-membrane region (Mynarcik et al., 1997, Ullrich et al., 1986, Hsu et al., 1994). Another receptor in the same family is the mannose-6-phosphate receptor also referred to as type 2 insulin-like growth factor receptor (IGF-2R) (Brown et al., 2008, Oshima et al., 1988).

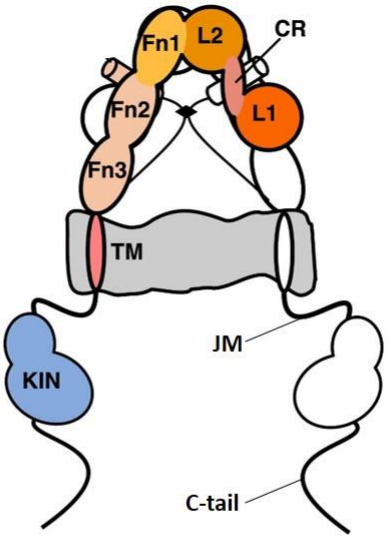


Figure 1-1: **Cartoon representation of the IGF-1 receptor**. The tetrameric protein consists of two α-subunits and two β-subunits; each containing specific regions serving a particular purpose. The cysteine-rich (CR) region and two L domains (L1 and L2) together form the ligand-binding site. There are also three fibronectin type domains. The intracellular portion of the β-subunit contains the catalytic tyrosine kinase domain, the juxta-membrane and the regulatory C-tail. Modified from (Kavran et al., 2014)

1.1.2. Receptor Activation

The IGF-1 receptor is activated upon specific ligand binding interactions with insulin-like growth factors IGF-1 and IGF-2. However, IGF-1 is a more potent activator because it binds with higher affinity to the IGF-1R (Favelyukis et al., 2001, Baker et al., 1993). It is reported that the key IGF-1 residues involved in ligand-receptor binding interactions are Phe23 and Tyr24 in the B region, Tyr31 in the C domain and Tyr60 in the A region of the ligand's structure. The first three are arranged structurally along with surrounding residues to form a hydrophobic patch that interacts with the IGF-1 receptor (Jansson et al., 1997, Bayne et al., 1990).

In the inactive state, the IGF-1R kinase activity is inhibited by an auto-inhibitory loop, referred to as 'A-loop', lodging within the kinase catalytic site which hinders ATP binding

and recruitment of downstream signalling substrates (Favelyukis et al., 2001, Pautsch et al., 2001). Interaction with an activating ligand causes a structural rearrangement resulting in the auto-phosphorylation of three tyrosine residues Tyr1135, Tyr1131, Tyr1136 on the A-loop, in a specific order (Favelyukis et al., 2001, Kavran et al., 2014). Phosphorylation of these residues triggers the displacement of the inhibitory loop from the active site as the receptor undergoes a conformational change that renders the catalytic site accessible to ATP binding. All three tyrosine residues need to be phosphorylated to destabilise the A-loop out of the catalytic site. Freeing of the active site enables the second wave of auto-phosphorylation events to take place, inducing the formation of phospho-tyrosine residues called 'docking sites' on the β-subunit. The activated IGF-1 receptor shows enhanced catalytic activity and increased affinity for ATP and its substrates (Favelyukis et al., 2001, Pautsch et al., 2001). The activated IGF-1R downstream signalling is mediated by the insulin receptor substrate family of proteins (IRS1-4) and Shc adapter proteins (Shc A-D) that are able to dock onto the receptor via their phospho-tyrosine binding (PTB) domain (Dey et al., 1996, Craparo et al., 1995). Shc proteins localise to the membrane by interacting with plasma membrane phospholipids through their PTB domain whilst IRS proteins use their pleckstrin homology (PH) domain which allows them to bind to phospholipids containing acidic motifs such as the phosphatidylinositol 4,5-trisphosphate (PIP2) molecules (Burks et al., 1998, Ravichandran, 2001).

1.1.3. IGF-1R downstream signalling pathways

Shc association with IGF-1R triggers phosphorylation on critical residues within its CH1 domain that induce a conformational change allowing recruitment of SH2 domain-containing adapter protein Grb2 (Ravichandran, 2001). Grb2, in turn, recruits the guanine nucleotide exchange factor SOS through its SH3 domain and the resulting activated

complex Shc-Grb2-SOS induce a cascade of activation events targeting effectors of the MAPK (mitogen-activated protein kinase) signalling, starting with RAS (Ravichandran, 2001).

Among the IRS family members (IRS1-4), IGF-1R signalling is predominantly mediated by IRS-1. Similarly to Shc adapter proteins, docking of IRS to phosphorylated Tyr950 on the activated IGF-1 receptor leads to the phosphorylation of several residues in its C-terminal region that serve as binding sites for downstream partner molecules such as class I PI3 kinase and Grb2 via their SH2 domain (Myers et al., 1992, Valverde et al., 2001).

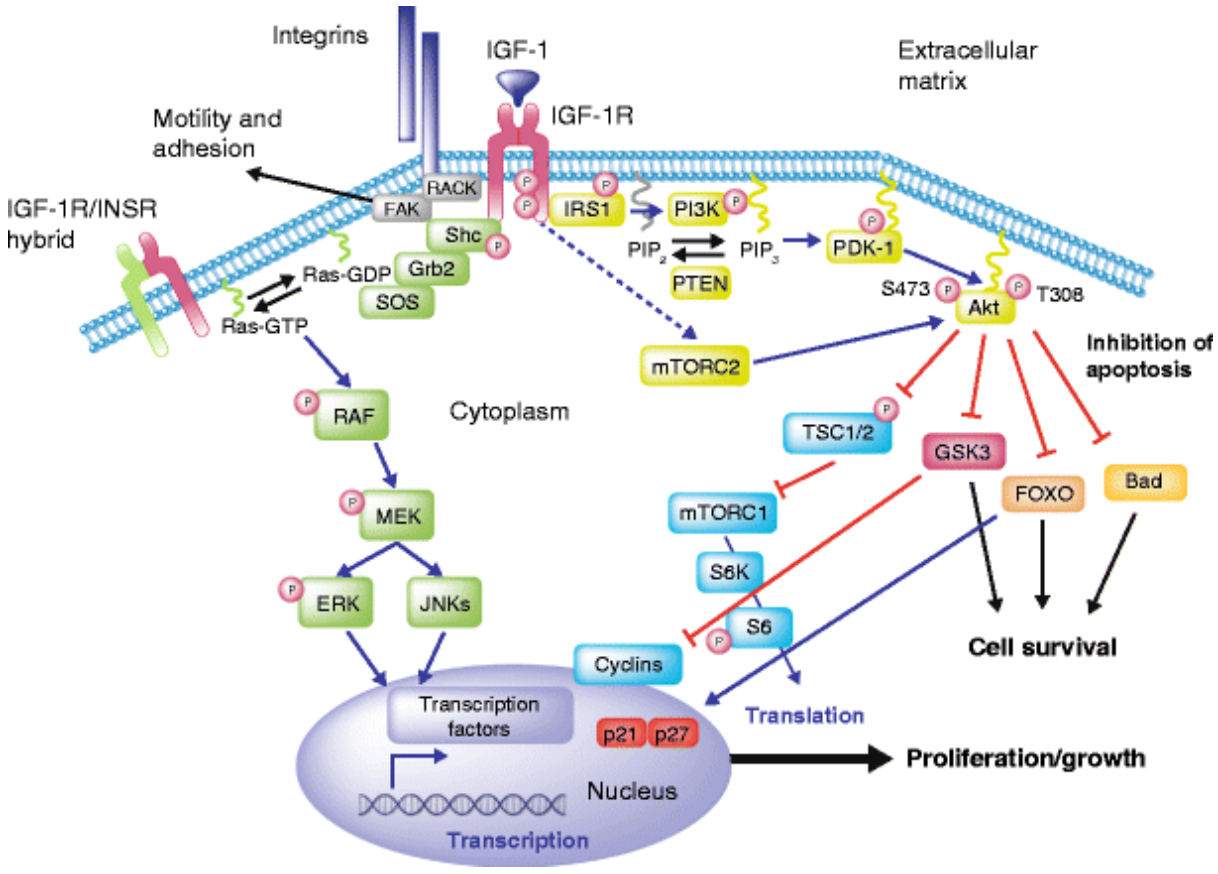


Figure 1-2: **Downstream signalling pathways associated with IGF-1R**. Upon IGF-1R activation, auto-phosphorylated tyrosine residues on the kinase domain serve as docking sites for signalling molecules such as Shc and IRS proteins. Downstream activation of the MAPK (ERK) and AKT pathways affects several cellular processes that stimulate cell growth and proliferation. Copied with permission from (Simpson et al., 2017).

1.1.3.1. Activation of PI3K-AKT pathway and downstream effectors and cellular effects

Binding of the PI3-kinase (PI3K) to IRS-1 via its p85 regulatory subunit triggers a conformational change within the P110 catalytic subunit that activates PI3 kinase activity and the catalytic production of PIP_3 (phosphatidylinositol 3,4,5-trisphosphate) from PIP2 (Jiménez et al., 2002). PIP3 allows the recruitment of PDK1 (phosphoinositide-dependent kinase-1) and AKT to the membrane via their PH domain; these are important mediators of PI3K signalling to downstream effectors. AKT is only partially activated upon phosphorylation of residue Thr308 on its activation loop by PDK and full activation results when Ser473 on its C-terminus is also phosphorylated by the mTORC2 complex (Alessi et al., 1996, Sarbassov et al., 2005, Wick et al., 2000). AKT promotes cell survival and proliferation through multiple downstream targets (Hemmings and Restuccia, 2012).

AKT, in turn, causes the activation of mTORC1 activator 'RHEB' and the inhibition of mTORC1 negative regulator PRAS40. TSC2, a GTPase-activating protein that prevents RHEB from becoming loaded with GTP molecules, is phosphorylated by AKT thereby allowing GTP-bound RHEB to stimulate the kinase activity of mTORC1 (Zhang et al., 2003). PRAS40 is phosphorylated on Thr246 by AKT, promoting its association with 14-3-3 inhibitory binding proteins and release from the mTORC1 complex (Nascimento et al., 2010). mTORC1 activation promotes protein synthesis via key substrates including nuclear cap-binding protein (CBP80), eukaryotic elongation factor 2 kinase (eEF2K), S6 kinase 1 (S6K1) and, elF4Ebinding protein 1 (4EBP1) (Zoncu et al., 2011). Through its modulatory function on protein synthesis, mTORC1 influences metabolism, angiogenesis, lipid biogenesis and autophagy (Zoncu et al., 2011).

AKT has also been shown to promote glucose metabolism through the downstream targets glycogen synthase kinase 3- β (GSK3β), the glycolytic enzymes phosphofructokinases PFK1/2, the Rab GTPase-activating protein TBC1D4 (Hemmings and Restuccia, 2012). In

addition to this, AKT has been shown to interact with key proteins involved in the regulation of the apoptosis/cell survival balance. AKT promotes cell survival by modulating the activation status and/or sub-cellular localisation of target proteins like caspase 9, BAD, CREB, MDM2 and FoxO transcription factors (Tzivion et al., 2011, Hemmings and Restuccia, 2012, Mayo and Donner, 2001).

1.1.3.2. Activation of the RAS/MAPK pathway

Although the Ras/MAPK pathway is predominantly activated through Shc-mediated signalling, there is evidence suggesting that IRS-1 can also lead to MAPK pathway activation. RAS becomes active through SOS-mediated GDP to GTP exchange (Downward, 2003). Activated RAS (RAS-GTP) facilitates recruitment of auto-inhibited RAF proteins to the plasma membrane through their RAS-binding domains. RAF interaction with RAS-GTP triggers dephosphorylation of RAF on Ser259 and the consequent displacement of the inhibitory 14-3-3 protein (Lavoie and Therrien, 2015). The removal of 14-3-3 from dephosphorylated Ser259 induces a rearrangement that forces the RAF kinase regulatory region out of its catalytic domain, thereby exposing key activating residues for phosphorylation. Full activation of RAF proteins ensues as a result of dimerization (Lavoie and Therrien, 2015). Activated RAF phosphorylates the dual specificity kinases MEK1 and MEK2 MAPK kinases, inducing their activation. Activated MEK, in turn, catalyses the phosphorylation of ERK1/2 on Tyr204/Thr202 resulting in the dissociation of the MEK-ERK complex which allows the formation of active ERK dimers. Targeted substrates of ERK1/2 include nuclear and cytosolic proteins to modulate a number of cellular processes. These substrates include Elk1, c-Fos and cAMP phosphodiesterase (PDE4) (Roskoski, 2012).

1.1.3.3. Other activated signalling pathways

Activation of the IGF-1R has also been associated with integrin signalling which can be mediated via interactions with the scaffold protein RACK1. The latter is reported to bind on residues Tyr1250/Tyr1251 of the receptor's C-terminal region (Blakesley et al., 1998, Kiely et al., 2005). For instance, it has been shown that IGF-1R facilitates PP2A displacement from RACK1-Tyr302 to promote binding of β1 integrin instead, resulting in the formation of the tri-molecular complex IGF-1R-RACK1-β1 integrin (Kiely et al., 2008, Beattie et al., 2010). In addition to this, it has been demonstrated that IGF-1 stimulation induces dephosphorylation of the focal adhesion kinase thereby triggering a series of downstream events that modulate cellular motility and migratory abilities through coordinated signalling with Src and Rho-GTPases proteins (Guvakova and Surmacz, 1999, Kiely et al., 2009). It is also possible that Wnt signalling is modulated in response to the IGF-1R signalling through IRS-1 mediated interaction with beta-catenin (Playford et al., 2000, Cox et al., 2015).

More so, IGF-1R has been reported to associate with receptor tyrosine kinases EGFR and INSR, Grb10, SOCS1/2, SHP2, 14-3-3 binding proteins, the stress-activated protein kinases p38 and JNK, TIMP2 and even with G-proteins. Although the resulting functional consequences for some of these associations are not thoroughly understood, binding to some of these partner molecules have been shown to modulate the stability, sub-cellular localisation and signalling of the IGF-1 receptor (Riedemann et al., 2007, Belfiore et al., 2009, Zheng et al., 2012, Dey et al., 1998, Fernandez et al., 2010, Dalle et al., 2001, Luttrell et al., 1995, O'Connor, 2003).

1.2 IGF-1R signalling in physiology and disease

Widely expressed across many cell types in foetal and postnatal tissues, the IGF-1 receptor is involved in important physiological processes at the whole-organism, cellular and sub-cellular levels that include somatic growth, longevity and aging, angiogenesis, cell differentiation, proliferation and metabolism (Baserga et al., 1997, Hellström et al., 2002, Junnila et al., 2013, Aguirre et al., 2016); signalling via this receptor is consequently subjected to a complex array of regulatory networks. Abnormalities affecting the IGF-1R signalling pathway are associated with important pathophysiological conditions such as dwarfism, cancer and metabolic diseases.

1.2.1. How is the IGF-1R signalling regulated?

This is an expanding area of research and several studies have shown that the IGF-1R signalling can be regulated at different levels. Herein, we will focus solely on the regulation at the levels of ligand and receptor availability.

1.2.1.1 Regulation at the ligand level

The IGF-1R signalling pathway can be regulated via modulation of IGF ligands bio-availability at the systemic but also tissue levels. At the systemic level, IGF-1 production by the liver is dependent upon stimulatory signals from the growth hormone (GH) (Boni-Schnetzler et al., 1991, Berelowitz et al., 1981). Circulating IGF-1 ligands are mostly found in ternary complexes with insulin-like growth factor binding proteins (IGFBPs) and the 85kDa glycoprotein acid-labile subunit (ALS) or in binary complexes with IGFBPs alone (Baxter, 2014, Twigg and Baxter, 1998, Payet et al., 2003). IGF-1 can also be secreted at the peripheral level in several tissues (D'Ercole et al., 1984). It is generally thought that the

production context determines the ligand's mode of function; systemic production might be mainly associated with endocrine signalling whilst expression at the peripheral level characterises its paracrine and autocrine signalling effect.

IGF-1 ligands form very stable complexes with IGFBPs which block binding and activation of the IGF-1R. It is therefore not surprising that IGFBPs themselves are subjected to regulatory mechanisms mostly at the post-transcriptional level in the form of protease-mediated cleavage inactivation, phosphorylation and *N*-linked glycosylation (Baxter, 2014).

Furthermore, there is growing interest in the regulation of the IGF-1 ligand bio-availability by microRNAs. A number of studies have revealed that the messenger RNA encoding for the IGF-1 ligand is the target of a small number of micro-RNAs that bind to its 3'UTR, repressing mRNA translation and negatively affecting transcript stability with the resulting effect being reduced IGF-1 mRNA and protein levels (Peng et al., 2013, Hu et al., 2013, Elia et al., 2009). However, these regulatory factors might be cell type-dependent as dysregulation has been associated with a variety of pathological conditions.

1.2.1.2 Regulation at the receptor level

IGF-1R signalling can be modulated at the transcriptional, post-transcriptional and post-translational levels. In this thesis, we will not provide a comprehensive review of regulatory mechanisms associated with IGF-1R signalling but we aim to give a brief overview based on recent and past findings.

At the post-transcriptional level, several microRNAs have been identified as targeting the *IGF1R* mRNA. MicroRNA-mediated regulation of the IGF-1R signalling has been associated with several physiological and pathological processes including postnatal cardiac remodelling, chronic skin inflammation, glucose metabolism and cancer (Jung and

Suh, 2014). Transcription of the *IGF1R* gene can be negatively or positively regulated by a number of proteins. Tumour suppressor protein p53 has been shown to prevent transcription of *IGF1R* DNA sequence through its interaction with the transcription factor 'TATA'-box binding protein (TBP), hindering it from binding to the *IGF1R* promoter region (Werner et al., 1996). Similarly, tumour suppressors BRCA1 and VHL have been shown to associate with the zinc finger protein Sp1 in order to prevent it from binding to the *IGF1R* gene promoter and induce its transcription (Abramovitch et al., 2003, Yuen et al., 2007).

Ligand-mediated activation of IGF-1R triggers downstream signalling pathways that induce internalisation of the receptor for recycling, degradation or nuclear translocation via incorporation into caveolin- or clathrin-coated vesicles (Sehat et al., 2008, Romanelli et al., 2007, Miura and Baserga, 1997, Aleksic et al., 2010). IGF-1R has been shown to translocate to the nucleus following ligand-activation where, in concert with accessory molecules, it is thought to regulate the transcriptional expression of a number of genes, including its own expression levels (Sarfstein et al., 2012). Our group showed that full receptor internalisation in clathrin-coated vesicles occurred upon IGF1-mediated activation (Aleksic et al., 2010). Subsequently, other groups have shown that apart from ligand-mediated activation, sumoylation at residues Lys1025, Lys1100, and Lys1120 within the tyrosine kinase domain of the IGF-1R is also required for nuclear translocation (Deng et al., 2011, Sehat et al., 2010).

IGF-1R signalling can be attenuated by ubiquitin-mediated targeted degradation in the proteasome or lysosome. Proteasome-mediated degradation of the IGF-1R is mediated by the E3 ubiquitin ligases MDM2 and c-Cbl (Sehat et al., 2008). The two ligases are thought to be activated through distinct ligand-dependent mechanisms: low doses of IGF-1 stimulate MDM2-mediated ubiquitination of the receptor whereas high doses of the ligand are required to trigger c-Cbl-mediated receptor internalisation and proteasome degradation

(Sehat et al., 2008). Lysosomal degradation of the IGF-1R is mediated by the E3 ubiquitin ligase NEDD4 (Monami et al., 2008, Higashi et al., 2008). Whilst it is not clear whether c-Cbl binds directly to the receptor, adapter proteins β-arrestins and Grb10 are required for MDM2- and NEDD4-mediated IGF-1R internalisation, respectively (Vecchione et al., 2003, Morrione et al., 1999, Girnita et al., 2005). It is possible that these adapter proteins dock onto binding sites located on the C-tail region of the IGF-1R because its deletion abrogates receptor ubiquitination (Sehat et al., 2007).

The C-tail region has also been pinpointed as harbouring regulatory phosphorylation sites. Indeed, there is experimental evidence suggesting that serine phosphorylation at Ser1248 on the C-tail of the IGF-1R by GSK3β restrains full kinase activity by promoting an auto-inhibitory conformation that also masks potential docking sites for downstream substrates thereby negatively regulating downstream signalling (Kelly et al., 2012). The phosphorylation is also purported to regulate IGF-1R trafficking from the plasma membrane (Kelly et al., 2012). In addition to this, it has been shown in breast adenocarcinoma cells that IGF-1R pro-mitogenic signalling can be blocked through a feedback regulatory mechanism involving JNK-mediated stimulation of SHP1 expression, a tyrosine phosphatase (Amin et al., 2011). Another phosphatase that has been shown to dephosphorylate phospho-tyrosine binding sites on the IGF-1 receptor is PTP1B (Blanquart et al., 2005, Buckley et al., 2002). In addition to this, there is a complex cross-talk regulatory relationship between IGF-1R and integrins signalling pathways. It has been shown that SHP2-mediated cross-talk between αVβ3 integrin and IGF-1R potentiates ligand-induced IGF-1R activation and signalling (Clemmons and Maile, 2005, Kuemmerle, 2006).

1.2.2 IGF-1R signalling and energy metabolism

A number of studies have demonstrated the role of the IGF-1 ligand in the regulation of glucose and lipid metabolism. This is mainly attributed to the activation of the AKT signalling pathway through IGF-1R or IGF1R-INSR hybrid receptors although IGF-1 has been shown to also have poor affinity for the INSR (Sakai et al., 2002, De Ita et al., 2015).

IGF1-mediated signalling can modulate carbohydrate metabolism by promoting glucose uptake in peripheral cells, by encouraging insulin sensitivity and also, by influencing the expression of genes involved in glucose metabolism (Yakar et al., 2001, De Ita et al., 2015, Sakai et al., 2002). There is increasing evidence showing that abnormally low levels of IGF-1 ligands correlate with glucose intolerance and increased risk of developing type 2 diabetes (Sandhu et al., 2002, Sesti et al., 2005). A large cohort study in individuals aged 55 and older revealed that those exposed to low circulating IGF-1 levels are at increased risk of developing type 2 diabetes compared to those who had 18% higher levels of the hormone (Vaessen et al., 2001). Furthermore, IGF-1 has been shown to promote trafficking of glucose transporters to the membrane and, reduced expression of IGF-1 leads to hyperglycaemia, with decreased expression of key glycolytic and TCA cycle enzymes (Furling et al., 1999, Baumann et al., 2014, De Ita et al., 2015).

It could be debated whether the above-mentioned effects associated with IGF-1 are related to IGF-1R signalling but, there is evidence showing similar effects in mice carrying partial IGF-1R deficiency due to ablation of the *IGF1R* gene in one allele and even in experimental models where a mutation abrogating the kinase function of the receptor has been introduced (Bokov et al., 2011, Fernandez et al., 2001).

In consistency with these, a recently published paper revealed that, in murine xenograft model of lung cancer, citrate administration was able to block tumour growth by

downregulating IGF-1R activation and its downstream AKT signalling pathway, with consequent suppression of glucose metabolism via the glycolytic pathway and TCA cycle (Ren et al., 2017). The study also reported enhanced cytokine release in treated cells along with increased immune cells infiltration, alluding to a potential IGF-1R-mediated immune modulation.

1.2.3 IGF-1R signalling and Cancer

Evidence from a number of studies conducted at the epidemiological level and in laboratory settings have helped establish a link between IGF-1R signalling and cancer. There is a large body of evidence pointing towards the role of the IGF-1R at the different stages associated with cancer disease, from malignant transformation to metastasis. Although it is generally accepted that IGF-1R signalling contributes to the acquisition and maintenance of a malignant phenotype, there is no experimental evidence demonstrating that it is the main initial driver of malignant transformation because mutations in the *IGF1R* gene are not frequent in cancers. Nonetheless, a few somatic mutations in the IGF-1R have been identified in human cancers but their effect on receptor activity and signalling remain unknown. For instance, gene amplification in the *IGF1R* gene locus on chromosome 15 has been reported in primary breast tumours and osteosarcomas although observed in a very small number of patients (Berns et al., 1992, Greenman et al., 2007, Behjati et al., 2017). Evidence from a group claiming that some of the reported mutational changes in the *IGF1R* gene are activating mutations that increase the basal activity of the receptor is highly disputable (Craddock and Miller, 2012).

1.2.3.1 IGF-1R, the risk of developing cancer & its role in malignant transformation

There is clear evidence showing that high levels of circulating IGF-1 ligands positively correlate with increased risk of developing most non-smoking related cancers (Renehan et al., 2004, Travis et al., 2016, Hankinson et al., 1998). Indeed, no association between IGF-1 levels and the risk of cancer was reported in cohort studies including heavy smokers, highlighting that IGF-1R signalling (Woodson et al., 2003, Spitz et al., 2002). Studies have shown that IGF-1 levels strongly correlated with the risk of developing ovarian cancer in women before turning 55 years old (Lukanova et al., 2002). Similarly, the risk of developing pre-cancerous squamous intra-epithelial lesions in the cervix increased with the level of IGF-1 (Wu et al., 2003a).

Consistent with these findings, there is evidence that IGF-1 deficiency may protect against developing malignant diseases (Guevara-Aguirre et al., 2011, Steuerman et al., 2011). A cohort study conducted in individuals with congenital IGF-1 deficiency revealed that the incidence of cancer in this group compared to their family members that do not show the deficiency was very negligible as individuals in the former group were approximately six times less likely to develop cancer. This is also supported by evidence from animal models of breast cancers showing that reduced IGF-1 levels in the circulation resulted in a delay in the onset of cancer upon exposure to chemical carcinogens (Wu et al., 2003b). Moreover, a study investigating the effect of reduced calorie intake on tumour progression in p53-deficient mice demonstrated that although mice with pre-neoplastic lesions under dietary restriction showed slower cancer progression compared to the controls, this protective effect was abolished when caloric reduction was combined with IGF-1 administration (Dunn et al., 1997).

Beyond the association with cancer risk, IGF-1R signalling is important for malignant transformation as evidenced by reports showing that inducing high expression levels of

IGF-1 in the basal epithelium of the prostate in transgenic murine models led to abnormal tissue growth (neoplasia) (DiGiovanni et al., 2000). Furthermore, contrary to their wild-type counterparts, mouse embryonic fibroblast cells unable to express IGF-1R (commonly referred to as R^- cells) do not undergo oncogenic transformation when transfected with plasmid containing genomic DNA encoding an oncoprotein (SV40 TAg) known to promote tumour development (Ahuja et al., 2005, Sell et al., 1993). Similarly, the chimeric oncoprotein ETV6-NTRK3 associated with constitutive activation of the RAS-MAPK signalling pathway was not able to induce transformation in R^- cells to the extent that was observed in cells with functional IGF-1R (Morrison et al., 2002); implying that IGF-1R signalling is important in the process of malignant transformation.

1.2.3.2 IGF-1R is involved in tumour growth and progression

Evidence for the involvement of the IGF-1R signalling in tumour progression has been building-up. Apart from a few reported mutations, highly active IGF1R signalling in cancer is generally attributed to a failure of the different regulatory mechanisms that modulate its expression or downstream signalling due to inherited or acquired somatic mutations (Berns et al., 1992, Greenman et al., 2007, Behjati et al., 2017). Several studies have pointed towards a relationship between IGF-1R expression levels and disease outcome in several cancer types. Our group has shown that IGF-1R levels correlated with poor prognosis in HPV negative head and neck squamous cell cancer (Dale et al., 2015). Tumour samples obtained from patients with the oropharyngeal squamous cell carcinomas showed significantly higher levels of cytoplasmic IGF-1R compared to normal non-malignant tissues from the same patients. Total IGF-1R positively correlated with high tumour grade, HPV-negativity and poor overall survival at five years from the diagnosis. Strikingly, this was independent

of the therapeutic strategy the patients had undergone to attempt to clear their tumour (Dale et al., 2015).

These findings are consistent with results from another group demonstrating that high IGF-1R expression positively correlated with increased probability of cancer recurrence and reduced overall survival in patients with laryngeal cancer that had undergone surgical therapy (Mountzios et al., 2013). A cohort study on primary breast cancer tissue samples revealed that overexpression of the IGF-1R correlated with poor prognosis while a worse outcome was identified in IGF-1R^{+ve}/ER^{-ve} patients compared to those with no detected overexpression of both receptors (IGF-1R^{-ve}/ER^{-ve}) in their tumour samples (Railo et al., 1994). Similar conclusions were drawn based on studies conducted in several other cancers including renal, colorectal and ovarian cancers (Takahari et al., 2009, Spentzos et al., 2007, Parker et al., 2003).

Our group has reported that the sub-cellular localisation of the receptor may influence its prognostic value in certain cancers such as renal carcinomas where poorer disease outcome correlated with stronger nuclear IGF-1R staining (Aleksic et al., 2010). In a small cohort study of individuals with non-operable and locally advanced/metastatic sarcomas treated with anti-IGF1R antibody, patients with tumours that showed exclusively nuclear IGF-1R levels derived greater benefits from the therapy with significantly better progression-free survival (Asmane et al., 2012).

1.2.3.3 IGF-1R is involved in cancer metastasis

In certain cancers, IGF-1R signalling has been linked with increased metastatic potential. A study carried out in patients with gastric cancer revealed that high pre-operative levels of the IGF-1R correlated with increased metastasis to regional lymph nodes (Jiang et al., 2005). Interestingly, these patients also showed overexpression of Sp1, a transcription

factor that has been shown to drive IGF-1R expression (Abramovitch et al., 2003). The authors confirmed their findings in xenograft models of gastric cancer, showing that Sp1 knockdown led to reduced IGF-1R levels and although tumours did develop, no liver metastasis was observed in this group compared to the control group which showed higher IGF-1R expression levels (Jiang et al., 2005). This confirms that dysfunction in proteins linked with the IGF-1R complex regulatory network can affect metastatic potential as well as mitogenic and transforming potential. There are other reports associating high IGF-1R expression levels with cancer metastasis (All-Ericsson et al., 2002, Yamamoto et al., 2012).

Indeed, IGF-1R signalling is thought to play a very important role at the different stages associated with the acquisition of metastatic potential in cancer, especially in epithelial to mesenchymal transition (EMT) (Zielinska et al., 2015). EMT is a process characterised by loss of cell-cell contacts and the ensuing loss of cell polarity, remodelling of cell-matrix adhesion and acquisition of mesenchymal properties (Nieto et al., 2016). Therefore, EMT promotes metastasis and drug resistance by bequeathing onto cells migratory, invasive and stem cell-like properties (Thiery et al., 2009, Nieto et al., 2016). IGF-1R signalling is involved in EMT through its role in modulating the expression of the Snail family of transcription factors known to repress the expression of genes encoding for adhesion molecules and tight junction proteins (Graham et al., 2008, Bachelder et al., 2005, Kim et al., 2007, Playford et al., 2000, Peinado et al., 2007, Wang et al., 2007). IGF-1R can also regulate the expression of matrix metalloproteinases (MMPs) which break down collagen in the matrix thereby altering the tumour micro-environment. Experimental studies have revealed that depending on the cell context, various MMPs can be upregulated and/or downregulated through activated IGF-1R signalling (Zhang et al., 2004, Mira et al., 1999, Adachi et al., 2009). Apart from matrix breakdown, MMPs have also been implicated in mediating activation of latent TGF-β, a potent EMT inducer (Walsh and Damjanovski, 2011). The cross-talk between the

IGF-1R and the integrin signalling pathways has also been pinpointed as a key player in tumour invasion and motility through modulation of the cytoskeletal architecture and sending through pro-survival signals amidst EMT-induced changes (Sayeed et al., 2012, Burnier et al., 2011, Metalli et al., 2010).

1.3 IGF-1R targeting and DNA damage

The term 'DNA damage' is used to describe any alteration in the chemical structure of the DNA molecule that may result from breaks in the molecular structure, damage to the sugar ring of the DNA nucleotide or modifications to the DNA base (De Bont and van Larebeke, 2004). These lesions can block replication and transcription and can therefore be cytotoxic to the cell if left unrepaired. It is estimated that a single cell is subjected to numerous DNA lesions arising from endogenous and exogenous sources (Lindahl, 1993, De Bont and van Larebeke, 2004). Such endogenous sources include spontaneous hydrolytic reactions and reactive chemical species like superoxide, peroxynitrite, malondialdehyde and S-adenosylmethionine arising from physiological processes (Chaudhary et al., 1994, Rydberg and Lindahl, 1982, Richeson et al., 1998, Lindahl, 1993, Jackson et al., 1998). Lesions in the DNA can be caused exogenously through exposure to physical or chemical agents such as alkylating agents, topoisomerase inhibitors, UV irradiation and radioisotopes (Cadet et al., 2005, Jackson and Bartek, 2009, Helleday et al., 2014). DNA damage has been widely used as a therapeutic strategy in the clinical management of cancers because, compared to normal cells, cancer cells often present defective DNA repair mechanisms or intrinsically much higher levels of genomic instability (Meindl et al., 2010, O'Connor, 2015, Windhofer et al., 2008, Bentley et al., 2004, Ding et al., 2008).

1.3.1. IGF-1R can mediate resistance to radiotherapy

There is evidence for the implication of the IGF-1R signalling in the resistance to radiation treatment. One of the most compelling piece of evidence came from a cohort study performed in 94 patients with local recurrence of primary breast cancer after surgical tumour removal accompanied with radiotherapy (Turner et al., 1997). The study revealed that IGF-1R overexpression strongly correlated with early breast cancer recurrence within the irradiated site as tumour specimens collected from just over half of the patients (52%) that presented themselves with aggressive recurrent carcinoma within 4 years from the date of the diagnosis showed stronger membranous and cytoplasmic IGF-1R staining compared to the group of individuals that had undergone the same therapeutic treatment and where no tumour relapse was observed within the same time-frame (Turner et al., 1997). A similar finding was reported 10 years later in patients with cervical carcinoma treated with a combination of radiotherapy and cisplatin (Lloret et al., 2007). The study demonstrated a strong positive correlation between high IGF-1R levels and cancer relapse within a group of patients that were initially confirmed as clinically disease-free after treatment. Out of 31 patients with tumour samples showing strong IGF-1R positivity after staining, up to 25 relapsed within 5 years compared to none out of the 19 patients with low IGF-1R (Lloret et al., 2007). These two studies pointed towards a link between IGF-1R overexpression in cancers and the likelihood of cancer recurrence following radiotherapy. Contradictory conclusions have been reported by a group showing that in early stage non-metastatic breast cancer tumour patients, those showing high IGF-1R levels are more likely to benefit from the lumpectomy plus radiotherapy treatment regimen and are at lower risk of local cancer recurrence (Peiró et al., 2009).

IGF-1R as a mediator of radio-resistance has also been demonstrated in laboratory-based studies. For instance, in a xenograft model of small cell lung cancer, targeting IGF-1R with

a monoclonal antibody significantly delayed tumour progression and prolonged survival when combined with ionising radiation, cisplatin treatment or both as opposed to either treatment alone (Ferté et al., 2013). In mouse melanoma cells, downregulation of the IGF-1R to protein levels approximately 70-80% less compared to the controls resulted in enhanced sensitivity to irradiation (Macaulay et al., 2001). Investigations from several other groups in different cancer cells using various IGF-1R blockade strategies have confirmed that targeting the IGF-1R signalling pathway can sensitise cancer cells to radiotherapy (Riesterer et al., 2011, Iwasa et al., 2009, Yavari et al., 2010, Wang et al., 2009, Osuka et al., 2013, Isebaert et al., 2011). Our group has shown that IGF-1R depletion in prostate cancer cell lines that are androgen-independent results in radio-sensitisation (Turney et al., 2012). The lack of sensitisation in cells still relying on stimulatory growth signals from the androgen receptor possibly indicates that IGF-1R targeting as a strategy to ameliorate the sensitivity to radiotherapy may be most effective in cancer cells that have developed a reliance on IGF-1R signalling for tumour survival and proliferation. Indeed, increased IGF-1R expression has been reported in androgen-independent prostate cancers (Nickerson et al., 2001, Krueckl et al., 2004).

1.3.2 Mechanisms of IGF1R-induced radio-resistance

1.3.2.1 Radiotherapy-induced DNA damage

Radiotherapy in the treatment of cancers can be in the form of photon beams such as X-rays and γ-rays or, particle radiation such as electron, proton and neutron beams. Because of associated cost with the latter, it is mostly used in radio-resistant cancers whilst photon beams are more commonly used in cancer therapy (Baskar et al., 2012). Photon beams are also considered low linear energy transfer ionising radiation that is, a small quantity of

photon energy is deposited in exposed cells. Nonetheless, these energy depositions in the cells induce chemical alterations to the DNA molecule (Goodhead, 1994, Nikjoo et al., 1994). Whilst the cell routinely deals with a high number of endogenous DNA lesions as described earlier, it is generally accepted that the cytotoxic ability of ionising radiation results not from the number of DNA lesions induced but from the complexity of these and their spatial distribution (Lomax et al., 2002, Nikjoo et al., 1994).

Indeed, the majority of endogenously induced DNA lesions are sparsely distributed along the molecule (sometimes referred to as isolated lesions) whereas, the passage of the ionising track of radiation does not only yield isolated but cluster lesions; these are lesions located within a few nanometres of each other that show reduced reparability compared to isolated lesions due to their complexity (Semenenko and Stewart, 2004, Goodhead, 1994, Lomax et al., 2013, Gulston et al., 2002, Sutherland et al., 2000). Overall, lesions caused by ionising radiation include single and double-strand breaks which arise as a result of breaks in the phosphodiester backbone of the DNA molecule either on one or both DNA strands and, nucleotide damage due to alterations on the base or sugar ring (Dizdaroglu and Jaruga, 2012, Cadet et al., 2008, Pouget et al., 2002, Hanai et al., 1998, Van Der Schans, 1978). The cell has in place robust repair mechanisms to deal with these lesions among which double-strand breaks are considered to be the most harmful (Vamvakas et al., 1997, Jackson and Bartek, 2009).

1.3.2.2 Understanding the main double-strand break repair pathways

Ionising radiation-induced double-strand breaks trigger a series of signalling mediated by post-translational modifications of several key proteins (Polo and Jackson, 2011, Thompson, 2012). Whilst replication-fork associated double-strand breaks trigger ATR activation, double-strand breaks directly resulting from a break in the two DNA strands separated by

about 10 base pairs or less with 3' blocking ends lead to ATM activation (Maréchal and Zou, 2013). There are two main cellular repair pathways responsible for tackling the danger of double-strand breaks which are homologous recombination (HR) and non-homologous end joining (NHEJ). These two do not only differ by the cellular proteins they engage but are also subjected to different cell cycle regulatory mechanisms. It has been shown that NHEJ can be active throughout the cell cycle whereas HR is most active during the S and G2 phases (Mao et al., 2008, Shibata et al., 2011, Kim et al., 2005). This is particularly important as HR relies on homology-directed search and therefore requires the availability of newly-synthesised sister chromatids as repair templates for what is generally considered a less error-prone process compared to NHEJ (Rodgers and McVey, 2016).

Homologous recombination

It has emerged recently that PARP1 may play an important role during early HR, detecting double-strand breaks and catalysing addition of poly-ADP-ribose modifications on chromatin flanking the break site, a reaction referred to as PARylation (Ray Chaudhuri and Nussenzweig, 2017). This facilitates the rapid recruitment of the DNA end-processing MRN (MRE11-RAD50-NBS1) complex which in turn mediates the recruitment of ATM (Costanzo et al., 2004, Uziel et al., 2003). Upon contact with free dsDNA ends, ATM auto-phosphorylates thereby activating its kinase function (Bakkenist and Kastan, 2003). Activated ATM then phosphorylates a number of substrates, including chromatin remodeller KAP1, histone variant H2AX, cell cycle checkpoint protein CHK2 (Vignard et al., 2013, Kim et al., 2005, Shibata et al., 2011, Goodarzi et al., 2008, Ziv et al., 2006, Thompson, 2012). Phosphorylation of H2AX in turn leads to MDC1 recruitment commonly referred to as the signal amplifier as it is important for the recruitment of many more factors including the E3 ubiquitin ligases RNF8/RNF168 responsible for the poly-ubiquitination of histones H2A and H2AX on Lys63 which targets the BRCA1A complex (RAP80-BRCA1-

BRCC36-CCDC98) to sites of DNA damage (Huen et al., 2007, Doil et al., 2009, Stewart et al., 2003, Kolas et al., 2007). BRCA1 localisation at the break sites stimulates CtIP-mediated 5'-3' DNA end-resection together with the MRN complex. Extension of resected ends is mediated by EXO1 and DNA2 nucleases, including the BLM helicase, yielding 3' ssDNA overhangs that become coated with the heterotrimeric protein RPA (Escribano-Diaz et al., 2013, Hoa et al., 2015, Sartori et al., 2007, Nimonkar et al., 2011, Huertas and Jackson, 2009). Next, via PALB2 interaction with BRCA1, BRCA2 is recruited to the site of damage where it promotes RAD51 loading on the ssDNA in place of RPA (Buisson et al., 2010, Liu et al., 2010). The RAD51-ssDNA nucleoproteins formed are stable structures for homology search and strand invasion, a critical step during HR which leads to the formation of a D-loop after which a double Holliday junction is formed. The latter is processed into damage-free DNA strands through the action of resolvases and other key proteins (Jasin and Rothstein, 2013, Wu et al., 2006, Raynard et al., 2006, Cejka et al., 2010).

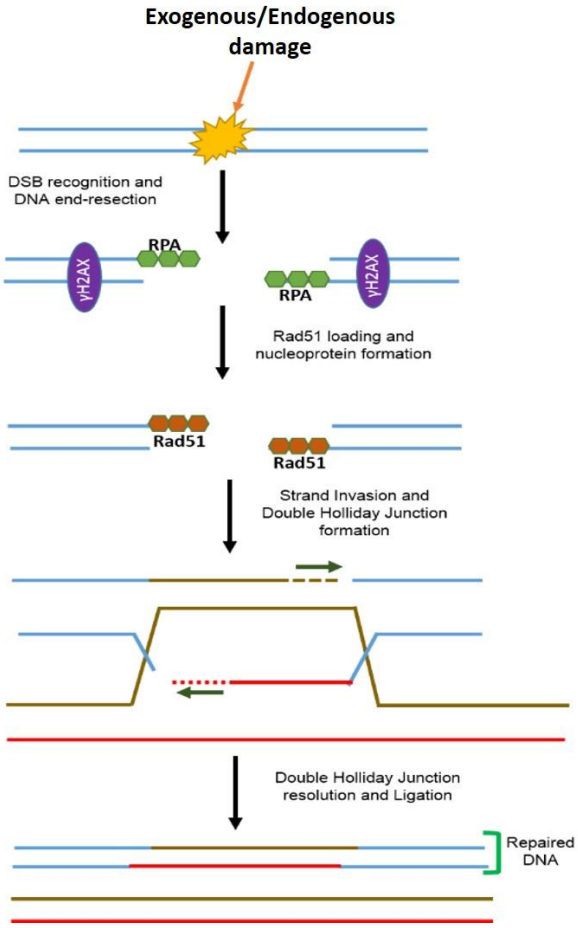


Figure 1-3: **Double-strand break repair via Homologous Recombination**. DSBs can be caused by endogenous and exogenous sources. HR-mediated repair is restricted to cell cycle phases S and G2 and, DSB processing involves the following steps: (1) DSB recognition by the MRN complex which activates ATM signalling; ATM then phosphorylates histone H2AX which in turn promotes MRN complex retention at damage sites and 5'-3' DNA end resection; replication protein A (RPA) molecules are recruited and coat single-stranded DNA (ssDNA), then RPA is displaced by RAD51; (4) RAD51-ssDNA nucleoprotein filaments form to perform homology search and strand invasion resulting in the formation of double Holliday junction (dHj); (6) dHj resolution and ligation.

Non-homologous end-joining

The NHEJ pathway is engaged upon recruitment of 53BP1 protein to sites of damage by MDC1. This is achieved through the action of the RIF1-53BP1 complex which prevents BRCA1 recruitment and, in addition to the CDK-dependent activation of CtIP effectively blocks DNA end resection thus hindering HR (Chen et al., 2008, Wang et al., 2013, Fugger and West, 2016, Chapman et al., 2013). The double-strand break sensor protein Ku is also recruited to the break site and, depending on the conformation of the DNA ends, different

downstream proteins are recruited to complete the NHEJ process (Chang et al., 2016, Downs and Jackson, 2004). Ionising radiation-induced double-strand breaks that are recognised and processed via NHEJ are mainly blunt ends, 3' and 5' incompatible ends that may involve minimal resection and, 3'-phosphoglycolated ends (Chang et al., 2017).

The heterodimer Ku70/80 not only recognises and binds to double-strand breaks but it also facilitates loading of downstream factors. It is generally accepted that the repair of blunt DNA ends only require the action of XRCC4-LigaseIV-Ku complex. Ku binds to the DNA then, ligase IV in complex with XRCC4 catalyses the ligation of the DNA ends (Sibanda et al., 2001, Ahnesorg et al., 2006, Grawunder et al., 1998). In cases when the double-strand break has generated incompatible DNA ends, the DNA-PKcs is recruited to the Ku protein. Contact with DNA ends triggers DNA-PKcs auto-phosphorylation and formation of the DNA-PK complex which facilitates recruitment and activation of the endonuclease Artemis for end processing (Goodarzi et al., 2006, Uematsu et al., 2007). Artemis processes both 5' and 3' overhangs to reveal small regions of micro-homology that can facilitate repair (Niewolik et al., 2006). End resection is followed by end ligation involving XLF, XRCC4 and PAXX but if required, DNA polymerases are first recruited to synthesise short patch of DNA prior to end joining (Chang et al., 2017, Ochi et al., 2015, Tadi et al., 2016). Repair of double-strand breaks with 3'-phosphoglycolated ends requires prior processing by TDP1 before recruitment of necessary NHEJ proteins depending on the configuration of the resulting DNA ends (Inamdar et al., 2002).

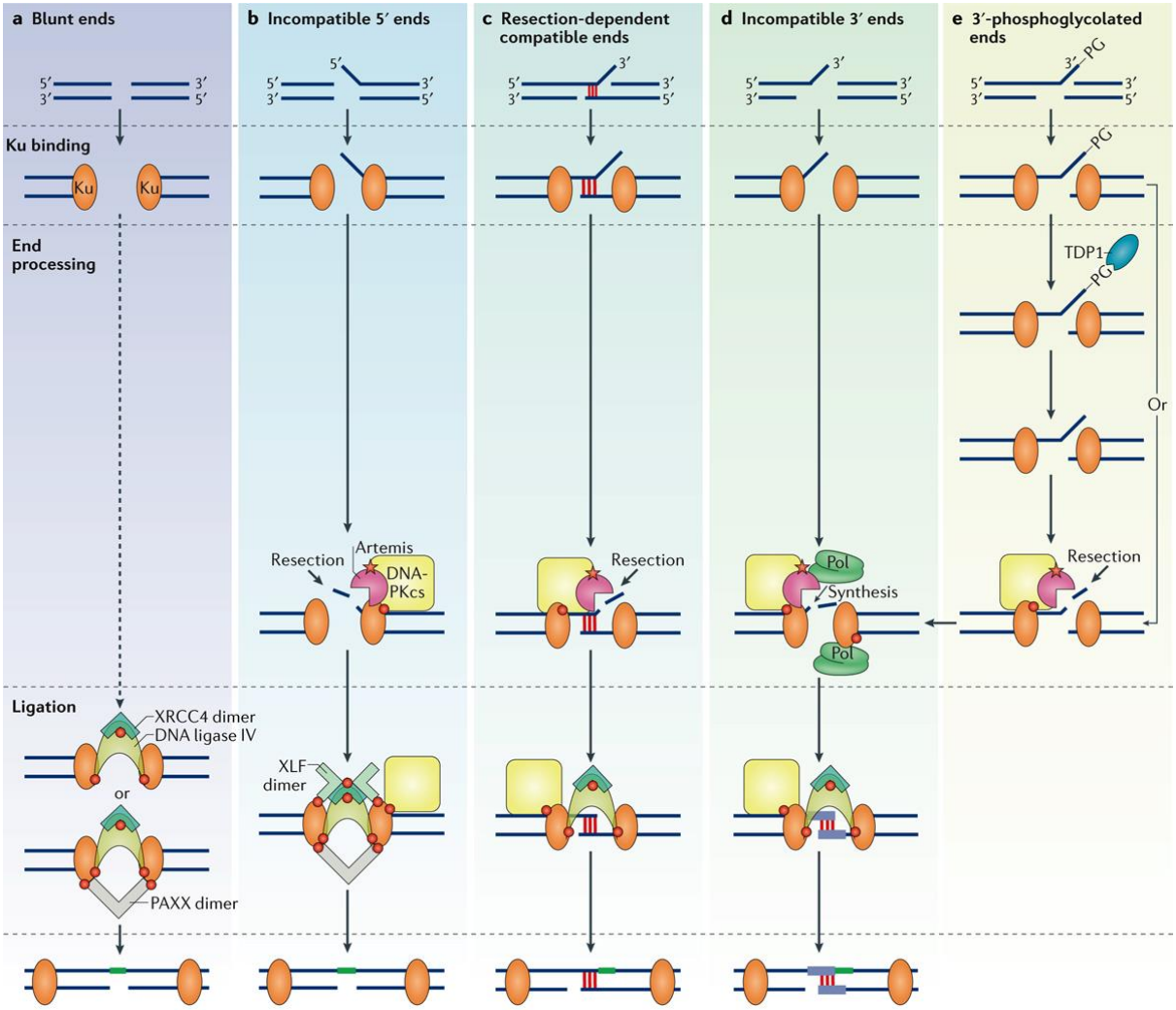


Figure 1-4: **Non-homologous end joining processing of various double-strand break ends**. The known protein-protein interactions as described in the text are depicted. Although ligation of the top strand only is represented, this process is also replicated with the bottom strand. Copied with permission from (Chang et al., 2017).

1.3.2.3 Proposed mechanisms of radio-resistance

For many years now, mechanistic insights concerning the role of the IGF-1R in conferring radio-protective abilities have been investigated. There is more to be uncovered as complex and sometimes unrelated results have been reported. In summary, IGF1R-mediated radio-resistance has been attributed to its canonical signalling pathways driving survival and cellular proliferation and, a yet to be fully understood possible involvement in the DNA damage response to ionising radiation.

Protection from irradiation-induced apoptosis

As detailed earlier (section 1.1.3), activation of the AKT and ERK pathways triggers a wide range of cellular changes to promote cell survival and proliferation. There is experimental evidence suggesting that IGF-1R signalling can protect haematopoietic stem and differentiated cells from irradiation-induced apoptosis by activating cell survival mechanisms and encouraging proliferation and differentiation (Zhou et al., 2013, Sanders et al., 1998). Moreover, it has been shown *in vivo* that activating IGF-1R signalling post-exposure to a lethal dose of whole-body irradiation via IGF-1 administration can attenuate the effects of irradiation on the haematopoietic system and increase the chances of survival (Zhou et al., 2013).

Other studies have shown that IGF-1R signalling mitigated irradiation-induced cell death in intestinal cells via activation of the AKT pathway leading to repression of the expression of pro-apoptotic proteins like BAX and PUMA (Qiu et al., 2010, Wilkins et al., 2002). Indeed, AKT activation has been pinpointed as a potent mechanism for IGF1R-mediated anti-apoptotic signalling (Kulik et al., 1997). The activation of ERK signalling pathway has also been implicated in IGF1R-mediated protection against irradiation (Yu et al., 2003, Peruzzi et al., 1999). Interestingly, it has been reported that IGF-1R influence on apoptotic induction following ionising radiation does not always correlate with clonogenic survival (Tezuka et al., 2001); implying that there might be other mechanisms in place underlying IGF1R-mediated radio-resistance.

The ATM – IGF-1R reciprocal regulation

A number of studies have hinted at a relationship between IGF-1R signalling, ATM function and response to ionising radiation. In murine melanoma cells, it was reported that downregulation of IGF-1R impaired ATM kinase activation in response to irradiation,

resulting in radio-sensitivity. The authors also proposed that IGF-1R may promote ATM stability because, despite no changes at the mRNA level, experimental evidence suggested that downregulation of IGF-1R reduced the half-life of the ATM protein (Macaulay et al., 2001). On the other hand, another group demonstrated that radio-sensitive A-T cells lacking functional ATM showed lower levels of IGF-1R than the control and that this could be reversed upon complementation with ATM cDNA (Peretz et al., 2001). The same group also showed that complemented A-T cells expressing functional ATM are unable to correct the radio-sensitivity profile of the cells when IGF-1R signalling is blocked; thereby suggesting that appropriate response to DNA damage in ATM-complemented A-T cells relies on a functional IGF-1R signalling (Peretz et al., 2001). These findings stimulated interest for the investigation of the potential influence of IGF-1R on the double-strand break repair process triggered following irradiation-induced ATM activation.

IGF-1R signalling cross-talking with double-strand break repair progression

Earlier investigations by our group revealed that depletion or inhibition of IGF-1R can cause a delay in the resolution of irradiation-induced γH2AX foci, a marker of DNA double-strand breaks, in prostate cancer cells (Chitnis et al., 2014, Turney et al., 2012). Interestingly, the effect on the resolution of irradiation-induced γH2AX foci was only observed in cell lines that showed radio-sensitisation upon depletion of IGF-1R (Turney et al., 2012), highlighting that the between IGF-1R signalling and radio-protection might be mediated through the modulation of the double-strand break repair. Further insight into the underlying mechanism of radio-protection was provided through repair reporter assays performed in HEK293 cells and the results indicated that IGF-1R inhibition resulted in significant suppression of NHEJ (Chitnis et al., 2014). The authors explained that this might account for the absence of an additive effect despite co-inhibition of IGF-1R and a key NHEJ protein 'DNA-PKcs' on the sensitivity of prostate cancer cells to γ-irradiation when

compared to treatment with a DNA-PKcs inhibitor alone. Furthermore, they demonstrated that glioblastoma cells lacking DNA-PKcs failed to show increased sensitivity to ionising radiation when IGF-1R activation was inhibited as opposed to the cells that were proficient for DNAPKcs (Chitnis et al., 2014).

Another study has also reported that IGF-1R can mediate radio-resistance by promoting NHEJ (Cosaceanu et al., 2007). The authors showed that irradiation triggered IGF-1R activation in serum-starved lung cancer cells which led to activation of anti-apoptotic signalling via the PI3K/AKT pathway. In addition, IGF-1R signalling modulated the sub-cellular localisation of the NHEJ protein Ku80 which is required for double-strand break detection and to facilitate the recruitment of other factors necessary for NHEJ-mediated double-strand break repair (Cosaceanu et al., 2007).

However, there is evidence from some studies suggesting that IGF-1R can also influence double-strand break repair via HR. IGF-1R activation was shown to stimulate RAD51 recruitment to the nucleus for the repair of cisplatin-induced DNA damage in mouse embryo fibroblast cells. Having demonstrated that IRS-1 co-localises with RAD51, the authors speculated that IGF-1R signalling supported HR by inducing IRS-1 re-localisation to the cytoplasm, thereby resulting in increased level of unbound RAD51 which may then enable it to perform its function in double-strand break repair (Trojanek et al., 2003). In support of this finding, the same group reported that IGF-1 stimulation was able to attenuate nuclear localisation of IRS-1 in JCV T-Ag expressing cells and relieve HR suppression (Trojanek et al., 2006). There is one main issue with the group's experimental evidence, and that is the fact that they failed to demonstrate activated IGF-1R signalling upon IGF-1 stimulation in both papers. There is no western blot establishing the levels of IGF-1R pre- and post-IGF1 stimulation in the cells used in their investigation. Moreover, from their later

publications, it seems problematic that although the cells used contain a disruption in the *IGF1R* gene, these are still considered as IGF-1R proficient.

Some of the above-mentioned studies do no concord with earlier reports that IGF-1R may influence ATM kinase activation, a much earlier event in IR-induced double-strand break repair; prompting the question whether mechanisms by which IGF-1R signalling mediate radio-protection might be cell context-dependent. Our group is very interested in furthering our understanding on the functional role IGF-1R might play in the repair of double-strand breaks as the studies described above pointed out.

1.3.3 Approaches to studying the influence of IGF-1R on double-strand break repair

1.3.3.1 Abrogating the activation of the IGF-1R signalling pathway

Strategies devised to block or suppress the IGF-1R signalling pathway in order to study its function vary greatly. These sometimes involve the use of inhibitors which target the ligand or the receptor directly. Alternatively, deletion/modification of the coding gene or, targeting the transcribed mRNA for degradation to block its expression at the protein level can also be considered: this is referred to as gene silencing.

Use of small molecule inhibitors

Among the types of inhibitors used to target the IGF-1R signalling pathway are neutralising monoclonal antibodies directed either against the receptor itself or its activating ligand. Anti-IGF mAb bind to circulating IGF ligands and prevent them from lodging into the ligand-binding region of the receptor, thereby blocking receptor activation. Antibodies directed against the receptor are thought to trigger receptor internalisation thereby limiting its availability at the plasma membrane and subsequent ligand-induced receptor activation

(Sachdev et al., 2003). Similarly, tyrosine kinase inhibitors block ligand-induced receptor autophosphorylation which impedes on the subsequent recruitment and phosphorylation of downstream substrates, mediators of IGF-1R signalling, since no phospho-tyrosine docking sites are available (Levitzki and Gazit, 1995). The efficacy of these different classes of drugs has been tested experimentally and in clinical trials (Simpson et al., 2017).

Gene silencing: transient and permanent

Loss of function can be induced transiently or permanently, depending on the methodology used and, each method has its own advantages and disadvantages. Routinely used methods of gene silencing include RNA interference and the CRISPR-Cas9 genome editing technique. RNA interference is a process whereby the translation of targeted mRNA transcripts is repressed through cleavage of the mRNA molecules or by modulating the stability of the transcripts (Pasquinelli, 2012, Rao et al., 2009). This can be achieved using either short interference RNA (siRNA) or short hairpin RNA (shRNA) which, through complementary base-pairing with the transcribed mRNA, targets it for degradation. The effects of siRNA are transient and not sustainable.

For long-term gene silencing, some of the methods employed are shRNA transfection or the CRISPR/Cas9 technology. The use of CRISPR/Cas9 leads to insertions or deletions in the coding sequence of the target gene that can potentially interfere with gene expression (Cho et al., 2013, Rao et al., 2009, Wang et al., 2016, Doudna and Charpentier, 2014) (Figure 1-5). Whereas the use of shRNA almost inevitably results in off-target effects and, depending on the mode of delivery, toxicity (due to immune response activation) and random integration into the genome can ensue, the CRISPR/Cas9 system carries no risk of genome integration and off-targeting requires a combination of different factors that are still not thoroughly understood (Kim and Eberwine, 2010, Rossi, 2008, Cho et al., 2013, Mali et al., 2013).

In addition to this, apart from the requirement for a more complex library design, shRNA-mediated knockout has been reported to sometimes result in hypomorphic effects which, in some instances, may not result in detectable phenotypic effects while CRISPR/Cas9 often results in true loss of function (Housden and Perrimon, 2016). Furthermore, CRISPR/Cas9 has been reported as more reliable than shRNA for large-scale genetic perturbation screens (Evers et al., 2016, Housden and Perrimon, 2016).

For the work conducted in this thesis, we opted for the use of CRISPR/Cas9 technology to generate IGF-1R knockout cells and used siRNA for transient downregulation of IGF-1R.

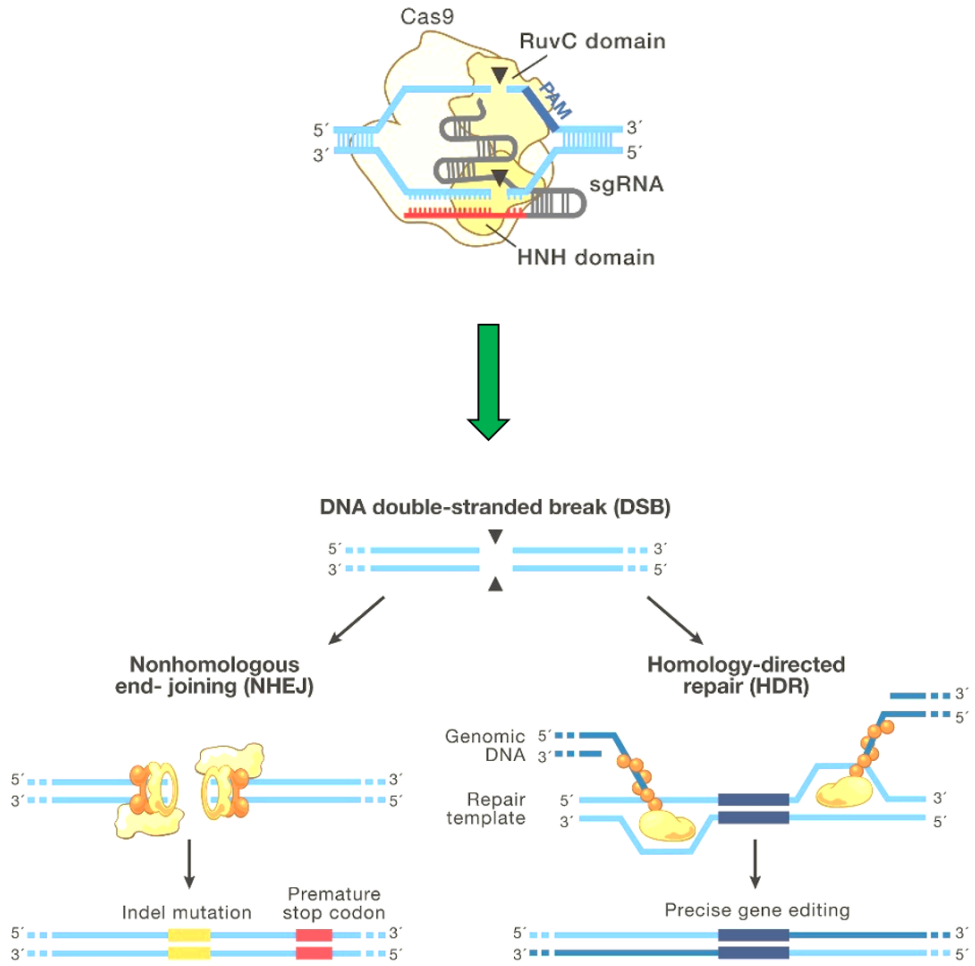


Figure 1-5: **CRISPR/Cas9-mediated genome editing**. The CRISPR system relies on a non-coding RNA sequence referred to as guide RNA (gRNA) or short guided RNA (sgRNA) to direct the Cas9 nuclease to specific genomic DNA region for cleavage. Heteroduplex formation between the guide RNA and the complementary target DNA triggers a structural change that releases Cas9 from an auto-inhibitory conformation as the nuclease catalytic sites become available upon removal of steric hindrance (Sander and Joung, 2014, Wang et al., 2016). The Cas9 nuclease contains two functional catalytic domains, RuvC and HNH, that catalyse cleavage of the target DNA at specific sites following structural activation. The resulting blunt-ended DNA double-strand break can be repaired either by non-homologous end joining (NHEJ) or homologous recombination (also called Homology-directed repair). Error-prone NHEJ leads to inaccurate repair with indels resulting to frameshift mutations that could, in turn, lead to the emergence of one or more stop codon(s) prematurely within the target gene's DNA sequence. Copied with permission from (Hsu et al., 2014).

1.3.3.2 Inducing DNA double-strand breaks

Double-strand breaks in the DNA can be induced directly or indirectly upon conversion of other forms of DNA damage into double-strand breaks. Apart from ionising radiation, various tools can be used to induce double-strand breaks; one such agent that indirectly

cause replication-associated double-strand breaks is the DNA alkylating drug Temozolomide (TMZ).

Simple methylating agents like TMZ can result in N-methylations or O-methylations as a methyl group is added either to the N or O atom of a DNA base (Beranek, 1990). *N*-methylations are reportedly more cytotoxic and less mutagenic whereas *O*-methylations are considered more mutagenic (Kondo et al., 2010). The former is dealt with efficiently by the base excision repair mechanism (BER) or the human AlkB homologue (hABH) depending on the type of adduct (Kaina et al., 2007). O^6MeG is the most common form of O-alkylation. O^6MeG adducts are repaired in a one-step process during which the Alkyl transferase enzyme MGMT removes the methyl group from the oxygen in the guanine residue and becomes inactivated as the methyl group is transferred and becomes covalently linked to a cysteine residue in the enzyme's catalytic pocket (Margison and Santibanez-Koref, 2002). Hence, cells lacking O^6-Methyl Guanine Methyl Transferase (MGMT) are more sensitive to TMZ (Brennand and Margison, 1986, Pollack et al., 2006, Christmann and Kaina, 2016).

Unrepaired O^6MeG gives rise to O^6MeG:C and O^6MeG:T pairs in the next round of replication. These are recognised by the MutSα complex, a component of the mismatch repair (MMR) machinery (Margison and Santibanez-Koref, 2002). The activated MMR causes nicks in the opposite strand to allow for incorporation of the correct base but, when the DNA lesion is on the template strand, MMR substrates are persistently generated by the repair machinery, trapping the cell in a 'futile repair' cycle (Wang et al., 2008). Strand nicks and gaps created by the MMR machinery can cause replication-fork stalling and give rise to replication-fork associated double-strand breaks that require repair by homologous recombination (HR) (Kondo et al., 2011, Roos et al., 2009, Cortés-Ledesma and Aguilera, 2006) (Figure 1-6). This is thought to occur after the cell has gone through at least two rounds of

replication (Margison and Santibanez-Koref, 2002). The 'futile repair' cycle in itself is generally acknowledged not to induce cell death but it is the resulting DNA double-strand breaks that are highly cytotoxic (Olive, 1998, Tominaga et al., 1997).

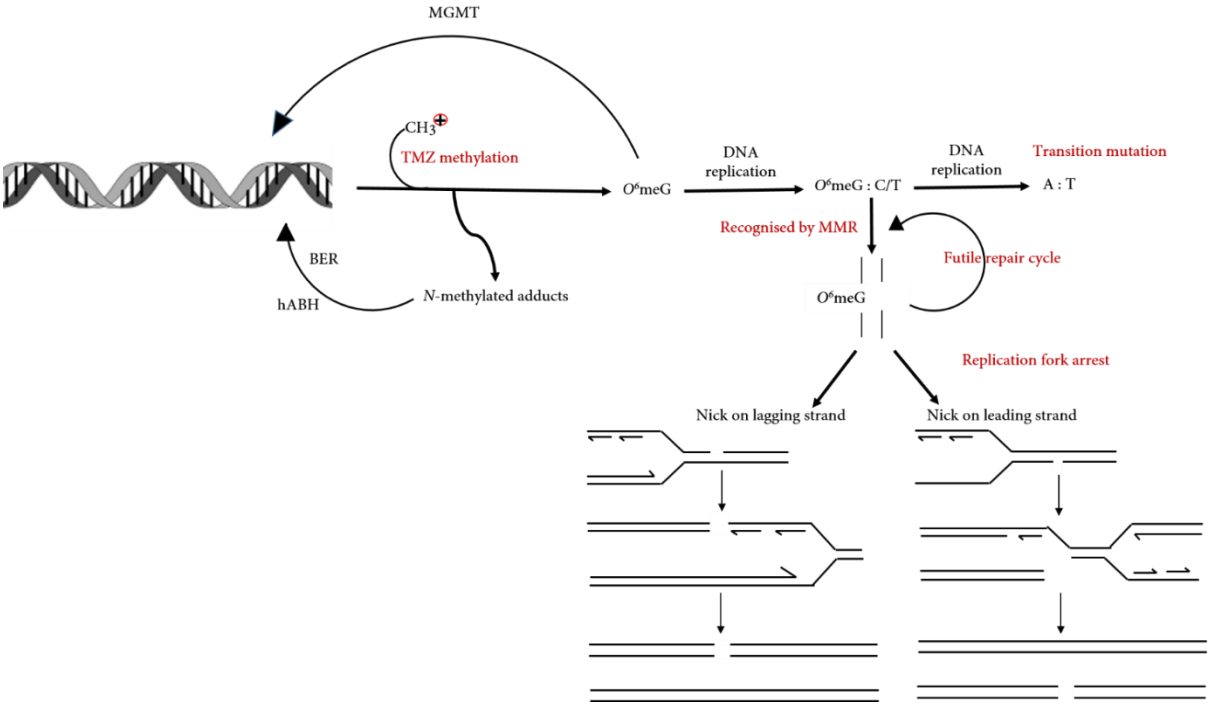


Figure 1-6: **Schematic representation of temozolomide-induced DNA damage.** TMZ can give rise to N-methylated adducts which are removed by the base excision repair (BER) machinery and the human AlkB homologue (hABH), and O^6meG adducts dealt with by the O6-methylguanine-DNA methyltransferase (MGMT) that removes the methyl adduct from O^6meG in one step. If O^6meG left unrepaired, O^6meG:C ambiguous pairs or O^6meG:T mismatch pairs can form during replication and these are recognized by the mismatch repair (MMR) system. MMR causes nicks in the opposite strand to allow for incorporation of correct base. Because the DNA lesion (methylated guanine residue) is on the template strand, repair attempts persistently generate MMR substrates, trapping the cell in a 'futile repair' cycle. MMR-produced nicks and single-strand breaks can cause replication arrest which can eventually lead to double-strand break formation.

1.4 Hypothesis and Aims of this study

HYPOTHESIS

Since previous studies carried out in our group demonstrating that IGF-1R inhibition and its depletion delayed DNA repair in prostate cancer cell lines following γ-irradiation. We hypothesised that the IGF-1R signalling influences the cellular response to DNA damage and that studying the molecular response to DNA damaging agents in other cancer cells where IGF-1R has been depleted (either permanently or transiently) or inhibited would help uncover the underlying molecular mechanisms by which it does so. This was tested through the use of a small molecule inhibitor targeting the IGF-1R kinase activity to block IGF-1R phosphorylation and later on, by generating IGF-1R knockout mutants through the use of genome editing.

In summary, the overarching goals of our study were:

AIM 1: To investigate whether targeting IGF-1R would delay the repair of exogenously-induced DNA double-strand breaks in cell types other than prostate cancer cells.

AIM 2: To generate IGF-1R mutant cells using CRISPR/Cas9 genome editing.

AIM 3: To confirm the importance of the IGF-1R signalling pathway in mediating radio-protection using IGF-1R deficient cells.

AIM 4: To understand the molecular basis of the IGF-1R's influence on the repair of irradiation-induced DNA double-strand breaks.

2. Materials and Methods

2.1. Cell lines

Melanoma CHL-1 cell line was purchased from ATCC whereas A375M and SK-MEL-23 melanoma cell lines were provided by Professor Colin Goding, Ludwig Institute for Cancer Research in Oxford, UK and Professor V Cerundolo, Weatherall Institute of Molecular Medicine respectively. These were cultured at 37˚C, in Dulbecco's Modified Eagle medium (DMEM, #41966, Life Technologies) containing 10% foetal bovine serum (FBS, #10500, Life Technologies) and supplemented with 1% Penicillin/Streptomycin (#15140, Life Technologies); cells were maintained at 10% CO_2. Ewing Sarcoma cell lines TC-71 and SK-N-MC were obtained from Professor Nicholas Athanasou, Nuffield Orthopaedic Centre, Oxford, UK; while TC-32 and TC-106 were obtained from the Childhood Cancer repository COG resource laboratory (Philadelphia, US). They were cultured at 5% CO_2, 37˚C, in 10% FBS containing RPMI medium 1640 (#42402, Life Technologies) supplemented with 1% Penicillin/Streptomycin and glutamine. The U2OS Osteosarcoma cell line was purchased from ATCC and cultured at 10% CO_2, 37˚C, in DMEM supplemented with 10% FBS and 1% Penicillin/Streptomycin. All cell lines were authenticated in June 2016 by Eurofins medigenomix GmbH (Germany) using Short Tandem Repeat genotyping.

Ewing sarcoma cell lines TC-32, TC-71 and also SK-N-MC were selected to conduct our experiments because they have been used in previous studies evaluating their drug sensitivity profile (May et al., 2013). TC-106 was also added to our panel because it lacked the friend leukaemia insertion (Fli-1) in chromosome 11, t(11;22) which is characteristics of TC-32 and TC-71 Ewing's sarcoma cell lines (Childhood Cancer repository COG

resource laboratory). Melanoma cell lines CHL-1, A375M and SK-MEL23 were used for the purpose of continuity with previous work carried out in the group.

Osteosarcoma U2OS cell line was used to carry out our investigation because it is widely used in DNA damage studies. Thus, it was hoped that findings obtained with this cell line revealing the role of IGF-1R in double strand break repair could be easily compared with previous research findings from other DNA repair studies performed with this same cell line and thereby enlighten our understanding of the link between IGF-1R signalling and radio-resistance. In addition to this, we planned to do in-vivo work and U2OS cells have been shown to form tumours when inoculated in mice and characterisation studies have proven it to generate acceptable in-vivo tumour models of osteosarcoma (Mohseny et al., 2011).

2.2. Drugs and Ligand

AZ12253801 is an ATP-competitive IGF-1R tyrosine kinase inhibitor which was provided by AstraZeneca as a dry powder. It was dissolved in Dimethyl Sulfoxide (DMSO, #41641, Sigma Aldrich) and aliquots of 10mM were stored at -20˚C. Drug concentrations were obtained after serial dilution of the stock. Temozolomide was obtained from Dr Geoff Margison (Manchester CRUK Cancer Centre) as a dry powder and was made up fresh every time by dissolving in DMSO at 100mM. Camptothecin was obtained from Dr Madalena Tarsounas, supplied as working solution of 10mM dissolved in aqueous solution (ddH_2O). Cisplatin was purchased from Cayman chemical (#13119) supplied as a crystalline solid and was dissolved in DMSO to obtain a 33mM solution. Etoposide dissolved in DMSO was purchased from Biovision (#1043-100) as a stock concentration

of 100mM. Vincristine was purchased from Selleckchem (S1241) as a stock solution of 10mM in DMSO.

The IGF-1 ligand was purchased from Sigma-Aldrich (#Sigma-I4657), dissolved in 10mM HCL (Hydrochloric acid) and aliquots of 110µM were stored at -80˚C.

2.3. Ionising Radiation

Cells were subjected to gamma-irradiation using a Caesium-137 irradiator, GSR D1 (Gamma service). Dishes or plates to be irradiated were taken out of the cell culture incubator and taken to the irradiation room. There, they were kept in a 5% CO_2 incubator at 37˚C until brought out for irradiation. The duration of irradiation was adjusted to give the correct irradiation dose according to the calculated dosage spreadsheets made available to users by the Radiation research unit at the Department of Oncology, Oxford University.

2.4. Western Blotting

Cells were harvested in ice-cold phosphate-buffered saline (PBS) and lysed in IGF1R lysis buffer (composition: 1% Triton X-100, 50mM HEPES pH 7.5, 100mM Sodium Chloride, 10mM EDTA, 4mM Sodium pyrophosphate, 2mM Sodium orthovanadate, 10mM Sodium fluoride, ddH_2O) or RIPA buffer (0.1% Sodium dodecyl sulphate SDS, 1% Triton X-100, 25mM Tris pH 7.5, 150mM Sodium Chloride, 0.5% Sodium deoxycholate). Lysis buffer was always supplemented with serine protease inhibitor Pefabloc-SCplus (#11873601001-Roche Life Sciences) at a final concentration of 0.8mM; 20µL of a 25X stock solution cOMPLETE EDTA-free protease inhibitor (#11873580001-Roche Life Sciences) per 1mL of lysis buffer; Phosphatase cocktail inhibitors 2 & 3 (#P5726 and #P0044 –SIGMA

Aldrich), each used at a final concentration of 2% (v/v, 20µL of cocktail solution per 1mL lysis buffer). Lysates were incubated on ice for 30 min. If the cells were lysed in RIPA supplemented with 0.3% SDS to facilitate detection of γH2Ax for instance, samples were first sonicated in a water bath at 4˚C for 20 cycles (30 sec on – 15 sec off) before centrifugation at 4˚C for 15 min at ≥13,000rpm.

The supernatant from each tube was then transferred to new Eppendorf tubes and protein content was quantified by Pierce bicinchoninic acid (BCA) assay using the BCA reagent kit (#23225-Thermo Fischer Scientific) and analysing samples at 562nM with a POLARstar Omega plate reader (BMG Labtech). Samples were prepared for gel electrophoresis by mixing the required volume of lysates (same protein amount was loaded for all samples) with 5X Laemmli buffer (70mM Tris pH6.8, 40% (v.v) glycerol, 3% (w/v) SDS, 0.05% (w/v) Bromophenol blue, 5% (v/v) ß-mercaptoethanol or 5mM Dithiothreitol (DTT). The samples were boiled for 7-8 min at 95˚C, centrifuged for 3 min at 11,000 rpm in a bench-top centrifuge at room temperature and loaded onto SDS-polyacrylamide gels or NuPAGE Novex 4-12% Bis-Tris mini protein gels (Invitrogen) for protein separation at 70-125Volts.

Proteins were transferred to nitrocellulose or Polyvinylidene difluoride (PVDF) membrane under semi-dry transfer at 35mA per gel for 3hours per gel or Trans-blot TURBO transfer system (BioRad) at 25V for 9 min per gel. The membrane was then blocked for 1 hour with 5% non-fat milk in Tris-buffered saline-0.1% Tween (TBS-T) at room temperature and then incubated with primary antibodies diluted in 5% non-fat milk or 5% bovine serum album (BSA) in TBS-T overnight at 4˚C or, for 1 hour at room temperature. Before and after incubation with secondary HRP-linked antibodies in 5% non-fat milk in TBS-T for 1 hour at room temperature, the membrane was washed three times with TBS-T for 7-10 min

intermittent incubation on a rocker. Signal was detected on X-ray film using enhanced chemi-luminescence reagent (ECL, Amersham Corporation, UK).

2.5. Gene silencing with short interference RNA (siRNA)

Gene silencing was performed using forward transfection. Cells were grown in a monolayer in 10cm dishes and were transfected when the dish was 30-40% confluent (generally the next day). The reagents used for the transfection were: Oligofectamine 2000 reagent (#12252011, Invitrogen) as transfection reagent, Opti-MEM-reduced serum medium GlutaMAX (#51985034, Life Technologies), AllStars siRNA (#1022076, Qiagen) as negative control non-silencing siRNA, Hs_IGF1R_1 (#SI00017521, Qiagen) and IGF1R silencer (AM51333, Life Technologies) as siRNAs targeting *IGF1R* mRNA. The siRNA transfection mix for a 100nM siRNA knockdown consisted of:

Tube A: 13.7µL of 20µM IGF1R siRNA or AllStars siRNA + 1516.6µL Opti-MEM

Tube B: 12.3µL Oligofectamine + 410µL Opti-MEM

Tube A and B were prepared separately, left to incubate for 10 min at room temperature after which the two were mixed and incubated for 25 min. In the meantime, the cell culture medium was discarded and culture dish rinsed twice with Opti-MEM. To this, 780µL Opti-MEM was added to the cells and the dish incubated at 37˚C. To this, a volume of 1952 µL from tubes A+B was then added onto each dish to be transfected. After 4 hours of incubation at 37˚C, 11mL of 10% FBS/DMEM was added to the dish in addition to 273µL of FBS. The tissue culture dish was then incubated at 37˚C until further analysis.

2.6. Flow cytometry and cell cycle analysis

2.6.1. Flow cytometry

Cells were grown in dishes/wells and transfected the next day. Cells were collected at different time-points after transfection by using trypsin (#BE02-007E, Lonza) to cause cells to detach from the substratum. Cells were collected in 15mL falcon tubes with the culture medium or fresh medium. Afterwards, cells were centrifuged at 1000 rpm for 5 min at room temperature. The supernatant was discarded and the pellet re-suspended in 200µL of phosphate-buffered saline (PBS). The resuspension mix was centrifuged again at 1000 rpm for 5 min and the supernatant discarded. The pellet was loosened by gentle vortex before adding 1mL of ice-cold 70% ethanol in a dropwise manner to fix and permeabilise the cells. The falcon tubes were incubated on ice for 30 min or overnight at -20˚C and cells were centrifuged again at 1000 rpm for 5 min at 4˚C. The pellet was resuspended in 2mL of the blocking buffer (2% FBS/PBS) and centrifuged again at 2000 rpm for 5 min at room temperature. The supernatant was discarded and the pellet was resuspended in 200µL of blocking buffer containing primary antibodies and incubated overnight at 4˚C.

The next day, 2ml of blocking buffer was added to each tube then, followed another round of centrifugation at 1000 rpm for 5 min at room temperature to reduce non-specific binding. After discarding the supernatant, the pellet was then resuspended in 100µL of blocking buffer containing fluorescent secondary antibodies. The tubes were incubated at room temperature for 1 hour in the dark. After this, there was another wash with 2mL of blocking buffer and then centrifugation at room temperature for 5 min at 1000rpm. The pellet was resuspended in 0.5mL PBS containing a DNA dye: DRAQ5 diluted 1:5000 or 50µg/mL propidium iodide (#P4864, Sigma Aldrich). Samples were analysed on a Beckman Coulter

CyAn Analyser or FACScalibur (BD Biosciences). Flow cytometry data analysis was performed using the FlowJo software version 10.0.

2.6.2. BrdU cell cycle analysis

5-bromo-2'-deoxyuridine (BrdU) is a synthetic thymidine analogue incorporated into newly synthesised DNA hence routinely used to identify proliferating cells (Dolbeare et al., 1983). Cells were grown in dishes and pulse-labelled for 30min with 10μM BrdU prior to cell harvest. Cells were collected, fixed and permeabilised as previously described in section 2.6.1. To enhance the accessibility of anti-BrdU antibodies to the BrdU nucleoside that has been incorporated during DNA synthesis, samples were put through DNA denaturation. To do so, 0.5mL of 2M HCl+0.5% Triton-X-100 added dropwise to degrade RNA and denature DNA for 30 min, at room temperature after fixation with ethanol. At the end of the incubation period with HCL, tubes were centrifuged again at 1000 rpm for 5 min at room temperature. The supernatant was discarded and residual acid was rinsed off with 0.5mL PBS. Then, after another round of centrifugation at 1000 rpm for 5 min at room temperature, the cells were incubated in blocking buffer and all subsequent steps were performed as described in section 2.6.1. Samples were analysed on a Beckman Coulter CyAn Analyser or FACScalibur (BD Biosciences). Flow cytometry data analysis was performed using the FlowJo software version 10.0.

2.7. Immunofluorescence

Cells were cultured on sterile coverslips in 6-well plates or directly into 96-well plates, then treated the day after with either solvent or drug. At collection, cells were fixed with 4% paraformaldehyde containing 0.1% Triton-X-100/PBS for 10-20 min at room temperature.

Thereafter, the cells were permeabilised in ice-cold 100% methanol for 30 min at -20˚C or with 0.5% Triton-X-100/PBS for 10 min at room temperature. This step was followed by 3 washes with PBS at 5 min intervals and incubation in 5% BSA/PBS for 1 hour at room temperature for non-specific epitope blocking. Afterwards, the coverslips or plates were incubated in 5% BSA/PBS solution containing primary antibodies for 1 hour at room temperature or at 4˚C overnight. This step also was followed by 3 washes with PBS after which the coverslips or plates were incubated in secondary antibodies diluted in a volume of 5% BSA/PBS for at least 1 hour in aluminium foil in the dark. When staining cells in 96-well plates, 4µM Hoechst was added to the secondary antibody solution to stain DNA. Non-specifically bound antibodies were washed off with 3x PBS washes. Coverslips were mounted on slides in Fluoromount G (#TA-030-FM, ThermoScientific) with 2µg/mL DAPI (4',6-diamidino-2-phenylindole) then, incubated overnight at room temperature in the dark to dry. Images were acquired using the Zeiss Observer Z1 light microscope, taking images in Z-stacks. For 96-well plates, images were acquired using the IN Cell Analyser 1000 (GE Healthcare) or the Nikon Eclipse TE2000 microscope (NIKON).

2.8. Foci counting

With the assistance of Dr Dominic Waite, a post-doctoral scientist in CBRG (Computational Biology Research Group) based in the WIMM, I developed a Fiji script written in the IJ1 Macro language to help me process immunofluorescence images and perform automated foci counting (See script in appendix 8). Some images were analysed by Mr Steve Taylor at the CBRG in the WIMM.

Unless stated otherwise, foci counting was also performed using the in-built foci counting software on the IN cell analyser 2000 machine (GE healthcare life sciences).

2.9. Cell viability assays

Cells were seeded in 96-well plates in triplicate wells. Twenty-four hours after seeding, the cells were either solvent-treated or treated with selected drug agent. Cell viability was measured using the CellTiter-Glo or CellTiter-Blue assays (Promega). CellTiter-Glo (#G7572) is a luminescent assay based on ATP quantitation from metabolically active cells. The reagent for this assay contains a firefly luciferase which uses ATP molecules released into the medium upon lysis of viable cells to generate light from its substrate luciferin. It is this catalytic reaction that acts as a direct measurement of ATP levels and therefore, of cell viability (Riss et al., 2004). As per manufacturer's protocol, an equal volume of the already lyophilised CellTiter-Glo substrate was added to the cell culture medium to induce cell lysis. The plate was then left to incubate in the dark for 30 min after which luminescence was recorded with a POLARstar Omega plate reader (BMG Labtech).

The CellTitre-Blue assay relies on the metabolic activity of the cells to convert resazurin into an end product called resorufin which emits a fluorescence signal that was detected with a plate reader recording fluorescence at 560/590mm. According to the manufacturer's protocol, the CellTitre-Blue reagent was added in a ratio of 1:6 (e.g. 20µL to 100µL culture volume) to wells and incubated at 37˚C for 2 hours before reading the signal on a POLARstar Omega plate reader (BMG Labtech).

2.10. Clonogenic assays

These assays were performed to determine the ability of a single cell to survive and form a colony of >50cells (Munshi et al., 2005). Cells were seeded in 10cm dishes or 6-well plates in triplicate. The next day, cells were subjected to treatment with drug, solvent or irradiation

after which they were incubated until the formation of visible colonies. Dishes/plates were fixed with 0.1% Coomassie brilliant blue stain solution composed of (per litre): 1g brilliant blue, 430ml distilled H_2O, 500mL methanol and 70mL acetic acid. Colony numbers were quantified using the GelCount colony counter from Optotronix, Oxford.

2.11. Genome editing: gRNA design, sub-cloning and bacterial transformation

2.11.1. gRNA design

Guide RNA (gRNA) oligonucleotides were generated by inputting exon 2 sequence for the *IGF1R* gene into the online CRISPR design tool developed by the Zhang Lab at the Massachusetts Institute of Technology (http://crispr.mit.edu/ - 2015). The oligonucleotide sequences are shown in the table below.

gRNA pairs	**Forward strand (5'-3')**	**Reverse strand (5'-3')**
Pair 1 (gRNA-1A)	CACCGGCTCTTCTACAACTACGCCC	AAACGGGCGTAGTTGTAGAAGAGCC
Pair 2 (gRNA-1B)	CACCGGCCAGCCGCGGATGACCGTG	AAACCACGGTCATCCGCGGCTGGCC
Pair 3 (gRNA-2A)	CACCGGAGAACTGCACGGTGATCG	AAACCGATCACCGTGCAGTTCTCC
Pair 4 (gRNA-2B)	CACCGGCAGCTGCTGATAGTCGTTG	AAACCAACGACTATCAGCAGCTGCC

Table 2-1: **List of CRISPR guideRNAs**. These were ordered as oligonucleotides with overhanging ends (underlined) compatible with ends produced on BbsI-digested PX458 Addgene plasmid.

2.11.2. Oligonucleotides ordering and subcloning

gRNA Oligonucleotides (ODN) were ordered as desalted single-stranded, lowest synthesis scale 0.025µmol (Sigma-Aldrich) and dissolved in nuclease-free H_2O to a 100µM solution. Double-stranded oligonucleotides (dsODN) were prepared by annealing the forward and reverse strands. The reaction mixture was composed as follows: 10µL forward ODN

ssDNA, 10µL reverse ODN ssDNA, 10µL NEB buffer 2.1 (#B7202S, New England Biolabs) and ddH_2O to a total volume of 100µL. The reaction mixture was incubated at 99˚C for 5 min and then slowly cooled. The dsODN was precipitated after addition of 30µL 3M NaOAc pH 5.6 then 300µL 100% ethanol and centrifugation at 1500 rpm for 30 min at 2˚C. The pellet was washed with 70% ethanol, air-dried and re-suspended in 100µL ddH_2O. Next, the dsODN ends were phosphorylated in a reaction mix consisting of: 2µL 10x T4 DNA ligase buffer (#M0202, New England Biolabs), 0.5µL T4 PNK (T4 Polynucleotide Kinase - #M0201, New England Biolabs), 1µg dsODN and ddH_2O to a total volume of 20µL. The reaction was incubated for 1 hour at 37˚C. Each phosphorylated dsODN (dsODN-P) was cloned into BbsI-digested PX458 plasmid (pSpCas9(BB)-2A-GFP, Addgene plasmid #48138). The BbsI digested PX458 plasmid was obtained from Dr Philip Hublitz, Genome engineering facility, Weatherall Institute of Molecular Medicine, Oxford, UK. The ligation mix consisted of: 1µL BbsI-digested PX458 (20ng), 0.5µL dsODN-P (~25ng), 0.5µL T4 DNA ligase, 1.0µL 10x T4 DNA ligase buffer, 7µL ddH_2O. The reaction mix was incubated for 1 hour at room temperature.

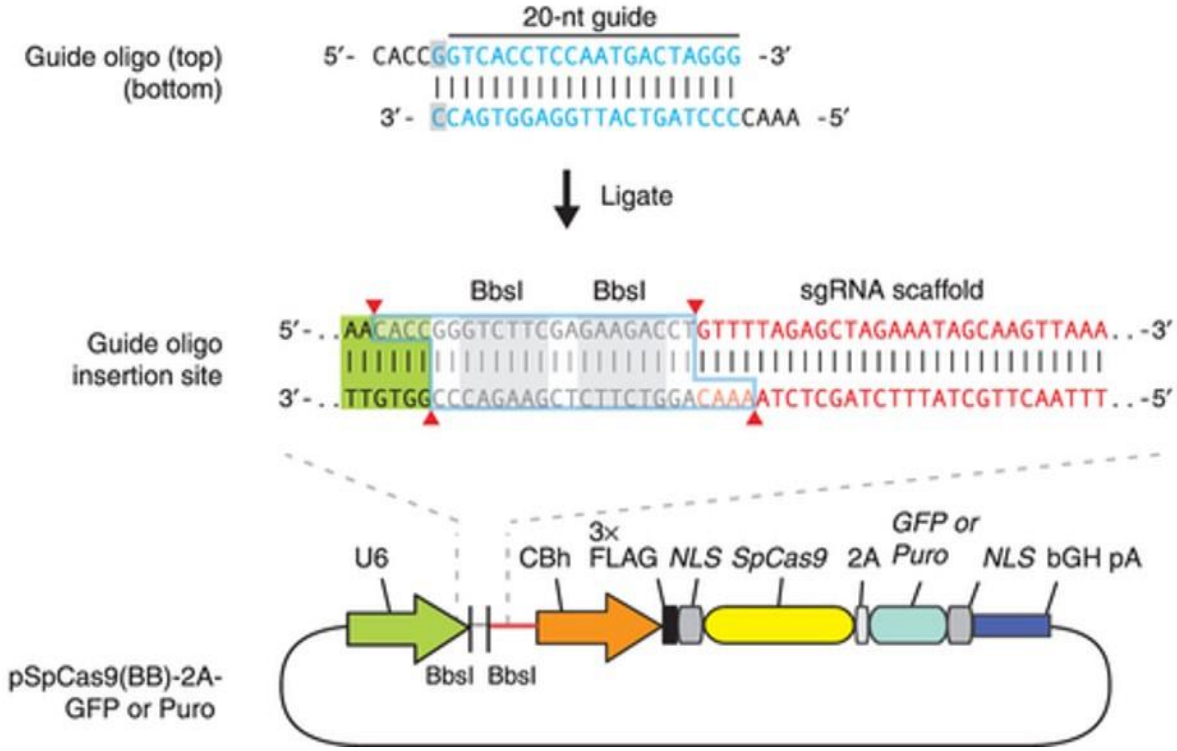


Figure 2-1: **Schematic for cloning of the gRNA into pSpCas9(BB)-2A plasmid**. The designed oligonucleotides are annealed to form dsODN with overhangs for ligation into the pair of BbsI sites in pSpCas9(BB)-2A-GFP (PX458). The GFP gene aids in the selection of successfully transfected cells. Copied with permission from (Ran et al., 2013).

2.11.3. Bacterial transformation

For transformation, maximum cloning efficiency DH5α competent cells (#18258-012, Invitrogen) were used. A volume of 10µL of the plasmid ligation reaction was added to 35µL of DH5α competent cells. The mixture was incubated on ice for 30 min, then heat shocked for 1 min at 42˚C and put back on ice for 3 min. To this, 1mL S.O.C. medium (#15544-034, Invitrogen) was added and the tube containing competent cells was incubated at 37˚C for 1 hour in a water-bath with shaking at 225rpm. Afterwards, the tube was centrifuged at 600 rpm for 1 min, 300µL of the supernatant was discarded and the residual supernatant re-suspended. After resuspension, a volume of 50 to 150µL of the transformation mix was spread on LB plates containing 100µg/ml ampicillin. The plates were incubated at 37˚C overnight for colony growth.

2.12. Plasmid DNA purification

From an ampicillin plate freshly streaked with bacterial transformation reaction mix and incubated overnight, a single colony was picked to inoculate a starter culture of 2–5ml LB medium containing the ampicillin (100ug/mL). This was incubated for approximately 8 hours at 37°C with vigorous shaking at 220rpm. From this, 50µL was inoculated in 25mL of LB culture medium containing the ampicillin (100ug/mL) and incubated at 37°C with vigorous shaking at 220rpm for 12-16 hours. Bacterial cells were harvested by centrifugation at 4500 x g for 20 min at 4˚C. The DNA midi-prep kit from QIAGEN (#12143) was used for plasmid purification. Pelleted bacterial cells were resuspended in 4mL Buffer P1 (supplemented with 100µg/ml RNaseA). To this, one volume of buffer P2 was added, mixed and incubated at room temperature for 3-5 min for cell lysis. To stop the lysis reaction and prevent extensive degradation of DNA, 4mL of Buffer P3 were added to the reaction mix, followed by incubation on ice for 15 min and then, centrifugation at 4500 x g for 45 min at 4˚C. The clear lysate was transferred to a new falcon tube and centrifuged at 4500 x g for 15 min at 4˚C.

In the meantime, the Qiagen-tip was equilibrated with 4mL buffer QBT after which the supernatant from the previous step was applied to the tip and left to flow-through at room temperature. Thereafter, the tip was washed twice with 10mL buffer QC and the DNA was then eluted with 5mL buffer QF into a fresh collection tube. Using 3.5mL isopropanol and centrifugation at 4500 x g for 45 min at 4˚C, the DNA was precipitated. To remove impurities, the pellet was washed with 2mL of 70% ethanol and centrifuged at 4500 x g for 25 min at 4˚C. After air-drying, the pellet was dissolved in 200µL nuclease-free water. The DNA quality and yield were determined by Nanodrop (ND-100 Spectrophotometer) and the DNA samples were stored at -20˚C.

2.13. Genomic DNA isolation

DNA extraction was performed using the AllPrep DNA/RNA Mini kit (#80204, QIAGEN) according to the manufacturer's protocol. Cells grown in monolayer were detached using trypsin and collected in DNase-free falcon tubes. The tubes were centrifuged at 300 x *g* for 5 min at room temperature. The pellet was lysed in 350µL (for dishes containing $<5\times10^6$ cells) of lysis buffer RLT containing 1% β-mercaptoethanol which inactivates ribonucleases during cell lysis. The lysate was homogenised by passing the lysate five times through a 20-gauge needle (0.9 mm diameter) fitted to a RNase-free syringe. The homogenised lysate was transferred to an AllPrep DNA spin column and centrifuged at 8000 x *g* for 30 sec at room temperature. The spin column was then placed in a new collection tube and proteins bound to the resin were washed off by adding 500µL of buffer AW1. The resin-bound DNA was further purified by addition of 500µL of buffer AW2 to remove salts; each wash step was followed by centrifugation at 8000 x *g* at room temperature. The purified genomic DNA was then eluted with 30µL nuclease-free water directly added onto the resin and collected after centrifugation at 8000 x *g* at room temperature for 1 min. DNA yield and quality were determined by Nanodrop (ND-100 Spectrophotometer), measuring the absorbance at 260nm and calculating the A260/230 and A260/280 ratios to estimate the purity of the sample. Samples were stored at -20˚C.

2.14. Surveyor mutation detection assay

The Surveyor mutation detection assay or Surveyor assay is a mismatch cleavage assay that is commonly used to test for gRNA targeting efficiency (Ran et al., 2013). The mutation detection technology relies on the function of the surveyor CEL nuclease enzyme, a mismatch-specific DNA endonuclease isolated from the CEL nuclease family which has

been demonstrated to cleave both DNA strands 3' to any mismatches (sites of base substitution or insertion/deletion) and shows high sensitivity in detecting mutations (Qiu et al., 2004). The Surveyor assay is a technique that involves four major steps. The first step is a Polymerase Chain Reaction (PCR) during which DNA extracted from cells is amplified using a high-fidelity DNA polymerase. The second step is DNA duplex formation, followed by digestion of the duplexes with the surveyor CEL nuclease enzyme, the products thereof are detected on an agarose gel (Figure 2-2).

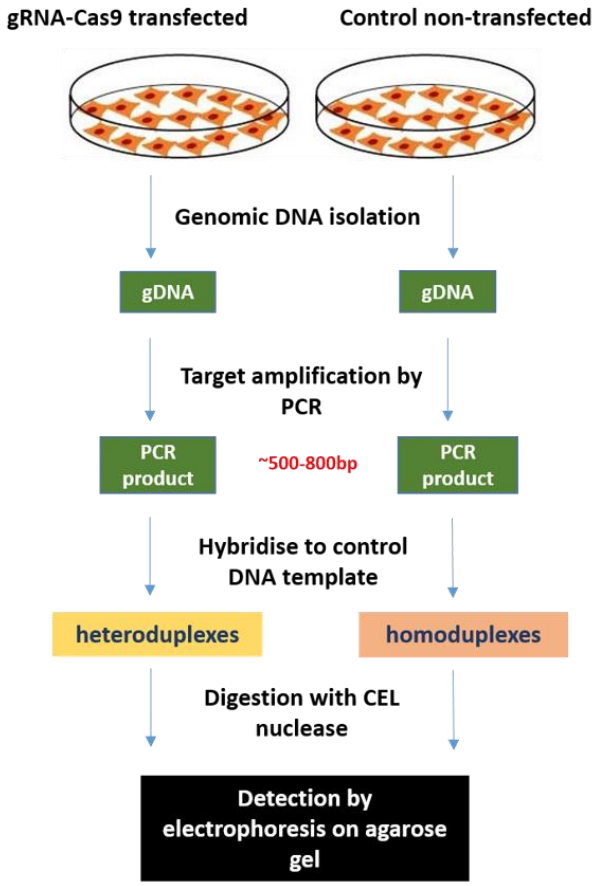


Figure 2-2: **The Surveyor mutation detection technique**. This flowchart depicts the steps required to complete a surveyor assay.

2.14.1. HEK293T cells transfection

Cells were seeded in antibiotic-free 10% FBS/DMEM. The next day, as per transfection protocol described in this chapter (see section 2.13), the cells were transfected with PX458-

gRNA (Cas9-gRNA transfected) or mock transfected (control non-transfected cells). Cells were harvested 3 days after transfection for genomic DNA isolation (see section 2.13).

2.14.2. Surveyor assay Step one: PCR reaction

From the isolated genomic DNA, the region spanning the predicted Cas9 cut site was amplified by PCR using a high-fidelity DNA polymerase with proofreading activity. To avoid non-specific amplification, surveyor primers were chosen using Primer-BLAST, a web-based tool for primer design developed by the National Center for Biotechnology Information (NCBI), USA. The primers were designed to be 18 to 25nt long with melting temperatures of ~60 °C. To allow clear differentiation of cleavage products by gel electrophoresis, primer pairs were designed to flank the Cas9 cut site unevenly i.e. 200–400bp on either side. Primers were ordered as desalted single-stranded, lowest synthesis scale 0.025µmol (Sigma-Aldrich) and dissolved in nuclease-free H_2O to a 100µM solution.

Surveyor primer pair (code name)	**Forward strand (5'-3')**	**Reverse strand (5'-3')**	**Amplifies DNA region targeted by**
SP_1	GTCTGGTCCAGTGTTGGCAC	TGTAGAAGAGTTTCCAGCCGC	gRNA-2A & gRNA-2B
SP_4	TAAACTGTCAGTCTGCAACCCA	ACAGTGGAGAGGTAACAGAGGT	gRNA-2A
SP_8	GACATCCGCAACGACTATCAGCA	CCAGCAGCGGTAGTTGTACTCAT	gRNA-1A

Table 2-2: **List of Surveyor primer pairs**. Primers were designed using Primer-BLAST, a web-based tool for primer design developed by the National Centre for Biotechnology Information.

The reaction mix for PCR amplification was composed as follows:

Component	Volume (µL)	Final Concentration
Herculase II PCR buffer 5x	10	1x
dNTP, 100mM (25mM each)	1	2mM
Forward Primer, 10µM	1	0.2µM
Reverse Primer, 10µM	1	0.2µM
Herculase II fusion polymerase	1	
MgCl2, 25mM	2	1mM
DNA template 150ng/µL	1	1.5ng/µL
ddH_2O	33	
	50µL	

Reagents used include: Herculase II fusion polymerase with 5x reaction buffer (#600679, Agilent Technologies); 100mM dNTP mix, 25mM each (#N205L, Enzymatics); $MgCl_2$ 25mM (#R0971, ThermoScientific).

PCR was performed for 32 amplification cycles as follows: one cycle of denaturation at 95˚C for 2 min; then 30 cycles of denaturation at 95˚C for 20 sec, annealing at 60˚C for 20 sec and extension at 72˚C for 30 sec; and a final cycle of extension at 72˚C for 3 min.

2.14.3. Surveyor assay Step two: DNA duplex formation

For this step, two tubes A and B were set up. In tube A, equal volumes of solution containing the DNA templates (20ng/µL) from cas9-gRNA transfected cells and wild-type cells (non-transfected) was mixed whilst tube B contained only DNA template from non-transfected cells. See detailed composition below:

Tube A: 2µL 10x Taq PCR buffer + 9µL DNA from Cas9-gRNA transfected+ 9µL wild-type DNA

Tube B: 2µL 10x Taq PCR buffer + 18µL wild-type DNA

Separate reactions were set up with controls C and G from the Surveyor Assay detection kit (#706025, Integrated DNA Technologies) to facilitate interpretation and troubleshooting. Controls C and G are two plasmid DNAs with inserts that differ at a single base pair.

A thermo-cycling program of 17 steps was performed under the conditions described below to promote DNA duplex formation using the Peltier Thermal Cycler (MJ Research, PTC-200).

Conditions	
95˚C, 10 min	55-45˚C, -0.3˚C per sec
95-85˚C, -2˚C per sec	45˚C, 1 min
85˚C, 1 min	45-35˚C, -0.3˚C per sec
85-75˚C, -0.3˚C per sec	35˚C, 1 min
75˚C, 1 min	35-25˚C, -0.3˚C per sec
75-65˚C, -0.3˚C per sec	25˚C, 1 min
65˚C, 1 min	25-4˚C, -0.3˚C per sec
65-55˚C, -0.3˚C per sec	4˚C, hold
55˚C, 1 min	

2.14.4. Surveyor assay Step three: Digestion of DNA duplexes with surveyor CEL nuclease

The CEL nuclease is an enzyme isolated from celery which detects single base mismatches between two hybridised DNA strands (Till et al., 2004). At the end of the annealing reaction,

9µL of each reaction mix was placed into a fresh tube to which the following reagents were added on ice: 1.2µL 25mM $MgCl_2$, 0.5µL ddH_2O, 1µL Surveyor nuclease S, 1µL Surveyor enhancer S. The reagents were mixed and the tubes were incubated at 42˚C for 30 min. At the end of the incubation period, 1.2µL of the STOP solution provided with the Surveyor kit was added to the reaction mix. All reagents were taken from the Surveyor Mutation Detection Kit (#706025, Integrated DNA Technologies).

2.14.5. Surveyor assay Step four: Detection of DNA products

From each reaction, 10µL of digested DNA products were mixed with 2µL of 6x loading dye (#R0631-New England Biolabs) and analysed on 2% TBE (Tris/Borate/EDTA) agarose gels. DNA fragments were separated by electrophoresis at 100 volts for 60 mins.

2.15. PCR product purification

Following PCR amplification as described in section 2.14.2, PCR products were purified prior to sequencing using the QIAGEN PCR purification kit (#28104) as per manufacturer's recommendations: 5 volumes of buffer PB were added to 1 volume of the sample containing the PCR product and mixed thoroughly without vortexing. The reaction mixture was added to a spin column, centrifuged at 17,900 x g for 60 sec, washed with 750µL buffer PE and centrifuged twice at 17,900 x g for 1 min each time. After discarding the flow-through, the column was put in a clean DNase-free collection tube into which the DNA bound to the resin was eluted with 30µL of nuclease-free water. The yield and quality of the purified DNA were determined by Nanodrop (ND-100 Spectrophotometer). DNA sequencing was performed by Source BioScience (UK) using the Sanger sequencing

method with primer pair SP-4. Samples were submitted at a concentration of 1ng/µL per 100bp and primer concentration of 3.2pmol/µL.

2.16. Transfection with CRISPR gRNAs

In 10cm dishes, $6x10^5$ U2OS cells were seeded in antibiotic-free 10% FBS/DMEM and transfected the next day at ~40% confluency with plasmid PX458 or one of the two selected gRNA individually cloned into PX458 (PX458-gRNA). The transfection procedure was conducted as detailed below:

Tube A: 10µg PX458 (or PX458-gRNA) + 1225µL Opti-MEM (#51985034, Life Technologies) + 25µL PLUS reagent (#15338100, Invitrogen)

Tube B: 40µL Lipofectamine LTX (#15338100, Invitrogen) + 1210µL Opti-MEM

The tubes were incubated at room temperature for 5 min before the contents were combined and once again incubated at room temperature for 20 min. Then, 2mL of the mixture was added to cells in 10cm dishes containing 8mL of antibiotic-free 10% FBS/DMEM. The culture medium was changed the next day with yet again antibiotics-free 10% FBS/DMEM. At 48 hours post-transfection, cells were then culture in antibiotic-containing medium.

2.17. Cell sorting, Clonal isolation & expansion and Clone screening

The PX458 plasmid contains GFP cDNA to aid in the selection of successfully transfected cells and its expression is driven by the same promoter as that for the Cas9 cDNA (Figure 2-1). Therefore, it is generally assumed that Cas9-expressing cells are GFP-positive cells

(Ran et al., 2013). GFP-expressing cells (GFP positive) were sorted 72 hours after transfection. Cells were detached using trypsin and collected in a 15ml falcon tube with 2% FBS/DMEM. After centrifugation at 800rpm for 5 min, the supernatant was discarded. The cell pellet was resuspended in 2% FBS/DMEM and cells were collected into a clean tube through a 0.40μm cell strainer. Tubes containing the cells remained on ice during transportation to the flow cytometry facility for sorting. Five days after selecting successfully transfected cells by GFP positivity, cells were sorted again to discard GFP-expressing cells whilst GFP-negative cells were retained and collected into tubes. These were then seeded into 15cm dishes at a density of $1x10^4$ for clonal isolation as previous attempts of single cell sorting into 96-well plates had been unsuccessful. The cells were incubated under regular growth conditions until visible colonies formed.

Separate cell colonies were then gently disaggregated with trypsin and placed into individual wells of 96-well plates and cultured under regular growth conditions. Once the wells reached a confluence >70%, cells from individual wells were detached and half of the content from each well was placed into separate wells to obtain a duplicate 96-well plate. This was done so that one plate could be used to screen for IGF1R-mutant clones whilst the twin-plate remained in culture. The screening for mutant clones was a two-stage process, the first consisted of staining cells in 96-well plates with anti-IGF1R antibodies and, by immunofluorescence, to identify clones showing either weak or no fluorescence signal. Clones of non-transfected parental U2OS cells were used as positive control for IGF-1R staining. As a negative control, U2OS parental cells lacking primary antibody staining was used. Clones showing weak or no fluorescence signal were then cultured in 6-well plates. When the confluence reached about 70%, the cells were collected for analysis by western blotting and probed for IGF-1R. Cell sorting was performed in collaboration

with Mick Woodcock from the Department of Oncology (Oxford, UK) using a BD FACS Aria III cell sorter.

2.18. RNA extraction and Transcriptome profiling

For RNA extraction, the PureLink RNA extraction kit (#12183018A, Ambion, Life Technologies) was used according to manufacturer's recommendations. Cells grown in monolayer were detached using trypsin and collected in RNase-free falcon tubes. The tubes were centrifuged at 2000 x *g* for 5 min at 4˚C. The pellet was lysed and homogenised in 0.6mL (for total 1×10^6–5×10^6 cells) of lysis buffer containing 1% β-mercaptoethanol. The latter prevents RNA degradation by inactivating ribonucleases during cell lysis. To this, one volume of 70% ethanol was added and mixed thoroughly to dissolve salts in the solution and maximise DNA/RNA binding to the resin. The homogenised solution was transferred to a spin cartridge and centrifuged at ≥12000 x *g* for 15 sec at room temperature. The spin cartridge containing resin-bound RNA was then placed in a new collection tube to which 350µL of Wash Buffer I was added.

After centrifugation at 12,000× *g* for 15 sec at room temperature, the flow-through was discarded and 80µL of PureLink DNase mix (#12185010, Invitrogen) was added directly to centre of the spin cartridge and not on the walls in order to digest DNA bound to the resin so as to elute RNA only from the samples that were lysed. DNase treatment required 15 min incubation at room temperature. After the treatment, 350µL of Wash Buffer I was added to the spin cartridge followed by centrifugation at 12,000 x *g* for 15 sec at room temperature. The cartridge was then inserted into a new collection tube, washed with 500µL Wash Buffer II with ethanol and centrifuged at 12,000 *x g* for 15 sec at room temperature. This step was repeated once and the cartridge was placed in a RNase-free collection tube.

Approximately 30µL of RNase free water was used to elute the RNA from the resin. The yield and quality of the purified RNA were determined by Nanodrop (ND-100 Spectrophotometer), measuring the absorbance at 260nm to determine the yield and the A260/230 and A260/280 ratios to estimate the purity of the sample. The 260/280 ratio was between 1.8-2.0 and the 260/230 ratio close to 1.8.

2.18.1. Sample preparation for RNA microarray and Data analysis

Extracted RNA samples were submitted as 500ng in 12µl of RNase free water for sample processing and 100 to 500ng in 5µl for quality control (QC). RNA samples were plated into a 96 well 0.2µl skirted plate (#AB-800, ABgene) in rows (A1, A2, etc) and stored at -80˚C until ready for analysis. RNA Integrity Number was assessed for each sample and confirmed to be greater than 7 with a 28S/18S ratio greater than 1.6. These checks were performed by the High Throughput Genomics group at the Welcome Trust Centre for Human Genetics in Oxford headed by Dr Christine Blancher. They performed transcriptome profiling using an Illumina GEX array.

Analysis of gene expression raw data generated from the microarray screen was performed by Dr Anastasia Samsonova at the Bioinformatics core of the Department of Oncology.

2.19. Reverse transcription, quantitative PCR (qPCR) & primers

Using the Superscript III first strand cDNA synthesis super mix from Invitrogen (#18080400) according to the manufacturer's protocol, purified RNA extracts from mammalian cell lines were reverse-transcribed into cDNA. In microcentrifuge tubes, the following reaction mix was prepared: 2x RT Reaction Mix (10µL), RT enzyme mix (2µL),

1µg of purified RNA (X µL) and DEPC-treated water to a final volume of 20µL. The thermal cycling reaction consisted of 10 min incubation at 25˚C, a further 30 min incubation at 50˚C and finally 5 min at 85˚C. The tubes were removed from the thermocycler and put on ice. To degrade all remaining RNA within the reaction mix, 1µL (2U) of RNaseH was added to each tube and incubated at 37˚C for 20 min. The cDNA samples were stored at -20˚C and used in qPCR reactions.

We used SYBR Green PCR Master Mix (#4309155, Applied Biosystems) for amplification on a 7500 fast real-time system v.2.0.5 (Applied Biosystems). The PCR reactions were prepared on ice as follows using primers listed in Table 2-3 :

Tube A: 10µL SYBR green master mix + 1µL primers (10µM forward + 10µM reverse)

Tube B: 8µL nuclease-free H_2O + 1µL cDNA from RT reaction

These components were pipetted into 96-well semi-skirted PCR plate (#AB0900, Thermo Scientific), with each well containing 11µL of Tube A mix and 9µL of Tube B mix. Thereafter, the plate was centrifuged at 700rpm speed for 90 sec to ensure no content remained on the walls of the wells. The reaction was performed using the standard run method which consists of: a holding stage of 95˚C for 20 sec; a cycling stage of 95˚C for 3 sec then 60˚C for 30 sec and a continuous melt curve stage running for 40 cycles as 95˚C for 15 sec ➔ 60˚C for 1 min ➔ 95˚C for 30 sec ➔ 60˚C for 30 sec.

Relative quantification of expression levels

Comparative C_T ($\Delta\Delta C_T$) method was used as the quantitation method to determine the target quantity in samples. The fold change in gene expression level was calculated using the $2^{-\Delta\Delta CT}$ method (Livak and Schmittgen, 2001):

(1) Both the reference and the target gene were amplified from the same cDNA input.

ΔC_T = average target C_T – average reference C_T

(2) Experimental control used as calibrator

$\Delta\Delta C_T$ = (average $\Delta C_{T\ test}$ – average $\Delta C_{T\ calibrator}$)

(3) Amount of target normalised to reference (endogenous control) and relative to calibrator

Amount of target = $2^{-\Delta\Delta CT}$

Primer pair code	**Forward primer (5'->3')**	**Reverse Primer (5'->3')**	**Target mRNA**
ACTIN	TGGCTCCTAGCACCATGA	CCACCGATCCACACAGAG	*ACTB*
CC_1	AATCAATGCCCCAGTCACCT	CTTCTTTGGGACACTTGCTGC	*CCL2*
DDB1_A	TGAAGACCAAGGGCGACTTC	ACAGCACTCATCCAGTTGGG	*DDB1*
DDI_1	GTTTGCACAGGTACATTCAGG	ACTGGCATCTGAACCTTGTCC	*DDIAS*
DRM_1	CTCGACATGCCACATACGGA	TCACAGATCGCACTCACTACG	*DRAM1*
FAM_1	CAGCCAGGCCAAAACCATTG	AGGCCCTCATTTATGTCGCAA	*FAM24B*
GD_1	GGATGGATAAGGTGGGGGATG	CTGACGCGCAGGATGTTGAT	*GADD45*
IBP_1	GATCTTCCGGCCCAAACACA	GGTCAGCTTCTTTCTGCGGT	*IGFBP5*
IGF1R_1	GCCCAAACCCTTAACTGACA	GGACAGGGACAGAGTGAGGA	*IGF1R*
IGF1R_2	TGCCCAAACCCTTAACTGAC	GGACAGGGACAGAGTGAGGA	*IGF1R*
MBP_1	TGCTTGGATGACCGAAAAGC	ACAGGAGATGGAAGAGGGCT	*MTBP*
MDC1_A	ACTTGCTCTGCCAGTACCATC	TCTCCCTGTACTCTGGGTGT	*MDC1*
TUBULIN	CCCCTTCAAGTTCTAGTCATGC	ATTGCCAATCTGGACACCA	*TUBA6*

Table 2-3: **List of primer pairs**. Primers were designed using Primer-BLAST, a web-based tool for primer design developed by the National Centre for Biotechnology Information.

2.20. Metabolite extraction, sample preparation and analysis

2.20.1. Metabolite extraction

For each cell line, cells were seeded in six different T75 flasks and grown at regular culture conditions (10% CO_2, 37˚C in 10% FBS/DMEM). The cells were grown for 4 days until the flasks were 70% confluent and metabolites were extracted from cells thereafter. Prior to extraction, one representative flask for each cell line was harvested with trypsin and the cell number was determined using the Countess Automated Cell counter (Invitrogen). This was done in order to estimate the number of cells in the five other replicate flasks as the cells were directly lysed in methanol while still inside the flask. Before the addition of methanol, cells were detached with 500µL of trypsin for 2 min at 37˚C because a test experiment suggested that the cells did not lyse with 100% methanol only. Then, 1.5mL of ice-cold 100% methanol was added to the cells and the flasks incubated for 5 min at room temperature in the tissue culture hood while swirling intermittently. The contents were then individually collected into cooled 15mL flasks which were kept on ice. From this, 1.25mL of each biological replicate was transferred into Eppendorf tubes and stored at -80˚C until further analysis.

2.20.2. Sample preparation for metabolomics

The samples were transported on dry ice to Dr James McCullagh's Chemistry laboratory (Oxford University). To remove impurities such as cell debris and other soluble proteins, 500µL of each sample was transferred to a tube containing a 10kDa molecular weight cut-off filter which allows only small molecules such as metabolites to pass through. The tubes were centrifuged at room temperature for 30 min at ≥13,000rpm. A test run for the metabolite concentration performed by Dr Elisabete Pires in Dr McCullagh's lab revealed

that the samples were too dilute so, the metabolite solution in each individual tube was evaporated to dryness. The samples were then reconstituted in milli-Q H_2O, adding 200µL per 1million cells. Thereafter, 300µL of each sample were transferred into recovery vials. Further preparation (see below) was performed to facilitate amino acid identification by derivatised LC/MS (Liquid chromatography–mass spectrometry) method.

2.20.3. Sample preparation for Amino Acid Analysis

Samples were prepared according to the waters amino acid analysis (AAA) method using the AccQ-Tag ultra-derivatisation kit (#186003836, WATERS) as follows:

	Volume (of Standards or samples)	Borate buffer	AccQTag Derivatising Solution
Individual Samples	10µL	70µL	20µL
Amino Acid Standards	10µL	70µL	20µL
Blank	0µL	100µL	0µL
Reagent Blank	0µL	80µL	20µL

The samples were vortexed, left to stand for 1 min and then placed on a heating block for 10 min at 55˚C. Afterwards, they were stored at room temperature to be analysed within a week.

2.20.4. Metabolite identification and Statistical evaluation

Amino acid analysis and identification were performed by Dr James McCullagh's group. All compounds identification and metabolomics data analysis including statistical analyses for hits identification were done by Dr Elisabete Pires and Dr James McCullagh.

2.21. Graphing and statistical analysis

Mean, standard deviation, standard error of the mean (SEM) and statistical analyses were performed with GraphPad Prism version 6.00, later upgraded to version 7.00 (GraphPad Software Inc, USA).

2.22. Generating Heatmaps

In order to generate heatmaps with raw intensity data from the expression matrix, we wrote scripts in the R programming language and used RStudio to run them (RStudio Team, 2016). We acknowledge Paka (Ludwig Cancer Institute, Oxford) for his assistance in this process. Scripts are included in appendix 8.6.

Table 2-4**: List of Antibodies** used for Western Blotting, Flow Cytometry and Immunofluorescence (IF) experiments

Primary Antibodies	**Company**	**Catalog number**	**Primary Antibody dilution**	**Secondary Antibody dilution**
4EBP1	Cell Signaling Technology	#9644	1:1000	1:2000
5-bromo-2'-deoxyuridine (BrdU)	BD Biosciences	BD44	1:100	1:1000
Actin (HRP linked)	Sigma-Aldrich	A3854		1:10000
Akt	Cell Signaling Technology	#9272	1:1000	1:2000
Alexa Fluor 488- conjugated Cleaved-Caspase-3	Cell Signaling Technology	#9603		1:50
ATM	Abcam	Ab32420	1:1000	1:2000
Cleaved-PARP	Cell Signaling Technology	#5625	1:800	1:1500
DRAQ5	Cell Signaling Technology	#4084	1:5000	
ERK1/2	Cell Signaling Technology	#4695	1:1000	1:2000
H3Ser10	Cell Signaling Technology	#9706	1:30	1:100
IGF1R-β subunit	Cell Signaling Technology	#3027	1:1000 // 1:100 (IF)	1:2000 // 1:1000(IF)
Insulin receptor	Calbiochem		1:500	1:1000
Ku70/80	Neomarkers	MS-286-P1	1:5000	1:10000
MGMT	Sigma-Aldrich	M3068	1:2000	1:5000
MGMT	Sigma-Aldrich	M3068	1:2000	1:5000
Myosin IIb	Cell Signaling Technology	#3404	1:5000	1:10000
p21	Santa Cruz Biotechnology	SC817	1:1000	1:2000

p53	Cell Signaling Technology	#9282	1:1000	1:2000
phospho-4EBP1 (Thr37/46)	Cell Signaling Technology	#2855	1:1000	1:2000
phospho-AKT (Ser473)	Cell Signaling Technology	#4095	1:500	1:1000
Phospho-ATM (ser1981)	Abcam	Ab81292	1:5000	1:8000
phospho-cdc2 (Tyr15)	Cell Signaling Technology	#4539	1:1000	1:2000
Phospho-CHK1 (ser345)	Cell Signaling Technology	#2348	1:1000	1:2000
Phospho-CHK2 (Thr68)	Cell Signaling Technology	#2661	1:1000	1:2000
phospho-ERK1/2 (Thr202/Tyr204)	Cell Signaling Technology	#9101	1:500	1:1000
phospho-IGF1Rβ (Tyr1135/1136)/IRβ (Tyr1150/1151)	Cell Signaling Technology	#3024	1:500	1:1000
Phospho-KAP1 (ser824)	Bethyl Laboratories	A300-767A	1:500	1:1000
Phospho-RPA (ser33)	Bethyl Laboratories	A300-246A	1:1000	1:2000
RAD51	Abcam	14b4	1:1000 // 1:500 (IF)	1:2000
β-tubulin	Sigma	T4026	1:5000	1:10000
γH2Ax (Ser139)	EMD Millipore	JBW301	1:1000 // 1:500 (IF)	1:2000

Note: For Western Blotting: HRP-linked anti-Mouse (#7076) and anti-Rabbit (#7074) from Cell signalling were used as secondary antibodies. For Flow Cytometry and Immunofluorescence, secondary antibodies used were: Alexa fluor (H+L) 488 Goat anti-Rabbit (A-11034), Alexa fluor (H+L) 568 Goat anti-Mouse (A-11031), Alexa fluor (H+L) 594 Goat anti-Mouse (A-11005) and Pacific blue (H+L) Goat anti-Rabbit (P-10994); All from Life Technologies.

3. IGF-1R in the response to temozolomide-induced DNA damage

Several studies have pinpointed IGF-1R as a mediator of resistance to chemotherapy in a number of cancers mainly through its influence on cell survival and growth (Min et al., 2003, Benini et al., 2004, Flanigan et al., 2010, Zhou et al., 2011, Cohen et al., 2005). It has been demonstrated by our group and others that blocking the IGF-1R signalling pathway can provide added benefit to treatment with cytotoxic drugs, including temozolomide (TMZ) (Flanigan et al., 2010, Geoerger et al., 2010, Yeh et al., 2006).

In a panel of MGMT-proficient melanoma cells lines, our group has shown that resistance to TMZ significantly correlated with IGF-1R activation (Ramcharan et al., 2015). This prompted the investigation of a possible combination of IGF-1R targeting and temozolomide in melanoma and it was found that IGF-1R inhibition enhanced the sensitivity of A375M and CHL-1 melanoma cell lines to TMZ (Ramcharan et al., 2015). However, we are yet to uncover the underlying mechanisms by which IGF-1R signalling influences the response to TMZ.

Preclinical testing of TMZ efficacy has been conducted in cancer types other than melanomas and high levels of anti-tumour activity have been observed in Ewing's sarcomas (Villano et al., 2009, Keir et al., 2013, Raverot et al., 2010). Therefore, in addition to CHL-1 and A375M melanoma cells previously used by my predecessor in the group and the SK-MEL23 melanoma cell line, we decided to include Ewing's sarcoma cell lines TC-71, SK-N-MC in our study; with the aim to decide based on chemo-sensitivity profiles which cell line would be a better model to help us dissect the role of IGF-1R in the response to TMZ-induced DNA damage. We conducted experiments that allowed us to:

1) Test whether IGF-1R targeting can induce chemo-sensitisation in selected melanoma and Ewing's sarcoma cell lines.
2) Examine the effect of IGF-1R targeting on the repair of TMZ-induced DNA damage.

3.1. Testing the effects of IGF-1R combination with TMZ in melanoma and Ewing's sarcoma cell lines

The effects of targeting IGF-1R signalling on the response to treatment with Temozolomide was evaluated in five cells lines including two Ewing's sarcoma (TC-71, SK-N-MC) and three melanoma cell lines (A375M, CHL-1 and SK-MEL23). First, we assessed the effect of IGF-1R inhibition alone.

3.1.1. The Effect of IGF-1R inhibition

The response of the cell lines to IGF-1R inhibition was evaluated by conducting colony formation assays and we calculated the drug concentration at which 50% of cells die (SF-50) in response to treatment with the IGF-1R inhibitor drug AZ12253801, which will be referred to as AZ3801 henceforth. AZ3801 is an ATP competitive small molecule inhibitor that blocks phosphorylation of IGF-1R as described in a previous paper from our group (Aleksic et al., 2010). The SF-50 values were extrapolated from the survival curves on GraphPad Prism. These were 25nM for melanoma cell lines A375M and SK-MEL23, and 20nM for Ewing's sarcoma cell lines TC-71 and SK-N-MC (Figure 3-1). Previous studies on CHL-1 from our group showed that the SF-50 was approximately 65nM when treated with AZ3801 (Ramcharan, 2014).

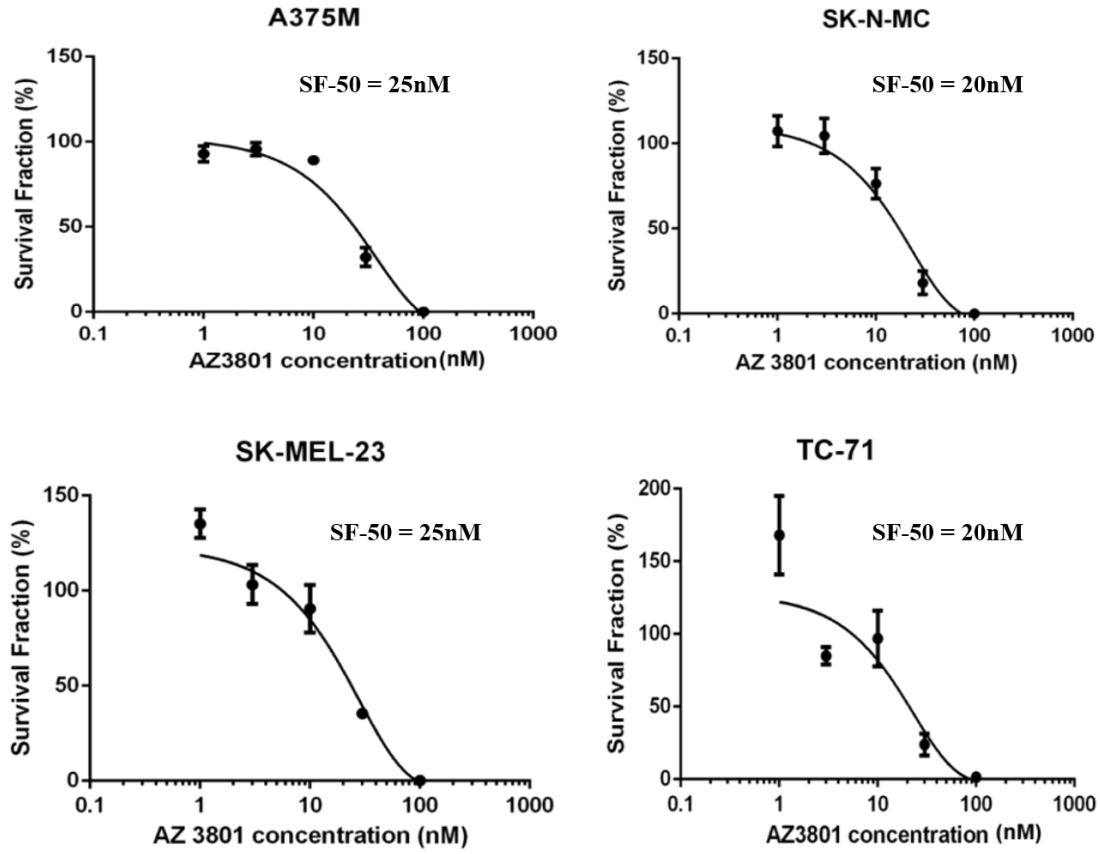


Figure 3-1: **Effects of IGF-1R inhibition on cell survival in melanoma and Ewing's sarcoma cells**. Cells were seeded in 10cm dishes in full medium (3000-10,000 cells per dish) and treated the following day with AZ3801 (1, 3, 10, 30, 100nM). Cell colonies were fixed and stained 6-12 days after seeding. Colonies were counted and expressed as a percentage of survival in comparison to solvent-treated controls (DMSO <0.1%). The graphs show mean ± standard deviation. Results were compiled from two independent experiments and expressed as the percentage of survival in solvent-treated dishes. GraphPad Prism software was used to curve-fit data and for SF-50 extrapolation.

To confirm that the effects observed on survival were due to inhibition of IGF-1R activation, we checked that AZ3801 was able to inhibit the phosphorylation of IGF-1R in the presence of the IGF-1 ligand. Our results showed that in a dose-dependent manner, AZ3801 prevented IGF1-induced phosphorylation of key residues Tyr1135, Tyr1136 on IGF-1R which are required for receptor activation (Figure 3-2). We noticed that ligand-induced activation of AKT was also suppressed by the drug.

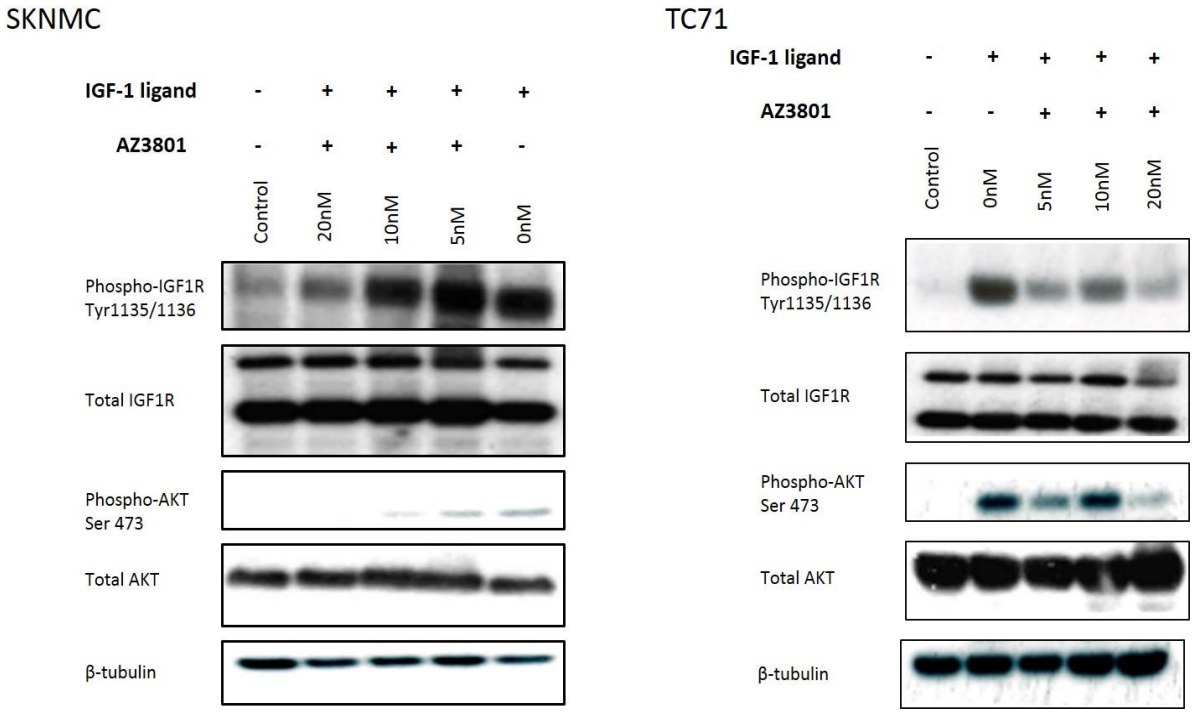
Downregulation of AKT phosphorylation was observed in all cell lines, except in CHL-1 cells. Surprisingly, PTEN mutant SK-MEL23 also showed increased suppression of AKT

activation in a dose-dependent manner (Figure 3-2). It is possible that basal phospho-AKT levels in SK-MEL23 were negligible despite harbouring a deactivating PTEN-mutation because the cells were incubated in serum-free medium, thereby lacking growth factors susceptible to stimulate the AKT signalling pathway. It would be interesting to have quantified data comparing the effect of the AZ3801 IGF-1R kinase inhibitor on both ERK and AKT downstream signalling pathways.

Consistent with the fact that the AZ3801 inhibitor blocks ligand-mediated receptor auto-phosphorylation, no changes were observed in the total protein levels of the IGF-1R in cells treated with the inhibitor.

Having confirmed that AZ3801 can suppress IGF-1R activation and can reduce downstream AKT signalling, we next determined the combinatorial effect of IGF-1R inhibition plus TMZ treatment in these five cell lines.

A)


SKNMC
IGF-1 ligand - + + + +
AZ3801 - + + + -
Control
20nM
10nM
5nM
0nM
Phospho-IGF1R Tyr1135/1136
Total IGF1R
Phospho-AKT Ser 473
Total AKT
β-tubulin
TC71
IGF-1 ligand - + + + +
AZ3801 - - + + +
Control
0nM
5nM
10nM
20nM
Phospho-IGF1R Tyr1135/1136
Total IGF1R
Phospho-AKT Ser 473
Total AKT
β-tubulin

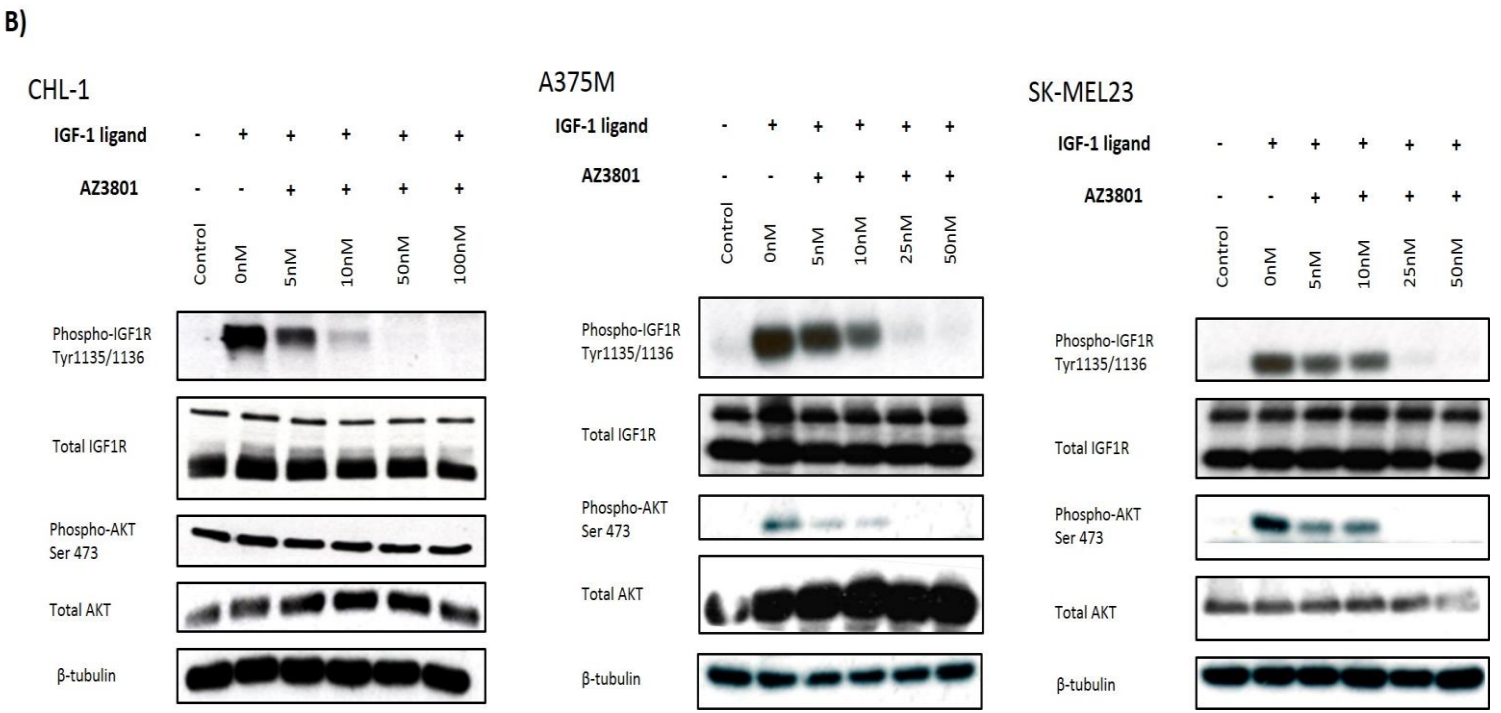


Figure 3-2: **Effect of the kinase inhibitor drug AZ3801 on IGF-1R activation and AKT signalling in Ewing's sarcoma (A) and melanoma cell lines (B).** Control cells were incubated in serum-free medium without inhibitor and no IGF-1 ligand. In the other conditions, cells were serum-starved and the following day treated with either AZ3801 or DMSO (<0.1%) for 1 hour in full medium. IGF-1 ligand (50nM) was added in the final 15 min in full medium. Cells were lysed and analysed by western blot on SDS-PAGE. Important: We later found out that the SK-N-MC cell is a neuroblastoma and not a Ewing's Sarcoma cell line.

3.1.2. Response to TMZ treatment as a single agent and in combination with IGF-1R inhibition

Using the colony formation assay, we assessed the response to treatment with temozolomide in combination with AZ3801 in order to determine whether simultaneous administration of the IGF-1R inhibitor could further enhance the sensitivity of these cell lines to the alkylating agent.

Upon treatment with temozolomide alone, we noted that all five cell lines showed reduced cell survival as the drug concentration increased, reflecting a dose-dependent sensitivity to the alkylating agent. As expected, SK-MEL23 cells were more sensitive to treatment with TMZ because they lack the MGMT enzyme required to remove harmful TMZ-induce O^6MeG DNA adducts. Among MGMT-proficient cells, SK-N-MC cells showed greater sensitivity to TMZ-induced damage whilst TC-71 was the most resistant. The mean percentage of cell survival at the dose of 200μM was 5%, 46%, 55% and 68% for SK-N-MC, A375M, CHL-1 and TC-71 respectively (Figure 3-3).

Simultaneous treatment with AZ3801 at sub SF-50 doses of the IGF-1R inhibitor for each particular cell line had no significant effect on the cell survival except in SK-N-MC cells where we observed that co-treatment with 20nM of AZ3801 and 200μM of TMZ was lethal (Figure 3-3). That MGMT-null SK-MEL23 did not show increased chemo-sensitisation as a result of IGF-1R targeting could indicate that either the burden of unrepaired O^6meG adducts is the predominant cause of death in these cells or that, IGF-1R inhibition exerted its effect via a route/pathway involving MGMT function.

When the concentration of AZ3801 was increased to doses greater than or equal to SF50 values corresponding to 20nM, 50nM and 100nM for TC-71, A375M and CHL-1 respectively, we observed a dramatic effect on the response to TMZ treatment in CHL-1

and A375M cells but not with TC-71 (Figure 3-3). This was consistent with previously published findings from our group (Ramcharan et al., 2015).

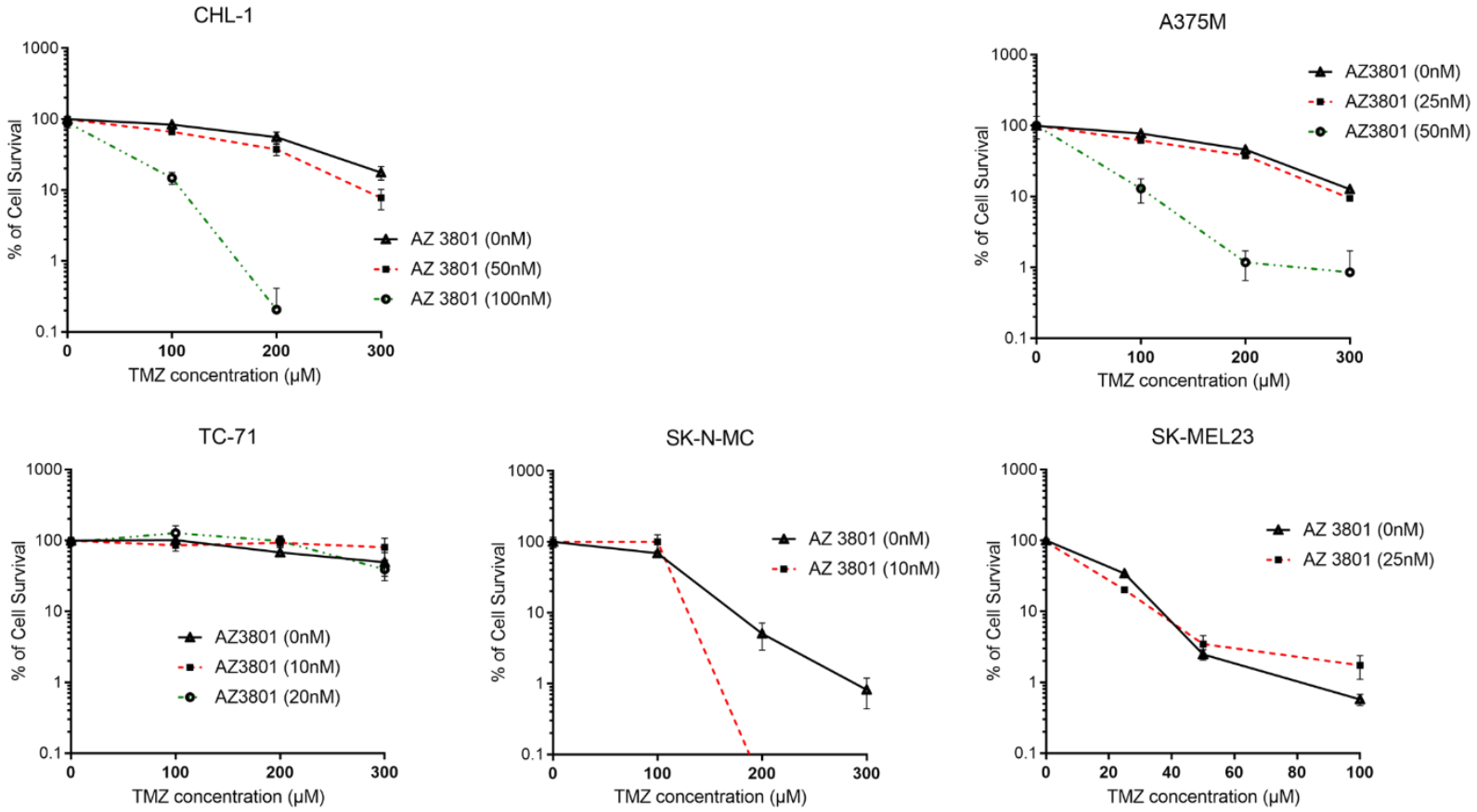


Figure 3-3: **Effects of IGF-1R inhibition (AZ3801) in the response to temozolomide (TMZ) treatment.** Cells were seeded in a triplicate set of 10cm dishes in full medium. The following day, these were treated with TMZ (100μM-300μM) or (25-100μM for SK-MEL23) on its own or simultaneously with AZ3801. Colonies were fixed and stained with Coomassie blue 7-12 days after seeding, then counted and values were expressed as a percentage of survival relative to solvent-treated controls (mean ±SEM). This result represents data obtained from 2-3 independent experiments.

3.2. Investigating the mechanisms of chemo-sensitisation to Temozolomide in IGF-1R inhibited melanoma cells

Results showing that IGF-1R inhibition potentiated the effect of TMZ treatment in melanoma cells prompted the question whether IGF-1R signalling could influence the efficient repair of TMZ-induced DNA damage or, that IGF-1R inhibition negatively affected cell survival independently of the effects of TMZ-caused damage. To tackle this, since an important amount of work had already been done to uncover how IGF-1R inhibition can promote sensitivity to TMZ in CHL-1 melanoma cells by a previous student in our group, it seemed logical to continue our investigation with this particular cell line.

Previous work has shown that although blocking IGF-1R signalling with AZ3801 did result in increased apoptosis in CHL-1 as evidenced by their sensitivity to single treatment with the IGF-1R inhibitor, the proportion of apoptotic cells at different doses did not correlate with the pattern of chemo-sensitisation observed when inhibition is combined with TMZ (Ramcharan et al., 2015); thereby suggesting that IGF1R-mediated effects on promoting cell survival can only partially account for the chemo-sensitisation observed in inhibited cells .

Because the activity of MGMT can also influence the response to TMZ treatment, the student checked whether IGF-1R hindered MGMT function. His results showed that IGF-1R inhibition did not affect MGMT levels. Also, blocking MGMT function using O^6-Benzylguanine did not prevent IGF-1R inhibition to induce chemo-sensitisation to TMZ (Ramcharan, 2014). Furthermore, neither MGMT activity nor that of Alkyladenine DNA glycosylases 'AAG' were affected by treatment with AZ3801. More interestingly, the

student demonstrated that the proportion of TMZ-induced toxic DNA adducts was not increased in IGF-1R inhibited cells (Ramcharan, 2014).

Because, the chemo-sensitisation of IGF-1R inhibited cells could not be accounted by the role of IGF-1R on cell survival and that there was no evidence of increased levels of TMZ-induced cytotoxic DNA adducts nor any negative effect on MGMT-mediated repair as a result of the inhibition of IGF-1R signalling, we were led to hypothesise that the repair of replication-associated double-strand breaks might be impaired in IGF-1R inhibited CHL-1 cells.

3.2.1. Assessing the influence of IGF-1R signalling on HR-mediated double-strand break repair

Studies have demonstrated that repair of TMZ-induced double-strand breaks requires functional homologous recombination (HR) and downregulation of BRCA2 has been shown to enhance sensitivity to the alkylating agent (Kondo et al., 2011, Roos et al., 2009). Replication-associated double-strand breaks trigger ATR signalling activation for fork protection in order to prevent subsequent genomic instability. ATR activation leads to phosphorylation of histone H2AX on Ser139 (Yeeles et al., 2013). Phosphorylated H2AX (γH2AX) facilitates the recruitment of a number of proteins that amplify the DNA damage response. RAD51 recruitment to the break site results in the formation of RAD51-ssDNA nucleoprotein filaments for strand invasion and homology searching (Jasin and Rothstein, 2013, Chen et al., 2008). Both γH2AX and RAD51 play critical roles during HR. While the former acts as a double-strand break marker, the latter stabilises ssDNA and facilitates strand invasion so, we hypothesised that any influence IGF-1R inhibition may exert on HR might be detected by determining whether the formation or resolution of γH2AX and RAD51 foci at the sites of DNA damage was impaired in AZ3801-treated cells.

First, we checked that HR-mediated repair was indeed triggered upon TMZ-induced damage. This was confirmed by staining CHL-1 cells for γH2AX and RAD51 proteins following treatment with TMZ (Figure 3-4). Our results showed that γH2AX and RAD51 foci can be detected 24 hours post-treatment with the alkylating agent, implying not only that breaks were detected and signalled but also that homologous recombination was activated in these cells. The number of γH2AX and RAD51 foci appeared to decrease dramatically at later time-points; a return to basal levels which implied that double-strand breaks repair was not impaired in these cells (Figure 3-4).

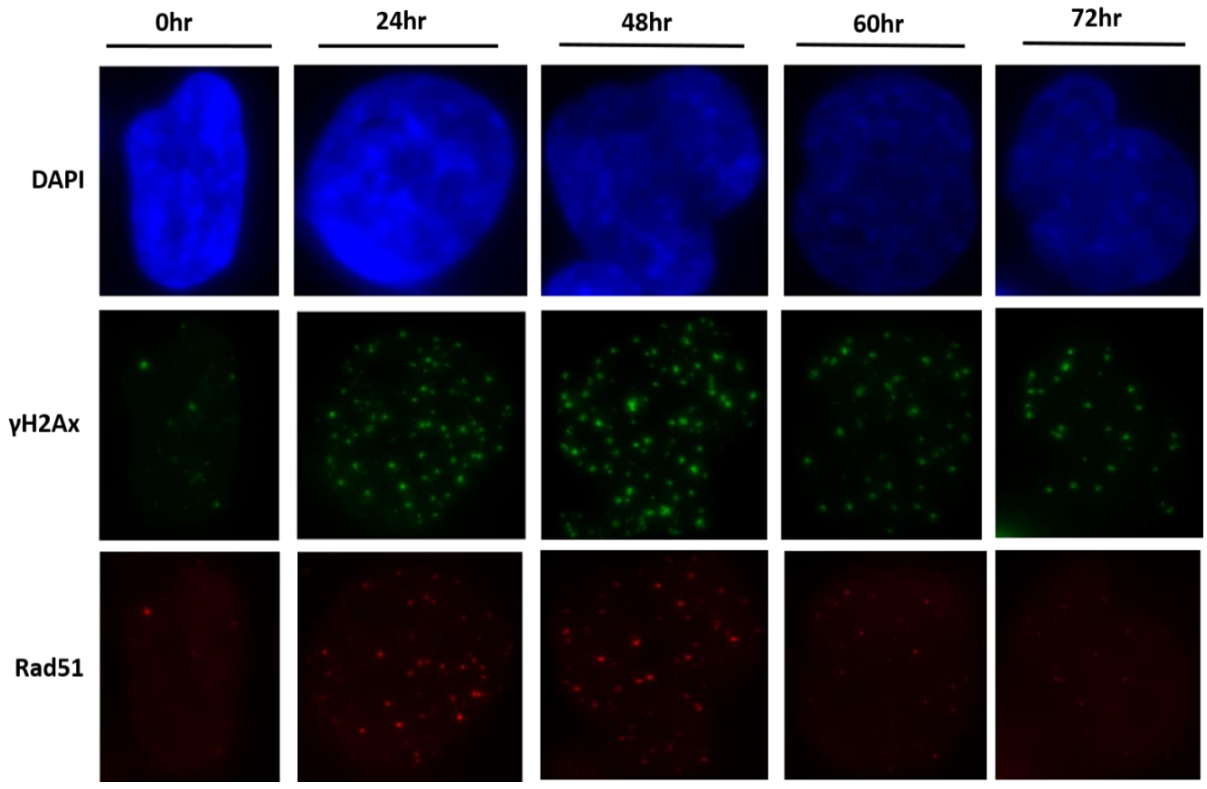


Figure 3-4: **Induction of γH2AX and RAD51 foci upon treatment with TMZ**. CHL-1 cells were cultured on coverslips placed in 6-well plates, treated 24 hours later with TMZ (300μM) and collected at time-points up to 72 hours, fixed and stained for RAD51, γH2AX (green) and DNA (DAPI, blue). Note: the 0hr time-point represents solvent-treated cells fixed and stained at the same time as TMZ-treated cells collected at the 24-hour time-point.

Next, we devised a similar experiment, tracking by immunofluorescence the induction and resolution of γH2AX and RAD51 foci in the nucleus but this time comparing TMZ-treated

cells with CHL-1 cells co-treated with TMZ and AZ3801. Foci counting was performed using two different quantitative methods notably a Fiji script that was written by myself (see appendix 8) and a programme developed by Dr Steve Taylor (Computational Biology Research Group, WIMM, Oxford).

Under basal conditions (0 hour time-point), endogenous damage can be observed in CHL-1 cells as depicted by the low levels of detectable γH2AX and RAD51 foci. IGF-1R inhibition did not abolish TMZ-induced increase in the levels of nuclear γH2AX and RAD51 foci in cells treated with the combination as evidenced by the similar increase from basal foci numbers measured 24 hours after treatment (Figure 3-5). This implied that in spite of IGF-1R inhibition, TMZ was able to cause DNA damage.

No significant difference in foci numbers between TMZ-treated cells versus cells co-treated with both TMZ and AZ3801 was detected; the same trend in foci numbers over the duration of the time-course was observed under both conditions. Indeed, just as with the single treatment, the rise γH2AX levels was followed by a dramatic decrease to near basal levels 48 hours after simultaneous treatment with AZ3801 (Figure 3-5). Similarly, RAD51 foci levels dropped to basal levels at the 60-hour time-point after the 48-hour peak (Figure 3-5).

Altogether, these findings led us to conclude that blocking IGF-1R signalling did not prevent the formation of replication-associated double-strand breaks when cells were treated with temozolomide. Also, we deduced that targeting IGF-1R did not affect double-strand break detection as the Serine 139 phosphorylation on histone H2AX was not impaired. In addition to this, our data revealed that blocking IGF-1R activation, which resulted in suppression of ERK1/2 phosphorylation as described earlier, did not prevent RAD51 accumulation in the nucleus following DNA damage. This is of particular importance since it has been suggested that IGF1R-dependent recruitment of IRS proteins

to the cytoplasm might be an important event allowing the disassembly of the nuclear IRS-RAD51 complex thereby freeing RAD51 so that it may be available for HR-mediated repair (Trojanek et al., 2006). More importantly, we noted that inhibiting the activation of IGF-1R did not delay the resolution of both γH2AX and RAD51 foci.

Our results therefore support the conclusion that HR-mediated repair of TMZ-induced replication associated double-strand breaks was able to proceed seemingly unhindered despite inhibition of IGF-1R downstream signalling in CHL-1 cells. We therefore reasoned that it was highly likely that the underlying mechanisms of chemo-sensitisation to TMZ were HR-independent and were prompted to determine whether the combination caused changes to the cell cycle that could account for the chemo-sensitisation phenotype.

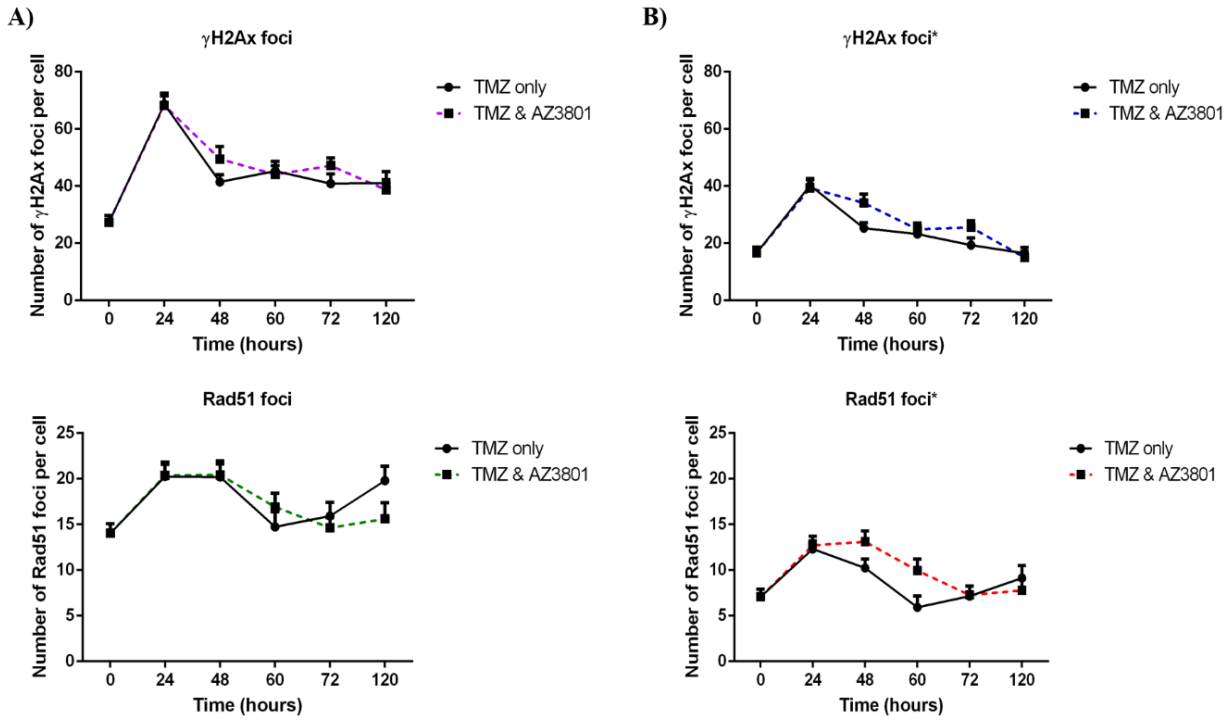


Figure 3-5: **Time-course of induction and resolution of TMZ-induced DSBs. A)** Graph plots based on Foci count generated using Fiji-script written by myself in collaboration with CBRG (WIMM, Oxford). **B)** Graph plots based on Foci count generated using software developed by Dr Steve Taylor. CHL-1 cells were cultured on coverslips placed in 6-well plates, treated the following day with AZ3801 (100nM) and/or TMZ (300µM). These were collected at time-points up to 120 hours, fixed and stained for RAD51, γH2AX (green) and DNA (DAPI, blue). The 0hr time-point represents solvent-treated cells fixed and stained at the same time as TMZ-treated cells collected at the 24-hour time-point. The results are represented as the average foci count per cell and the standard error of the mean. To estimate the average, more than 50 cells were counted. This result represents data obtained from at least three independent experiments.

3.2.2. Effects of the combination treatment on the cell cycle

Cells were treated either with DMSO (control), TMZ, AZ3801 or a combination of TMZ and AZ3801. As described in the methods chapter (see section 2.6.2), cells were incubated with BrdU prior to collection at different time-points (24, 48 and 60 hours post-treatment) so that BrdU staining could be used to identify the S-cycling cells. Our results showed that whilst the highest proportion of solvent-treated cells where in the G1 phase throughout the experimental time-course, drug-treated cells (with TMZ, AZ3801 or both) displayed a significant number of cells in the G2 phase that reflected G2 accumulation (Figure 3-6). For instance, at 24 hours after treatment, solvent-treated cells exhibited the highest percentage

of cells in G1 (63%) and the lowest percentage of cell in the G2 phase (7%) whilst co-treatment with TMZ and AZ3801 resulted in reduced proportion of cells in G1 (4%) and a dramatic increase in the proportion of cells in G2 (78%). We also observed a population of polyploid cells (DNA content >4N); a phenotype that was most pronounced under conditions of treatment with AZ3801 alone (Figure 3-6).

At the 48-hour time-point, we noticed a 3-fold increase in the G1 population for TMZ-treated cells. On the other hand, there was a significant reduction in the proportion of cells in the S-phase (>3-fold). A similar observation was made with cell subjected to combination treatment where the proportion of S phase cells decreased by more than 10-fold (Figure 3-6). Interestingly, we noted that compared to the earlier time-point, the percentage of polyploid cells increased by more than 2-fold under treatment conditions with AZ3801 alone or in combination with TMZ.

We found it intriguing that although treatment with TMZ or AZ3801 resulted in G2 accumulation, the combination did not seem to yield additive effects. However, it appeared that treatment with TMZ could protect against polyploidy because, throughout the entire timecourse, a far greater proportion of polyploid cells was counted under treatment with AZ3801 alone compared to the combination.

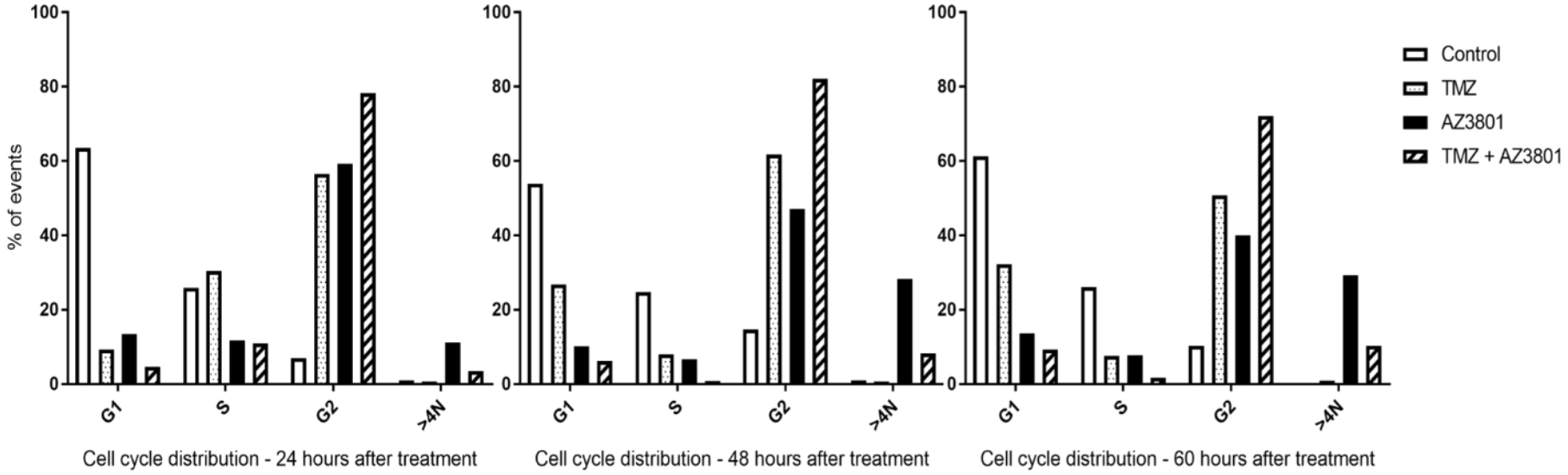


Figure 3-6: **Effects of the combination treatment on cell cycle distribution in CHL-1 cells**. Cells were seeded in 10cm dishes and treated the following day with either solvent (DMSO<0.3%), temozolomide (TMZ-300μM) alone, AZ3801 (100nM) alone or in combination with TMZ (300μM). Prior to harvest, cells were pulse-labelled with BrdU (10μM) for 30mins. Propidium iodide was used to stain DNA. Flow cytometry data were analysed using Flowjo software to determine the percentage of cells in each cell cycle stage. Graphs were plotted using GraphPad Prism. This figure was produced with data from a single experiment. Cell cycle raw data added in section 8.2.1.

It is generally accepted that when cells experience mitotic defects, polyploidy can result; yielding cells with DNA content greater than 2N (Glotzer, 2001). Because polyploidy was observed only under treatment conditions involving the administration of AZ3801, we questioned whether this phenotype could possibly be the result of off-target effects associated with this drug. To do so, we decided to assess cell cycle distribution in cells where IGF-1R signalling has been downregulated using an IGF1R-targeting siRNA.

3.2.3. Effects of IGF-1R depletion on the cell cycle

CHL-1 cells were transfected with siRNA targeting the *IGF1R* mRNA to induce downregulation of IGF-1R at the protein level thereby leading to reduced IGF-1R signalling in cells. Prior to collection, cells were incubated with BrdU and later stained with an antibody able to detect the synthetic nucleoside, thus allowing us to identify S-cycling cells. Changes in the cell cycle distribution were examined at 48 and 120 hours after transfection with the IGF1R-targeting siRNA or the non-targeting 'Allstars' siRNA. As the non-transfected control, we used cells that did not undergo the transfection process and were cultured under normal growth conditions. We confirmed by western blot that the siRNA used to induce the degradation of the *IGF1R* mRNA led to a marked reduction in the protein levels of the IGF-1 receptor (Figure 3-7).

Cell cycling data revealed that IGF-1R depletion induced G1-S cell cycle arrest 48 hours after siRNA transfection, with approximately 70% of the cell population being in the G1 phase compared to only ~36% in cells treated with non-targeting siRNA (Figure 3-7). In contrast, the proportion of S-cycling cells was twice lower under conditions of IGF-1R depletion relative to the non-targeting control. These distinct features of IGF-1R depleted cells were no longer observed at the 120-hour time-point. More importantly, very little if any polyploidy (<2%) was observed following IGF-1R depletion. These results therefore

supported the argument that the polyploidy phenotype was likely not caused by suppression of the IGF-1R signalling but could be a drug-related off-target effect. Polyploidy and consequently death resulting from mitotic defects might therefore account for the increased cytotoxic effects associated with the TMZ+AZ3801 combination treatment in comparison to treatment with TMZ alone.

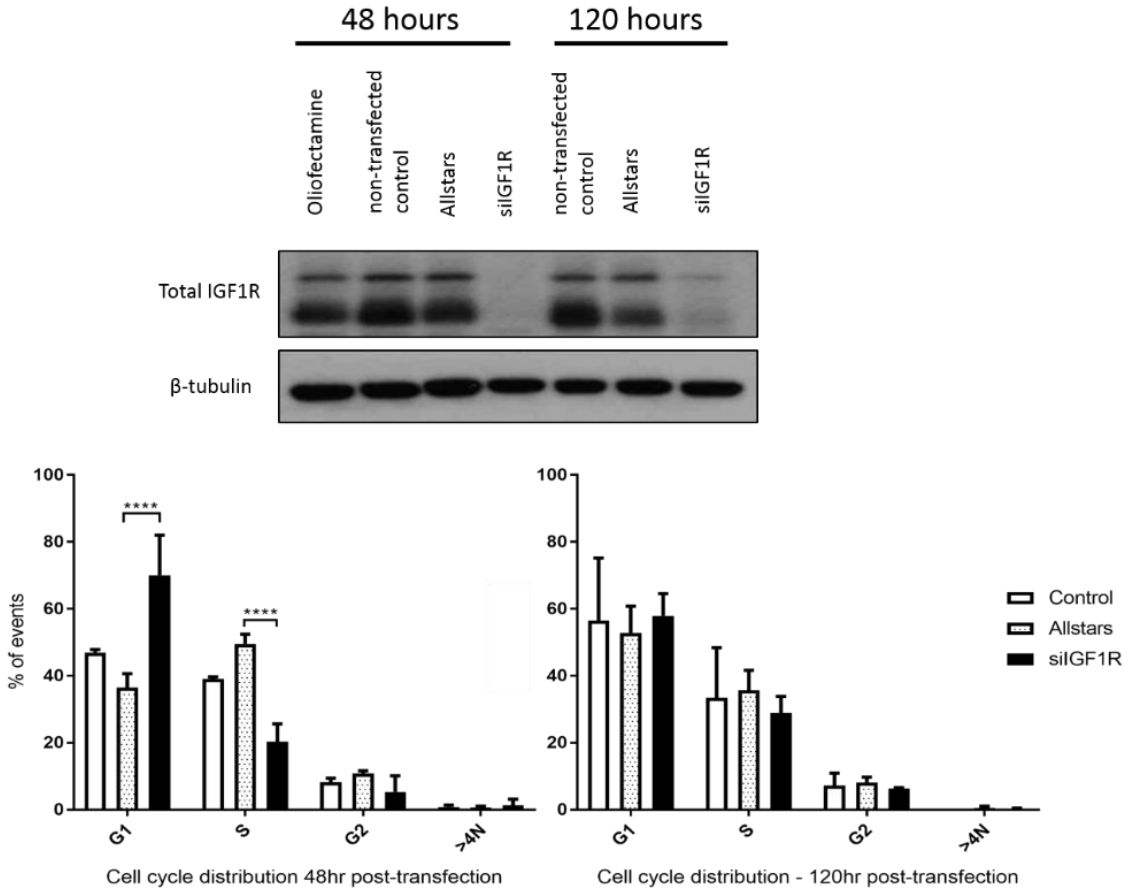


Figure 3-7: **Effects of IGF-1R depletion on Cell cycle distribution in CHL-1 cells**. CHL-1 cells were seeded in 10cm dishes. The next day cells were transfected either with 200nM of non-targeting siRNA (Allstars) or 200nM of IGF1R siRNA (siIGF1R). The non-transfected control cells did not undergo transfection but the cell culture medium was changed to maintain consistency across samples. Cells were collected 48 hours and 120 hours after transfection. Prior to harvest, cells were pulse-labelled with BrdU (10μM) for 30 mins. Propidium iodide was used to stain DNA. Flow cytometry data were analysed using Flowjo software to determine the proportion of cells in each cell cycle phase. Results from two independent experiments were analysed and presented herein as the mean ± standard deviation. Cell cycle raw data added in section 8.2.2.

3.3. Discussion

Our data confirmed that treating cells with temozolomide caused DNA damage which consequently triggered the HR-mediated repair machinery, as evidenced by the surge in RAD51 and γH2AX foci numbers observed in temozolomide-treated cells in comparison to solvent-treated cells. We also noticed that treatment with TMZ triggered the accumulation of cells in G2, which was consistent with previous reports showing that the methylating agent methylnitronitrosoguanidine (MNNG) can induce activation of the G2/M DNA damage checkpoint (Mojas et al., 2007, Quiros et al., 2010).

IGF-1R inhibition enhanced the sensitivity of CHL-1 and A375M melanoma cells to treatment with TMZ. Based on previous work conducted on CHL-1, we were prompted to find out whether chemo-sensitisation as a result of IGF-1R inhibition was mediated through negative effects on HR-directed repair. However, our investigation revealed that the inhibition of IGF-1R activation did not hinder TMZ-induced DNA damage, nor did it result in the induction of more double-strand breaks. Our results suggested that the sensitisation of IGF-1R inhibited cells to treatment with TMZ might be HR-independent.

Interestingly though, both A375M and CHL-1 harbour mutations in the *CDKN2A* gene encoding for the cell cycle protein $p16^{INK4A}$ that is responsible for regulating the G1/S cell cycle transition through its inhibitory function on cell cycle kinases CDK4 and CDK6 (Ohtani et al., 2004). IGF-1R inhibition was reported to synergise with Palbociclib, a CDK4/6 inhibitor, to suppress the growth of $p16^{INK4A}$-deficient pancreatic cancer cells (Heilmann et al., 2014). Although, the authors failed to describe the underlying cause of the synergy we, thought this was of particular importance in the context of our study because whilst siRNA-mediated depletion of IGF-1R resulted in transient G1/S arrest, treatment with the inhibitor induced accumulation of cells in G2 instead and, G2/M accumulation as

a result of IGF-1R inhibition has also been reported in other studies (Liang et al., 2014, Strömberg et al., 2006).

In addition to this, we noticed an increase in the percentage of polyploid cells under conditions of IGF-1R inhibition. This caused us to suggest that IGF-1R inhibition may promote chemo-sensitisation by inducing tampering with cell cycle progression and inducing mitotic defects. However, because polyploidy was exclusively observed in cells treated with AZ3801 either alone or in combination with TMZ and not with depletion of IGF-1R, we questioned whether the drug had potential off-target effects. This was followed-up with Elaine Kilquor of AstraZeneca (the company that synthesised the drug) who confirmed that the Aurora A kinase, an important player during mitosis, was also inhibited by AZ3801 and may account for the resulting mitotic catastrophe (Marumoto et al., 2005).

Because of off-target effects associated with kinase inhibitor drugs making it difficult to tear apart phenotypic effects specifically associated with IGF-1R signalling, we decided to develop and use an isogenic cell line model lacking IGF-1R to question the influence of IGF-1R function in the repair of exogenously-induced double-strand breaks.

4. Generating IGF-1R knockout isogenic cells

Due to concerns about off-target effects from the use of the IGF-1R receptor tyrosine kinase inhibitor AZ3801, performing loss of function experiments by genetic manipulation was considered to be the best approach to dissect the role of IGF-1R in the repair of DNA double-strand breaks. Successfully carrying out our investigation necessitated that the influence of the IGF-1R signalling is interrogated in a cell line that showed dependence and reliance on this pathway for cell survival. This was therefore taken into account when deciding on a suitable cell line where the IGF-1R function should be permanently abrogated. In this chapter we will report on:

1) The selection of an appropriate cell line model
2) The design and validation process of a suitable gRNA for CRISPR/Cas9 mediated genome editing
3) The characterisation of CRISPR-generated IGF-1R mutants

4.1. Cell line model selection

The IGF-1R signalling pathway has been shown to be very important for cell survival in Ewing's sarcoma and osteosarcoma cell lines (Cao et al., 2014, Olmos et al., 2010). Therefore, as candidate cell lines wherein the *IGF1R* gene could be manipulated to prevent its expression at the protein level, we considered the Ewing sarcoma cell lines TC-32, TC-106 and the osteosarcoma cell line U2OS in addition to the melanoma cell line CHL-1 on which previous work was carried (as exhibited in chapter 3).

We hypothesised that reduction in survival would reflect the extent to which a given cell line relies on pro-proliferative signals triggered by the activation of the IGF-1 receptor and consequently assessed their proliferative ability in response to siRNA-mediated transient depletion of IGF-1R by colony formation assay to determine which cell line was the most appropriate for our study. Because, as explained earlier, successfully carrying out our investigation necessitated that the influence of the IGF-1R signalling on the response to DNA damage is interrogated in a cell line that showed dependence and reliance on the IGF-1R signalling pathway for survival.

CHL-1, TC-32, TC-106 and U2OS cells were transfected with either non-targeting Allstars siRNA or siRNA targeting the *IGF-1R* mRNA. Different molar concentrations of the siRNA were used in some instances to determine the most effective concentration at which IGF-1R depletion could be achieved. Downregulation of the IGF-1R protein was apparent in all cell lines. However, suppression of IGF-1R protein expression was less effective in the TC-106 cell line (Figure 4-1). Consequently, this cell line was not included when we went ahead to determine the effect of IGF-1R depletion on the cell survival.

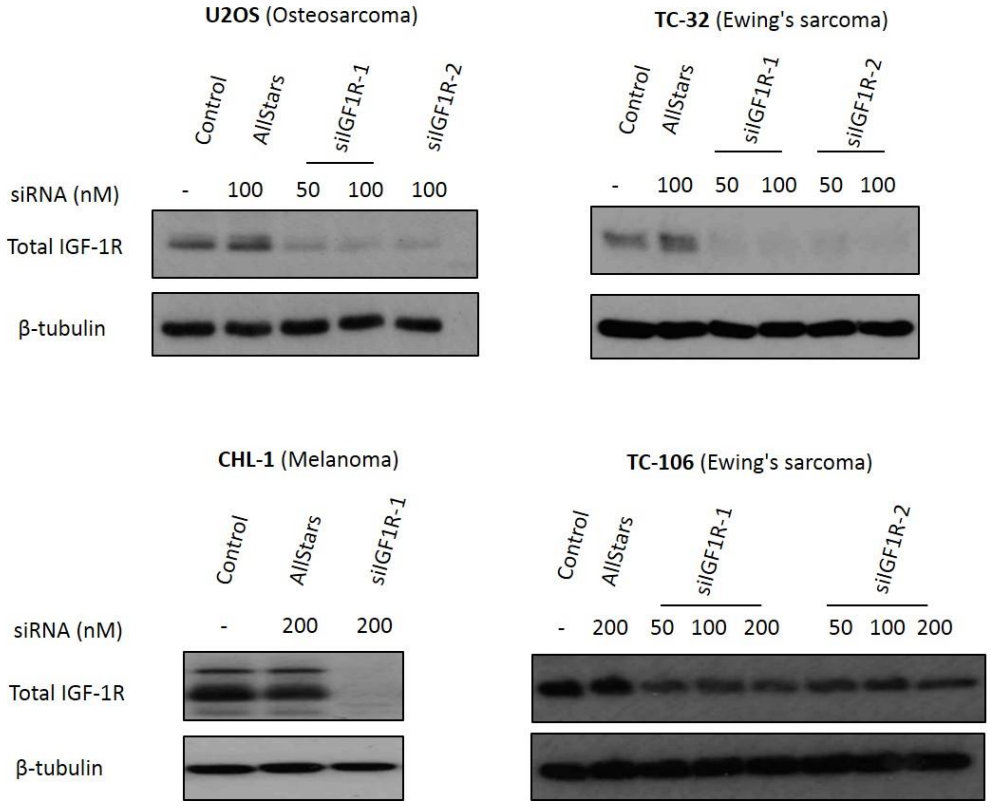


Figure 4-1: **siRNA-mediated depletion of IGF-1R**. Cells were seeded in 10cm dishes and transfected the next day either with non-targeting siRNA 'Allstars' or with increasing concentrations of IGF1R siRNA (siIGF1R-1, siIGF1R-2). Non-transfected control samples did not undergo transfection but the cell culture medium was changed to maintain consistency across samples. Cells were lysed 48 hours post-transfection and analysed by western blot.

Although IGF-1R depletion was apparently very effective in the melanoma cell line CHL-1, we noticed that the proliferative ability of these cells was not strikingly affected as the cell survival was only reduced by 35% (mean percentage) in comparison to the 'Allstars-transfected' negative control (Figure 4-2). In contrast, the downregulation of IGF-1R signalling induced a remarkable reduction in cell survival in U2OS (75% - mean value) and TC-32 (80% - mean value) cell lines. Hence, we concluded that the latter two cell lines do show significant dependence on IGF-1R function for survival and would consequently represent the most appropriate models for testing the role of the receptor in

the repair of DNA double-strand breaks because canonical pathways such as AKT and ERK signalling would be mostly activated through the IGF-1 receptor tyrosine kinase.

Taking into account the extreme sensitivity of TC-32 cells to transient depletion of the IGF-1R protein relative to U2OS cells, we reasoned that permanent depletion of the receptor in the former would likely fail to yield viable cells. Indeed, the highest mean percentage survival following depletion of IGF-1R in TC-32 was only up to 18%, observed at the concentration of 100nM with siIGF1R-1 whereas the lowest survival percentage in IGF-1R depleted U2OS cells was 29% (Figure 4-2). Consequently, we decided to perform CRISPR/Cas9-mediated genome editing of the *IGF1R* gene in U2OS cells. Our decision was supported by evidence pointing towards a critical role of the IGF-1R signalling pathway for determining sensitivity to DNA damaging agents in osteosarcoma cells (Wang et al., 2009, Wang et al., 2010, Kuijjer et al., 2013).

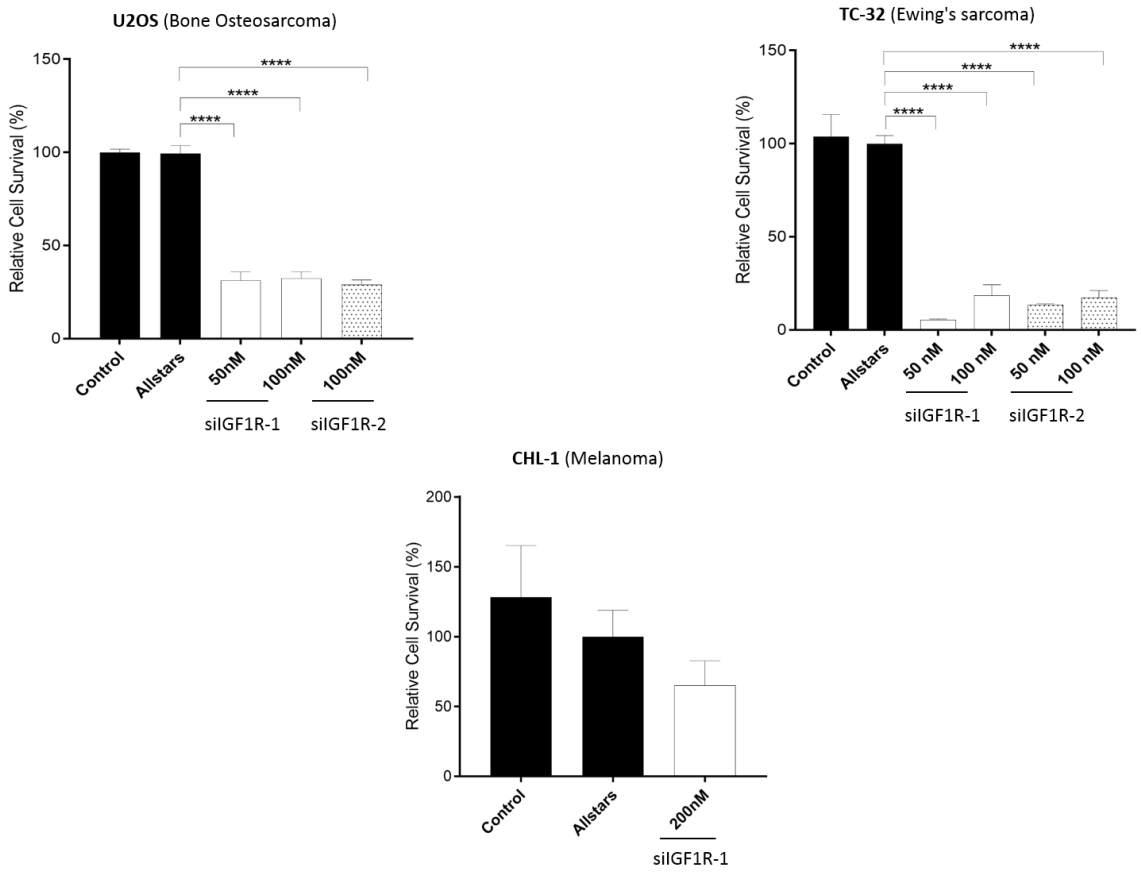


Figure 4-2: **The effect of IGF-1R depletion on the survival of CHL-1, U2OS and TC-32 cell lines**. Cells were seeded in 10cm culture dishes and the next day, they were either not transfected with siRNA (control) or transfected with non-targeting siRNA 'Allstars' or IGF1R siRNA (siIGF1R-1, siIGF1R-2). After 24 hours following transfection, cells were seeded for colony formation assay in triplicate dishes. Colonies were fixed and stained with Coomassie blue 7-12 days after, counted using a GelCount (Oxford-Optotronix) and the results were expressed as a percentage of survival relative to Allstars-transfected negative control. One-way ANOVA analysis was performed to assess for statistical significance (p-value < 0.05).

4.2. guide RNA design and validation

CRISPR/Cas9 genome engineering relies on a short oligonucleotide sequence referred to as guide RNA (gRNA) to direct the Cas9 enzyme to a specific DNA region in the genome where it induces a double-strand break (in the case of a wild-type Cas9 nuclease). It is therefore important when designing and deciding on which gRNA to use to take into account its specificity for the target region and the probability of non-specific targeting.

Several software programs have been developed to aid the researcher in this task and we opted for the online CRISPR design tool developed by the Zhang group at the Massachusetts Institute of Technology, USA (http://crispr.mit.edu/ - 2015).

4.2.1. gRNA design

The *IGF1R* gene consists of 21 exons and since the first exon encodes mostly for the signal peptide which is cleaved off during post-translational processing, we decided to design gRNAs targeting the second coding exon (Ullrich et al., 1986). The targeted exon (exon 2) contains sequences coding for the cysteine-rich region and a portion of the L domains, both of which assemble to constitute the ligand binding site (see section 1.1.1). The specificity of selected gRNA nucleotides for exon 2 was evaluated using the BLASTn (nucleotide Basic Local Alignment Search Tool) programme from the National Center for Biotechnology Information (USA) which searches for sequence homology against the human genome including mRNA transcripts.

The search results revealed that although other transcripts were predicted as potential targets, the sequence homology with *IGF1R* mRNA was the most significant for all gRNAs, with the expect (E) value at least 58 times smaller than that of the next hit (Table 4-1). We also noticed that the sequence for gRNA-2A showed the best alignment score with the *IGF1R* mRNA transcript in comparison to the other three gRNA sequences (Table 4-1).

guideRNA	Forward sequence (5' -3')	BLASTn hits (E value; Alignment score)
gRNA-1A	GGCTCTTCTACAACTACGCCC	*IGF1R* mRNA (0.089; <40); *RBM26* (86; <40)
gRNA-1B	GGCCAGCCGCGGATGACCGTG	*IGF1R* mRNA (0.089; <40); *CSPP1* mRNA (86; <40)
gRNA-2A	GGAGAACTGCACGGTGATCG	*IGF1R* mRNA (0.017; 40-50); *HERC2* mRNA (1.0; <40)
gRNA-2B	GGCAGCTGCTGATAGTCGTTG	*IGF1R* mRNA (0.089; <40); *SMIM19* mRNA (22; <40)

Table 4-1: **BLASTn search results with selected guide oligonucleotides**. As described in the text, a megablast search was performed for each of the indicated guideRNAs and their corresponding sequences, searching for sequence homology in the human genome. Only the top 2 mRNA transcript hits are presented in the table. In brackets, the expect value (E value) for each hit is shown, as well as the alignment score between the input sequence and the hit.

To date, there are seventeen known *IGF1R* transcript variants resulting from alternative splicing of the *IGF1R* gene, of which five are protein-coding (Aken et al., 2016) (Table 4-2). The information available on the Ensembl database suggests that there are two consensus coding sequences (CCDS) for the *IGF1R* gene which differ by only 3 nucleotides and, we confirmed by DNA sequence alignment that this small nucleotide difference was not located in the DNA region expected to form base-pairing with each of the selected four gRNAs. In addition to the differences with the CCDS, 3 out of the 5 protein-coding splice variants yield truncated proteins, two of which lack exon 2 and the other one contains a truncated version of exon 2. However, after checking the structures encoded by retained exons, we noted that none corresponded to key structural domains that could assemble to produce a functional tyrosine kinase receptor (Figure 4-3). Hence, we concluded that exon 2 was a valid target for CRISPR/Cas9-mediated editing of the *IGF1R* gene.

Name	Transcript ID	bp	Protein	Biotype	CCDS
IGF1R-201	ENST00000268035.10	11803	1367aa	Protein coding	CCDS10378
IGF1R-206	ENST00000558762.5	11726	1366aa	Protein coding	CCDS73785
IGF1R-207	ENST00000558898.1	1034	212aa	Protein coding	-
IGF1R-204	ENST00000558355.1	572	190aa	Protein coding	-
IGF1R-216	ENST00000560972.1	310	103aa	Protein coding	-
IGF1R-211	ENST00000560144.1	525	90aa	Nonsense mediated decay	-
IGF1R-215	ENST00000560432.1	657	No protein	Processed transcript	-
IGF1R-202	ENST00000557873.5	583	No protein	Processed transcript	-
IGF1R-203	ENST00000557938.5	574	No protein	Processed transcript	-
IGF1R-209	ENST00000559582.1	567	No protein	Processed transcript	-
IGF1R-212	ENST00000560186.5	551	No protein	Processed transcript	-
IGF1R-205	ENST00000558751.1	548	No protein	Processed transcript	-
IGF1R-213	ENST00000560277.5	526	No protein	Processed transcript	-
IGF1R-208	ENST00000558947.1	303	No protein	Processed transcript	-
IGF1R-210	ENST00000559925.5	2280	No protein	Retained intron	-
IGF1R-217	ENST00000561049.1	682	No protein	Retained intron	-
IGF1R-214	ENST00000560343.1	343	No protein	Retained intron	-

Table 4-2: **List of *IGF1R* human transcripts**. The table lists down all 17 splice variants including their names, the transcript ID on the Ensembl database, the length of the transcript and whether or not it is protein coding. Highlighted in red are the five variants that are known to yield protein products. This information was accessed by searching the Ensembl database for the *IGF1R* gene with the reference 'ENSG00000140443' (Aken et al., 2016). CCDS = consensus coding sequence

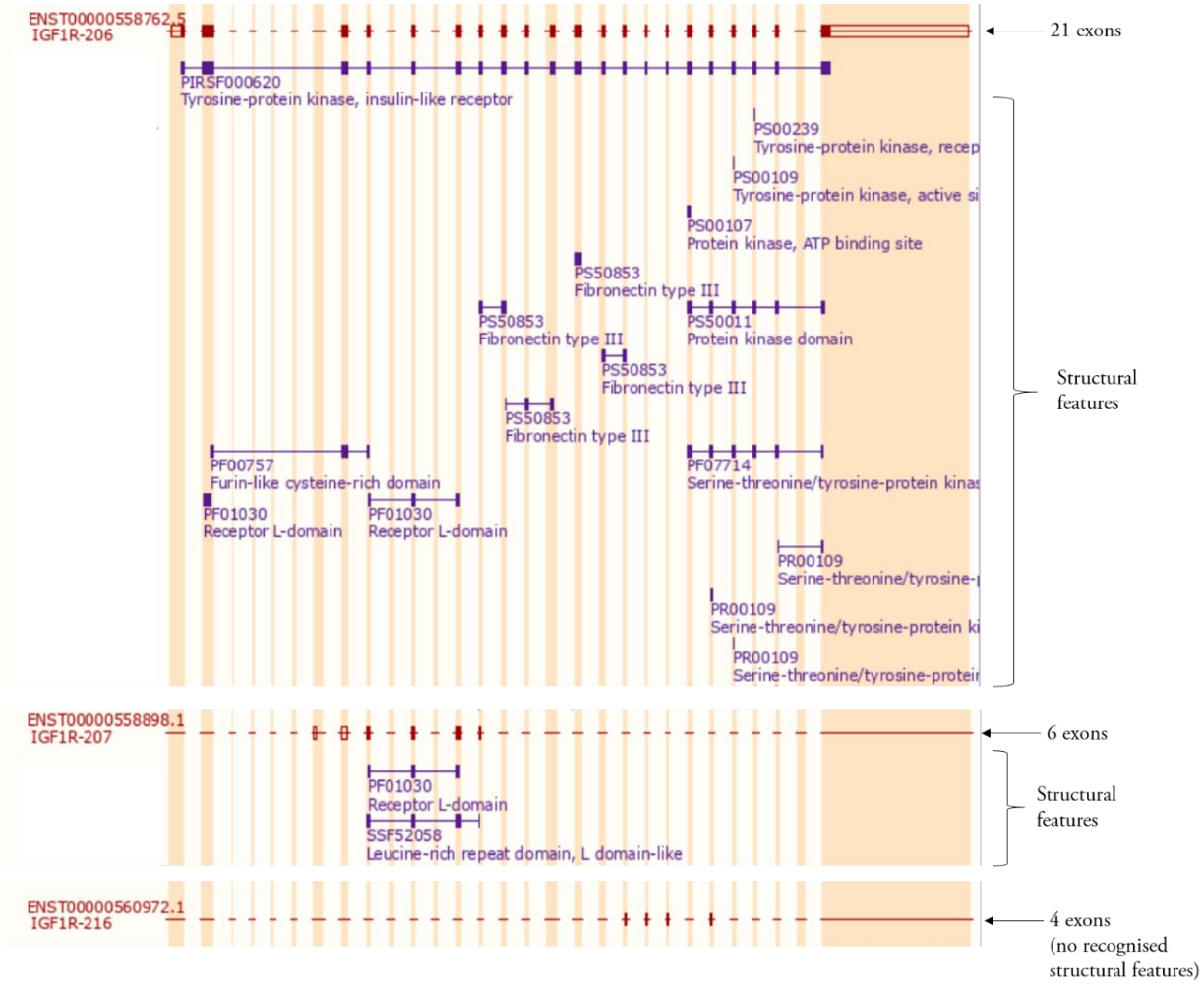


Figure 4-3: **Graphical representation of three protein-coding *IGF1R* splice variants**. Three transcripts are represented including the number of exons retained. In addition, structural features encoded by the exons that constitute each individual splice variant are indicated in blue as per the information on the Ensembl database (Aken et al., 2016). The full list of the five IGF-1R protein-coding variants can be found in appendix 8.3.

Since the CRISPR/Cas9 technique relies on the likelihood of one or more premature stop codons arising within a coding sequence as a result of indels, it was paramount that we confirmed whether a -1/+1 or -2/+2 frameshift in the reading frame would cause stop codons to arise prematurely using the software programme SerialCloner (version 2.6.1). Frameshift analyses indicated that a -1/+1 frameshift mutation would yield 3 premature

stop codons within exon 2 whilst a -2/+2 frameshift mutation should yield 5 stop codons within the same exon. This further confirmed that exon 2 of the *IGF1R* gene was a valid target for CRISPR/Cas9 genome editing because the presence of stop codons within exon 2 would result in a truncated protein lacking important functional features.

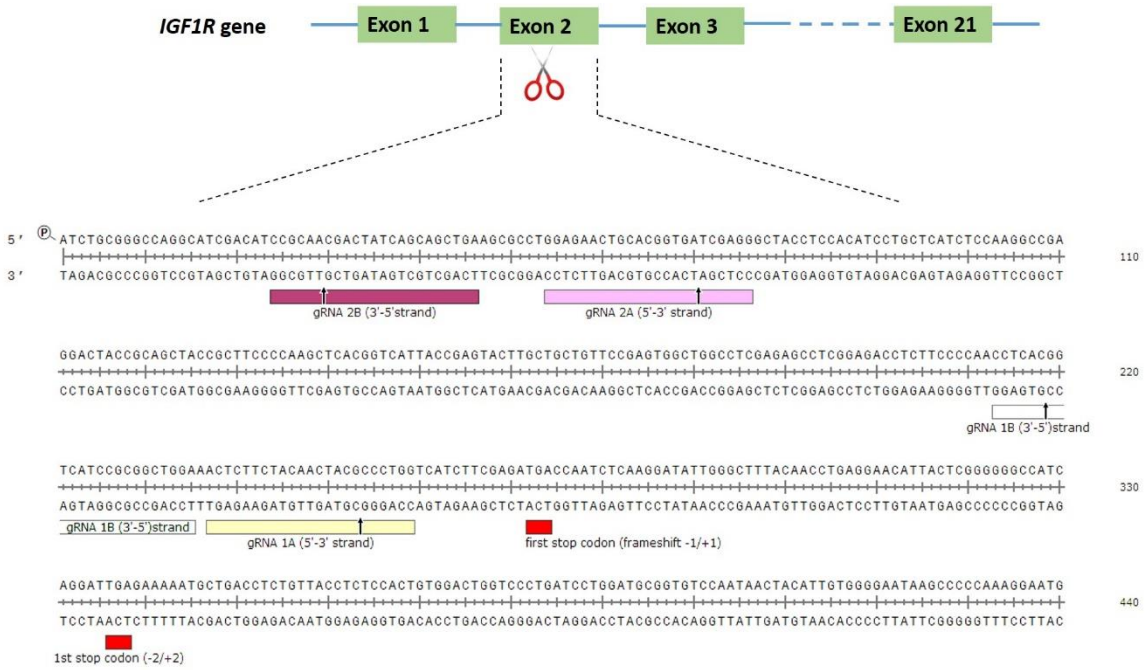


Figure 4-4: **Map showing predicted stop codons as a result of indels**. The human *IGF1R* DNA sequence encoding for a portion of exon 2 (<500bp) was uploaded onto the SnapGene viewer software in order to visualise complementary sequences to all four of the selected gRNAs (gRNAs 1A, 1B, 2A, 2B in colourful rectangles). Alongside each specified gRNA, we have indicated in brackets the orientation of the DNA strand that harbours the sequence identical to that of each individual gRNA which corresponds to the non-complementary target sequence. The upward-facing black arrows indicate the expected cleavage site of the wild-type Cas9 nuclease depending on the gRNA. The red boxes highlight the location of the first premature stop-codon according to the frameshift mutation that would occur.

4.2.2. gRNA validation

Validation of designed gRNAs consists of evaluating the efficiency of each individual gRNA to direct the Cas9 nuclease to the targeted DNA sequence. Base-pairing between the gRNA and the complementary DNA sequence allows the nuclease to cut the target and the DNA fragments can be detected on agarose gel by electrophoresis. This is a multi-step

process referred to as ‘the surveyor assay’ and has been described in greater details in the Materials and Methods chapter of this thesis (see section 2.14).

HEK293T cells were transfected with non-replicating plasmid DNA (PX458) into which the *Cas9* gene, one of the four selected gRNA and the *GFP* gene had been cloned. GFP expression was used as a marker of transfection and by quantifying the percentage of GFP-expressing HEK293T cells 72 hours after transfection, we were able to calculate the efficiency of transfection in these cells. This was particularly important because an above average percentage would allow us to run the surveyor assay without prior sorting for GFP-expressing cells only. To identify live cells, transfected HEK293T were stained with propidium iodide prior to conducting flow cytometry and non-transfected HEK293T cells were used as controls.

The results showed that plasmid transfection caused significant cell death in HEK293T as the proportion of dead cells post-transfection was 6 times more than that observed in the control (32% vs 5.7% respectively) (Figure 4-5). As expected, virtually no GFP expression could be detected in non-transfected cells whilst the percentage of GFP-expressing live cells was 62% in HEK293T cells transfected with the gRNA containing PX458 (PX458-gRNA) plasmid (Figure 4-5). Such level of transfection efficiency allowed us to perform a surveyor assay without prior sorting for GFP-expressing cells only. Thus, we proceeded with designing primers that would be used to amplify the region around the gRNA target site.

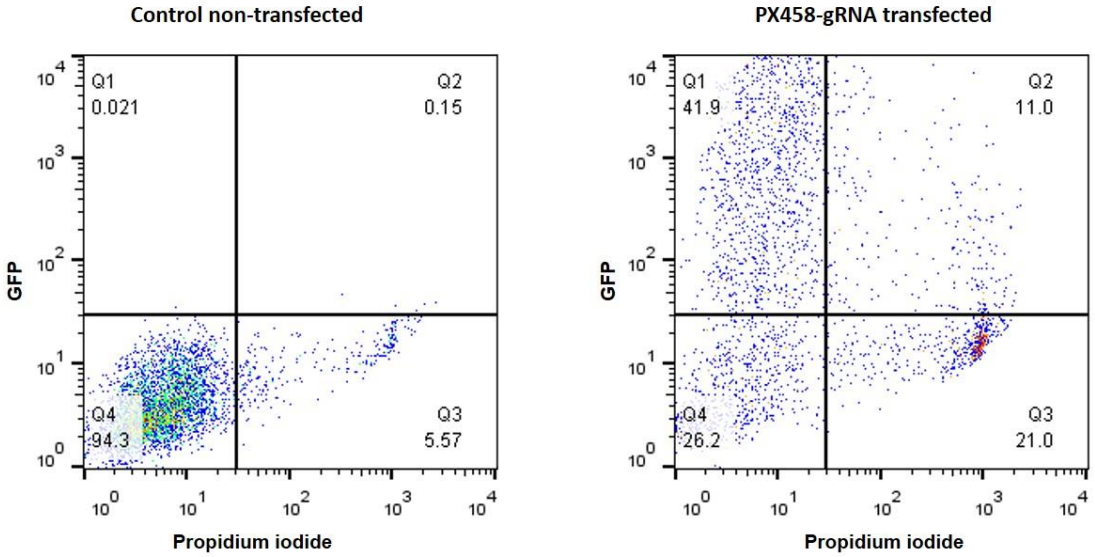


Figure 4-5: **Efficiency of plasmid transfection in HEK293T cells**. HEK293T cells were seeded in 6 well plates and either transfected the next day with plasmid DNA containing gRNA-2B (PX458-gRNA2B) or not. Cells were harvested 72 hours after transfection and stained with Propidium iodide. Flow cytometry results were analysed with FlowJo and cell events were segregated into four separate quartiles: Q1 = GFP positive, PI negative; Q2 = GFP positive, PI positive; Q3 = GFP negative, PI positive; Q4 = GFP negative, PI negative. The percentage of transfection efficiency was calculated as: [Q1/(Q1+Q4)]*100.

Primer pairs spanning the target DNA sequence for each individual gRNA were generated using Primer-BLAST (National Centre for Biotechnology Information, USA) and used in PCR reactions with the goal to amplify that genomic region and use the PCR products in subsequent reactions. PCR reactions containing primer pairs SP1, SP4 and SP8 designed to amplify the genomic region containing sequences complementary to gRNA-1B, gRNA-2A and gRNA-2B yielded PCR products. PCR products from transfected cells obtained with each individual primer pairs were hybridised with the same corresponding genomic region amplified from HEK293T non-transfected cells (wild-type DNA). The DNA duplexes were then digested with the CEL nuclease and the digestion products were loaded onto agarose gel where these DNA products were separated by electrophoresis.

As controls, we used duplexes formed as a result of the hybridisation between two homologous wild-type DNA sequences and also included controls C and G from the

surveyor kit to help confirm that the enzyme used had nuclease activity. Controls C and G are similar DNA sequences with one nucleotide difference which results in a mismatch when the two sequences are hybridised to each other.

From the top gel image, we noticed that the mismatch between the kit controls was recognised by the CEL nuclease as it can be deduced from the additional 2 bands that did not appear when C+C homoduplexes were treated with the nuclease, nor when C+G heteroduplexes were not treated with the nuclease (Figure 4-6). It was inferred from these results that the CEL nuclease specifically cleaved duplexes at sites of mismatches. Additional DNA bands also appeared for heteroduplexes from genomic regions amplified by primers SP1 and SP4 that were treated with the nuclease but not from amplification products with the SP8 primer; implying that cells transfected with plasmid containing gRNA-1B did not undergo genome editing by Cas9 which subsequently led to the absence of mismatches between DNA from transfected cells and the wild-type (Figure 4-6). In contrast, the image showed that cells transfected with gRNA-2A and gRNA-2B contain indels within the region amplified by the SP4 primer, recognised by the CEL nuclease.

Consistent with the fact that the target sequences within exon 2 for each individual gRNA differ, CEL nuclease processing yielded different DNA fragment sizes implying that as expected, the Cas9 cleavage site is specific to each gRNA (Figure 4-6). Having confirmed that both gRNA-2A and gRNA-2B were able to effectively direct Cas9 to their target region in the genome, we sought to determine which of the two was the most efficient.

To do so, the common practice is to ascertain by eye the intensity of the bands generated following CEL nuclease processing. It is generally assumed that the stronger the band intensity, the more effective the gRNA is because it is reasoned that the band intensity strength should reflect the amount of DNA heteroduplexes containing mismatches which

in turn would indicate a greater amount of transfected DNA harbouring indels. From the gel image, we were able to ascertain that gRNA-2A was the better guide as the bands generated as a result of CEL nuclease digestion appeared less fuzzy (Figure 4-6). Moreover, because no mismatch was detected from the duplexes formed between DNA from PX458 (empty vector – no gRNA) transfected cells and wild-type DNA, we concluded from these experiments that in addition to the fact that the Cas9 cleavage site was gRNA-dependent, the cleavage activity of the Cas9 nuclease required a guide RNA (Figure 4-6).

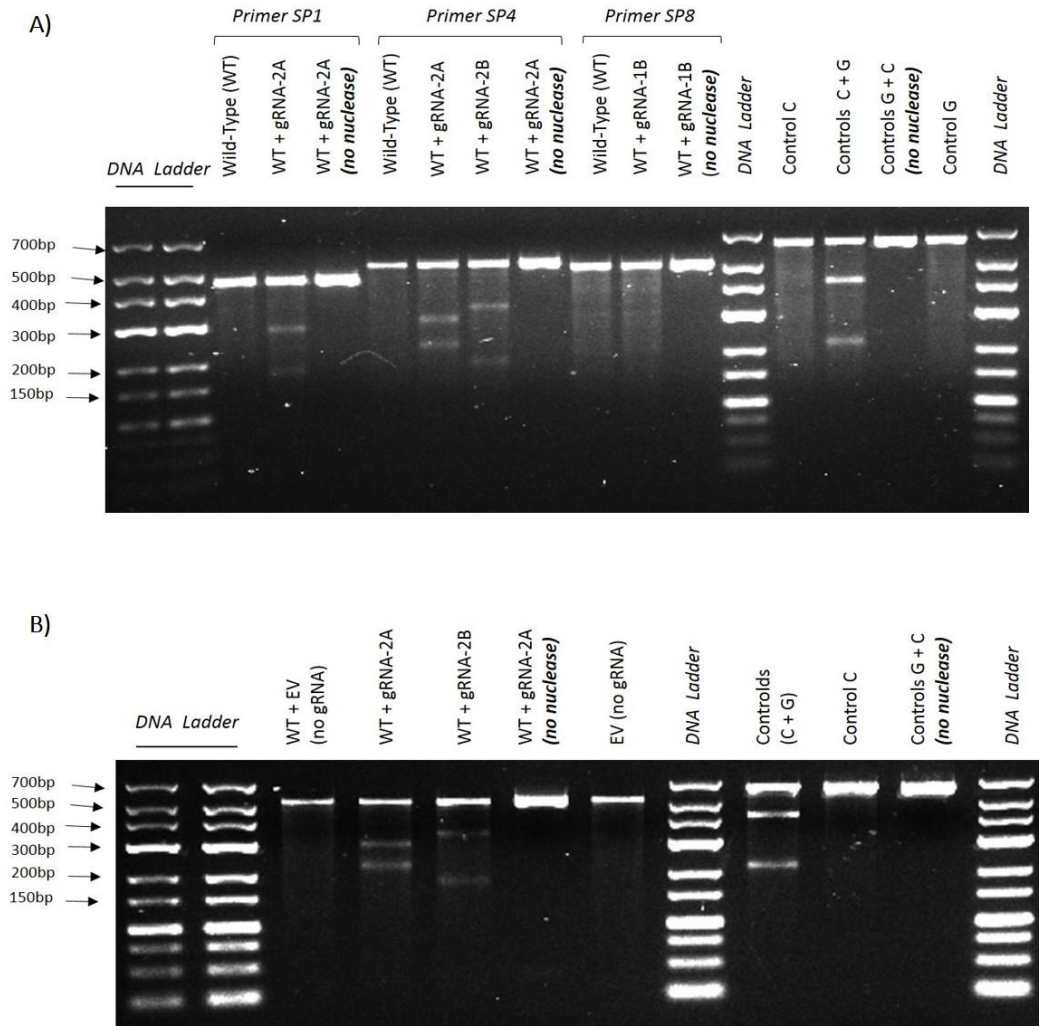


Figure 4-6: **Surveyor Assay - validation of selected gRNAs**. HEK293T cells were transfected with PX458 (empty vector – EV, no gRNA) or PX458-gRNA1B/2A/2B or not transfected (wild-type – WT). Genomic DNA was isolated from the transfected and non-transfected cells of which 150ng/µL were used in the PCR reaction aimed at amplifying the DNA sequence spanning each individual gRNA target site with primer pairs SP1, SP4, SP8 (**A**) or SP4 only (**B**). PCR products were mixed to form DNA duplexes and then either treated with the Surveyor CEL nuclease or not. The reaction product after nuclease treatment was loaded on agarose gel for detection and DNA fragments were separated by electrophoresis. Note: Genomic DNA for controls C and G were obtained from the Surveyor assay Kit.

4.3. Characterisation of IGF-1R mutant U2OS cells

U2OS cells were transfected with the modified PX458 plasmid which had the gRNA-2A sequence cloned into; a process described in details in the Methods chapter (see section 2.14.1). Following transfection, GFP-positive cells were sorted then followed clonal

isolation and expansion. All steps have been described in the Methods chapter of this thesis (see section 2.17) so herein, we will only give a brief account.

4.3.1. Screening for IGF-1R knockout cells

Mutants lacking the IGF-1R protein were identified by immunofluorescence and western blotting. Immunofluorescence allowed us to screen for mutant clones showing little or no IGF-1R staining before confirming the observations by western blotting. As controls for IGF-1R protein expression, we included non-transfected U2OS cells that grew from a single clone. This was done so as to confirm that any lack of detectable IGF-1R at the protein levels could be confidently attributed to CRISPR/Cas9 mediated genome editing and not simply as a consequence of the various pressures during the process of clonal isolation and expansion that may have been applied to U2OS cells transfected with the gRNA2A-containing plasmid.

By western blotting, we tested six potential IGF-1R mutants that showed little or no IGF-1R staining by immunofluorescence. Interestingly, 50% of isolated potential mutant clones showed a band corresponding to the IGF-1R pro-receptor but no mature IGF-1R protein was detectable whilst the other 3 clones showed no band corresponding to the pro-receptor or the proteolytically processed protein (Figure 4-7). In contrast, both forms could be detected in the controls which showed the IGF-1R pro-receptor band (180kDa) and the mature IGF-1R (95kDa). This prompted us to conclude that whilst gRNA targeting of exon 2 had successfully abrogated protein expression in mutant clones 1, 3 and 4, the same event resulted in a different outcome for mutant clones 2, 5 and 6. We speculated that in the latter cases, indels in exon 2 could have caused 'in-frame' mutational changes within the *IGF1R* gene sequence that did not prevent mRNA translation but rather impeded on the processing of the pro-receptor protein into the mature IGF-1R. It is reported that the R739Q

mutation in exon 11 of the *IGF1R* gene results in impaired cleavage of the pro-receptor into the mature form of the receptor and might be causally-linked with intra-uterine growth retardation (Kawashima et al., 2005).

Noteworthily, there was no difference overall in the protein expression levels of the insulin receptor (INSR) between wild-type clones and the mutants (Figure 4-7). Although we see reduced INSR levels in the wild-type clone 4 and in the mutant clone 5, this did not appear to be correlated with IGF-1R protein expression. Most importantly, mutants lacking the IGF-1R protein either in its pro-receptor or mature forms do not show reduced or increased INSR levels compared to the controls. Thus we concluded that tampering with IGF-1R protein expression did not affect INSR expression.

In addition, when we looked at downstream signalling targets of the IGF-1R, there were some differences in AKT and ERK1/2 levels between the mutant and wild-type clones especially with the phosphorylated form of these proteins. Interestingly, whilst most mutants showed decreased phospho-AKT levels, some of them showed higher levels of phospho-ERK1/2 compared to the wild-type (Figure 4-7). Noteworthily, mutant clones showing the band corresponding to the IGF-1R pro-receptor showed higher levels of activated ERK1/2.

Since downstream signalling pathways associated with the IGF-1R was not completely abrogated in the mutants, we deduced that they might have developed alternative mechanisms of activation of these cellular pathways to sustain cell growth and proliferation.

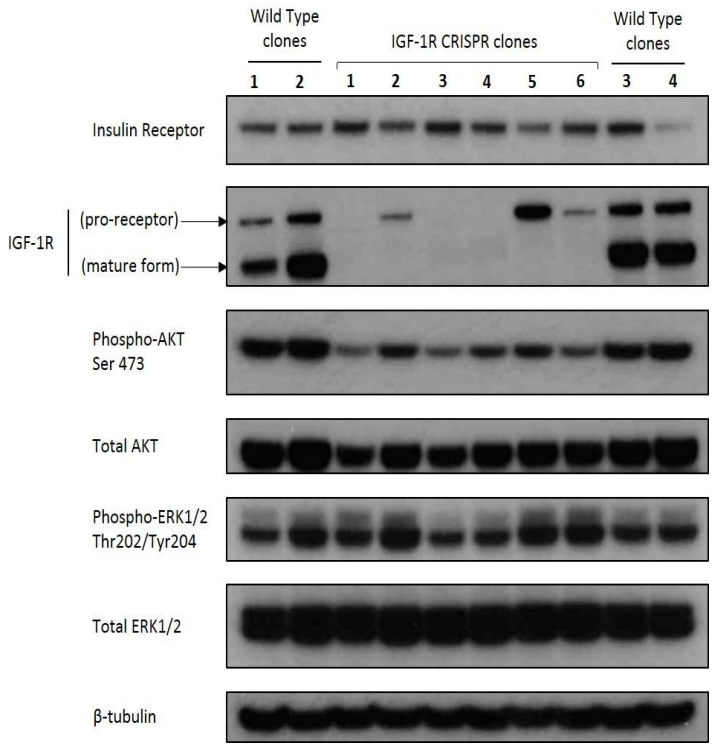


Figure 4-7: **IGF-1R protein levels in CRISPR-generated mutant clones**. Mutant and wild-type clonal cells were seeded in separate 10cm dishes and cultured in serum-supplemented DMEM growth medium until reached a confluency of ~70%. Cell lysates were prepared as described in section 2.4 of the Methods chapter and loaded on SDS-PAGE.

4.3.2. DNA sequence verification

Despite the puzzling occurrence of mutant clones showing detectable levels of the IGF-1R pro-receptor, we did not seek to determine whether the IGF-1R signalling pathway was still functional in these clones and they were excluded from subsequent experiments as we focused on the other three mutant clones which we will refer to as 'full' knockouts or mutant #1, #3, #4.

Next, we sequenced the DNA region spanning the gRNA-2A target site to check whether indels were introduced during the processing of Cas9-induced DNA breaks in mutant #1, #3 and #4. To achieve this, we used the EMBOSS Needle pairwise sequence alignment tool from The European Bioinformatics Institute (EMBL-EBI), comparing the sequence from full knockout clones to that of a wild-type clone.

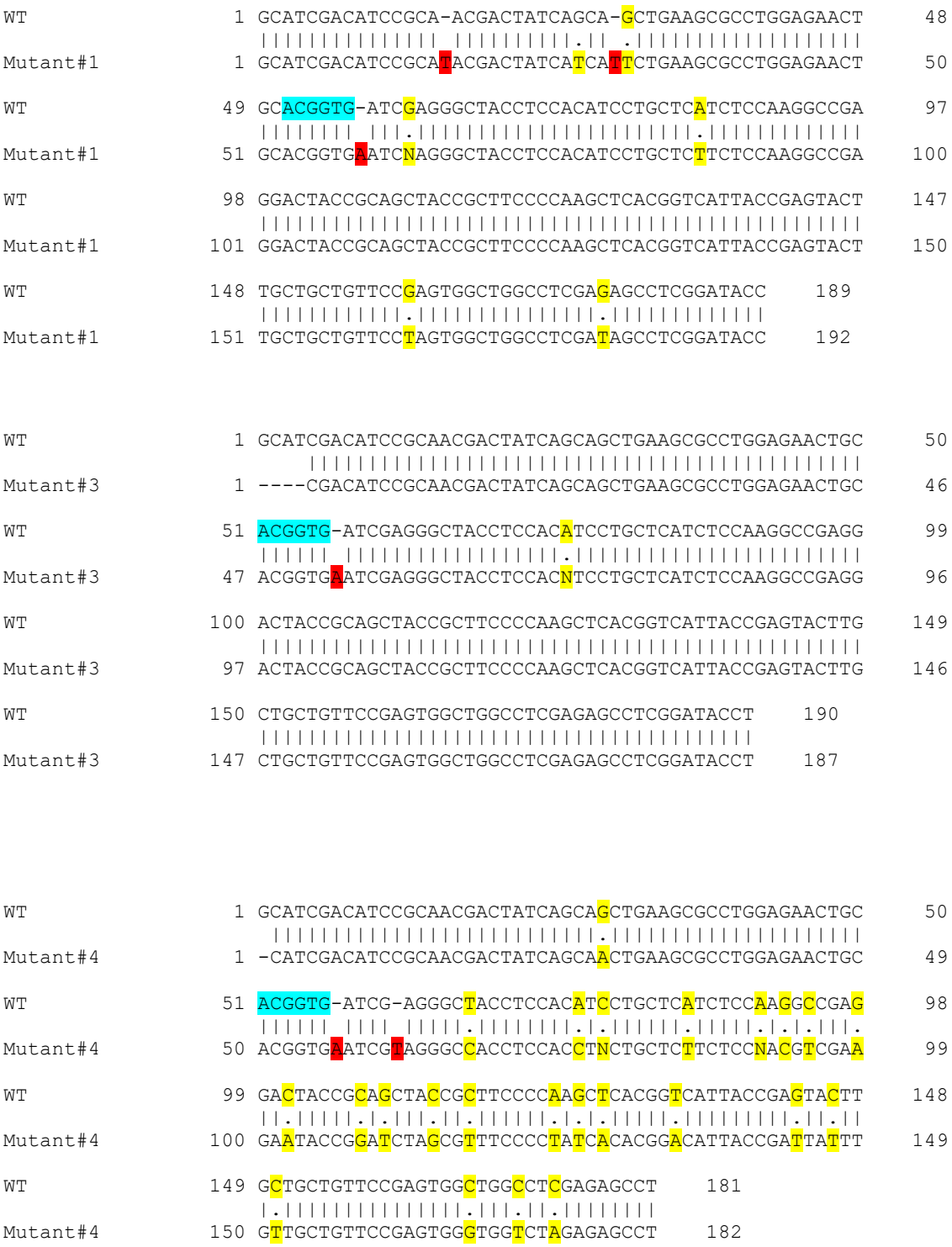


Figure 4-8: **DNA sequence alignment of IGF-1R mutants with wild-type**. DNA was isolated from a wild-type clone and each of the three 'full' IGF-1R knockouts. The DNA region spanning the gRNA target site was amplified by PCR using the primer pair SP4. The PCR product was sent for sequencing. Using the EMBOSS Needle pairwise sequence alignment tool from The European Bioinformatics Institute (http://www.ebi.ac.uk/Tools/psa/emboss_needle/nucleotide.html), DNA sequence from wild-type DNA was aligned to that of IGF-1R knockouts to identify regions of genomic differences. Highlighted in yellow are regions of nucleotide mismatches whilst red highlighted nucleotides indicate insertions. The five nucleotides preceding the predicted Cas9 cleavage site are highlighted in blue.

We observed no nucleotide deletions in the mutants but only insertions. Strikingly, at the predicted Cas9 cleavage site, all mutants harboured the same nucleotide insertion at the same position although the number of insertions varied from mutant to mutant. This was taken as confirmation that Cas9 targeting to exon 2 did indeed induce DNA breaks at that site which, upon repair resulted in additional nucleotide insertions. Only one nucleotide was additionally inserted in the gRNA-targeted DNA sequence for mutant clone 3 whilst mutant clone 4 showed 2 insertions and mutant clone 1 harboured 3 nucleotide insertions. Apart from these, there were many base mismatches located several base pairs away from the Cas9 cleavage site. We thought these might be due to genomic variations between gene copy numbers or most likely poor quality of the sequencing data.

4.4. Discussion

Altogether, based on western blot results, gRNA2A-mediated targeting of Cas9 to the second exon of the *IGF1R* gene in U2OS cells yielded mutant clones that do not express the IGF-1R protein. However, among the CRISPR-generated clones, we noticed that some showed a band of a molecular size corresponding to that of the IGF-1R pro-receptor. This prompted us to suggest that repair of Cas9-induced breaks in the DNA may have caused indels that did not disrupt full IGF-1R protein expression but rather resulted in gene sequence changes that could have hindered the proteolytic processing of the pro-receptor into its mature form of the protein. Since post-translational processing of newly synthesised proteins generally occurs in the endoplasmic reticulum (ER), it is possible that the synthesised IGF-1R pro-receptor is not trafficked to the plasma membrane wherefrom most known IGF-1R functions have been reported. Moreover, the IGF-1R pro-receptor lacks the functional abilities of the mature IGF-1R (Lehmann et al., 1998). Nevertheless, we thought it best not to work with these 'partial' knockouts to carry out our investigation in order to avoid any possible artefacts in subsequent experiments as the entire biology of IGF-1R is not thoroughly understood.

Three out of the six mutant clones were considered as 'full' knockouts because they did not appear to express IGF-1R in its mature or pro-receptor form. The genomic region flanking the gRNA targeted DNA was sequenced in order to examine the mutational changes that may have resulted from Cas9-induced DNA cleavage. Our results showed insertion within the sequenced region, resulting in +1 and +2 frameshift mutations in the mutants #3 and #4 respectively. These frameshift mutations, as detailed earlier in this chapter, were predicted to yield 3 or 5 premature stop codons within exon 2. Therefore, we were able to confirm with the DNA sequence that Cas9 genome editing led to abrogation

of IGF-1R protein expression in the mutant clones 3 and 4 as a result of frameshift mutations within exon 2 of the *IGF1R* gene. However, that a +3 frameshift mutation in mutant clone 1 generated a knockout was a puzzling occurrence which we were not able to fully explain. Because the first two insertions appeared several base pairs upstream of the predicted Cas9 cleavage site, we reasoned that these may not be 'CRISPR-induced' insertions and may simply reflect inherent sequence variations between copy numbers of the *IGF1R* gene in this clone.

Indeed, although some base mismatches observed in the mutants' DNA sequences can be attributed to the inaccurate repair of Cas9-induced DNA breaks, many of those occur at distal sites and could be due to intrinsic genomic variations and/or poor sequencing data quality. U2OS cells are generally categorised as triploid cells because most chromosomes have more than 2 copy numbers (Halling-Brown et al., 2012, Janssen and Medema, 2013). Hence, it would have been beneficial to assess the penetrance of the knockout phenotype in these mutants using such assays as TOPO-TA cloning to elucidate whether all or most gene copies harboured frameshift mutations leading to premature stop codons within exon 2.

5. Investigating the role of IGF-1R in the response to DNA damage induced by ionising radiation in U2OS

The link between IGF-1R function and radio-resistance has long been established thanks to a great body of experimental evidence and several epidemiological studies. However, we are yet to elucidate the mechanisms underlying this phenotypic observation. There is evidence, from studies carried out by our group in DU145 prostate cancer cells that, IGF-1R may play an important function in the repair of double-strand breaks induced by ionising radiation (IR) and we sought to elucidate if these findings could be replicated in other types of cancer cells. To help us interrogate the function of IGF-1R in the repair of IR-induced double-strand breaks in U2OS (osteosarcoma cell line), we have engineered IGF-1R mutants using the CRISPR/Cas9 technology. Out of the six mutant clones obtained, we selected out three which appeared to be 'full' knockouts (see section 4.3.1). We did not use partial knockouts because of the possibility that the presence of pro-IGF1R at the protein level may trigger unknown signalling pathways.

In this chapter, we will:

- Assess the validity of selected mutant clones as models lacking functional IGF-1R signalling by evaluating their response to ionising radiation.
- Evaluate the DNA damage response to irradiation in IGF-1R mutants.
- Investigate the mechanisms of radio-sensitisation in IGF-1R mutants.

5.1. IGF-1R and the DNA damage response to γ-irradiation

5.1.1. Testing the response to ionising radiation

Previous studies carried out in the Saos-2 osteosarcoma cell line showed that downregulation of IGF-1R using shRNA increased the sensitivity to ionising radiation (Wang et al., 2009). This, in addition to evidence that depletion or inhibition of IGF-1R in a number of cancer cell types was shown to promote radio-sensitivity (Riesterer et al., 2011, Rochester et al., 2005, Turney et al., 2012), prompted us to hypothesise that similar observations would be made in the mutated U2OS osteosarcoma cells lacking the IGF-1R protein. Hence, we tested the response of the mutant clones to 5Gy of γ-irradiation by assessing their proliferative ability in the colony formation assay. As controls, we used wild-type clones (WT 3 and 4).

In the absence of ionising radiation, the proliferative abilities of mutant clones seemed comparable to that of the wild-type (Figure 5-1). We noticed that the number of colonies did not differ significantly across the different clones and the average number of colonies was 407, 499, 349, 350, 352 for WT3, WT4, and IGF-1R knockout clones 1, 3 and 4 respectively. This was inconsistent with the data described in the previous chapter which showed that the basal activity of AKT in the IGF-1R mutants was reduced compared to that of the wild-type controls (Figure 4-7).

Ionising radiation significantly suppressed the proliferation of both wild-type and mutant clones (Figure 5-1). However, whilst mutants #3 and #4 showed significantly diminished proliferative abilities compared to the controls (wild-type U2OS cells), mutant #1 was surprisingly more resistant to ionising radiation than the controls. The average cell survival in irradiated mutant #1 was 15%, twice that of the wild-type controls which was 6% and

7% for WT3 and WT4 respectively. In comparison, the cell survival for the other two mutant clones following irradiation was more than 5x lower than that of their mutant counterpart (Figure 5-1).

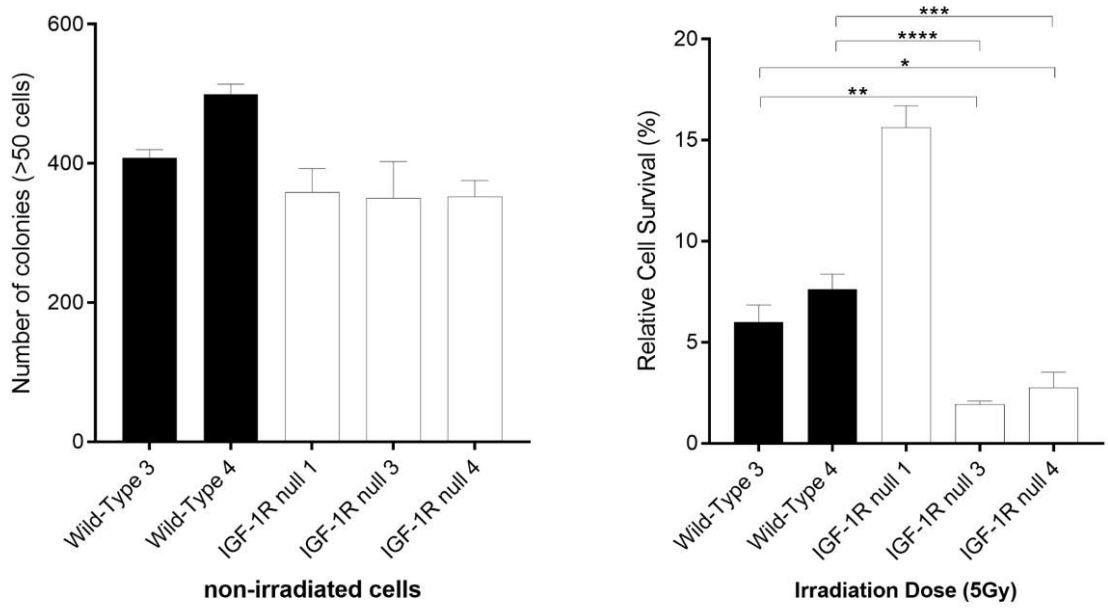


Figure 5-1: **Differential response of the IGF-1R knockouts to ionising radiation**. Wild-type and knockout cells were seeded in triplicates in 6-well plates and either irradiated the next day with 5Gy or not. The number of colonies per well was determined 9-10 days after seeding using the GelCount colony counter (Optotronix, Oxford). The percentage of cell survival for mutants and wild-type clones was calculated in proportion to the number of colonies that grew under conditions of no irradiation. The graph was plotted with GraphPad Prism as mean ± standard error of the mean (SEM). Statistical significance was calculated by one-way ANOVA using Prism (p-value <0.05). These are results compiled from three independent experiments.

Such variability among 'full' knockout clones was interesting and, considering that activation of the AKT pathway has been linked with radio-resistance (Gupta et al., 2002, Kim et al., 2006, Toulany and Rodemann, 2015, Oeck et al., 2017, Li et al., 2009), we tested whether phosphorylated AKT (ser473) levels differed between mutant #1 and the wild-type controls in response to irradiation. Our results showed that AKT activity in the wild-type was greater than that observed in all three mutant clones (see Figure 8-2 in appendix 8.4.2); thereby suggesting that AKT activity may not account for the distinctive radio-resistant phenotype displayed by mutant #1. But we did however noticed that ERK1/2

phosphorylation occurred at an earlier timepoints in the more radio-sensitive null mutant clones #3 and #4 compared to the wild-type and radio-resistant mutant clone #1. Nevertheless, the phenotype observed in mutant #1 in response to irradiation makes it difficult to know the true effect of IGF-1R loss. Although, two of the three 'partial' IGF-1R mutant clones that lacked only the mature form of the IGF-1R but expressed the pro-receptor were also shown to be more radio-sensitive than the wild-type clones (see Figure 8-1 in appendix 8.4.1).

We decided to conduct subsequent experiments solely with the two mutants that showed enhanced sensitivity to ionising radiation with calculated dose enhancement ratio values of 3.6 and 2.4 for IGF-1R mutant clones 3 and 4 respectively.

5.1.2. Assessing the activation of the DNA damage response

Irradiation yields several toxic products in the cell among which the most cytotoxic are thought to be DNA double-strand breaks (Lomax et al., 2013, Vamvakas et al., 1997). As detailed in Chapter 1, ATM/ATR activation and the downstream signalling are key for mounting the appropriate response to IR-induced DNA double-strand breaks and ensure that these are repaired (Polo and Jackson, 2011, Thompson, 2012). Because previous studies have suggested a link between functional IGF-1R and ATM activation in the response to ionising radiation (see section 1.3.2.3), we hypothesised that mutants #3 and #4 might show impaired activation of ATM signalling which could result in delayed resolution of γH2AX foci.

To assess this, we irradiated the most radio-sensitive IGF-1R knockout (mutant #3) and wild-type (WT4) cells with 5Gy in order to monitor ATM activation and that of other downstream signalling components known to play a role in the response to ionising

radiation at different time-points over the course of 50 hours. The time-points were decided based on the work from others investigating ATM signalling following exposure to ionising radiation (Goodarzi et al., 2008).

Under normal growth conditions, wild-type U2OS cells did not show detectable levels of ATM in its auto-phosphorylated form (Figure 5-2). Upon exposure to ionising radiation, phospho-ATM levels rose dramatically, peaking at 30 mins post-IR before decreasing back to near basal levels 24 hours after irradiation. We noticed that the expression level of phospho-ATM at 50 hours post-IR was 3x higher than that at the 24-hour time-point (Figure 5-2). This late increase may be attributed to ATR-mediated activation of ATM signalling as a result of the conversion of unrepaired single-strand breaks into double-strand breaks upon encountering a replication fork (Maréchal and Zou, 2013). Just as with the wild-type, we noticed a dramatic increase in the levels of active ATM (pSer1981-ATM) in the first 30 minutes that followed irradiation of the knockout (Figure 5-2). However, whereas phospho-ATM levels quickly reduced towards basal levels in the wild-type, the recovery was much slower in the knockout (Figure 5-2). Moreover, in contrast to the wild-type, we were able to detect minimal levels of phosphorylated ATM in the non-irradiated knockout.

Within the first 30 minutes that followed irradiation of wild-type cells, ATM protein levels went up to levels almost 2x that observed under basal conditions (Figure 5-2). These changes in ATM levels in response to ionising radiation may have resulted from transcriptional changes, increased stability of the protein and mRNA transcripts or a combination of all. The IGF-1R mutant, in contrast, did not show increased ATM levels in response to IR-induced damage. But, we did notice a slow reduction in ATM protein levels in the hours that followed irradiation (Figure 5-2). Interestingly, under basal conditions, ATM levels in the knockout were almost twice that of the wild-type under the same conditions (Figure 5-2).

Consistent with evidence that IR-induced ATM activation leads to p53 accumulation (Fei and El-Deiry, 2003), we noticed from the wild-type that p53 levels increased sharply in response to ionising radiation, peaking 6 hours after irradiation with the expression levels almost 9x greater than that observed under basal conditions (Figure 5-2). Although p53 levels in the knockout were 5-fold lower compared the wild-type under basal conditions, ionising radiation also led to increased stability of the protein and we calculated a 10-fold increase in the knockout compared to ~7-fold in the wild-type in p53 levels at 30 mins post-IR (Figure 5-2). In contrast to the wild-type, the IR-induced p53 accumulation reached its highest level at the 2-hour time-point in the knockout when the levels were 31-fold higher than the basal levels and 3x higher than the levels at 30 mins after irradiation. Such dramatic fold increase was not observed in the wild-type where the fold-difference was only 8-fold between peak levels and basal p53 levels (Figure 5-2). Nevertheless, it was intriguing that despite considerable changes in p53 levels in the knockout after ionising radiation, they were still lower than that of the wild-type at each specific time-point. There was a striking difference in the pattern of recovery towards basal p53 levels between the wild-type and the knockout with the latter showing faster recovery (Figure 5-2). However, this was not observed in a recently conducted experiment wherein irradiation-induced p53 accumulation persisted up to 24 hours post-irradiation in mutant #3 to levels comparable to that of wild-type #4 (Figure 8-2).

Another downstream target of ATM is, chromatin remodeller KAP1 which also showed increased phosphorylated levels detected 30 minutes after ionising radiation (Figure 5-2). In response to ionising radiation, the 32-kDa subunit of the RPA protein becomes hyper-phosphorylated by ATM and ATR to promote DNA repair. However, the Ser33 phosphorylation site is largely attributed to ATR which is activated in response to IR-induced replication stress and is also responsible for the activation of the cell cycle

checkpoint protein CHK1 in order to provoke G2/M cell cycle arrest (Marechal and Zou, 2015, Binz et al., 2004). In accordance with this, we observed RPA phosphorylation in response to irradiation in both knockout and wild-type cells. Phospho-RPA levels seemed to steadily increase from their basal levels following irradiation, peaking at the 24-hour time-point (Figure 5-2). We also sought to determine whether the ATM-CHK2 pathway was not compromised in the mutant by probing for the phosphorylation of CHK2 kinase on Threonine 68 by western blot but were beset with technical difficulties despite several attempts (Figure 8-2).

Our data revealed a sharp increase in phosphorylated levels of the ATR target CHK1 in response to ionising radiation which was noticeable from 30 mins after irradiation in both wild-type and knockout cells (Figure 5-2). The levels of double-strand break marker γH2AX (pSer139-H2AX) rose dramatically within the 30 minutes that followed ionising radiation before steadily decreasing to near basal levels (Figure 5-2). The same trend in γH2AX levels was observed in the wild-type and knockout throughout the course of the experiment, suggesting that the IGF-1R mutant might not be defective in the induction or resolution of γH2AX foci following exposure to ionising radiation.

Altogether, our results showed that ATM activation, CHK1 induction and histone H2AX phosphorylation at Ser139 as key events of the cellular response to IR-induced DNA damage were neither delayed nor impaired in the IGF-1R mutant. This led us to conclude that DNA damage sensing mechanisms were active and unhindered in the IGF-1R mutant. We noted however that ATM activation persisted for longer in the mutant and that basal ATM levels were significantly higher. This may pinpoint a possible link between IGF-1R signalling and the regulation of ATM expression and activated levels. Although this has been proposed by others, our results are in conflict with previous suggestions that IGF-1R

is required for ATM activation in response to ionising radiation (Macaulay et al., 2001, Peretz et al., 2001).

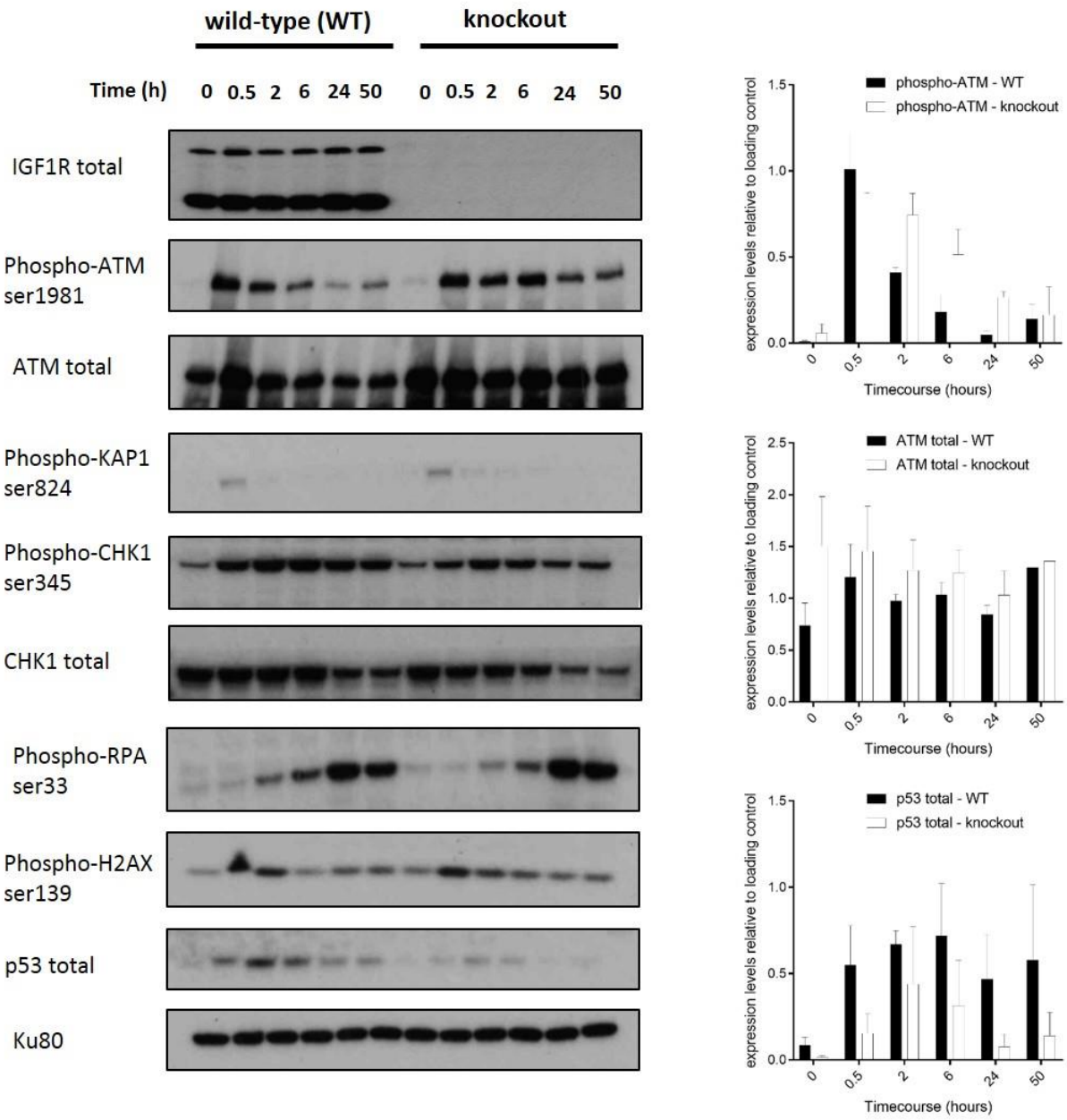


Figure 5-2: **DNA damage signalling induced in response to ionising radiation**. Cells were seeded in 10cm culture dishes and irradiated the next day with 5Gy. Cells were lysed at the indicated time-points after irradiation. The non-irradiated cells (0h) were lysed at 0.5h post-irradiation. The lysates were prepared for western blotting as described in the Methods chapter (section 2.4). Expression levels were quantified using ImageJ and graphs were plotted on GraphPad Prism as mean ± SD. This result represents data obtained from two independent experiments.

5.1.3. Evaluating γH2AX focus formation and resolution in response to ionising radiation

Routinely used in investigations as a marker of double-strand break damage in mammalian cells following exposure to ionising radiation, the method of choice to visualise and track γH2AX focus formation is by immunofluorescence. This is because γH2AX can also be detected in apoptotic cells. Imaging damaged but non-apoptotic nuclei thus gives the opportunity to quantify repair-associated IR-induced γH2AX levels more accurately (Ivashkevich et al., 2012, Kuo and Yang, 2008).

For this reason, despite observing no differences in γH2AX levels by western blot detection, we decided to check for potential differences in post-IR γH2AX levels between the wild-type clones and the IGF-1R mutants by immunofluorescence microscopy. These were irradiated with 5Gy and fixed at 2, 24 and 72 hours afterwards. Cells were stained with antibodies that recognise the phosphorylated Ser139 residue on the histone H2AX protein. To determine the basal levels of γH2AX, we used non-irradiated cells collected and fixed at the same time as cells that were irradiated and collected 2 hours after IR exposure.

Under conditions of minimal damage (endogenous only), very few nuclear γH2AX foci (3-4) could be observed in both the wild-type and mutant clones (Figure 5-3). Upon irradiation, the number of γH2AX foci increased dramatically as the levels at the 2-hour peak were ~8 times higher than basal levels for the wild-type group (WT3 and WT4) and the IGF1R mutant #4, and only ~5.5-fold higher for the IGF1R mutant #3 (Figure 5-3). By 24 hours after irradiation, γH2AX foci levels had dropped considerably to levels now only 4-fold greater than the basal levels. We continued to observe resolution of γH2AX foci 72 hours

after irradiation. Surprisingly though, the γH2AX foci count had not returned to basal levels yet. The average foci count was 9-10 across both wild-type and mutant groups (Figure 5-3).

Since both wild-type and mutants cells displayed the expected response to ionising radiation with γH2AX foci levels peaking within the first 2 hours following irradiation and subsequently decreasing to near basal levels afterwards (Figure 5-3), we deduced that the NHEJ pathway, which has been described as the first line of response to double-stranded breaks caused by ionising radiation, was likely functional not only in the wild-type but also in the mutant cells (Mahaney et al., 2009, Jeggo and Lobrich, 2006). Moreover, as there were no striking differences between the wild-type and the knockouts in the levels of γH2AX throughout the entire timecourse (Figure 5-3), our results pointed us to the conclusion that the permanent abrogation of IGF-1R signalling in U2OS cells did not hinder the sensing of IR-induced double-strand breaks. Furthermore, the lack of the IGF-1R protein did not cause any delay in the resolution of γH2AX in U2OS cells (Figure 5-3); encouraging us to find out whether other mechanisms might be responsible for the enhanced sensitivity of these IGF-1R mutants to ionising radiation.

Considering that protein expression levels of p53 were reduced in IGF-1R mutant #3 and that IR-induced p53 accumulation lasted a shorter time in this mutant compared to the wild-type (Figure 5-2), we hypothesised that although double-strand break repair pathways may be intact in these mutants, they might show defects in cell cycle checkpoint activation. Therefore, we next assessed the cell cycle checkpoint integrity in IGF-1R knockout cells.

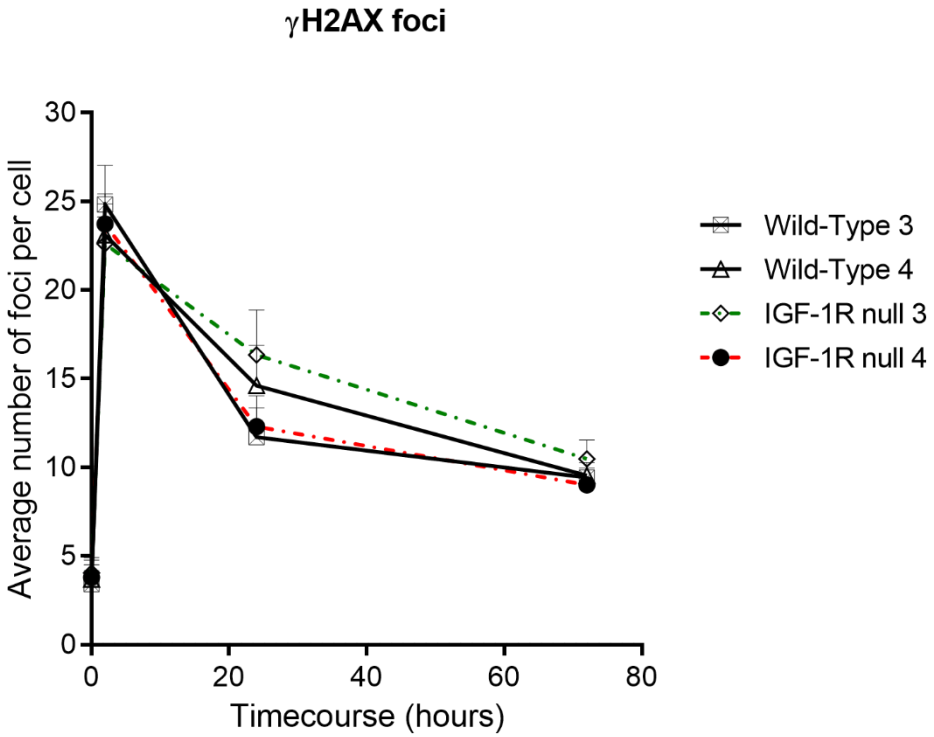


Figure 5-3: **Timecourse of induction and resolution of IR-induced γH2AX foci**. Cells were seeded in triplicates in 96-well plates and irradiated the next day with 5Gy. Cells were then collected and fixed at the time-points 2, 24 and 72 hours after irradiation. The non-irradiated cells (0h) were fixed at 2h post-irradiation. The cells were stained for γH2AX and DNA (Hoechst). Over 50 cells were counted per condition per time-point using the foci counting program on the In Cell Analyser 2000. The graph was plotted using GraphPad Prism as mean±SEM. This result presents data obtained from three independent experiments.

5.1.4. Assessing the cell cycle checkpoint integrity in the IGF-1R mutant

IR-induced double-strand breaks trigger a series of signalling events including CHK1 and p53 activation that promote cell cycle arrest at the G1/S, S and G2/M transitions in order to ensure that the cell has enough time to adequately repair damage in the DNA (Bunz et al., 1998, Agarwal et al., 1995, Liu et al., 2000, Sorensen et al., 2003). We did not expect to see a G1/S cell cycle arrest in these cells because the U2OS cell line is hemizygous for the *CDKN2A* gene which codes for the G1/S cell cycle regulator $p16^{INK4A}$ (Ottaviano et al., 2010).Using the BrdU labelling method, we determined the effects of irradiation on the cell cycle distribution in the wild-type (WT4) and the knockout (mutant #3). Irradiated cells

were collected at 10, 22 and 72 hours following irradiation. As controls for changes induced by ionising radiation, we used non-irradiated cells.

In the absence of ionising radiation, there were minor differences between the cell cycle distribution of the wild-type and to that of the knockout throughout the entire timecourse (Figure 5-4). At the 10-hour and 22-hour time-points, we noticed that the largest proportion of cells were in the S phase whilst the proportion of G2 cells was the lowest. However, 50 hours later, there were more cells in G1 than in the S phase indicating that cells that were in the S phase at the previous time-point progressed through the G2 phase, mitosis and back into G1; suggesting that the cell cycle progression proceeded unhindered in the mutant just as with the wild-type (Figure 5-4).

Compared to non-irradiated cells, the cell cycling pattern in irradiated cells was different; ionising radiation induced a late-G2/M cell cycle arrest in the wild-type and the IGF-1R mutant (Figure 5-4).

At 10 hours after irradiation, most cells were in the S phase, a much smaller percentage in G2 and even fewer in G1. This could be the result of intra-S phase checkpoint activation as the proportion of cells in G1 in the irradiated group is significantly smaller than that observed in the non-irradiated and there was overall a 15% difference in the proportion of S cycling cells between the two groups. Twelve hours after this time-point, the tendency shifted considerably and we noticed an accumulation of cells in G2 as the average percentage of cells significantly increased from 17% to 41% and 18% to 45% for the wild-type and the mutant respectively (Figure 5-4).

This late occurrence of G2 accumulation in response to ionising radiation is generally attributed to damaged S cells that have entered G2 without repairing the DNA damage and therefore become arrested in G2 to prevent them from undergoing mitotic catastrophe.

G2/M checkpoint activation in the mutant did not support our hypothesis that these cells might display defects in cell cycle checkpoints activation compared to the wild-type because they showed reduced and a rapid decrease of p53 levels after irradiation. However, we speculated that owing to the short-lived accumulation of p53 in response to ionising radiation, G2 accumulation in the mutant might be a transient event. Therefore, we extended our observation of the cell cycle distribution a further 50 hours after the 22-hour time-point.

At 72 hours post-IR, we observed that contrary to our expectation, G2/M cell cycle arrest was sustained in the mutant and yet again, there were no differences in the cell cycle distribution when compared to the wild-type. Nevertheless, compared to the distribution at the previous time-point, the average percentage of cells in the S phase decreased by 19% and 22% whereas the proportion of G2 cells increased by 12% and 16% for the wild-type and the mutant respectively (Figure 5-4). There was also a small increase in the proportion of cells in G1 which prompted us to think that some cells that were previously in G2 cycled back into G1.

From the cell cycle distribution experiments, we found no evidence that the activation of IR-induced G2/M cell cycle checkpoint was defective in the IGF-1R mutant. There were no pattern differences between the irradiated mutant and the irradiated wild-type except that, similar to what was observed in the absence of irradiation, the population of irradiated mutant cells in G1 was consistently smaller than that of the control, and the difference was the more striking at 22 hours after irradiation. This could be due to cells failing to re-enter the cell cycle either as a result of apoptosis or senescence following G2/M arrest. Indeed, it has been reported that depending on the intensity of the stress stimuli, the level of damage induced and intrinsic cell-type properties, the outcome of a p53-mediated cell cycle arrest in response to ionising radiation can vary (Murray-Zmijewski et al., 2008). Therefore, we

sought to uncover the intrinsic transcriptomic and metabolic changes in the mutant that might influence the cell's decision to undergo either senescence, apoptosis or recovery.

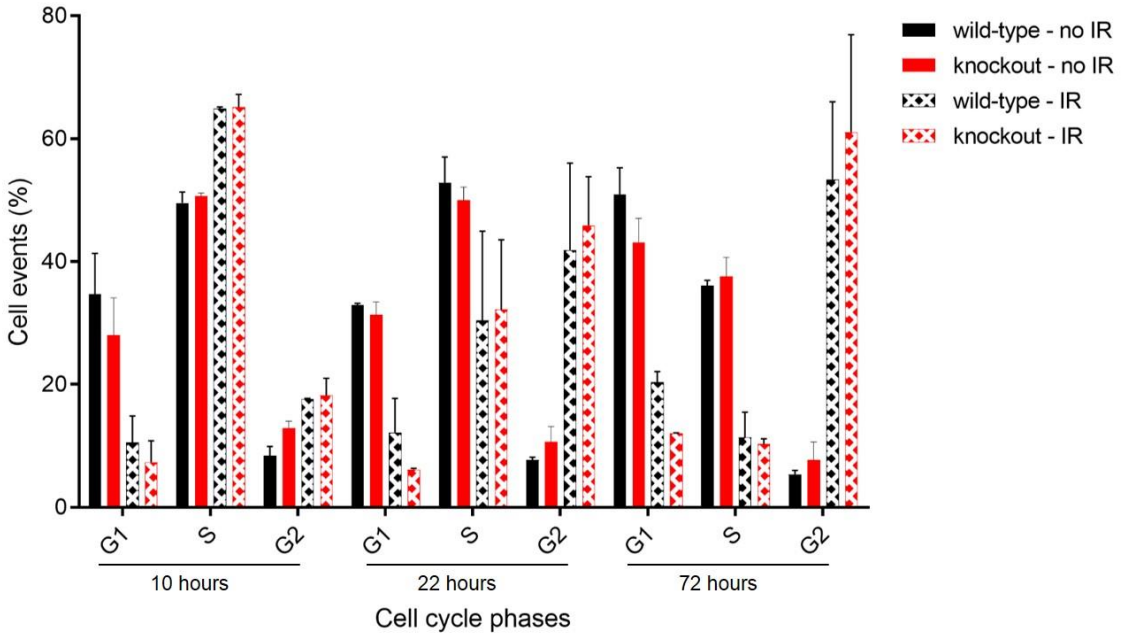


Figure 5-4: **Ionising radiation induces late G2-M accumulation in the wild-type and the knockout.** Cells were seeded in 10cm dishes and either irradiated the following day (IR) or not (no IR). Prior to harvesting at indicated time-points, cells were pulse-labelled with BrdU (10μM). Propidium iodide was used to stain the DNA after cell fixation. Flow cytometry data were analysed using the Flowjo software to determine the percentage of cells in each cell cycle stage. Graphs were plotted using GraphPad Prism as mean ±SD. This result presents data obtained from two independent experiments. See cell cycle raw data in section 8.2.3.

5.2. Transcript profiling of wild-type U2OS and IGF-1R mutants

We performed gene expression profiling in order to gain a global overview of the intrinsic cellular changes that may predispose IGF-1R mutants to greater sensitivity to IR-induced DNA damage. To do so, we extracted RNA from triplicate samples of two wild-type clones (WT3 &WT4) and the two radio-sensitive IGF-1R mutants (mutant#3 & mutant #4). The gene expression data from the Illumina GEX array was processed by Dr Anastasia Samsonova (bio-informatician at the Department of Oncology, University of Oxford) who performed clustering and outlier detection analyses, including fold change and statistical significance calculations. We used MetaCore (GeneGo™, Thomson Reuters, NY) to interpret the gene expression data in the context of biological processes, biological networks and gene ontology pathways. The questions we asked were: Are there transcriptional differences between the IGF-1R mutants and the wild-type? If so, what are the affected functional pathways and/or processes?

5.2.1. Does deficiency in IGF-1R signalling induce transcriptomic changes?

In order to answer this question, we decided to compare the gene expression profile of the IGF-1R mutants to that of the wild-type clones. Since our analysis included two wild-type clones (WT3 & WT4), it was important to find out whether they could be grouped as one and this was done by the bioinformatician who performed a dendrogram cluster analysis. In addition to that, we decided to compare the transcriptome profile of the two wild-type clones to assess the degree of similarity or dissimilarity between the two. Considering as

significant hits those with the adjusted p-value ≤ 0.05, we found that among the genes that were differentially regulated between WT3 and WT4, none were statistically significant. Hence, we decided to run subsequent data evaluation combining WT3 and WT4 as the 'wild-type group'. With the mutant clones, regardless of the fold-change values, there were over 600 genes that were regulated differently between mutant #3 and mutant #4. We then compared the transcriptome profile of each mutant to that of the 'wild-type' group, retaining only statistically significant hits (adjusted p-value ≤ 0.05) showing a fold-change of at least 2. Whilst there were 45 deregulated genes in mutant #3, there were 27 in mutant #4 and only one commonly deregulated gene between the two IGF-1R mutants (Figure 5-5). The heterogeneity between the two mutants supports the concept of intra-tumour heterogeneity in cancer which posits that cancer cells arising from the same niche can develop different adaptive mechanisms in response to environmental conditions (Meacham and Morrison, 2013). These differences may also have arisen from technical factors associated with sample manipulation. Profiling more mutant clones would have clarified which changes are strongly associated with IGF-1R null status.

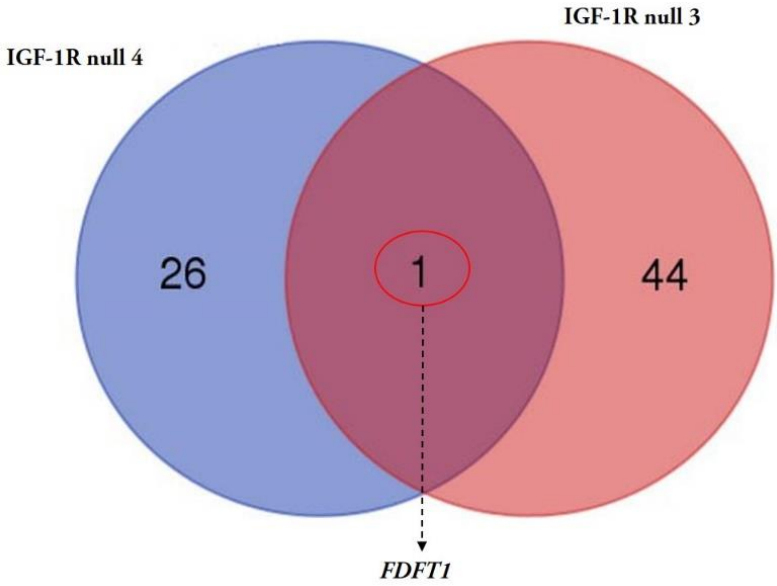


Figure 5-5: **Comparative diagram of deregulated genes between the IGF-1R knockouts**. This Venn diagram was produced using the list of deregulated genes in mutant clones IGF-1R null 3 vs IGF-1R null 4. Only hits with an adjusted p-value ≤ 0.05 and a fold-change value of at least 2 were considered as significantly deregulated genes. The Venn diagram was created using an online programme available on http://bioinformatics.psb.ugent.be/webtools/Venn.

As expected, the two mutants did not show downregulated levels of *IGF1R* mRNA transcripts, for the reason that CRISPR/Cas9 genome editing technique does not block the transcription of the targeted gene but rather, interferes with full mRNA translation as a result of premature stop codons within the coding sequence.

The only common feature at the transcriptome level between the two IGF-1R mutants was the upregulation of the *FDFT1* gene (Figure 5-5). The latter codes for the Squalene Synthase protein, an important player in the biosynthesis of cholesterol.

Next, we decided to uncover what were the deregulated cellular pathways and processes in each separate IGF-1R mutant.

5.2.2. Deregulated pathways & processes in the IGF-1R mutant #4

A large proportion (85%) of the 27 genes differentially expressed in the IGF-1R mutant clone 4 were upregulated and half of these encoded proteins from the GAGE cancer/testis antigens family (Figure 5-6). Using RStudio (RStudio Team, 2016), we generated a heatmap of the deregulated genes in this mutant and included samples from the wild-type group and mutant #3. In support of our initial findings, we noticed striking transcriptomic differences between the two mutants but there were also some unexplained differences within the wild-type group (Figure 5-6).

We used MetaCore^{TM} to run functional enrichment analyses in order to understand the functional pathways or processes that might be affected by the transcriptome changes in the IGF-1R mutant #4. The MetaCore results showed that GnRH signalling, calcium mobilisation and signalling, membrane biogenesis/assembly, endocytosis, blood vessel morphogenesis were among the processes associated with some of the hits (Table 5-1).

Because 70% of the differentially expressed genes in this mutant code for proteins that do not yet have known biological functions, we could not draw a functional map of the biological networks and processes deregulated in order to further our understanding of the cellular changes that occurred in this mutant.

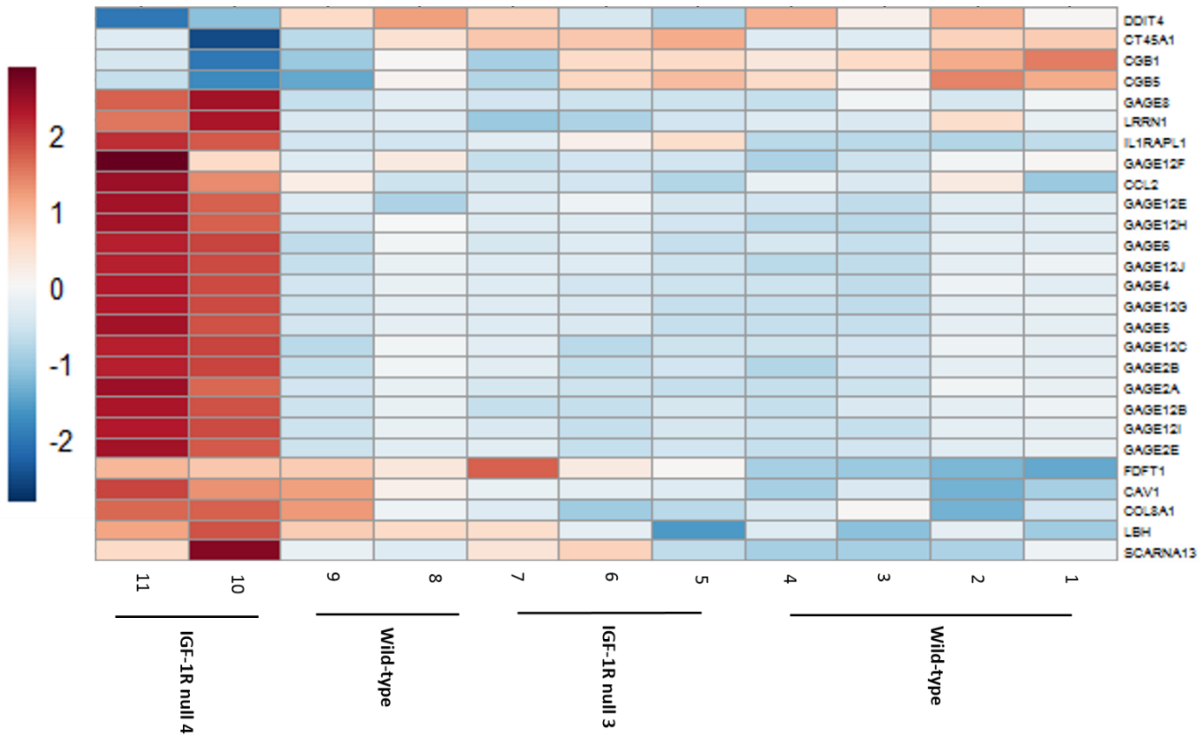


Figure 5-6: **Differentially expressed genes in IGF-1R mutant #4**. The heatmap shows the fold-change difference as per intensity on the gene matrix for all 27 genes transcriptionally deregulated in IGF-1R mutant #4 (IGF-1R null 4) in comparison to the wild-type and the other IGF-1R mutant. The colour spectrum corresponds to the fold difference as per intensity on the array, with downregulated genes lower than 0 in blue and upregulated genes higher than 0 in red. All hits were statistically significant, with the adjusted p-value ≤0.05. The heatmap was generated with RStudio. Note: there is a missing replicate sample for IGF-1R null 4 because it was flagged as an outlier when the outlier detection test was performed on the gene expression data.

Hits	Fold change (log)	Direction of Change	Associated Cellular Pathways/Processes	Adjusted p-value
CAV1	-1.05001	upregulated	Energy metabolism	0.005951319
CCL2	-1.47028	upregulated	Immune system	0.000444998
CGB1	1.173115	downregulated	GnRH signalling	0.023024539
CGB5	1.01634	downregulated	GnRH signalling	0.033222328
COL8A1	-1.30616	upregulated	ECM organisation	0.001859908
CT45A1	1.61787	downregulated	-	0.038136126
DDIT4	1.281383	downregulated	mTOR signalling pathway and metabolism	0.022493911
FDFT1	-1.34892	upregulated	cholesterol biosynthesis	0.000225302
GAGE 2,4,5,6,8,12 (all)	-1.44818 (minimum) & -3.34965 (maximum)	upregulated	-	Between 0.00170345 & 6.74E-12
IL1RAPL1	-1.22379	upregulated	Immune system	6.52E-05
LBH	-1.38453	upregulated	-	0.018461553
LRRN1	-0.99207	upregulated	-	0.002739195
SCARNA13	-1.02526	upregulated	-	0.004312137

Table 5-1: **Transcriptionally deregulated genes in the IGF-1R mutant #4**. This table contains the list of genes differentially expressed in IGF-1R mutant #4. The fold change is expressed in the log of 2, and the direction of change relative to the wild-type is indicated too. Also included are the cellular processes and/or pathways associated with each hit according to the results from functional enrichment analyses performed with MetaCore™. All hits were statistically significant, falling within the cut-off limit of 5% confidence interval for False Discovery Ratio FDR. See appendix8.5.2 for a full list containing all the genes of the *GAGE* family.

5.2.3. Deregulated pathways & processes in the IGF-1R mutant #3

Using MetaCore™, we ran functional enrichment analyses with all 45 deregulated gene hits from the IGF-1R mutant #3. From the enrichment output, we were able to classify these hits into six major groups according to the cellular pathways and biological processes associated with their functions (some hits belonged to more than one group). The top three were: the group of genes coding for proteins involved in mediating cell motility or extracellular matrix remodelling (38%), genes encoding proteins required in the cellular response to stress (20%) and, genes coding for proteins that have a role in intracellular metabolism (15%). This was recapitulated in the figure below (Figure 5-7) and we have generated separate tables containing a list of these genes according to the cellular processes

they are involved in. A heatmap highlighting the intensity fold in the expression level of the deregulated genes in this mutant compared to the wild-type and the other IGF-1R mutant was also generated, revealing differences between the transcriptome profiles of the two radio-sensitive IGF-1R mutants (Figure 5-8).

Indeed, the IGF-1R mutant clone 3 distinguished itself from mutant #4 in that, a large proportion of deregulated genes coded for proteins affiliated with the cellular functions of motility and extracellular matrix remodelling. Among these, 71% were upregulated while the remaining 29% were downregulated (Table 5-2).

Our results also showed that, out of the 7 deregulated hits associated with metabolism, all were downregulated (Table 5-5). These are genes coding for the glucose transporter GLUT1, the p53-regulated protein TIGAR and the hydrolase NUD14. The latter two are known to promote the shunting of glycolytic intermediates for use in the pentose phosphate pathway (PPP) which itself generates important intermediates for ribonucleotide synthesis (Safran et al., 2010) (Yagi et al., 2003).

Metabolic reprogramming is an important feature of cancer cells growing under various stress and it has been shown that partial IGF-1R deficiency can induce changes in glucose and lipid metabolism (DeBerardinis et al., 2008, De Ita et al., 2015). Hence next, we decided to perform metabolome profiling of this IGF-1R mutant and compare it to that of the wild-type.

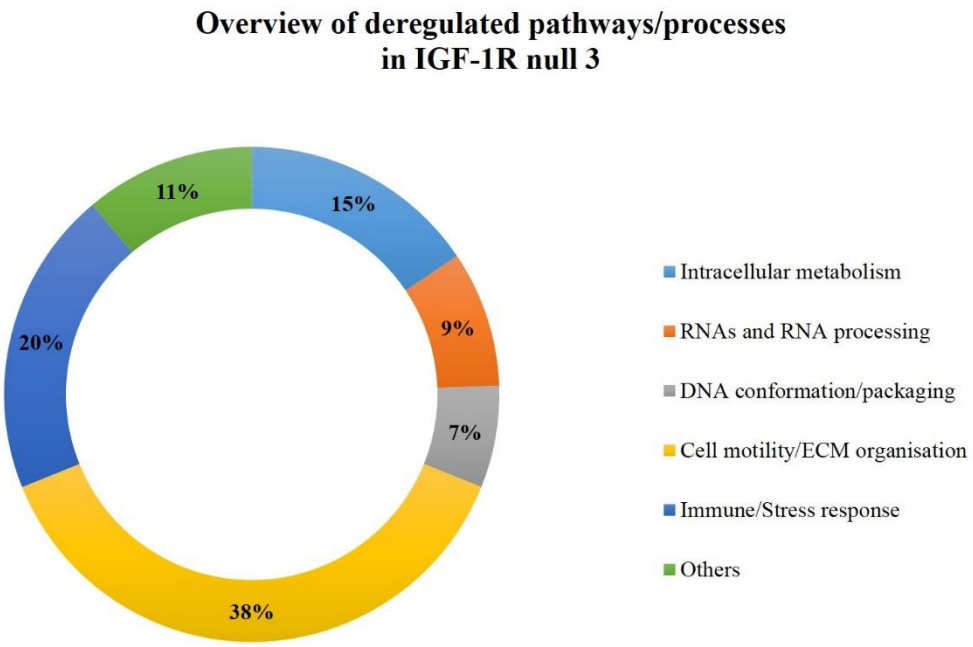


Figure 5-7: **Overview of deregulated cellular processes in IGF-1R null 3.** All 45 differentially regulated genes were classified into different categories according to results obtained from the functional enrichment analyses performed with MetaCore™. The information available on each gene from the GeneCards database was also taken into account (Safran et al., 2010). Only hits with an adjusted p-value ≤ 0.05 and a fold-change value of at least 2 were considered as significantly deregulated genes.

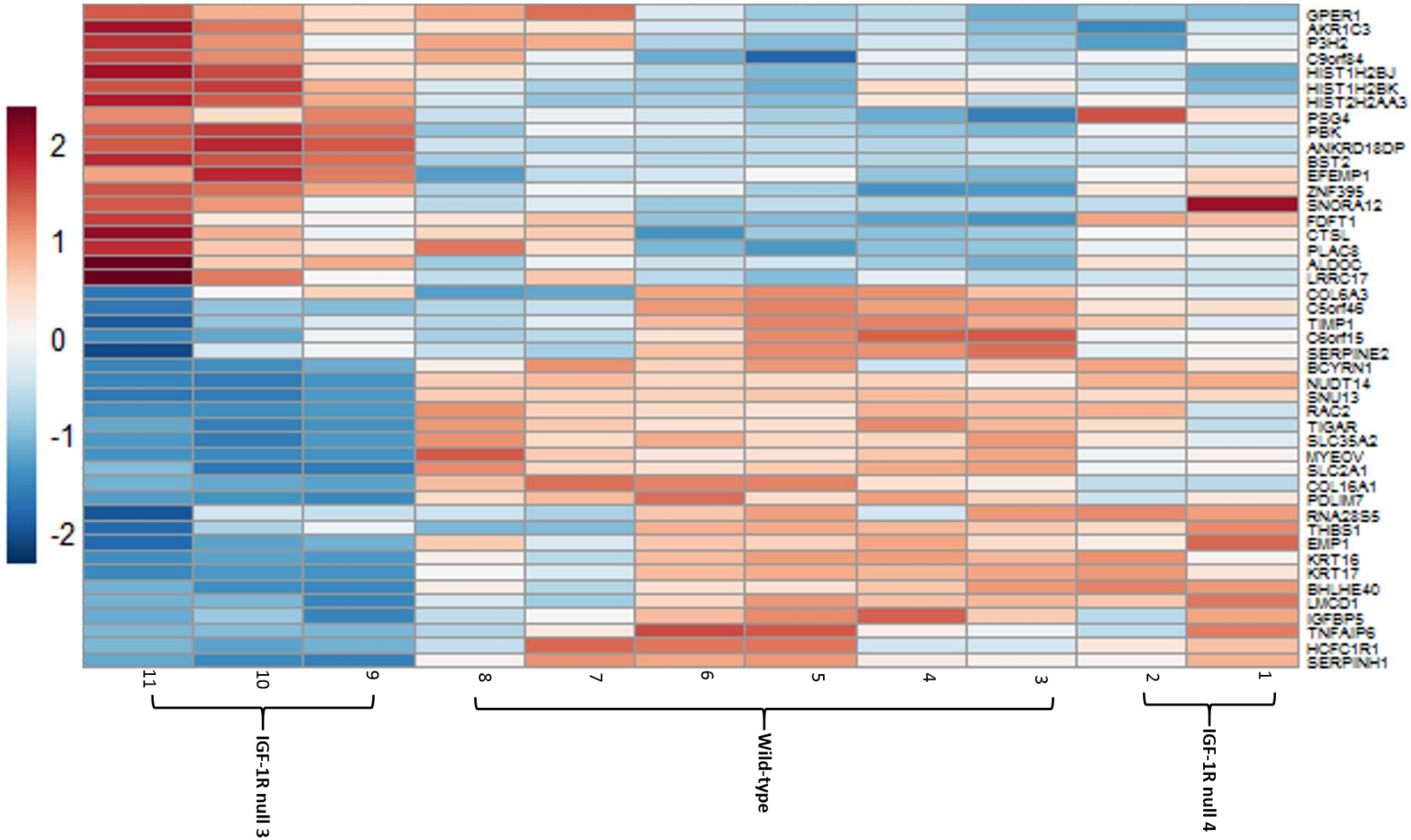


Figure 5-8: **Differentially expressed genes in IGF-1R null 3.** The heatmap shows the fold-change difference as per intensity on the gene matrix for all 45 genes transcriptionally deregulated in IGF-1R mutant #3 (IGF-1R null 3) in comparison to the wild-type and the IGF-1R mutant #4. The colour spectrum corresponds to the fold difference as per intensity on the array, with downregulated genes lower than 0 in blue and upregulated genes higher than 0 in red. All hits were statistically significant, with the adjusted p-value ≤0.05. The heatmap was generated with RStudio. Note: there is a missing replicate sample for IGF-1R null 4 because it was flagged as an outlier when the outlier detection test was performed on the gene expression data.

Hits	Fold change (log)	Direction of Change	Associated Cellular Pathways/Processes	Adjusted p-value
BST2	-1.46202	Upregulated	Cell Growth, Migration & Immune System	3.14E-08
C6orf15	2.026064	Downregulated	Heparin and Fibronectin Binding	6.01E-05
COL16A1	1.14258	Downregulated	ECM Organisation	8.52E-05
COL6A3	1.235264	Downregulated	ECM Organisation & RET Signalling	0.008236356
CTSL	-1.11587	Upregulated	Intracellular Protein Catabolism	0.000520418
EFEMP1	-1.10721	Upregulated	Cell Adhesion & Migration	1.45E-05
GPER1	-1.02238	Upregulated	Synthesis of PI3s & cAMP Production	0.000849251
IGFBP5	1.767032	Downregulated	Fibronectin And Insulin-like Growth Factor I Binding	2.10E-05
KRT16	1.23902	Downregulated	Cytoskeleton Remodelling & Immune System	1.50E-05
P3H2	-1.08792	Upregulated	Collagen Biosynthesis	0.002448284
RAC2	1.375175	Downregulated	Immune System & cell migration	0.001845234
SERPINE2	1.163934	Downregulated	ECM Remodelling	0.000261233
SERPINH1	0.993494	Downregulated	Collagen Biosynthesis	1.30E-05
SLC35A2	1.007438	Downregulated	Glycans Synthesis	2.26E-07
THBS1	1.026308	Downregulated	Cell-cell & cell-matrix Interactions	0.000223653
TIMP1	1.556766	Downregulated	ECM Organisation/Remodelling	1.60E-05
TNFAIP6	1.681453	Downregulated	Cell-cell & cell-matrix Interactions	0.001883701

Table 5-2: **Transcriptionally deregulated genes associated with extracellular matrix remodelling (ECM) in the IGF-1R mutant #3.** This table contains the list of genes differentially expressed in IGF-1R mutant #3. The fold change is expressed in the log of 2, and the direction of change relative to the wild-type is indicated. Also included are the cellular processes and/or pathways associated with each hit according to the results from functional enrichment analyses performed with MetaCore™ and these were confirmed by checking the information available on the GeneCards database (Safran et al., 2010). All hits were statistically significant, falling within the cut-off limit of 5% confidence interval for False Discovery Ratio FDR.

Hits	Fold change (log)	Direction of Change	Associated Cellular Pathways/Processes	Adjusted p-value
AKR1C3	-1.09926	Upregulated	Metabolism & Immune System	0.00043062
ALDOC	-1.24997	Upregulated	Metabolism & Immune System	0.000165299
BST2	-1.46202	Upregulated	Cell Growth, Migration & Immune System	3.14E-08
GPER1	-1.02238	Upregulated	Synthesis Of PIP_3 & cAMP Production	0.000849251
HIST1H2BJ	-1.1094	Upregulated	DNA Packaging	0.000258967
HIST1H2BK	-1.16944	Upregulated	DNA Packaging	0.000936835
HIST2H2AA3	-1.08824	Upregulated	DNA Packaging	0.000252319
KRT16	1.23902	Downregulated	Cytoskeleton Remodelling & Immune System	1.50E-05
LMCD1	1.054705	Downregulated	Co-repressor of GATA6 binding to DNA target sites	1.60E-05
PLAC8	-1.98391	Upregulated	Energy metabolism & Immune System	3.20E-05
RAC2	1.375175	Downregulated	Immune System & cell migration	0.001845234
SERPINE2	1.163934	Downregulated	ECM Remodelling	0.000261233
SERPINH1	0.993494	Downregulated	Collagen Biosynthesis	1.30E-05
SLC2A1	1.099496	Downregulated	Glucose Uptake	6.79E-06
THBS1	1.026308	Downregulated	Cell-cell & cell-matrix Interactions	0.000223653
TIGAR	0.988028	Downregulated	Energy Metabolism & DNA Damage	6.02E-05
TIMP1	1.556766	Downregulated	ECM Organisation/Remodelling	1.60E-05
TNFAIP6	1.681453	Downregulated	Cell-cell & cell-matrix Interactions	0.001883701

Table 5-3: **Transcriptionally deregulated genes associated with cellular response to stress in the IGF-1R mutant #3.** This table contains the list of genes differentially expressed in IGF-1R mutant #3. The fold change is expressed in the log of 2, and the direction of change relative to the wild-type is indicated. Also included are the cellular processes and/or pathways associated with each hit according to the results from functional enrichment analyses performed with MetaCore™ and these were confirmed by checking the information available on the GeneCards database (Safran et al., 2010). All hits were statistically significant, falling within the cut-off limit of 5% confidence interval for False Discovery Ratio FDR.

Hits	Fold change (log)	Direction of Change	Associated Cellular Pathways/Processes	Adjusted p-value
BCYRN1	1.031001	Downregulated	-	0.000281089
BHLHE40	1.13106	Downregulated	candidate tumor suppressor gene	2.12E-06
HIST1H2BJ	-1.1094	Upregulated	DNA packaging	0.000258967
HIST1H2BK	-1.16944	Upregulated	DNA packaging	0.000936835
HIST2H2AA3	-1.08824	Upregulated	DNA packaging	0.000252319
KRT17	1.8275	Downregulated	Hair cycle	7.18E-07
LRRC17	-1.04219	Upregulated	bone homeostasis	0.002971122
MYEOV	1.12967	Downregulated	-	0.000162586
PBK	-0.99057	Upregulated	DNA damage	0.000168208
SNORA12	-1.09706	Upregulated	RNA processing	0.009487205
SNU13	2.37103	Downregulated	mRNA splicing & rRNA processing	3.61E-14
ZNF395	-1.26520	Upregulated	-	0.000243198

Table 5-4: **Transcriptionally deregulated genes associated with DNA damage and other cellular processes in the IGF-1R mutant #3.** This table contains the list of genes differentially expressed in IGF-1R mutant #3. The fold change is expressed in the log of 2, and the direction of change relative to the wild-type is indicated. Also included are the cellular processes and/or pathways associated with each hit according to the results from functional enrichment analyses performed with MetaCore™ and these were confirmed by checking the information available on the GeneCards database (Safran et al., 2010). All hits were statistically significant, falling within the cut-off limit of 5% confidence interval for False Discovery Ratio FDR.

Hits	Fold change (log)	Direction of Change	Associated Cellular Pathways/Processes	Adjusted p-value
AKR1C3	-1.09926	Upregulated	metabolism & immune system	0.00043062
ALDOC	-1.24997	Upregulated	metabolism & immune system	0.000165299
FDFT1	-1.2111	Upregulated	cholesterol biosynthesis	6.79E-05
NUDT14	1.11382	Downregulated	nucleotide metabolism	3.14E-08
PLAC8	-1.98391	Upregulated	Energy metabolism & Immune System	3.20E-05
SLC2A1	1.099496	Downregulated	Glucose uptake	6.79E-06
TIGAR	0.988028	Downregulated	energy metabolism & DNA damage	6.02E-05

Table 5-5: **Transcriptionally deregulated genes associated with intracellular metabolism in the IGF-1R mutant #3.** This table contains the list of genes differentially expressed in IGF-1R mutant #3. The fold change is expressed in the log of 2, and the direction of change relative to the wild-type is indicated. Also included are the cellular processes and/or pathways associated with each hit according to the results from functional enrichment analyses performed with MetaCore™ and these were confirmed by checking the information available on the GeneCards database (www.genecards.org) (Safran et al., 2010). All hits were statistically significant, falling within the cut-off limit of 5% confidence interval for False Discovery Ratio FDR.

5.3. Metabolome profiling of U2OS wild-type and mutant cells

Metabolic changes induced in the IGF-1R mutant #3 were investigated by doing metabolomics. Metabolites were extracted from wild-type cells (WT4) and the IGF-1R mutant #3 according to the protocol described in the methods chapter (see section 2.20). A total of ten replicate samples were used for each condition. Outlier detection and statistical analyses were performed by Dr James McCullagh (Chemistry Research Laboratory, Oxford University). All hits with a p-value ≤ 0.05 and a fold-change value of at least 1.5 were considered as significantly deregulated. We used MetaCore™ to run functional enrichment analyses on the hits from this screen and validated metabolic pathways associated with each hit using the information available on the Human Metabolome Database (Wishart et al., 2013).

Lack of IGF-1R signalling induced a significant change in the abundance of 32 metabolites in the mutant which, compared to the wild-type, showed downregulated levels for 25 of them. Since the transcriptome profile of this mutant pointed towards possible suppression of glucose metabolism, we sought to map out the pathways associated with each of the 32 hits from the metabolome screen. First, we generated a heatmap to confirm whether replicate samples from the wild-type and the mutant behaved similarly. Although we noticed a few variations particularly with O-Phospho-4-hydroxy-L-threonine and iminoaspartic acid, the relative abundance was mostly the same across replicates from within each group (Figure 5-9).

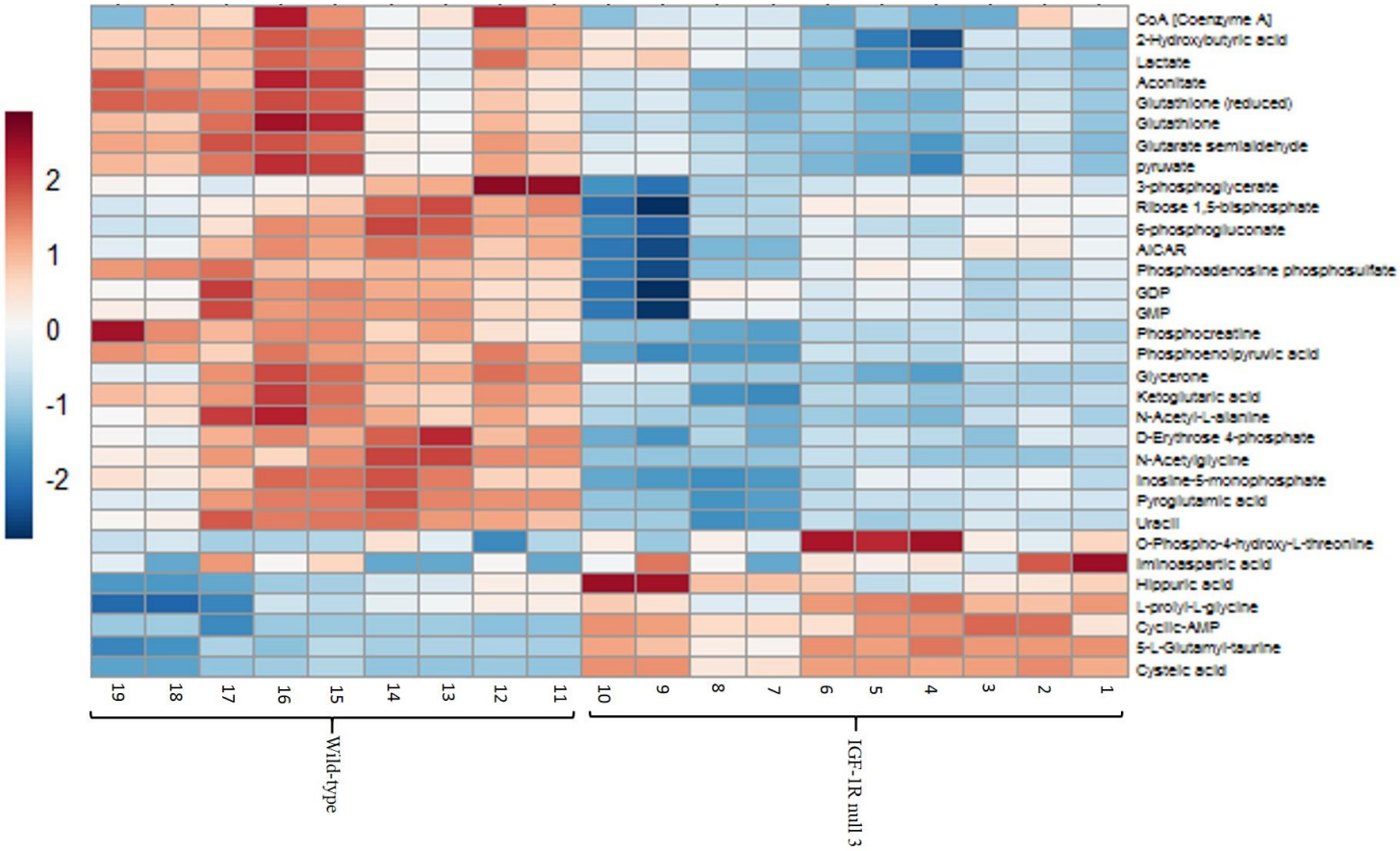


Figure 5-9: **Significantly upregulated and downregulated metabolites in IGF-1R mutant #3.** The heatmap depicts the abundance level of all 32 deregulated metabolites according to normalised abundance values per replicate sample. Metabolites of reduced abundance are colour-coded in shades of blue whilst those that are of increased abundance are coded in shades of red. The colour spectrum corresponds to the fold difference in abundance. All hits were statistically significant, with the p-value ≤0.05. The heatmap was generated with RStudio. Note: One replicate among the wild-type sample set was excluded because it failed the outlier detection test.

Among the metabolites that were downregulated in the mutant, just under half (48%) were linked with glucose metabolism and none of the upregulated metabolites were associated with this cellular process. Indeed, 12 out of the 32 metabolites were intermediates or products of glycolysis, the TCA cycle and the pentose phosphate pathway (Figure 5-10 & Table 5-6).

In this mutant, there was reduced abundance of metabolites associated with purine metabolism and glutathione metabolism (Figure 5-10). Purine synthesis relies on the availability of the PPP intermediate ribose-5-phosphate, the synthesis of which is itself promoted by NUD14. The mutant showed decreased metabolic levels of IMP (a precursor to adenine and guanine nucleotides), and also lower levels of AICAR, GMP and GDP which are important intermediates for IMP biosynthesis (Table 5-6). We also noticed that the levels of 2-hydroxybutyric acid and glutathione were significantly reduced (Table 5-6). The serine biosynthesis pathway, an off-shoot branch of the glycolytic flux is known to generate intermediates that are required for glutathione synthesis (Locasale, 2013).

Of the seven metabolites that were found in greater abundance in the mutant, two were affiliated with taurine metabolism and the others were linked with various other metabolic processes including amino acid synthesis and vitamin B6 metabolism (Table 5-7). Taurine is a molecule with cyto-protective properties that has been implicated in osmo-regulation (Ripps and Shen, 2012). The higher abundance of cAMP seemed to correlate with the upregulation of the *GPER1* gene noticed from the transcriptomic data (non-validated hit) and coding for the G-protein oestrogen receptor; receptor linked with cAMP production (Table 5-3).

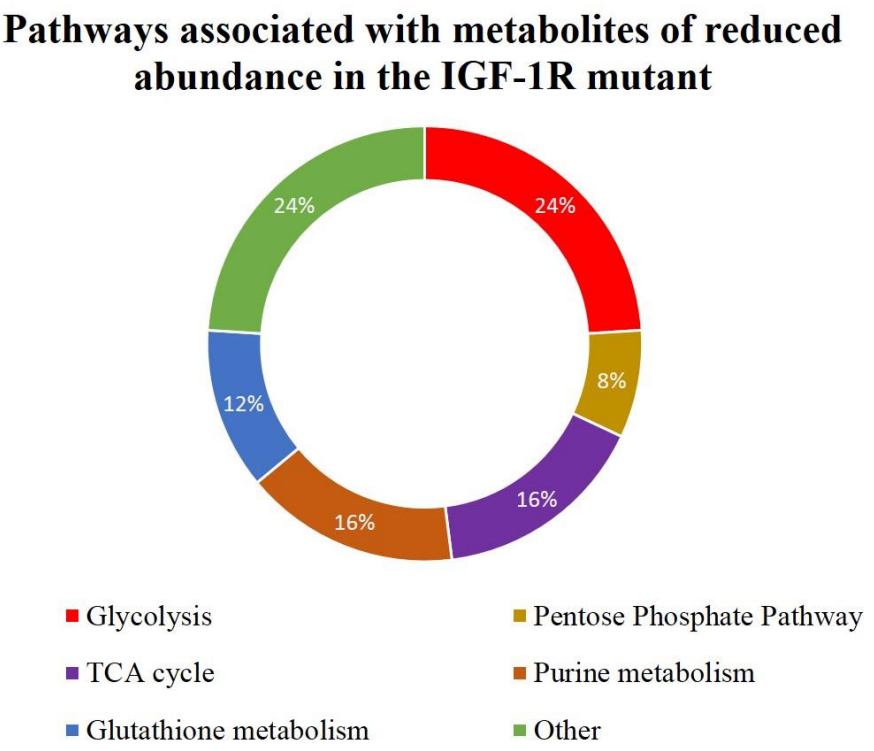


Figure 5-10: **Overview of downregulated metabolic processes in IGF-1R mutant #3.** All 32 metabolites that showed a statistically significant difference in their abundance between the wild-type and the IGF-1R mutant #3 were taken into account. Hits were classified into different categories based on the information available in the Human metabolome database (Wishart et al., 2013) and the results from functional enrichment analyses performed with MetaCore™. All hits had a p-value ≤0.05. The pie chart depicts the proportion of metabolites that fall into the categories described in the legend.

Compound ID	ANOVA (p-value)	Fold change	Associated pathways
2-Hydroxybutyric acid	0.001887851	1.575601116	Glutathione pathway
3-phosphoglycerate	0.004540884	1.658136401	Glycolysis
6-phosphogluconate	0.004724754	1.779780165	PPP
Aconitate	5.92E-07	2.287179413	TCA cycle
AICAR	0.003032695	1.517421131	IMP biosynthesis
CoA [Coenzyme A]	0.004980315	2.307560951	TCA cycle; a precursor for fatty acid synthesis
D-Erythrose 4-phosphate	2.20E-06	1.786845175	PPP
GDP	0.004749381	1.513469636	GTP metabolism/IMP biosynthesis
Glutarate semialdehyde	2.10E-07	1.80702325	Glycolysis
Glutathione	3.47E-07	4.656849581	Glutathione pathway
Glutathione (reduced)	7.67E-07	2.832733649	Glutathione pathway
Glycerone	2.03E-06	1.575150243	Glycolysis
GMP	0.003694748	1.676998104	GTP metabolism/IMP biosynthesis
Inosine-5-monophosphate	9.38E-06	1.510235819	Purine synthesis
Ketoglutaric acid	2.24E-08	1.764137541	TCA cycle
Lactate	0.000921299	1.50521166	TCA cycle
N-Acetylglycine	1.27E-07	22.851313	-
N-Acetyl-L-alanine	5.65E-08	1.842081233	Substrate for a number of proteins like GTP-binding nuclear protein Ran
Phosphoadenosine phosphosulfate	0.000687572	1.791935371	end product of sulfur metabolism
Phosphocreatine	4.30E-08	1.549025769	Reacts with ADP to yield ATP and creatine
Phosphoenolpyruvic acid	7.32E-07	1.760868442	Glycolysis
Pyroglutamic acid	8.97E-06	1.568646127	Cyclized derivative of L-glutamic acid
Pyruvate	8.72E-06	1.782842248	Glycolysis
Ribose 1,5-bisphosphate	0.038492191	1.583776775	Glycolysis
Uracil	1.82E-07	1.600725773	Carbohydrate metabolism

Table 5-6: **Downregulated metabolites in the IGF-1R mutant #3**. Based on the statistical analyses performed on the metabolomics data, 25 hits were identified as compounds significantly lower in abundance in the IGF-1R mutant compared to the wild-type (p-value ≤ 0.05; fold-change ≥ 1.5). The information displayed regarding associated pathways was gathered from functional enrichment analyses performed with MetaCore™ and from the Human metabolome database (Wishart et al., 2013).

Compound ID	Anova (p-value)	Fold Change	Associated pathways
Cyclic-AMP	3.65E-06	3.767845384	Synthesized from ATP
Cysteic acid	1.36E-11	1.974562157	Taurine metabolism
Iminoaspartic acid	0.081312093	1.933729638	Amino acid biosynthesis
Hippuric acid	0.001635005	1.780090049	Conjugation of benzoic acid with glycine
L-prolyl-L-glycine	0.002829966	1.701449577	Proteolytic breakdown product of larger proteins
O-Phospho-4-hydroxy-L-threonine	0.007851171	1.69208802	Vitamin B6 metabolism
5-L-Glutamyl-taurine	2.12E-08	1.572715603	Taurine and hypotaurine metabolism

Table 5-7: **Upregulated metabolites in the IGF-1R mutant #3**. Based on the statistical analyses performed on the metabolomics data, 7 hits were identified as compounds significantly higher in abundance in the IGF-1R mutant compared to the wild-type (p-value ≤ 0.05; fold-change ≥ 1.5). The information displayed regarding associated pathways was gathered from functional enrichment analyses performed with MetaCore™ and from the Human metabolome database (Wishart et al., 2013).

5.4. Discussion

Our study demonstrated that IGF-1R signalling confers some protection against the effects of ionising radiation in U2OS osteosarcoma cells. Out of the three genetically engineered IGF-1R 'full' knockout mutants, two showed significantly reduced clonogenic survival compared to the wild-type when exposed to γ-irradiation. We found it interesting that one of the mutant clones lacking the IGF-1R protein showed a 2-fold greater clonogenic survival than the wild-type. This raises the question whether assessing clonogenic survival is the best tool to interrogate the potential radio-protective role of IGF-1R signalling in U2OS cells. It may be used to challenge the IGF-1R specificity of the phenotypes observed in the full knockout mutants.

However, with the two other IGF-1R mutants, our findings were consistent with results from experimental studies carried out in mouse embryo fibroblasts lacking IGF-1R (R^- cells) which showed that blocking IGF-1R downstream signalling increased radio-sensitivity (Yu et al., 2003). Moreover, it has also been demonstrated in osteosarcoma cells that suppressing IGF-1R signalling leads to enhanced sensitivity to ionising radiation (Wang et al., 2009). It has been proposed that signalling via the PI3K and MAPK pathways are both important for IGF1R-mediated radio-resistance (Yu et al., 2003). But, no intricate details as to how these two pathways may confer radio-protection have been described thus far other than promoting cell survival and, since they are not exclusively associated with IGF-1R signalling, there is an urgent need to understand the mechanisms via which this receptor tyrosine kinase can promote cancer cell survival to radiotherapy.

IGF-1R signalling influence on irradiation-induced DNA damage response cascade

We have shown that the signalling cascade triggered following exposure to ionising radiation was not impaired or delayed in the IGF-1R mutant cells. Indeed, although we did

note differences in basal levels of p53 and that of ATM, all events that are known to be triggered by γ-irradiation from ATM induction to p53 accumulation, including the phosphorylation of CHK1, KAP1, RPA and histone H2AX occurred in both the wild-type and the IGF-1R mutant without any evidence of delay.

Consistent with this, it emerged from the transcriptome profile of both IGF-1R mutants that the lack of IGF-1R did not induce transcriptional changes in genes encoding key proteins involved in the repair of DNA damage. The transcriptomic data also did not suggest upregulation of pro-apoptotic genes in the mutants which might explain why their proliferative ability was no different to that of the wild-type cells in the absence of irradiation.

Interpreting the disparate results between our study and previously published ones is rendered challenging by the fact that the DNA damage response (DDR) cascade induced by γ-irradiation was not investigated in a similar way by other studies seeking to tackle this very question of IGF-1R influence on the response to DNA damage (Turney et al., 2012, Chitnis et al., 2014, Isebaert et al., 2011, Ferté et al., 2013, Cosaceanu et al., 2007). Whilst we followed in a timecourse the changes occurring at the protein level for key players in the DDR, the other studies only looked at a single time-point post-exposure to IR or, did not track changes in as many DDR proteins to enable understanding of what may be unravelling in the cells. Nevertheless, in consistency with our findings in the IGF-1R mutant, a previous investigation also demonstrated that inhibition of IGF-1R activation does not affect IR-induced ATM activation (Chitnis et al., 2014).

IGF-1R signalling influence on irradiation-induced cell cycle changes

Consistent with the IR-induced p53 accumulation and CHK1 phosphorylation detected by western blot, we confirmed that the integrity of the G2/M cell-cycle checkpoint was not

affected by IGF-1R deficiency and we did not detect any polyploidy in irradiated and non-irradiated IGF-1R deficient U2OS cells. This is particularly important because while the cell may undergo senescence, apoptosis or recovery upon induction of the G2/M cell cycle arrest, it protects it from mitotic catastrophe as evidenced by the polyploidy phenotype that was reported in IGF-1R inhibited DU145 cells which showed a modest increase in G2 population after γ-irradiation (Chitnis et al., 2014). Although the absence of G2/M arrest was likely due to the *TP53* mutant status of DU145 cells, because polyploidy was only noticed in cells treated with the IGF-1R inhibitor, unlike what we reported with our model, the radio-sensitisation in DU145 could be partly due to these mitotic defects.

Because the induction of double-strand breaks was not enhanced in IGF-1R deficient cells, nor was there evidence of impaired double-strand break repair to account for their enhanced sensitivity to γ-irradiation and the mutant cells showed activation of the G2/M cell cycle checkpoint, we reasoned that intrinsic differences with the IGF-1R proficient U2OS cells might predispose IGF-1R deficient cells to undergo enhanced apoptosis or senescence upon exposure to ionising radiation. This conclusion is supported by evidence from previous investigations suggesting that the cellular outcome following IR-induced damage can be influenced by various factors (El-Awady et al., 2003, Chitnis et al., 2014, Isebaert et al., 2011).

Conclusion

Our investigation suggested that intrinsic differences between the IGF-1R mutants and the wild-type which are thought to affect the interaction with the extracellular environment, the intracellular metabolism and the stress status of the cell could be responsible for the greater sensitivity that these mutants displayed to ionising radiation.

In order to clarify whether the various cellular changes observed in the IGF-1R mutants can be attributed specifically to the suppression of IGF-1R signalling and validate them as

possible contributing factors to radio-sensitisation, we decided to conduct further investigations in U2OS cells where the *IGF1R* gene was transiently silenced using short interference RNA (siRNA).

6. Discerning IGF1R-specific effects on the response to ionising radiation: Comparative analysis between IGF-1R mutants and IGF-1R depleted U2OS cells

Having established the phenotype of CRISPR/Cas9-engineered mutants and the intracellular changes resulting from the chronic lack of IGF-1R in U2OS osteosarcoma cells, we wished to confirm that the radio-sensitivity profile of the mutants as well as the suggested deregulated cellular processes could be attributed specifically to IGF-1R signalling. Therefore, we assessed in parental U2OS osteosarcoma cells the effects of siRNA-mediated IGF-1R depletion on the response to ionising radiation (IR), on the repair of IR-induced double-strand breaks and finally, on intracellular processes. Then, we compared the findings to that observed in the IGF-1R mutants. In this chapter, with the goal to deepen our understanding of the pathways underpinning radio-sensitisation, we will also evaluate the response of the IGF-1R mutants and the IGF-1R depleted cells to other drugs that induce different types of DNA damage.

6.1. IGF-1R depletion and the response to γ-irradiation

Previous studies have reported that suppressing IGF-1R growth signalling enhanced sensitivity to ionising radiation and we sought to find out if the same observations would be made in IGF-1R depleted cells (Riesterer et al., 2011, Rochester et al., 2005, Turney et al., 2012).

6.1.1. Testing the response to irradiation

U2OS cells were transfected with two different siRNA (siIGF1R-1 and siIGF1R-2), each targeting the *IGF1R* mRNA for degradation. Using the colony formation assay, we assessed the proliferative ability of the resulting IGF-1R depleted cells with or without γ-irradiation (5Gy) in comparison to the non-transfected U2OS cells (control) and non-targeting siRNA-transfected cells (Allstars/negative control).

IGF-1R depletion significantly impacted the proliferation of U2OS cells; whilst we counted an average of 470 and 429 colonies for the non-transfected and the negative control respectively, the numbers were 2-fold lower in the depleted cells where we registered an average of 168 and 213 colonies for siIGF1R-1 and siIGF1R-2 respectively (Figure 6-1). This striking effect was in contrast to the absence of any impairment on the proliferative ability of the IGF-1R mutants thereby highlighting the differential response of U2OS cells to chronic and transient suppression of the IGF-1R growth signalling. This further arose our curiosity regarding whether these cells would show radio-sensitisation.

In response to γ-irradiation, both the controls and IGF-1R knockdown cells displayed high sensitivity; the mean percentage of cell survival was reduced and IGF-1R depletion significantly enhanced the sensitivity of U2OS cells to ionising radiation by more than 3-fold (Figure 6-1). There were no notable differences within the knockdown group and the

controls also showed a relatively similar degree of sensitivity to irradiation and the mean survival percentage was 10.8%, 9.6%, 2.4% and 2.8% for the non-transfected control, Allstars, siIGF1R-1 and siIGF1R-2 transfected cells respectively (Figure 6-1). In comparison to what was observed with IGF-1R mutants, the dose enhancement ratio was not remarkably different; the calculated ratios were 3.3 and 3.8 for cells transfected with siIGF1R-1 and siIGF1R-2 respectively (Figure 6-2).

On the other hand, wild-type U2OS cells derived from parental clones were more sensitive to ionising radiation than the parental U2OS cells or the negative control (Figure 6-2). This further justified our decision to use wild-type U2OS clones as controls for experiments with IGF-1R mutant clones instead of parental U2OS cells because such differences could have significantly flawed interpretation of the results.

Next, we checked whether the radio-sensitisation effect conferred upon depletion of IGF-1R was caused by defects in the repair of IR-induced double-strand breaks repair by tracking the formation and resolution of γH2AX foci.

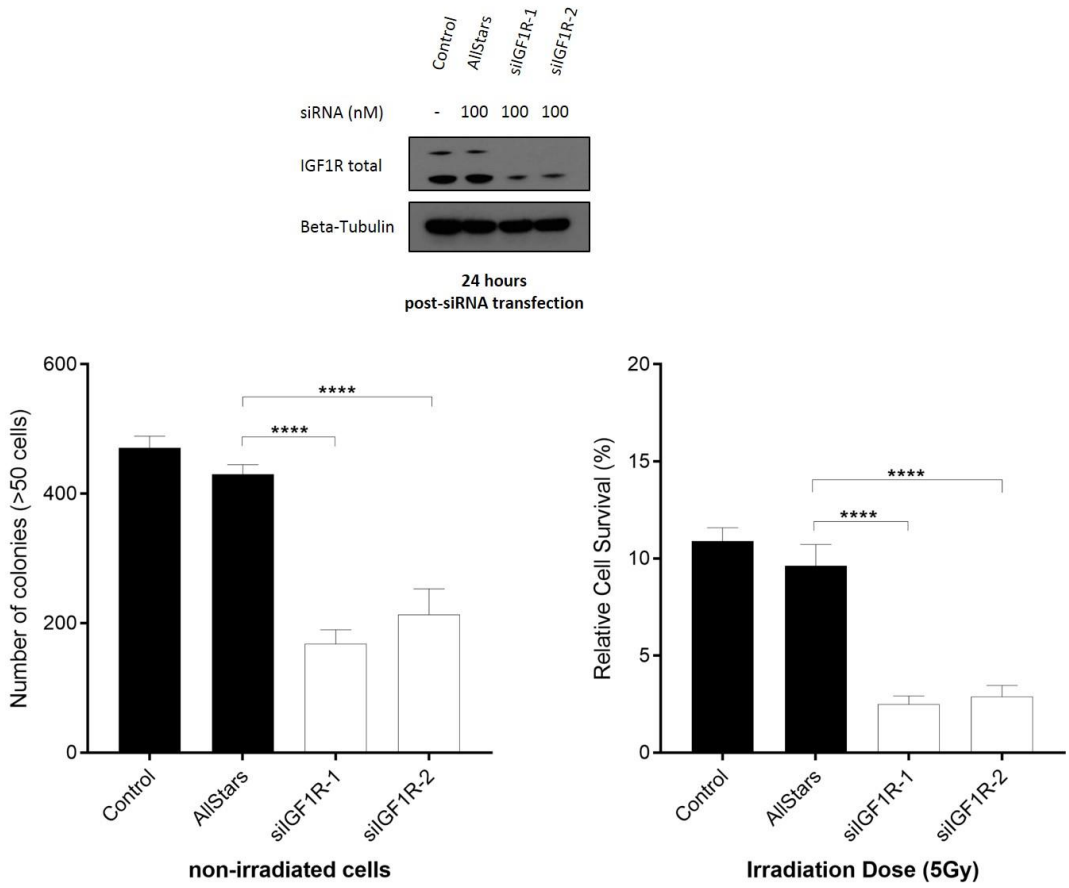
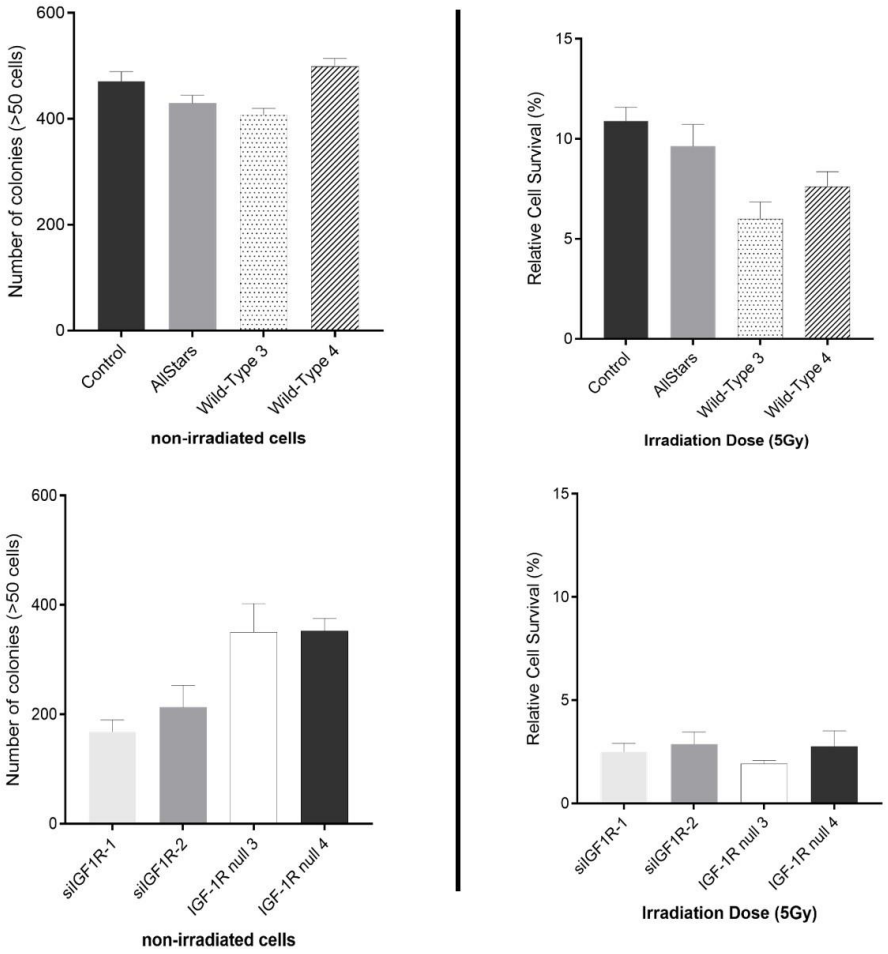


Figure 6-1: **IGF-1R depletion leads to reduced proliferation and increased sensitivity to ionising radiation**. Cells were seeded in 10cm dishes and transfected the next day either with non-targeting siRNA 'Allstars' or with IGF1R-targeting siRNAs (siIGF1R-1, siIGF1R-2). Non-transfected control samples did not undergo transfection but the cell culture medium was changed to maintain consistency across samples. The following day, both siRNA transfected and non-transfected cells were disaggregated and seeded in triplicates into 6-well plates and the remaining volume of cells was used to confirm the level of knockdown at 24 hours post-transfection by western blotting. Cells were irradiated the next with at a dose of 5Gy. The number of colonies (>50cells) per well was determined 9-10 days after seeding using the GelCount colony counter. The percentage of cell survival for the knockdown and control cells was calculated in proportion to the number of colonies that grew under conditions of no irradiation. The graph was plotted with GraphPad Prism as mean ± standard error of the mean (SEM). Statistical significance was calculated by one-way ANOVA using Prism (p-value <0.05). These are results from three independent experiments.



Condition	Survival at 5Gy (%)	DER
WT clones 3/4	6.8	
IGF-1R null 3	1.9	**3.6**
IGF-1R null 4	2.8	**2.4**
Allstars control	9.6	
IGF-1R siRNA 1	2.5	**3.8**
IGF-1R siRNA 2	2.9	**3.3**

Figure 6-2: **Dose enhancement Ratios and radio-sensitivity profile of IGF-1R depleted cells compared to the IGF-1R mutants**. Contrasting the sensitivity of wild-type clones and IGF-1R mutant clones relative to parental U2OS cells (non-transfected and negatively transfected) and IGF-1R depleted cells respectively. Using Prism, graphs were plotted as mean ±SEM. On the far right is a table showing the dose enhancement ratio (DER) calculations.

6.1.2. Assessing the effect of IGF-1R depletion on γH2AX focus formation and resolution following ionising radiation

Cells were irradiated with 5Gy, fixed at 2, 24 and 72 hours after, and then stained with antibodies that recognise phosphorylated Ser139 residue on histone H2AX. To determine the basal levels of γH2AX, we used non-irradiated cells that were fixed at the same time as cells that were irradiated and fixed 2 hours after exposure to γ-irradiation.

Ionising radiation triggered a dramatic increase in the levels of γH2AX foci with peak levels at least 6-fold greater than basal levels at the 2-hour time-point (Figure 6-3). This was followed by a sharp decline to levels 2-3 times higher than the baseline levels at the last recorded time-point after irradiation. Although it appeared that the number of γH2AX foci was slightly higher in cells transfected with siIGF1R-1 compared to the siIGF1R-2 transfected group at the 2-hour and 24-hour time-points, these differences were not statistically significant; neither were the differences between the siIGF1R-1 or siIGF1R-2 and the negative control (Allstars) (Figure 6-3).

We noticed that the decline to baseline levels was seemingly faster in the knockdown compared to the controls; irrespective of the peak levels reached at the 2-hour time-point, γH2AX levels at the 24-hour time-point in the controls (non-transfected and Allstars-transfected) had only decreased by 2-fold whereas we noted a 3-fold decrease in IGF-1R depleted cells within the same period (Figure 6-3).

Overall, our results indicate that detection of double-strand breaks induced by ionising radiation and their repair as tracked by the formation and resolution of γH2AX foci was not impaired in cells depleted of IGF-1R.

Next, we decided to search for intrinsic changes at the transcriptome level that may account for the enhanced sensitivity of IGF-1R depleted cells to damage caused by ionising radiation so, we performed a RNA microarray screen.

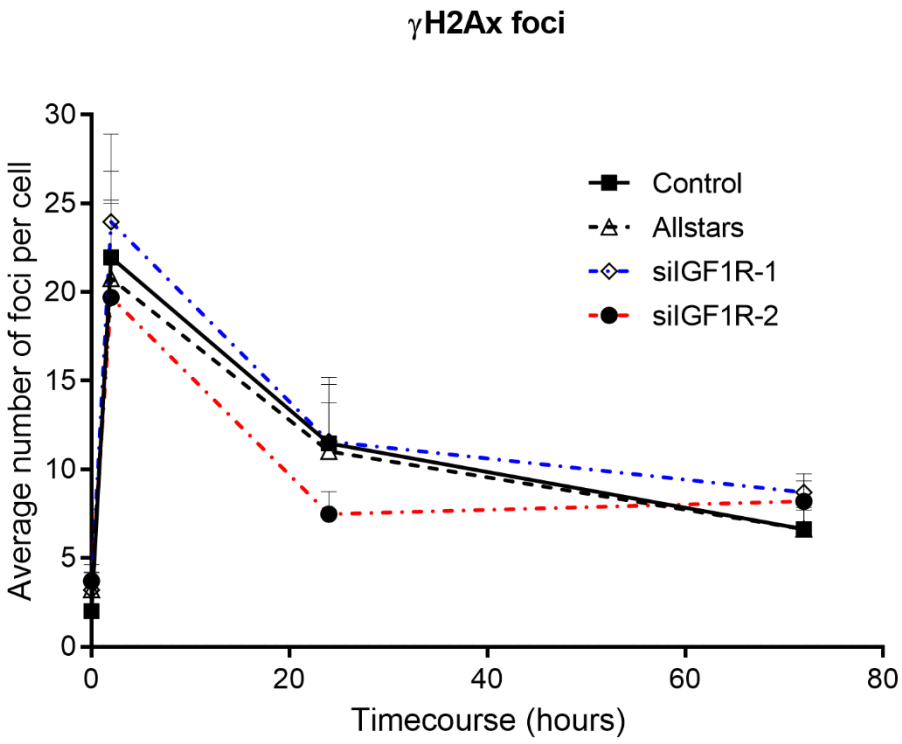


Figure 6-3: **Induction and Resolution of γH2AX foci upon exposure to ionising radiation**. Cells were seeded in 10cm dishes and transfected the next day either with non-targeting siRNA 'Allstars' or with IGF1R-targeting siRNAs (siIGF1R-1, siIGF1R-2). Non-transfected control samples did not undergo transfection but the cell culture medium was changed to maintain consistency across samples. The following day, both siRNA transfected and non-transfected cells were disaggregated and seeded in triplicates into 96-well plates and irradiated the next day with 5Gy. Cells were fixed at the time-points 2, 24 and 72 hours after irradiation. The non-irradiated cells (0h) were fixed at 2h post-irradiation. The cells were stained for γH2AX and DNA (Hoechst). Over 50 cells were counted per condition per time-point using the foci counting program on the In Cell Analyser 2000. The error bar represents the standard deviation. The graph was plotted using GraphPad Prism as mean ± standard deviation. This result represents data obtained from two independent experiments.

6.2. Effects of IGF-1R depletion on gene expression

We assessed the effects of IGF-1R depletion on U2OS in a bid to further uncover what intracellular changes might render them more sensitive to the wild-type upon exposure to ionising radiation. To do so, we extracted RNA 48 hours after transfection from triplicate samples of U2OS non-transfected control, Allstars-transfected negative control, siIGF1R1- and siIGF1R2-transfected cells. Prior to sending the RNA for microarray, we checked whether the levels of *IGF1R* mRNA were significantly downregulated in the cells transfected with IGF-1R targeting siRNA. Compared to the negative control, the levels of *IGF1R* mRNA were 3x or 5x lower when cells were transfected with siIGF1R-1 or siIGF1R-2 respectively (Figure 6-4).

The RNA microarray data were analysed and processed by Dr Anastasia Samsonova who performed sample validation assessment including the outlier detection tests and two sample outliers were identified; for each of the triplicate set of samples submitted for cell targeted with either siIGF1R-1 or siIGF1R-2, there was one outlier. This might be due to variations in the degree of IGF-1R knockdown across the three samples submitted because they were derived from three independent knockdown experiments.

Using MetaCore (GeneGo™, Thomson Reuters, NY), we performed Ingenuity pathway analyses in order to address the questions of interest: Does IGF-1R depletion induce transcriptomic changes? If yes, what are they and could they account for increased sensitivity to ionising radiation?

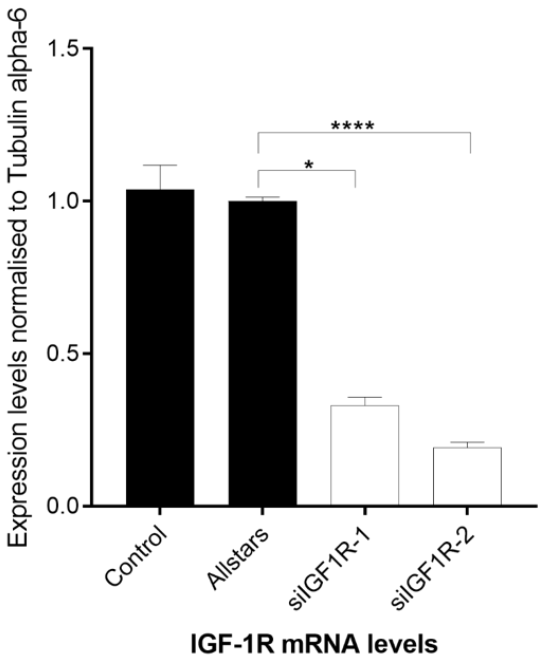


Figure 6-4: **Levels of *IGF1R* mRNA upon siRNA-mediated depletion**. Cells were seeded in 10cm dishes and transfected the next day either with non-targeting siRNA 'Allstars' or with IGF1R-targeting siRNAs (siIGF1R-1, siIGF1R-2). Non-transfected control samples did not undergo transfection but the cell culture medium was changed to maintain consistency across samples. RNA was extracted 48 hours later and *IGF1R* mRNA levels were determined by quantitative reverse transcription real-time PCR in triplicates and normalised to endogenous levels of mRNA coding for tubulin alpha-6. The graph was plotted with GraphPad Prism as mean ± standard error of the mean (SEM). Statistical significance was calculated by one-way ANOVA using Prism (p-value <0.05). These are results from three independent experiments. Note: unless stated otherwise, the siRNA concentration for Allstars, siIGF1R-1 and siIGF1R-2 was 100nM.

6.2.1. Does IGF-1R depletion induce gene expression changes in U2OS?

First, we needed to decide whether the negative and non-transfected controls could be grouped as one representing altogether the control group against which we would compare the transcript profile of siIGF1R-transfected cells to assess for differential gene regulation. So, we compared the RNA hits data of the negative and non-transfected controls to each other and checked for statistically significant differences and there were none. Next, we did the same with siIGF1R-transfected cells to find out if they could be combined as the 'knockdown group'.

In contrast to what was observed when the two IGF-1R mutants were compared, a large proportion of deregulated genes was found as hits with both siRNAs. Indeed, more than half of the genes significantly deregulated with siIGF1R-1 were also significantly deregulated with siIGF1R-2 (Figure 6-5). Consequently, we decided to group them although this meant that based on the intensity of each hit on the array, some of the hits that were not common to the two did not qualify as significantly deregulated in both. And so, overall there were 90 genes significantly deregulated and showing a fold-change of at least 2 in the 'IGF-1R depleted group'.

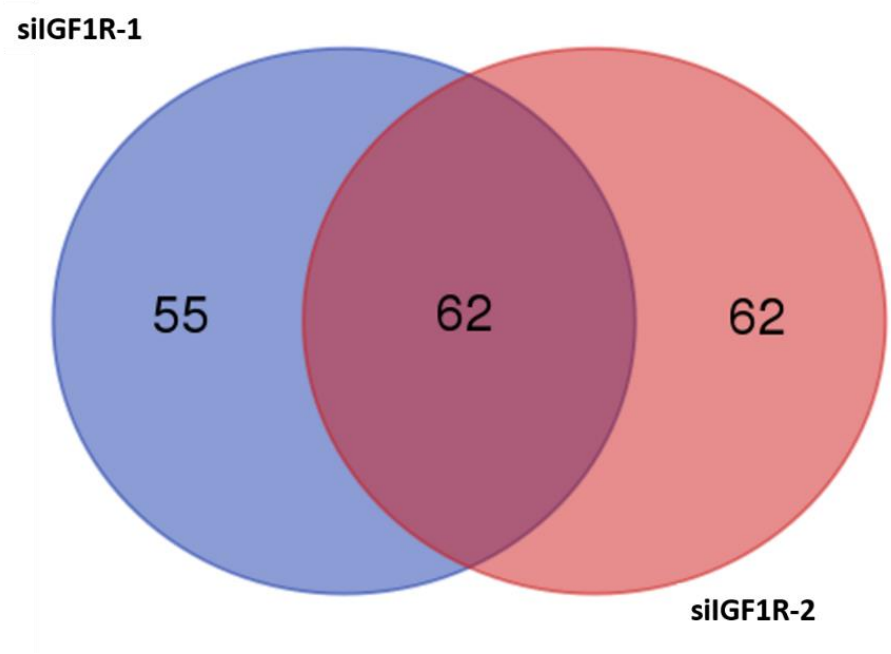


Figure 6-5: **Comparative diagram of deregulated genes upon siRNA-mediated IGF-1R depletion**. This Venn diagram was produced using the list of deregulated genes upon siIGF1R-1 vs siIGF1R-2 mediated transfection. Only hits with an adjusted p-value ≤ 0.05 and a fold-change value of at least 2 were considered as significantly deregulated genes. The Venn diagram was created using an online programme available on http://bioinformatics.psb.ugent.be/webtools/Venn.

6.2.2. Deregulated cellular pathways and processes upon IGF-1R knockdown

Using MetaCore™, ingenuity pathway analyses were performed with genes that showed transcriptional deregulation as a result of transient depletion of the IGF-1R protein. The most deregulated cellular pathways or processes were intracellular signalling transduction (31%), the stress/immune response (18%) and, 36% of the differentially expressed genes coded for proteins involved in processes pertaining to extracellular matrix remodelling (ECM), regulation of cell adhesion and cytoskeleton rearrangement (Figure 6-6). The latter three are key factors known to influence cellular motility and migration. Other less outstandingly affected processes included vesicle formation and trafficking, the metabolism of purines, glucose and amino-acids and, the regulation of IGF-1R signalling (Figure 6-6).

Similar to what was observed in IGF-1R mutant #3, the largest proportion of differentially expressed genes in IGF-1R depleted cells was associated with the remodelling of the extracellular matrix (ECM) and other players involved in cell-matrix or cell-cell interactions (Table 6-2). In addition to this, even though transient, IGF-1R deficiency also triggered a stress response in the knockdown cells with several of the hits associated with the stress response to bacterial lipopolysaccharide (LPS) induction (Table 6-1). It has been reported that siRNA-mediated downregulation of IGF-1R can inhibit tumour growth and stimulate the expression of pro-inflammatory cytokines in cancer cells (Durfort et al., 2012). Other studies have also demonstrated that IGF-1R signalling can modulate immune-related functions in mammalian cells (Smith, 2010, Van Valen et al., 2012).

In contrast to the IGF-1R mutant #3, IGF-1R depleted cells did not show many deregulated hits associated with glucose metabolism (Table 6-3).

Because some of the processes deregulated upon siRNA-mediated IGF-1R depletion were also deregulated in the IGF-1R mutants, we sought to find out if they shared the same differentially expressed genes.

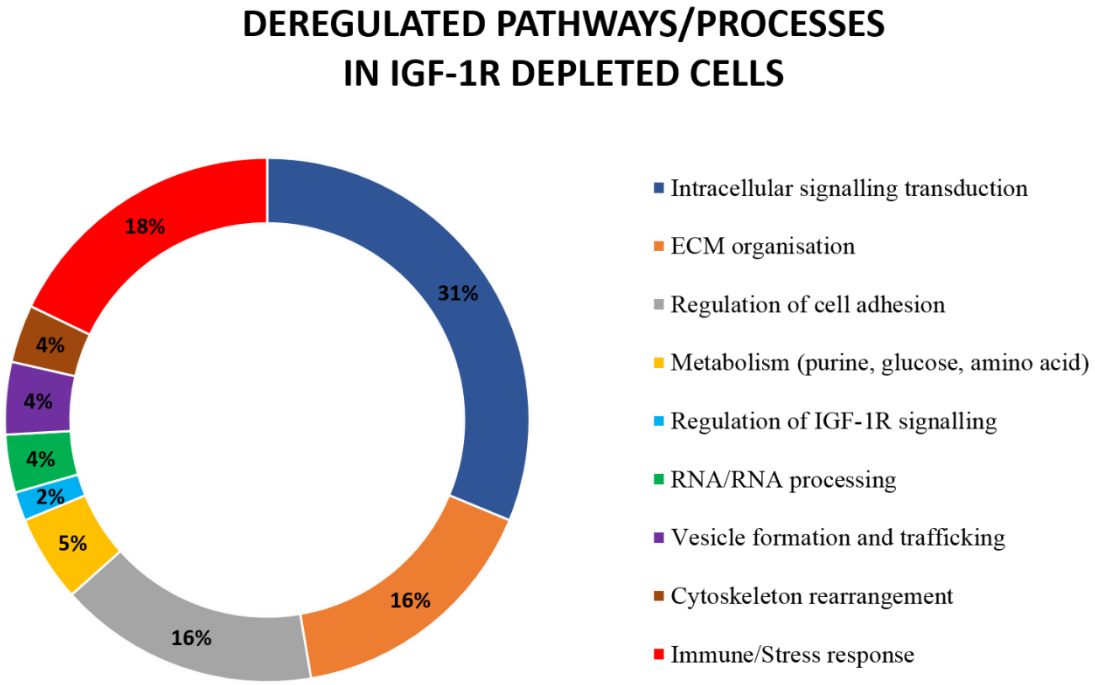


Figure 6-6: **Overview of deregulated cellular processes upon IGF-1R depletion.** All differentially regulated genes were classified into different categories according to results obtained from the functional enrichment analyses performed with MetaCore™. The information available on each gene from the GeneCards database was also taken into account (Safran et al., 2010). Only hits with an adjusted p-value≤0.05 and a fold-change value of at least 2 were considered as significantly deregulated genes.

Hits	Fold change (log)	Adjusted p-value	Direction of change
ADAMTS6	-1.37612	0.000119	Upregulated
ALPL	-1.12401	0.005308	Upregulated
CD163L1	-1.09521	3.42E-05	Upregulated
CXCL14	1.267984	0.013486	Downregulated
CXCL8	-2.00092	0.004011	Upregulated
DDIT4	0.987944	0.021718	Downregulated
DEFB103A	-1.71447	3.32E-06	Upregulated
EBI3	-1.13026	0.000532	Upregulated
FAM24B	-1.25336	1.85E-06	Upregulated
FOXD1	-1.02301	0.001398	Upregulated
GADD45A	-1.02046	4.39E-05	Upregulated
GLIPR1	-1.30629	0.001715	Upregulated
IL24	-1.17818	1.62E-05	Upregulated
LY96	-1.3562	4.14E-06	Upregulated
MARCH4	-1.68743	0.000169	Upregulated
NLRP3	-1.16936	4.14E-06	Upregulated
PLAU	-1.33275	3.80E-05	Upregulated
TNFRSF11B	-1.20509	1.91E-05	Upregulated
TRIB1	-1.18277	1.65E-06	Upregulated
VSTM1	-1.34256	2.55E-05	Upregulated

Table 6-1: **Transcriptionally deregulated genes associated with the immune/stress response upon IGF-1R depletion**. This table contains the list of mRNA transcripts differentially expressed in IGF-1R depleted cells. The fold change is expressed in the log of 2, and the direction of change relative to the control group (Allstars & non-transfected control) is indicated too. The list was compiled based on results from functional enrichment analyses performed with MetaCore™ and checked against information available on the GeneCards database (Safran et al., 2010). All hits were statistically significant, falling within the cut-off limit of 5% confidence interval for False Discovery Ratio FDR. Colour coded in purple are genes encoding for proteins involved in the LPS-induced inflammatory cellular response, as identified through pathway analysis on MetaCore™.

Hits	Fold change (log)	Adjusted p-value	Direction of change
ACKR3	1.588042	0.000616	Downregulated
ADAMTS6	-1.37612	0.000119	Upregulated
ALPL	-1.12401	0.005308	Upregulated
ANTXR2	-1.42865	1.42E-06	Upregulated
ARHGDIB	-1.49823	0.00052	Upregulated
BMP5	1.035569	5.46E-06	Downregulated
CNTNAP2	1.032524	2.63E-05	Downregulated
COL13A1	-1.41117	4.13E-06	Upregulated
COL17A1	-1.30873	3.60E-05	Upregulated
COL22A1	-1.43425	0.000435	Upregulated
CXCL14	1.267984	0.013486	Downregulated
CXCL8	-2.00092	0.004011	Upregulated
DCLK1	-1.37865	2.12E-05	Upregulated
EDIL3	1.027792	0.00016	Downregulated
EPHB1	-1.15209	5.21E-06	Upregulated
HAPLN1	1.444281	0.002378	Downregulated
IL1RAPL1	-1.1935	0.000275	Upregulated
KISS1	-3.2288	3.32E-05	Upregulated
LAMA5	1.123836	0.000908	Downregulated
LPXN	-2.19108	1.42E-06	Upregulated
MMP3	-2.71789	2.38E-05	Upregulated
P3H2	1.035864	0.014951	Downregulated
PLAU	-1.33275	3.80E-05	Upregulated
PLEK2	-1.03765	9.30E-06	Upregulated
SMAD6	1.248096	0.000407	Downregulated
SMAGP	-1.04167	1.78E-05	Upregulated
STXBP6	-1.14357	3.93E-07	Upregulated
THBS1	-1.04619	0.023343	Upregulated
TRIB1	-1.18277	1.65E-06	Upregulated
TUBB3	1.105915	1.42E-06	Downregulated

Table 6-2: **Transcriptionally deregulated genes associated with extracellular matrix reorganisation, cytoskeleton rearrangement and cell adhesion**. This table contains the list of mRNA transcripts differentially expressed in IGF-1R depleted cells. The fold change is expressed in the log of 2, and the direction of change relative to the control group (Allstars & non-transfected control) is indicated too. The list was compiled based on results from functional enrichment analyses performed with MetaCore™ and checked against information available on the GeneCards database (Safran et al., 2010). All hits were statistically significant, falling within the cut-off limit of 5% confidence interval for False Discovery Ratio FDR.

Hits	Fold change (log)	Adjusted p-value	Direction of change
AOX1	-1.43638	1.74E-06	Upregulated
CPE	1.009027	0.002481	Downregulated
PDE1C	-1.02974	0.000386	Upregulated
SCG5	-2.3844	1.42E-06	Upregulated
SLC2A12	1.358993	5.07E-06	Downregulated
SUGCT	-1.23711	0.000275	Upregulated

Table 6-3: **Transcriptionally deregulated genes associated with metabolism**. This table contains the list of mRNA transcripts differentially expressed in IGF-1R depleted cells. The fold change is expressed in the log of 2, and the direction of change relative to the control group (Allstars & non-transfected control) is indicated too. The list was compiled based on results from functional enrichment analyses performed with MetaCore™ and checked against information available on the GeneCards database (Safran et al., 2010). All hits were statistically significant, falling within the cut-off limit of 5% confidence interval for False Discovery Ratio FDR.

Hits	Fold change (log)	Adjusted p-value	Direction of change
BMP5	1.035569	5.46E-06	Downregulated
IGFBP5	1.418793	0.001979	Downregulated

Table 6-4: **Transcriptionally deregulated genes associated with IGF-1R signalling**. This table contains the list of mRNA transcripts differentially expressed in IGF-1R depleted cells. The fold change is expressed in the log of 2, and the direction of change relative to the control group (Allstars & non-transfected control) is indicated too. The list was compiled based on results from functional enrichment analyses performed with MetaCore™ and checked against information available on the GeneCards database (Safran et al., 2010). All hits were statistically significant, falling within the cut-off limit of 5% confidence interval for False Discovery Ratio FDR.

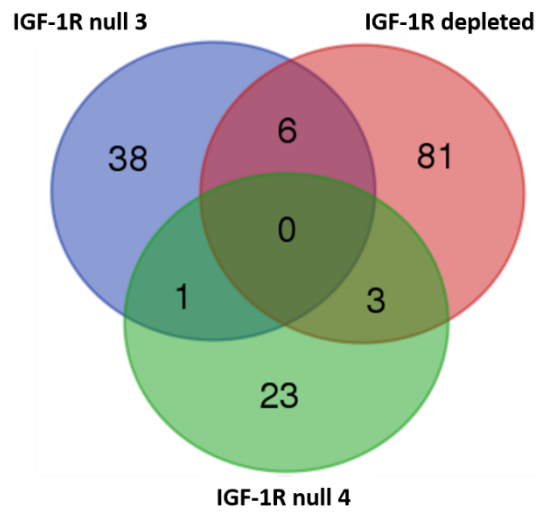
6.2.3. Differentially expressed genes 'in common' between the IGF-1R mutants and depleted cells

We did a Venn diagram in order to determine what RNA hits overlapped and only nine genes were deregulated in both the knockdown and the two radio-sensitive IGF-1R mutants. Surprisingly, only two of the nine overlapping hits encoded proteins with functions related to ECM remodelling or to the immune response. Also, the direction of change (upregulation or downregulation) mostly differed between the mutants and IGF-1R depleted cells (Figure 6-7).

The *IGFBP5* gene was downregulated in the knockdown and in one of the IGF-1R mutants, suggesting that IGF-1R signalling might directly or indirectly influence its expression (Figure 6-7). Interestingly, it has been reported that mTORC1 signalling can stimulate IGFBP5 expression and its subsequent secretion into the extracellular space in order to suppress IGF1-mediated growth factor signalling in a regulatory feedback loop (Ding et al., 2016).

Other common hits were genes encoding the DDIT4 protein (DNA damage-inducible Transcript 4) and IL1RAPL1 (Interleukin 1 Receptor Accessory Protein-Like 1) (Figure 6-7). DDIT4 or REDD1 is involved in the negative regulation of mTORC1 signalling and promotes p53-mediated apoptosis upon induction by DNA damage whereas ILRAPL1 has been linked with JNK activation in neuronal cells (Safran et al., 2010).

Next, we decided to validate by quantitative real-time PCR the hits generated from the RNA microarray, particularly the genes coding for proteins linked with the response to DNA damage or stress.



Overlapping hits	Function	Direction of change
C9orf84	Unknown	Opposite
EMP1	Unknown	Opposite
IGFBP5	IGF-1 signalling	Same (downregulated)
P3H2	Collagen biosynthesis	Opposite
SNORA12	RNA processing	Opposite
THBS1	ECM-related and immune response	Opposite
DDIT4	DNA damage	Same (downregulated)
IL1RAPL1	Immune system	Same (upregulated)
LBH	Transcriptional activator	Opposite

Figure 6-7: **Deregulated genes in common between IGF-1R depleted cells and IGF-1R knockout cells**. The Venn diagram shows overlapping hits across all three sample groups: IGF-1R knockdown, IGF-1R null3 & IGF-1R null4). These were listed down in the table on the right with the top six hits (blue colour coded) corresponding to differentially expressed genes in common between the knockdown and IGF-1R null 3 (mutant #3) whilst the green colour hits between knockdown and IGF-1R null3 and the bottom three (green colour coded) for common hits between IGF-1R depleted cells and IGF-1R null4. The direction of deregulation relative to their respective control is also indicated: 'opposite' = hit is downregulated in one but upregulated in the other; 'same' = hit upregulated or downregulated in both. The Venn diagram was created on http://bioinformatics.psb.ugent.be/webtools/Venn/.

6.2.4. Validation of some RNA hits by qRT-PCR

To validate the microarray data, we assessed by quantitative reverse transcription PCR (qPCR) the expression level of some genes that were identified as significantly deregulated and those that were not statistically significant, comparing the controls to IGF-1R depleted cells but also the wild-type clones to mutants #3 and #4. The genes considered code for proteins known to also be involved in the response to DNA damage or stress.

The validation experiment was performed using the same RNA samples from which a portion was used for the microarray. Primers for amplification were designed as detailed in the methods chapter (see section 2.19). Among the DNA damage related-hits we sought to validate were genes encoding: the growth arrest and DNA damage-inducible 'GADD45A', the damage-specific DNA binding protein 1 'DDB1', the DNA damage-

induced apoptosis suppressor 'DDIAS', the mediator of DNA damage checkpoint 1 'MDC1'. These four genes have all been suggested to influence the response to DNA damage (Lee and Zhou, 2007, Lovejoy et al., 2006, Im et al., 2016, Lee et al., 2017, Xiao et al., 2000). Other tested hits include genes coding for stress-related proteins such as the C-C motif chemokine ligand 2 (CCL2), DNA damage regulated autophagy modulator 1 (DRAM1) and the MDM2-binding protein (MTBP). Although not much is known about the product of the *FAM24B* gene, since the microarray data showed upregulation in IGF-1R depleted cells and that its promoter contains a binding site for the stress-activated protein NF-κB (Safran et al., 2010), we decided to include it too in the validation. Lastly, we assessed the effect of IGF-1R deficiency on the expression of IGFBP5.

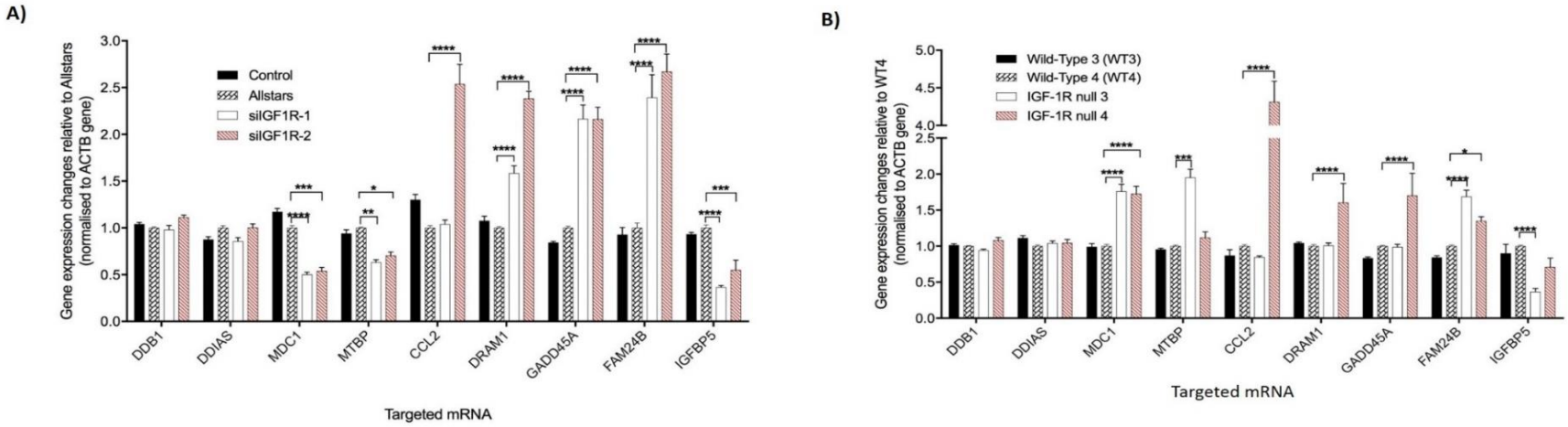
Consistent with the microarray data, the expression level of genes encoding the DNA damage-related proteins DDB1 and DDIAS were unchanged following IGF-1R knockout and siRNA-mediated depletion. However, we did notice significant changes in the expression levels of other genes (Figure 6-8).

In striking contrast to the mutant clones, *MDC1* mRNA levels were significantly reduced in IGF-1R depleted cells whereas these were upregulated in IGF-1R mutant #3 and #4. Likewise, while *MTBP* gene expression was upregulated in mutant #3, there was no deregulation in mutant #4 whilst a significant reduction was detected in IGF-1R depleted cells (Figure 6-8).

Interestingly, IGF-1R deficiency caused downregulation of *IGFBP5* mRNA levels except in the IGF-1R mutant #4 (Figure 6-8). Also, although this was not apparent based on microarray data, our results revealed that both IGF-1R depleted cells and the mutant clones have upregulated mRNA levels for the 'likely' stress-related protein FAM24B compared to their respective controls. Similarly, except for the IGF-1R mutant #3, IGF1R-deficient

cells showed upregulation of *GADD45A*, *CCL2* and *DRAM1* mRNAs coding for proteins associated with the response to stress (Figure 6-8).

Next, we decided to evaluate the phenotypic consequences of IGF-1R depletion in U2OS cells, especially on cell cycling since GADD45A has been shown to promote growth arrest (Wang et al., 1999).



	Expression changes (Microarray data vs qRT-PCR validation)		
Validated Hits	IGF-1R null 3	IGF-1R null 4	IGF-1R depleted cells
DDB1	No // No	No // No	No // No
DDIAS	No // No	No // No	No // No
MTBP	No // Yes	No // No	No // Yes
MDC1	No // Yes	No // Yes	No // Yes
IGFBP5	Yes // Yes	No // No	Yes // Yes
GADD45A	No // No	No // Yes	Yes // Yes
FAM24B	No // Yes	No // Yes	Yes // Yes
CCL2	No // No	Yes // Yes	No // Yes (only with siIGF1R-2)
DRAM1	No // No	No // Yes	No //Yes

Figure 6-8: **RNA hits validation by qRT-PCR**. RNA extracted from the non-transfected U2OS cells (control), the Allstars-transfected and siIGF1R transfected cells (siIGF1R-1 and siIGF1R-2) were reverse transcribed into complementary DNA (cDNA) in **A),** and from wild-type clones (WT3 & WT4) and IGF-1R null clones (mutant #3 & mutant #4) in **B)**. For each target gene, the abundance of cDNA copies was determined by quantitative real-time PCR. This graph shows the abundance levels normalised to the levels of the beta-actin coding gene *ACTB*, the expression of which was not affected by IGF-1R downregulation. The graph was plotted with GraphPad Prism as mean ± SEM as well as the two-way ANOVA statistical analysis (p-value < 0.05 connotes significance). The table at the bottom indicates whether or not there is gene expression change based on the RNA microarray versus qRT-PCR data. These are results from three independent experiments.

6.3. Phenotypic changes associated with IGF-1R depletion

6.3.1. Evaluating the effect of IGF-1R depletion on the cell cycle distribution

To determine the consequences of IGF-1R depletion on cell cycling, U2OS cells were transfected with the siRNAs 'siIGF1R-1' and 'siIGF1R-2' which target the *IGF1R* mRNA. As controls, we had the non-transfected U2OS cells and cells transfected with non-targeting siRNA 'Allstars' (negative control). We used the BrdU labelling method in combination with Propidium iodide staining to determine the proportion of cells at the various stages of the cell cycle. Cells were collected at 48 and 96 hours post-transfection and in parallel, we also evaluated IGF-1R protein levels by western blotting.

From the cell cycle distribution, we derived that IGF-1R depleted cells showed an increased proportion of cells in G2 (Figure 6-9). The proportion of cells in G2 was at least 1.7 fold greater for the knockdown cells (siIGF1R-2-transfected) compared to the negative control (Allstars-transfected) at the 48-hour time-point. At the 96-hour time-point, the fold difference in the percentage of cells in G2 between the negative control and IGF-1R depleted cells was ~2-fold with siIGF1R-1 and ~3-fold with siIGF1R-2 (Figure 6-9). Since this apparent G2 accumulation was only observed in IGF-1R knockdown cells, we deduced that the downregulation of IGF-1R signalling may have triggered G2 cell cycle arrest.

We also noticed that IGF-1R depletion with siIGF1R-2 induced a reduction in the proportion of S cycling cells (Figure 6-9). There was a 2-fold and 4-fold difference in the percentage of cells in the S phase between the negative control and siIGF1R-2 transfected cells respectively at 48 and 96 hours post-transfection. This correlated with an increased

proportion of non-BrdU stained cells between the G1 and the G2 cycle phases corresponding to non-cycling S phase cells (Figure 6-9). However, this was likely the result of off-target effects with the siRNA because similar observations were not made with cells transfected with siIGF1R-1 although we did see effective depletion of the IGF-1R protein with each siRNA at the 48 and 96-hour time-points (Figure 6-10). On the same note, the decreased percentage of cells in the G1 phase observed with siIGF1R-1 at the 96-hour time-point might result from off-target effects or could be due to increased cell death or senescence following G2 arrest (Figure 6-9).

Indeed, whilst there were minor differences in the percentage of cycling cells for the controls, we noted that the percentage of events occurring across the various cell cycle phases decreased dramatically between the 48-hour and 96-hour time-point in IGF-1R depleted cells (Figure 6-9). This was reflected by a more prominent sub-G1 population at the 96-hour time-point on the cell cycle profiles (Figure 6-9) and, together with earlier results depicting the impact of IGF-1R depletion on clonogenic survival of U2OS cells (Figure 6-1) suggested that IGF-1R depletion may have resulted in cell death. We decided to look further into this and assessed cell survival.

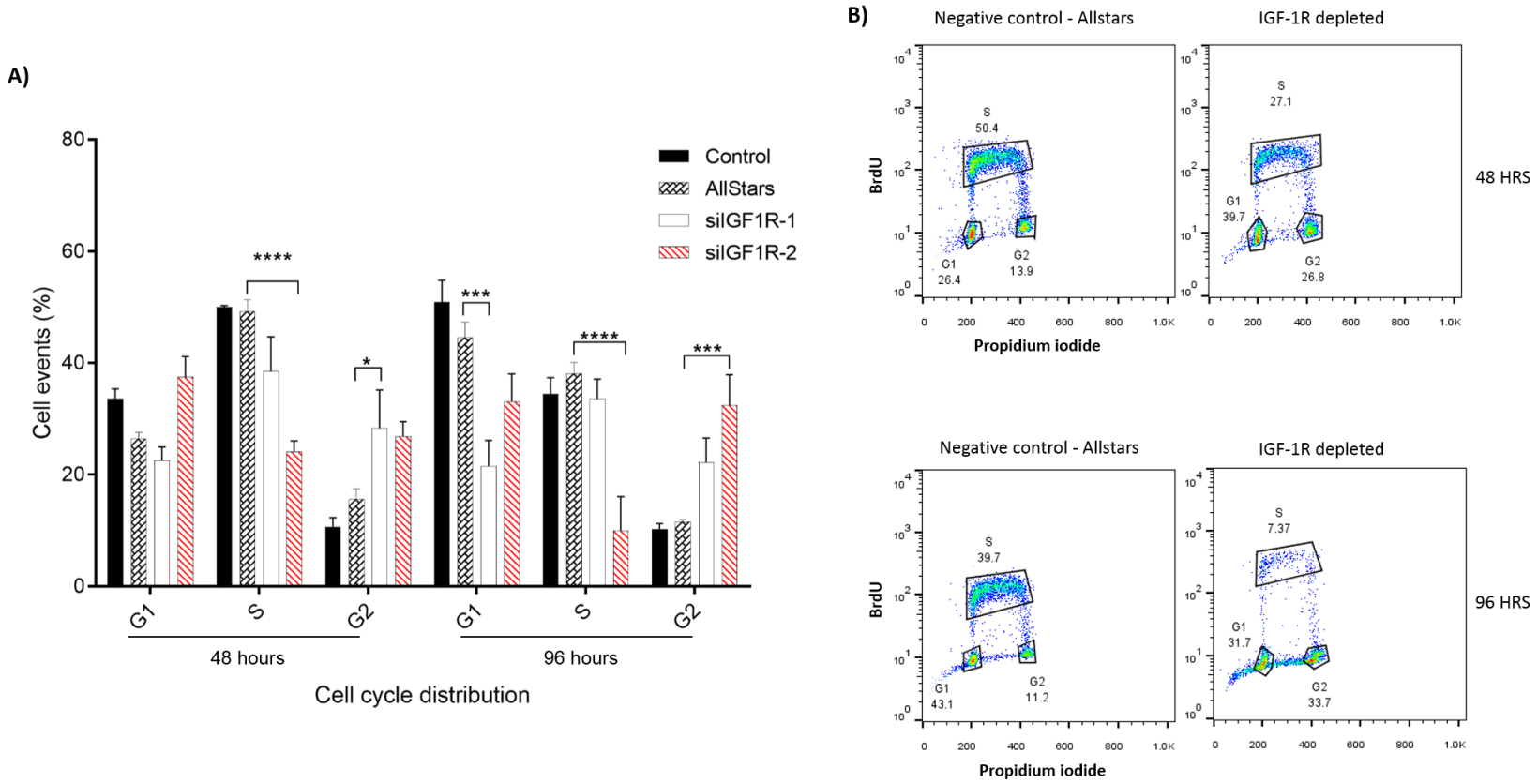


Figure 6-9: **IGF-1R depletion induces G2 accumulation.** Cells were seeded in 10cm dishes and transfected the next day either with non-targeting siRNA 'Allstars' or with IGF1R-targeting siRNAs (siIGF1R-1, siIGF1R-2). Non-transfected control samples did not undergo transfection but the cell culture medium was changed to maintain consistency across samples. Prior to harvesting at the indicated time-points, cells were pulse-labelled with BrdU (10μM) and Propidium iodide was used to stain DNA after fixation. Flow cytometry data were analysed using the Flowjo software to determine the percentage of cells in each cell cycle stage. A) The graph was plotted using GraphPad Prism as mean ±SEM. Statistical significance was calculated by two-way ANOVA using Prism (p-value <0.05). These are results from three independent experiments. B) This figure depicts the impact of IGF-1R knockdown on cell cycling as evidenced by the proportion of cells in the intra-S phase cells and the sub-G1 population. Note: unless stated otherwise, the siRNA concentration for Allstars, siIGF1R-1 and siIGF1R-2 was 100nM. See cell cycle raw data in 8.2.4.

6.3.2. Assessing the effect of IGF-1R knockdown on cell death

To evaluate whether siRNA-mediated depletion of the IGF-1R protein led to cell death in U2OS cells, we decided to quantify the sub-G1 population from the cell cycle profiles described in section 6.3.

The results showed that 48 hours following siRNA transfection, the sub-G1 population under conditions of IGF-1R depletion was 2-2.5 times higher than that observed with the negative control (Figure 6-10). The difference became even more significant at 96 hours post-transfection as the proportion of cells in sub-G1 was 8-9-fold greater when cells were transfected with siRNA targeting the *IGF1R* mRNA (siIGF1R-1, siIGF1R-2) compared to cells transfected with the non-targeting siRNA 'Allstars' (Figure 6-10). This confirmed the hypothesis that suppression of the growth signalling cascade from the IGF-1 receptor led to cell death in U2OS cells.

Probing for downstream signalling targets of the IGF-1R pathway revealed that AKT phosphorylation was suppressed in IGF-1R depleted cells (Figure 6-10). Intriguingly, mTORC1-mediated negative regulation of 4EBP1 function through phosphorylation of the latter appeared increased upon IGF-1R knockdown (Figure 6-10). We also noticed that IGF-1R depletion triggered a striking upregulation of phosphorylated levels of the ERK1 isoform, possibly as a mechanism of cell survival (Figure 6-10). These result might indicate that the ERK1 upregulation is important to prevent lethal damage upon depletion of IGF-1R or, depleted cells might be undergoing ERK-induced cell death (Cagnol and Chambard, 2010). That the function of the 4EBP1 protein is negatively regulated by inhibitory phosphorylation of sites usually attributed to mTORC1 in cells where AKT signalling is suppressed may indicate that other proteins can modulate 4EBP1 function (Gingras et al., 2001).

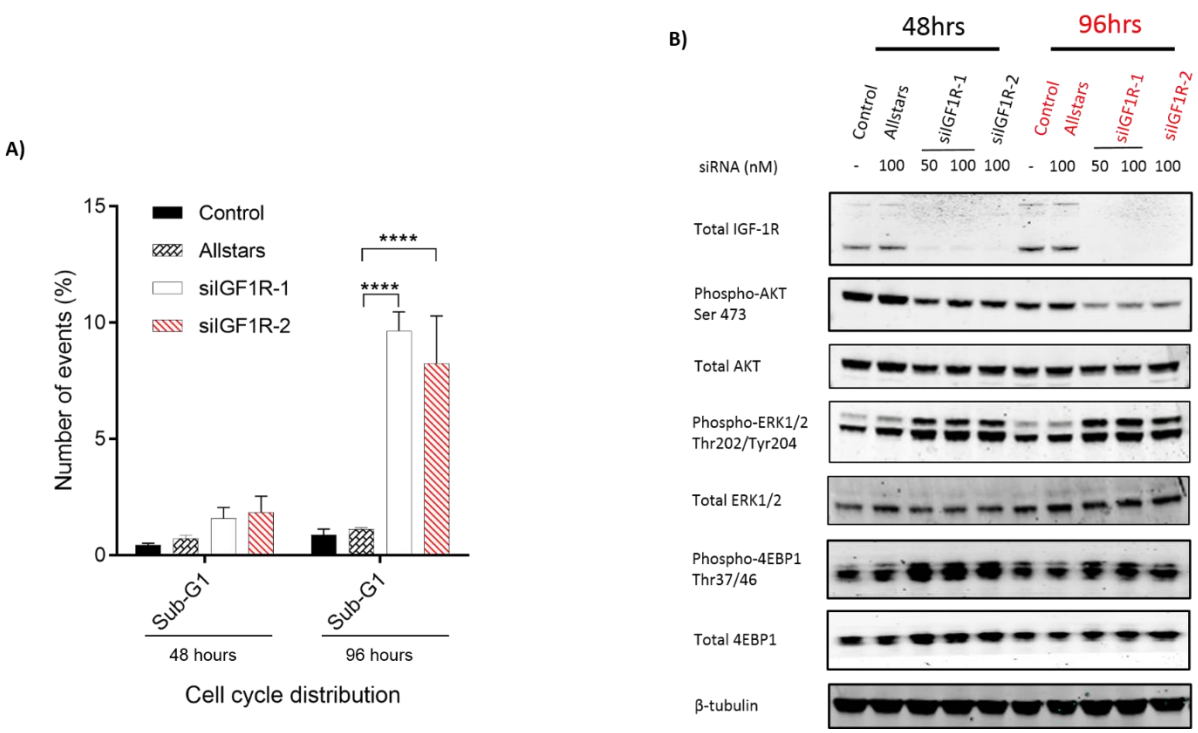


Figure 6-10: **IGF-1R depletion affects cell survival**. **A)** The proportion of cells in Sub-G1 was determined by analysing the data from flow cytometry experiments assessing the effects of IGF-1R depletion on cell cycling with FlowJo (see Figure 6-9). The graph was plotted as mean ± SEM and statistical significance was calculated by two-way ANOVA using Prism (p-value <0.05) on GraphPad Prism. These are results compiled from three independent experiments. **B)** This figure shows the effect of IGF-1R depletion on downstream signalling. Cells were seeded in 10cm dishes and transfected the next day either with non-targeting siRNA 'Allstars' or with the IGF1R-targeting siRNAs siIGF1R-1 (50nM, 100nM) and siIGF1R-2 (100nM). Non-transfected control samples did not undergo transfection but the cell culture medium was changed to maintain consistency across samples. Cells were lysed at the indicated time-points and the lysates were prepared for western blotting as described in the methods (section 2.4). This result shows data obtained from a single repeat.

Since the sub-G1 population can also include necrotic cells, it was not clear whether the cell death resulted from the upregulation in the expression levels of GADD45A. The latter has been shown to induce senescence, apoptosis or survival depending on other intracellular factors (Mak and Kültz, 2004, Gupta et al., 2006). Hence, we stained IGF-1R depleted cells for markers of apoptosis cleaved-PARP and cleaved-caspase 3 at the same time-points post-transfection (48 and 96 hours).

At 48 hours post-transfection, there were negligible differences in the levels of cleaved-caspase 3 and cleaved-PARP between the controls and cells transfected with siIGF1R-1

but, these levels were 2-fold greater when cells transfected with siIGF1R-2 (Figure 6-11). At the 96-hour-time-point, we observed that despite increased levels of cleaved-PARP and cleaved-caspase 3 with the negative control, the increase was much more important under conditions of IGF-1R depletion; the proportion of cleaved-PARP and cleaved-caspase 3 positive cells was at least ~4 times higher when IGF-1R was depleted from cells (Figure 6-11). These findings supported the conclusion that depletion of IGF-1R induced apoptosis in U2OS cells.

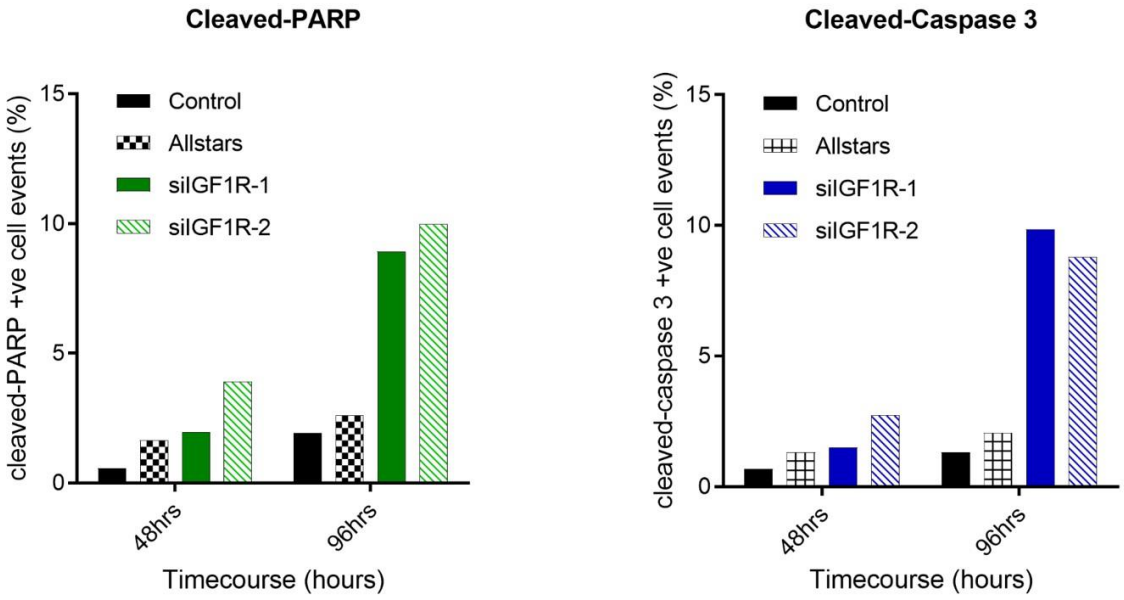


Figure 6-11: **IGF-1R depletion induces apoptosis.** Cells were seeded in 10cm dishes and transfected the next day either with non-targeting siRNA 'Allstars' or with the IGF1R-targeting siRNAs siIGF1R-1 (50nM, 100nM) and siIGF1R-2 (100nM). Non-transfected control samples did not undergo transfection but the cell culture medium was changed to maintain consistency across samples. Upon collection and fixation at the indicated time-points, cells were stained for cleaved-PARP and cleaved-caspase 3. We used DRAQ5 to stain the DNA. Flow cytometry data were analysed using the Flowjo software to determine the percentage of cells positive for the apoptotic markers. This is data obtained from a single repeat. Note: unless stated otherwise, the siRNA concentration for Allstars, siIGF1R-1 and siIGF1R-2 was 100nM. See cell cycle raw data in 8.2.5.

Based on these experiments, we derived that relative to the control, IGF-1R depleted cells might be more susceptible to damage by ionising radiation because, being already in a state

of activated stress may have primed them to undergo apoptosis in response to IR-induced DNA damage.

The findings described here and in the preceding chapter, raised the question whether the sensitisation observed in IGF-1R deficient cells was specific to DNA damage caused by ionising radiation or not. To answer this, the response of the IGF-1R mutants and IGF-1R depleted cells to cytotoxic drugs causing various types of DNA damage was assessed.

6.4. IGF-1R deficiency and the response to other DNA damaging agents

Herein we investigate the impact of chronic and transient lack of IGF-1R on the response of U2OS cells to DNA damaging agents that can cause certain types of DNA damage that do not result from exposure to ionising radiation. We used camptothecin, cisplatin and etoposide which are listed (or analogous compounds are) as chemotherapeutic agents for the treatment of osteosarcomas (American Cancer Society, 2017). These three differ in the type of DNA damage caused and consequently, the pathways solicited to repair the damaged DNA. To evaluate if the phenotypic responses to the drugs are specific to DNA damage or not, vincristine was added to the drug panel. The latter is a mitosis inhibitor which causes cell death by interfering with tubulin polymerisation during metaphase (Moudi et al., 2013).

6.4.1. Assessing the response of IGF-1R mutants to other DNA damaging agents

Wild-type U2OS cells (WT3 and WT4) and IGF-1R mutants (mutant #3 & mutant #4) were treated with solvent or increasing doses of cisplatin (0, 10, 20, 50μM), camptothecin (0, 3,

10μM), etoposide (0, 5, 25, 50, 150μM) and vincristine (0, 1, 2.5, 5, 10μM) for 24 hours and viability was measured 5 days later using the cellTitre blue assay. The drug concentrations were decided based on what had been done in other studies using these same drugs in U2OS (Smeenk et al., 2011, Yoo et al., 2005, Habel et al., 2013, Reinhardt et al., 2007, Dai et al., 2011).

In the response to camptothecin treatment, there were minor differences in cell viability between the IGF-1R mutants and the wild-type but these were not statistically significant (Figure 6-12). At the drug concentration of 3μM, the most sensitive wild-type control (WT3) showed an average survival percentage of 48% and this was 10% higher than that of the least sensitive IGF-1R mutant (mutant #4) and 14% higher than that of IGF-1R mutant #3 (Figure 6-12).

The IGF-1R mutants and the wild-type controls did not show striking differences in their response to the other DNA damaging drugs; the two groups showed a comparable degree of sensitivity to treatment with cisplatin and etoposide (Figure 6-12). Interestingly, whilst the wild-type controls behaved very similarly to each other, we noticed a non-negligible gap between the two mutants in their sensitivity to etoposide especially at the drug concentration of 25μM. IGF-1R mutant #4 appeared to be less sensitive to cellular damage caused by etoposide compared to its mutant counterpart and even the wild-type controls, particularly as the drug concentration increased (Figure 6-12). The average cell survival percentage for IGF-1R mutant #4 with 25μM of etoposide was twice higher than that of mutant #3.

Under treatment conditions with vincristine, the cell viability for both the wild-type and the knockout cells was significantly impaired (Figure 6-12). Just as with cisplatin, we did not notice any remarkable distinction between the mutants and the wild-type controls.

Altogether, these results showed that functional IGF-1R did not confer a selective advantage compared to the controls in the response to damage caused by camptothecin, cisplatin, etoposide and vincristine; implying that IGF-1R deficiency may not affect the cell survival response upon treatment with these drug agents. In order to confirm this, we decided to check the response of IGF-1R depleted cells to treatment with the same drugs.

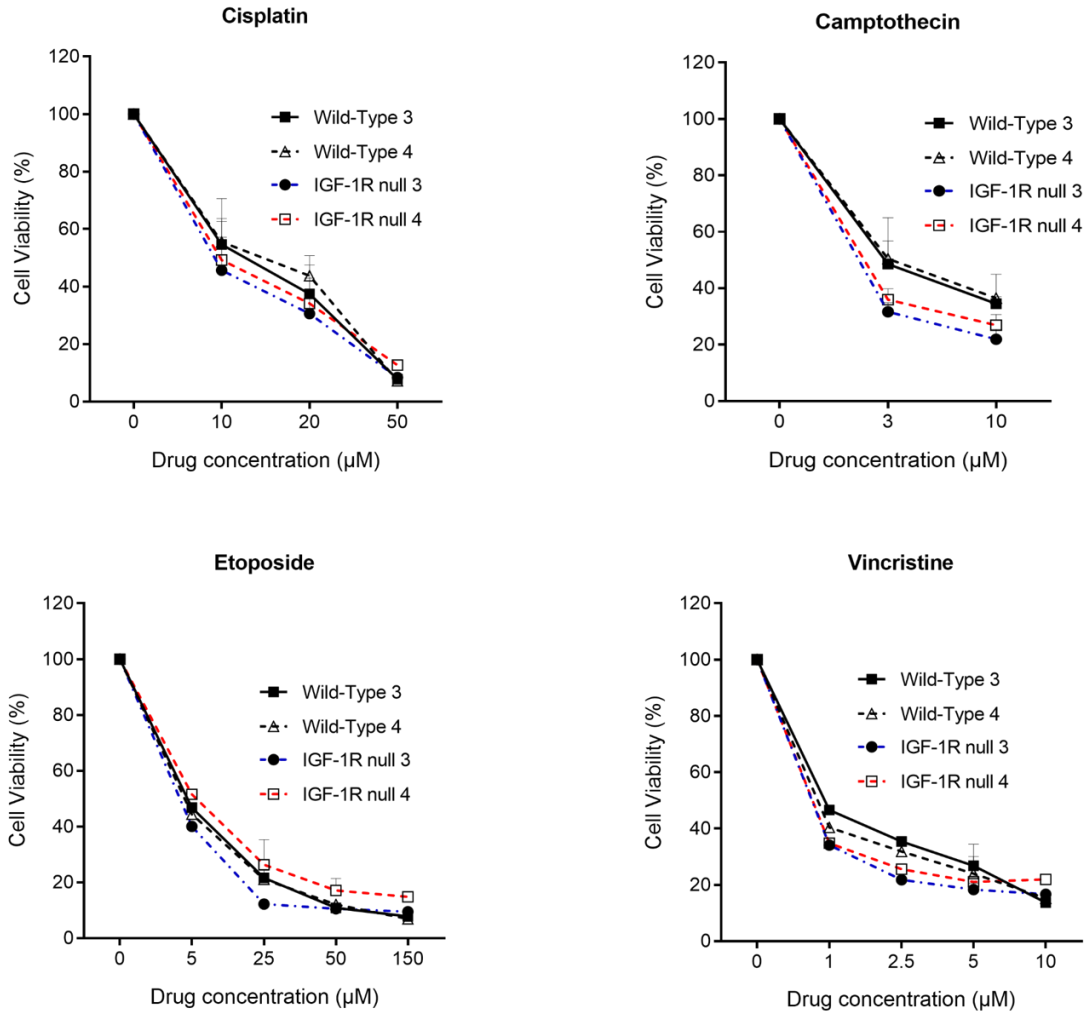


Figure 6-12: **chemo-sensitivity profile of IGF-1R mutants**. U2OS 'wild-type' and IGF-1R mutant cells were seeded into 96-well plates and treated the following day with camptothecin (0, 3, 10μM), cisplatin (0, 10, 20, 50μM), vincristine (0, 1, 2.5, 5μM), etoposide (0, 5, 25, 50, 150μM) or solvent treated. The drug or solvent was removed after 24 hours. Cells were then rinsed with DMEM and cultured for 5 more days in serum-supplemented DMEM until the confluence of the control well reached ~70% after which, viability was measured using the cellTitre Blue assay. POLARstar Omega plate reader was used for signal measurement. Using Prism, graphs were plotted as mean ±SEM on GraphPad Prism. This presents data from three independent experiments. Note: the number of independent repeats varied with some drug doses.

6.4.2. Testing the effects of IGF-1R depletion on the response to cytotoxic drugs

Cells were depleted of IGF-1R using the targeting siRNAs siIGF1R-1 and siIGF1R-2. The following day after transfection, cells were seeded into 96-well plates and treated the next day with solvent or increasing doses of camptothecin (0, 3, 10μM), cisplatin (0, 10, 20μM), etoposide (0, 5, 25μM) and vincristine (0, 1, 5μM).

Treatment with cisplatin was very cytotoxic to U2OS controls and IGF-1R depleted cells; cell survival in the two groups was reduced to less than 40% with 10μM of the drug (Figure 6-13). There was no distinction in the response of the controls from that of the knockdown. The treatment with vincristine also induced significant cell death with the controls and cells depleted of IGF-1R showing comparable levels of sensitivity (Figure 6-13). The same observations were made upon treatment with etoposide. Unlike what was seen with the mutants, the response of cells transfected with siIGF1R-1 to etoposide did not differ from that of siIGF1R-2 transfected cells (Figure 6-13).

Although cell viability was considerably reduced in the controls and IGF-1R depleted cells following treatment with camptothecin, the two groups could be distinguished by their degree of sensitivity to the drug (Figure 6-13). siIGF1R2-transfected cells showed statistically significant greater sensitivity to camptothecin especially at the drug concentration of 3μM when the difference in cell viability between the negative control and cells transfected with siIGF1R-1 and siIGF1R-2 was 20% and 12% respectively (Figure 6-13).

Also interesting was that U2OS controls demonstrated greater sensitivity to camptothecin compared to the wild-type clones (WT3 and WT4) and, IGF-1R depleted cells were also more sensitive than IGF-1R mutants (Figure 6-14).

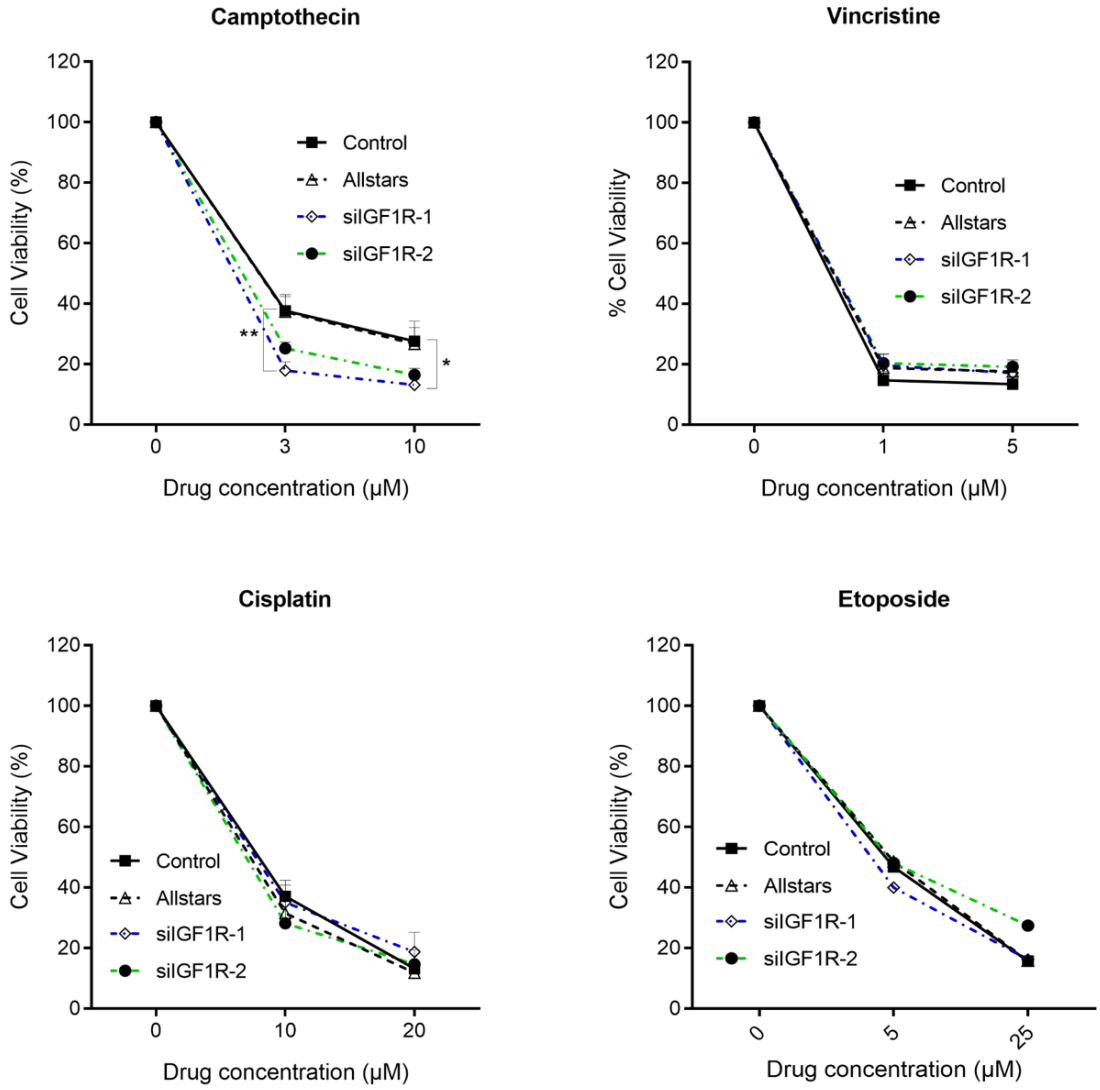


Figure 6-13: **Chemo-sensitivity profile of IGF-1R depleted U2OS cells**. Cells were seeded in 10 cm dishes and the next day either transfected with 100nM of siIGF1R-1, siIGF1R-2 or with the non-targeting siRNA 'Allstars' (negative control) or not transfected at all (control). The day after, these were disaggregated and seeded into a 96-well plate. The following day, triplicate wells were treated with camptothecin (0, 3, 10μM), cisplatin (0, 10, 20μM), vincristine (0, 1, 5μM), etoposide (0, 5, 25μM) or solvent treated. The drug or solvent was removed after 24 hours. Cells then were rinsed with DMEM and cultured for 5 more days in serum-supplemented DMEM until the confluence of the control well reached ~70% after which, viability was measured using the cellTitre Blue assay. POLARstar Omega plate reader was used for signal measurement. Using Prism, graphs were plotted as mean ±SEM for camptothecin and vincristine treatments or mean ±SD for cisplatin (two repeats) or mean only for etoposide (one repeat). Where applicable, statistical significance was calculated by two-way ANOVA using Prism (p-value <0.05) on GraphPad Prism.

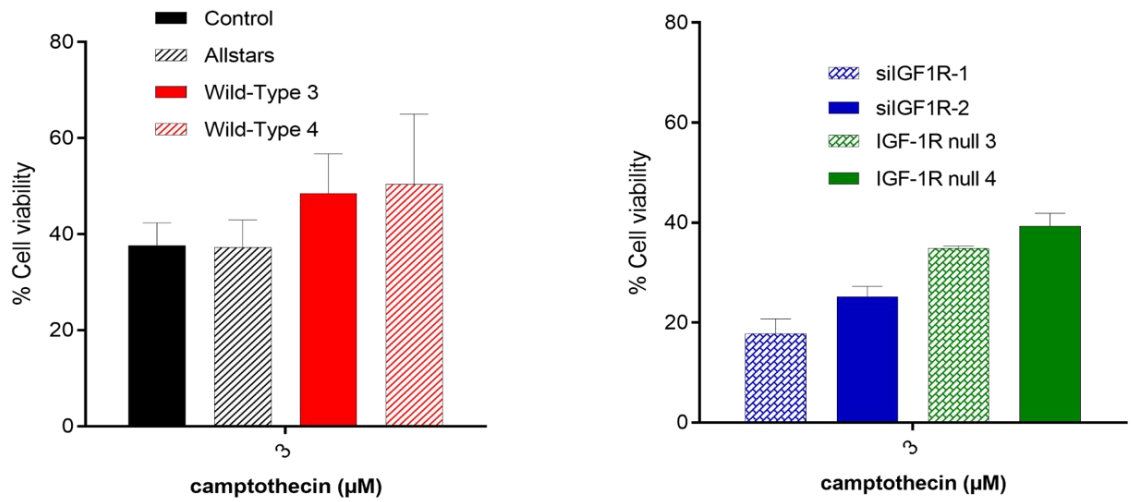


Figure 6-14: **Comparing the chemo-sensitivity profiles of IGF-1R deficient cells**. Comparison of the sensitivity of wild-type clones and IGF-1R knockout clones relative to parental U2OS cells (non-transfected and negatively transfected) and IGF-1R depleted cells respectively to treatment with camptothecin. Using Prism, graphs were plotted as mean ±SEM.

6.5. Discussion

In this chapter, we have shown that deficiency in IGF-1R, even transient, results in radio-sensitisation and that double-strand break repair upon exposure to ionising radiation as measured by γH2AX focus formation and resolution was not impaired in IGF-1R depleted cells. This prompted an investigation at the transcriptome level to determine whether IGF-1R depletion induced gene expression changes that may account for the enhanced sensitivity of knockdown cells to damage induced by γ-irradiation.

Similar to what was observed in IGF-1R mutants, most of the genes that were deregulated upon downregulating IGF-1R levels coded for proteins that function in cellular processes that determine cell motility, migration and metastatic potential. Whether changes in the transcriptional regulation of genes associated with extracellular matrix remodelling, cell adhesion and cytoskeleton rearrangement may also contribute to the radio-sensitivity profile of IGF-1R depleted cells is yet to be confirmed. It would be informative to conduct experiments that will help dissect the consequential effects of these changes on cell motility, anchorage-independent cell growth and metastatic potential and determine whether these are potentiated or repressed upon exposure to ionising radiation. But first, the hits identified in the transcriptome analysis should be validated by qPCR.

Validation of the microarray data revealed an interesting dichotomy between IGF-1R depleted cells and the mutant clones which does not allow to speculate that deregulated levels of *MDC1* expression might account for the enhanced radio-sensitivity phenotype displayed by cells lacking the IGF-1R protein. Lower expression levels of the *MDC1* gene support the hypothesis that the repair of radiation-induced double strand breaks could be impaired in IGF-1R depleted cells given that the MDC1 protein plays the role of a signal amplifier in the DNA damage response cascade, facilitating the recruitment of repair

proteins to the sites of DNA damage as evidenced in previous studies (Chen et al., 2017, Lee et al., 2017). However, what are we to make of the upregulation observed in the 'full' knockout cells? The answer might lie in the understanding of DDR-independent MDC1 functions that are progressively being unravelled (Eliezer et al., 2014, Li et al., 2017, Wang et al., 2015).

Another fascinating observation is that deregulated hits *MTBP*, *DRAM1* and *GADD45A* are all linked to the p53 pathway: *GADD45A* gene transcription can be stimulated via p53-dependent mechanisms (Fornace et al., 1989); the *DRAM1* gene encodes a lysosomal membrane protein that is required for the induction of autophagy and its expression is also regulated by the p53 pathway (Crighton et al., 2006). Meanwhile, *MTBP* encodes a protein that increases the stability of the MDM2 protein thereby promoting p53 ubiquitination and its subsequent degradation (Brady et al., 2005). Taken together, the changes in expression levels observed for these p53 target genes suggest that IGF-1R depletion may have resulted in p53 accumulation. Further experiments should be conducted to confirm this.

In correlation with the upregulation seen in the expression levels of GADD45A confirmed by qRT-PCR, we detected increased accumulation of cells in the G2 phase of the cell cycle although in different order of magnitude between cells transfected with either siIGF1R-1 or siIGF1R-2. Unlike what was seen in the IGF-1R mutant, depletion of IGF-1R impeded on the proliferative ability of U2OS cells as evidenced by the reduction in clonogenic survival under normal growth conditions, in the absence of ionising radiation.

GADD45A is thought to play an important role in the maintenance of genomic stability through its modulatory function on different cellular processes namely cell cycle control, DNA repair, apoptosis, survival and senescence (Salvador et al., 2013, Fornace et al., 1989, Jin et al., 2000, Wang et al., 1999, Carrier et al., 1999, Hollander et al., 2001). Although upregulated

levels of GADD45A is associated with cellular stress induction and subsequent activation of the G2/M cell cycle checkpoint, its upregulation alone is not sufficient to cause cell death (Asuthkar et al., 2011). Depending on the cellular context, high levels of GADD45A can promote survival, apoptosis or senescence via p53-dependent or –independent mechanisms (Gupta et al., 2006, Tront et al., 2006, Smith et al., 2000).

Indeed, it has been shown that co-upregulation of IL-24 and GADD45A suppresses tumour growth and promotes apoptosis (Su et al., 2003, Zerbini et al., 2006, Jiang et al., 1996). This is what was suggested by the transcriptome profile of IGF-1R depleted cells where we observed upregulated levels of both IL-24 and GADD45A and, the increased levels of apoptosis markers cleaved-PARP and cleaved-caspase3 in the IGF-1R depleted cells. This could therefore constitute a major contributing factor to the increased sensitivity of IGF-1R depleted cells to ionising radiation. Interestingly, co-upregulation of GADD45 proteins and IL-24 has previously been associated with radio-sensitisation in cancer cells (Su et al., 2003).

Previous investigations have shown that suppression of IGF-1R signalling can also promote chemo-sensitivity (Wang et al., 2010, Flanigan et al., 2010, Rochester et al., 2005, Singh et al., 2014, Duan et al., 2009). We observed a modest reduction in cell viability in IGF-1R depleted cells upon treatment with camptothecin compared to the controls. However, the biological significance of this effect should be ascertained by conducting clonogenic assay experiments.

7. Discussion

7.1. IGF-1R signalling and double-strand break repair

Previous studies have pinpointed double-strand break induction and repair kinetics as a major determinant of tumour cells' response to irradiation (Zaffaroni et al., 1994, El-Awady et al., 2003, Schwartz et al., 1988). We evaluated this by tracking the formation and resolution of γH2AX focus formation in the IGF-1R deficient and proficient U2OS cells. Our results did not suggest any delay in the induction nor in the repair of double-strand breaks following exposure to ionising radiation as a result of IGF-1R deficiency. There was no difference in IR-induced foci numbers between the mutant and the wild-type nor between IGF-1R depleted cells and the negative control throughout the course of the experiment. The same observations were made in CHL-1 melanoma cells where IGF-1R inhibition did not prevent the formation nor the resolution of γH2AX foci resulting from TMZ-induced double-strand breaks.

This was in conflict with previously published findings from our group which revealed that although γH2AX focus formation was not impaired, inhibition and depletion of IGF-1R resulted in delayed resolution of γH2AX foci in irradiated DU145 prostate cancer cells (Chitnis et al., 2008, Turney et al., 2012). This led us to question whether the disparity between our results might be cell-context dependent.

7.2. Limitations and future work recommendations

Although our study is a good attempt to examine the influence of IGF-1R in the response to DNA damage, there are several things that remain to be tackled. We confirmed previous

evidence suggesting that abrogation of IGF-1R signalling sensitise cancer cells to ionising radiation and gained some understanding of possible cellular processes underpinning radio-sensitisation. But, we are still short of in-depth mechanistic insights.

The Experimental approach

It would have been very informative if the effects of IGF-1R on the efficiency of homologous recombination and non-homologous end-joining were tested in DNA repair reporter assays, comparing the wild-type and the IGF-1R mutants or depleted cells (Seluanov et al., 2010). Moreover, in addition to tracking γH2AX focus formation and its resolution, it would have been interesting to confirm by immunofluorescence the recruitment and retirement of proteins known to be involved in the latter stages of homologous recombination such as members of the multimeric complex involved in the resolution of double Holliday junctions (Seki et al., 2006, Wu et al., 2006, Raynard et al., 2006).

Furthermore, while investigating the activation of the DNA damage signalling cascade, it would have been highly beneficial to probe for Serine 15 phosphorylation of p53 and also the phosphorylation of CHK2 at Threonine 68 since both are known to be targets of activated ATM following ionising radiation; ATM-mediated Thr68-CHK2 phosphorylation is a priming event triggering CHK2 activation (Ahn et al., 2000, Blackford and Jackson, 2017, Canman et al., 1998, Banin et al., 1998, Ahn et al., 2002). As well as being a signal amplifier in the DNA damage response signalling cascade, activation of CHK2 promotes cell cycle arrest. A number of studies have shown that CHK2 can mediate IR-induced G2/M cell cycle arrest (Hirao et al., 2000, Gogineni et al., 2011). However, experiments conducted in CHK2-deficient fibroblast cells suggest that while CHK2's function in G2/M arrest may be redundant, it remains an influential factor for p53-mediated G1 cell cycle arrest (Agarwal et al., 1995, Takai et al., 2002). Controversially, evidence from

another study conducted in mouse embryo fibroblast cells suggests that CHK2 is not required for IR-induced p53-mediated G1 cell cycle arrest (Jack et al., 2002).

Nonetheless, the key characteristic associated with CHK2-deficiency is radio-resistance, with evidence suggesting that CHK2 plays a critical role in the p53-mediated radiation-induced apoptosis by influencing p53 stability and its transcriptional activity (Hirao et al., 2002, Takai et al., 2002, Jack et al., 2002, Chen et al., 2005). It is generally accepted that phosphorylation of the serine15 residue on p53 by ATM following ionising radiation promotes p53 accumulation by disrupting its binding interactions with MDM2 and, increased levels of p53 can amount to different cell fates (cell cycle arrest, senescence or apoptosis) depending on a number of other factors (Shieh et al., 1997, Loughery et al., 2014, Sakaguchi et al., 1998, Zhang et al., 2011, Okaichi et al., 2011).

Thus, probing for phosphoThr68-CHK2 and phosphoSer15-p53 in IGF-1R deficient and wild-type U2OS cells could have provided clues to the mechanisms underlying the radiation response observed in these cells. Since Thr68-CHK2 phosphorylation is not exclusively ATM-dependent and that activated CHK2 can promote p53-mediated apoptosis in an ATM-dependent but also ATM-independent manner (Hirao et al., 2002, Matsuoka et al., 2000). Therefore, if future investigations were to pinpoint p53-mediated apoptosis as a contributing factor to the radio-sensitivity observed in IGF-1R null 3, IGF-1R null 4 and IGF-1R depleted cells, undertaking experiments to clarify the role of ATM in influencing the observed response to radiotherapy should be considered.

Another experimental procedure that could have been considered is the neutral comet assay to determine at the individual cell level the reparability of IR-induced double-strand breaks in the IGF-1R deficient U2OS cells versus proficient ones (Olive and Banath, 2006).

Also, assessing the impact of IGF-1R on replication fork restart would have greatly helped in clarifying whether IGF-1R deficient cells can resume DNA replication after fork stalling or collapse. This might be achieved by conducting DNA fibre assay, comparing the propensity of IGF-1R mutants to that of the wild-type in resuming with replication after hydroxyurea-induced fork stalling/collapse (Nieminuszczy et al., 2016).

Finally, it needs to be acknowledged that because IGF-1R has been shown to translocate to the nucleus and as such is likely involved in carrying out kinase-independent functions in the cell via protein-protein or DNA-protein interactions, it is paramount that the phenotypic observations made in IGF-1R deficient cells is tested with the use of a small molecule inhibitor targeting the IGF-1R signalling pathway or by complementing the deficient cells with kinase-dead IGF-1R (Aleksic et al., 2010, Sehat et al., 2010, Weiss et al., 2007). This would allow dissection of the nuclear role of IGF-1R from its membrane-bound function and reveal whether both are required to confer radio-protection.

Increased radio-sensitivity as a true consequence of IGF-1R loss

We have shown that out of the five mutant clones that were tested of which two were 'partial' knockouts and three were 'full' knockouts, four displayed increased sensitivity to irradiation relative to the wild-type controls. Moreover, IGF-1R depletion also resulted in the radio-sensitisation of U2OS cells. In order to decipher the molecular changes underpinning the reduced sensitivity displayed by one of the mutant clones, it might be beneficial to pursue in-depth understanding of the mechanisms underlying radio-sensitivity in more than two clones and use the radio-resistant clone to test subsequent findings.

Alternatively, it would also shed light to investigate by genomic sequencing methods whether there are amino acid changes in the chromosome locus specific to the *IGF1R* gene

in the radio-resistant mutant clone. The genome information should then be compared to that of the wild-type clones as well as other IGF-1R mutant clones.

Exploring qRT-PCR validated hits as mediators of radio-sensitivity

Although more microarray hits need to be validated in order to help uncover the molecular mechanisms underlying the radio-sensitivity observed upon depletion or knockout of IGF-1R, it would be important to assess the contribution of upregulated hits such as FAM24B, GADD45A and DRAM1 to this phenotype. This can be achieved by manipulating the expression levels of these targets and evaluate the effects on the response to irradiation.

Moreover, GADD45A has been implicated in modulating DNA accessibility to cellular proteins to promote genome stability (Carrier et al., 1999, Hollander et al., 2001, Xiao et al., 2000). Therefore, although there was no apparent delay in γH2AX focus formation and resolution in IGF-1R depleted cells, examining the changes triggered by ionising radiation on the activation and localisation of key DDR proteins in comparison to IGF-1R proficient controls may reveal important clues on their enhanced radio-sensitivity profile.

Furthermore, since GADD45A has been shown to interact with cell cycle regulator p21 and can also inhibit the activity of the protein complex cdc2/cyclinB1 (Kearsey et al., 1995, Zhan et al., 1999), it would be interesting to investigate whether post-irradiation cell cycle checkpoint integrity observed in mutant #3 and the wild-type controls which do not show deregulated *GADD45A* mRNA levels is compromised or heightened in mutant #4 and IGF-1R depleted cells.

However, given the large body of evidence showing that GADD45A is important for genome stability it might be unlikely that higher expression levels of this gene alone would affect cell survival post-irradiation.

AKT as an influential factor in the cellular response to irradiation

As discussed earlier in this report in sections 1.3.2.3 and 5.1.2, several studies have demonstrated the role of AKT signalling in the cellular radiation response through its effects on apoptosis and also on double strand break repair. While there is a large body of evidence supporting the function of AKT as a promoter of DNA-PK-dependent NHEJ (Toulany et al., 2012, Fraser et al., 2011, Toulany et al., 2008, Oeck et al., 2017), it has also been shown that AKT suppresses NHEJ-mediated repair via phosphorylation of the XRCC4-Like Factor (XLF) protein on Thr181 which may promote its association with 14-3-3 and could result in nuclear exclusion and subsequent degradation (Liu et al., 2015). However, this appears to be an isoform-specific interaction as the authors reported no XLF phosphorylation with AKT isoforms 2 and 3. Cells expressing a phospho-mimetic XLF mutant showed impaired NHEJ while those deficient in XLF-Thr181 phosphorylation were more tolerant to DNA damage and showed increased NHEJ repair capacity.

However, the contribution of AKT activation to the radiation response observed in the IGF-1R knockout U2OS cells is unclear. Because there were no sharp differences in phospho-AKT levels between IGF-1R mutant 1 which was significantly less sensitive to ionising radiation than mutants 3 and 4, it is difficult to ascertain whether reduced phospho-AKT levels observed in IGF-1R deficient cells may have resulted in reduced availability of Ser473-AKT phosphorylated by DNA-PKcs to promote NHEJ. At the same time, the opposite case that decreased levels of AKT-mediated XLF phosphorylation may account for the increased tolerance of IGF-1R null 1 to ionising radiation can also not be argued for. Nonetheless, the relationship between DNA-PKcs and AKT and, AKT and XLF should be interrogated in both IGF-1R knockouts and IGF-1R depleted cells.

Also, given that the PI3K/AKT signalling pathways has been reported to influence GADD45 gene expression in a FOXO3a-dependent manner following Myc activation (Amente et al., 2011), it would be informative to explore this relationship in the context of IGF1R-dependent cellular response to irradiation. This could be of particular importance since both IGF-1R depleted and IGF-1R null 4 cells showed significantly upregulated levels of GADD45A mRNA.

Conclusion

Altogether, beyond suggesting possible mechanisms by which the IGF-1R protein can confer radio-protection, our study points to a better way forward in the investigation of the intricate relationship between IGF-1R signalling and the response to radiotherapy in cancer. Because diverse cellular processes are influenced by IGF-1R function, because proteins function in multiple cellular networks and since, cell behaviour is governed by the integration of many and various intracellular and extracellular cues, it may not be possible to thoroughly understand how high levels of IGF-1R are associated with radio-resistance unless a systems-wide approach is adopted. That is what we have attempted to do in this work, searching through evidence at the proteome, transcriptome and metabolome level to better understand the different factors that may contribute together in defining how the IGF-1R signalling can affect the response to ionising radiation. It is hoped that adopting new approaches in tackling this question will take us closer to shaping more effective therapeutic strategies in the treatment of cancers that show dependence on the IGF-1R signalling pathway.

8. Appendix

8.1. ImageJ Macro language Script for Foci counting

```
run("Z Project...", "projection=[Max Intensity] ");
run("Split Channels");
selectWindow("C1-MAX_image");
setAutoThreshold("Otsu dark");
setThreshold(1292, 4095);
//run("Threshold...");
setOption("BlackBackground", false);
run("Convert to Mask");
run("Analyze Particles...", "size=50-Infinity show=[Count Masks] clear add");
run("glasbey");
saveAs("PNG", "C:\\Users\\The Apple of HIS Eye\\Desktop\\Count_masks_output\\"+title);
count = roiManager("Count");
run("Clear Results");
for (i=0;i<count;i++){
selectWindow("C2-MAX_image");
roiManager("Select", i);
run("Find Maxima...", "noise=300 output=Count");
selectWindow ("C3-MAX_image");
roiManager("select", i);
run("Find Maxima...", "noise=500 output=Count");
IJ.log("title:\t"+title+"\t gammaH2AX: \t"+getResult("Count", nResults-2)+"\t RAD51: \t"+getResult("Count", nResults-1)); }
```

8.2. Raw data for flow cytometry

The following tables represent raw data for corresponding flow cytometry figures in the text.

8.2.1. Cell cycle changes following drug treatment in CHL-1

This table contains data presented in Figure 3-6.

24 hours post-treatment	Control	TMZ	AZ3801	TMZ + AZ3801
G1	63.6	9.24	13.4	4.68
S	25.9	30.4	11.8	11
G2	7.04	56.6	59.3	78.3
>4N	0.99	0.73	11.2	3.5

48 hours post-treatment	Control	TMZ	AZ3801	TMZ + AZ3801
G1	54	26.8	10.2	6.17
S	24.8	8.07	6.67	0.82
G2	14.7	61.7	47.2	82.1
>4N	1.07	0.72	28.3	8.26

60 hours post-treatment	Control	TMZ	AZ3801	TMZ + AZ3801
G1	61.3	32.2	13.7	9.23
S	26.1	7.56	7.75	1.67
G2	10.3	50.8	40	72.1
>4N	0.38	0.87	29.3	10.3

Values denoted are in percentage (%)

8.2.2. Cell cycle changes following IGF-1R depletion in CHL-1

This table contains data presented in Figure 3-7.

48 hours post-transfection

	Control		Allstars		siIGF1R	
	expt #1	expt #2	expt #1	expt #2	expt #1	expt #2
G1	46.3	47.6	39.4	33.5	78.5	61.6
S	39.5	38.7	47.5	51.6	16.6	24.1
G2	7.46	9.12	10.2	11.4	1.94	8.75
>4N	0.42	1.24	0.45	0.96	0.08	2.59

120 hours post-transfection

	Control		Allstars		siIGF1R	
	expt #1	expt #2	expt #1	expt #2	expt #1	expt #2
G1	69.7	43.3	58.5	47.2	53.3	62.6
S	22.8	44	31.5	39.9	32.4	25.4
G2	4.6	9.86	6.91	9.25	6.51	6.14
>4N	0.24	0.25	0.26	0.9	0.27	0.43

expt = experiment Values denoted are in percentage (%)

8.2.3. Assessing checkpoint integrity in response to irradiation

This table contains data presented in Figure 5-4.

		Wild-type -- no IR		Knockout - no IR		Wild-type- IR		Knockout - IR	
10 hours		expt #1	expt #2	expt #1	expt #2	expt #1	expt #2	expt #1	expt #2
	G1	29.9	39.4	23.7	32.3	7.49	13.6	4.88	9.8
	S	50.8	48.3	51	50.3	65.1	64.7	66.6	63.7
	G2	7.37	9.47	13.7	12	17.7	17.5	16.3	20.2
22 hours									
	G1	33.1	32.7	29.9	32.8	16.1	8.19	6.28	6.04
	S	49.9	55.8	51.5	48.5	20.1	40.7	24.1	40.2
	G2	7.37	8.03	8.83	12.4	51.9	31.9	51.5	40.3
72 hours									
	G1	47.9	54	40.4	45.9	19.1	21.6	12	12.1
	S	35.5	36.7	39.8	35.3	14.3	8.5	10.9	9.69
	G2	4.89	5.81	5.67	9.78	44.4	62.3	49.9	72.3

expt = experiment Values denoted are in percentage (%)

8.2.4. Cell cycle changes following IGF-1R depletion in U2OS

This table contains data presented in Figure 6-9 and Figure 6-10.

48 hours post-transfection

	Control			Allstars			siIGF1R-1			siIGF1R-2		
	expt #1	expt #2	expt #3	expt #1	expt #2	expt #3	expt #1	expt #2	expt #3	expt #1	expt #2	expt #3
G1	34.5	30.2	36.1	28.4	24.5	26.4	26.7	18.5	22.5	39.7	30.3	42.4
S	49.4	50.4	50.2	52.1	45.4	50.4	44.8	26.1	44.6	27.1	20.6	24.7
G2	11.1	13.2	7.73	13.7	19.3	13.9	22.5	41.9	20.7	26.8	31.5	22.2
sub-G1	0.51	0.32	0.51	0.47	0.77	0.93	0.75	2.4	1.59	1.07	3.22	1.26

96 hours post-transfection

	Control			Allstars			siIGF1R-1			siIGF1R-2		
	expt #1	expt #2	expt #3	expt #1	expt #2	expt #3	expt #1	expt #2	expt #3	expt #1	expt #2	expt #3
G1	58.6	45.9	48.2	49.9	43.1	40.8	30.1	14.4	20.2	31.7	25.5	42.2
S	28.8	38.2	36.4	34.1	39.7	40.5	32.6	28.2	40.1	7.37	1.09	21.6
G2	8.41	11.7	10.6	12.2	11.2	11.4	17	30.8	18.9	33.7	41.2	22.4
sub-G1	0.83	0.49	1.33	0.98	1.15	1.23	10.2	10.7	8.07	9.21	11.2	4.35

expt = experiment Values denoted are in percentage (%)

8.2.5. Apoptotic markers in IGF-1R depleted U2OS cells

This table contains data presented in Figure 6-11.

Cleaved PARP levels

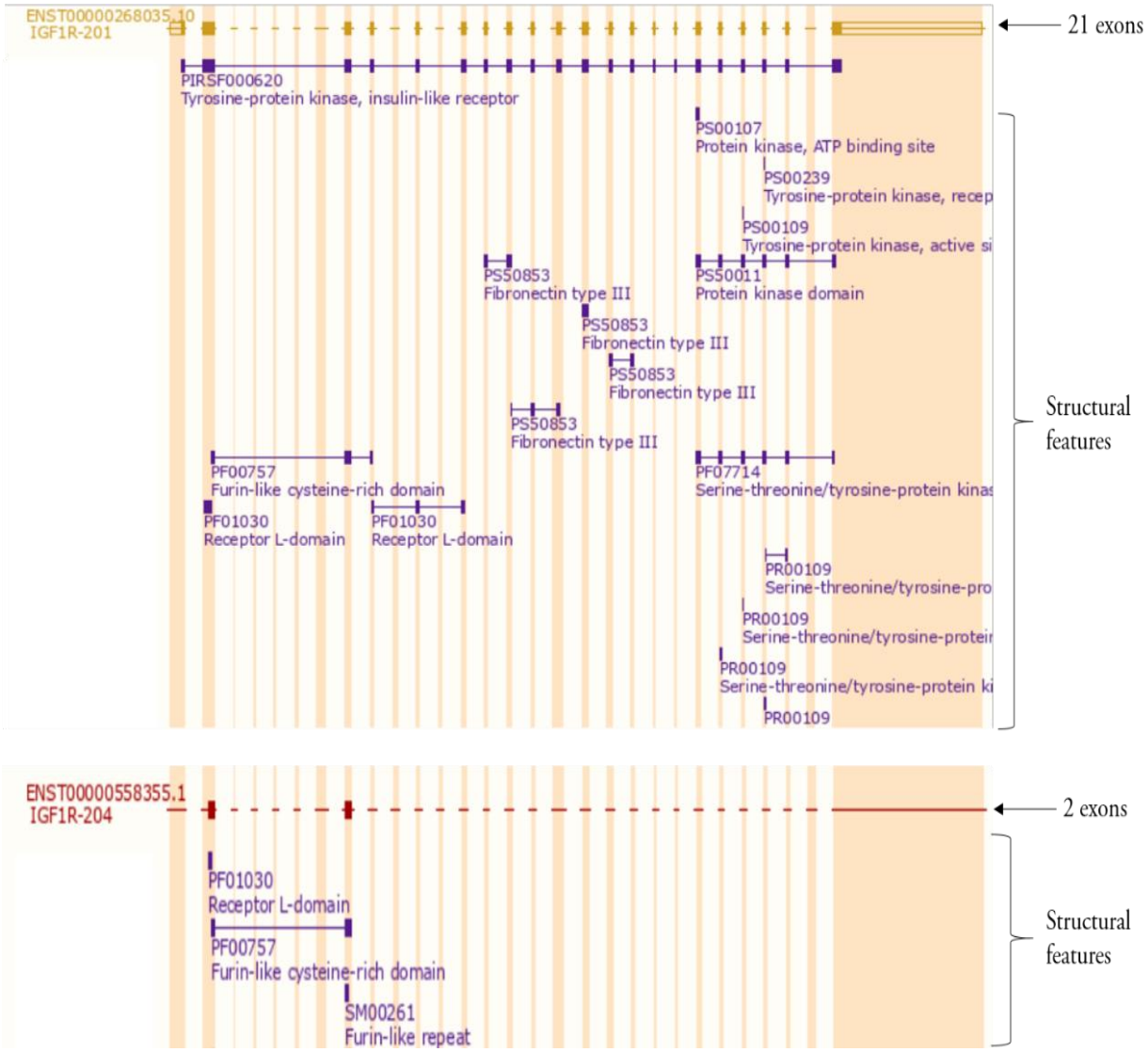
	Control	AllStars	siIGF1R-1	siIGF1R-2
48 hours	0.56	1.64	1.97	3.9
96 hours	1.93	2.61	8.91	9.98

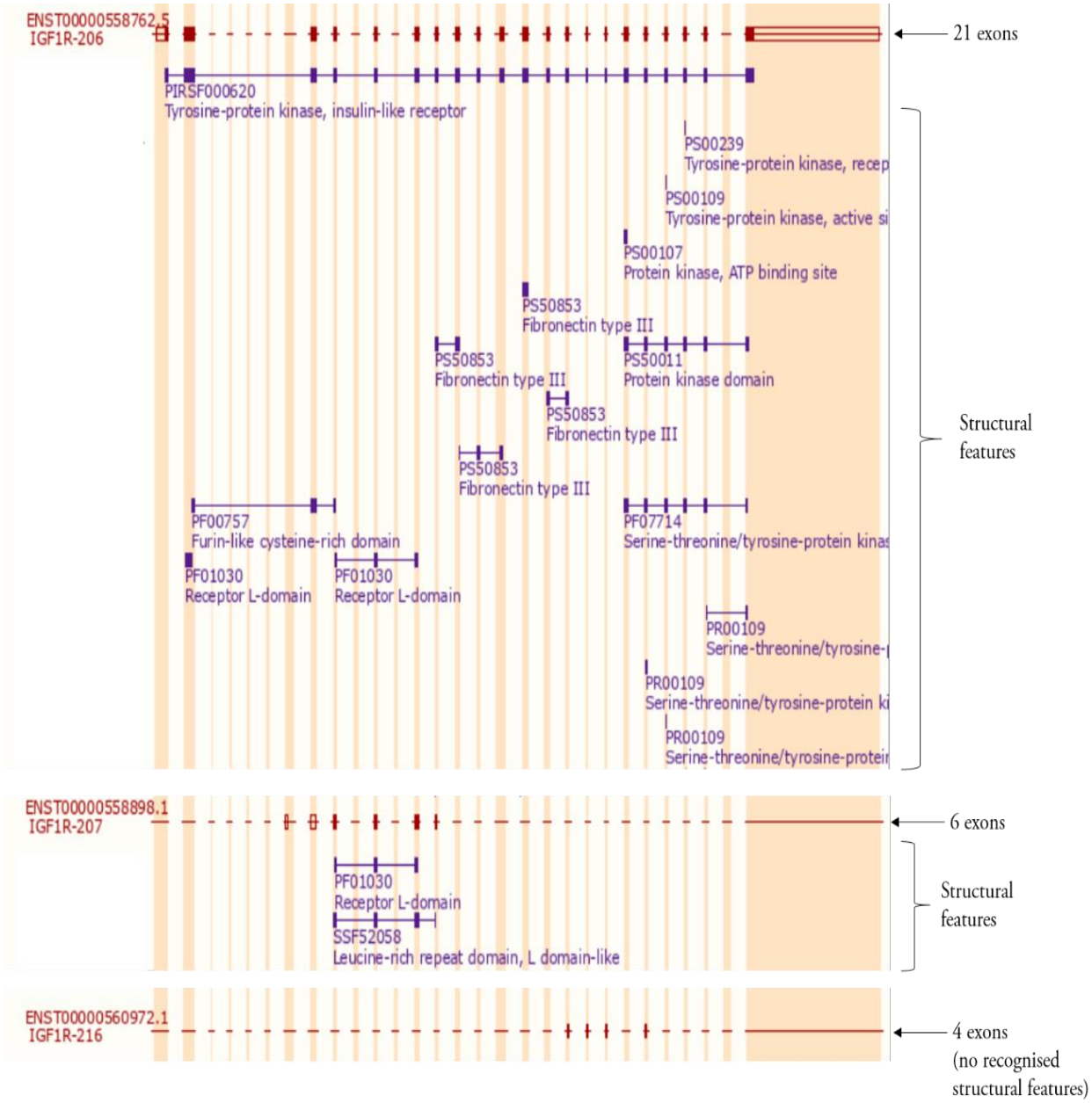
Cleaved caspase-3 levels

	Control	Allstars	siIGF1R-1	siIGF1R-2
48 hours	0.68	1.32	1.49	2.73
96 hours	1.31	2.06	9.84	8.79

Values denoted are in percentage (%)

8.3. Structural information on *IGF1R* protein coding splice variants




ENST00000558762.5
IGF1R-206
21 exons
PIRSF000620
Tyrosine-protein kinase, insulin-like receptor
PS00239
Tyrosine-protein kinase, recep
PS00109
Tyrosine-protein kinase, active si
PS00107
Protein kinase, ATP binding site
PS50853
Fibronectin type III
PS50853
Fibronectin type III
PS50011
Protein kinase domain
PS50853
Fibronectin type III
PS50853
Fibronectin type III
PF00757
Furin-like cysteine-rich domain
PF07714
Serine-threonine/tyrosine-protein kinas
PF01030
Receptor L-domain
PF01030
Receptor L-domain
PR00109
Serine-threonine/tyrosine-
PR00109
Serine-threonine/tyrosine-protein ki
PR00109
Serine-threonine/tyrosine-protei
Structural features
ENST00000558898.1
IGF1R-207
6 exons
PF01030
Receptor L-domain
SSF52058
Leucine-rich repeat domain, L domain-like
Structural features
ENST00000560972.1
IGF1R-216
4 exons
(no recognised structural features)

8.4. Response of IGF-1R mutant clones to irradiation

8.4.1. Clonogenic assay with four mutant clones

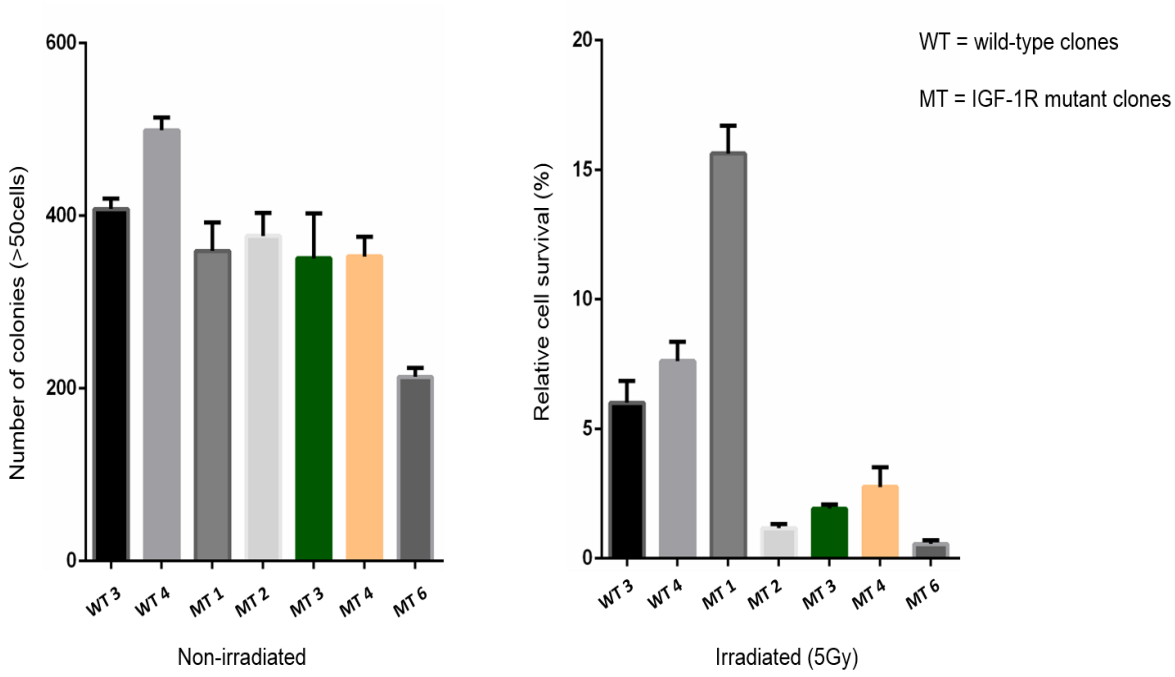


Figure 8-1: **Effect of ionising radiation on cell proliferation in 'full' and 'partial' IGF-1R knockouts**. Wild-type and knockout cells were seeded in triplicates in 6-well plates and either irradiated the next day with 5Gy or not. The number of colonies per well was determined 9-10 days after seeding using the GelCount colony counter (Optotronix, Oxford). The percentage of cell survival for mutants and wild-type clones was calculated in proportion to the number of colonies that grew under conditions of no irradiation. The graph was plotted with GraphPad Prism as mean ± standard error of the mean (SEM). Statistical significance was calculated by one-way ANOVA using Prism (p-value <0.05). These are results compiled from three independent experiments.

8.4.2. Post-irradiation timecourse in IGF-1R null and wild-type clones

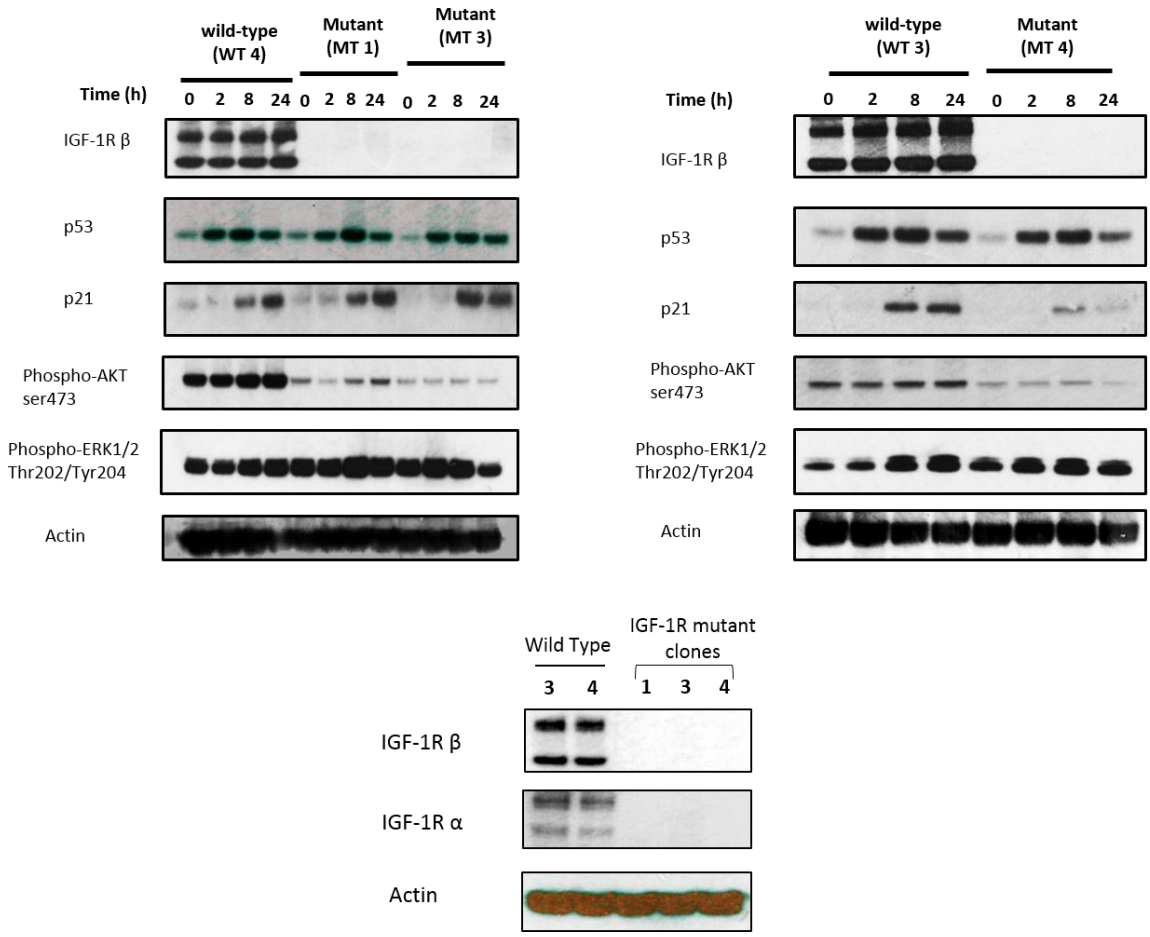


Figure 8-2: I**onising radiation induces molecular changes in 'full' knockouts and wild-type cells**. Cells were seeded in 10cm culture dishes and irradiated the next day with 5Gy. Cells were lysed at the indicated time-points after irradiation. The non-irradiated cells (0h) were lysed at 2h post-irradiation. The lysates were prepared for western blotting as described in the Methods chapter (section 2.4). The results depicted were obtained from a single experiment.

8.5. All hits from transcriptome analysis

8.5.1. Wild-type vs IGF-1R null 3

Gene Symbol	Gene Name	Fold-change (log)	Adjusted p-value
AKR1C3	aldo-keto reductase family 1, member C3	-1.099260241	0.00043062
ALDOC	aldolase, fructose-bisphosphate C	-1.249969477	0.000165299
ANKRD18DP	ankyrin repeat domain 18D, pseudogene	-2.192953469	3.61E-14
BCYRN1	brain cytoplasmic RNA 1	1.031001157	0.000281089
BHLHE40	basic helix-loop-helix family member e40	1.131059585	2.12E-06
BST2	bone marrow stromal cell antigen 2	-1.462020377	3.14E-08
C5orf46	chromosome 5 open reading frame 46	2.658654742	4.56E-10
C6orf15	chromosome 6 open reading frame 15	2.026064099	6.01E-05
C9orf84	chromosome 9 open reading frame 84	-1.137497628	0.000324342
COL16A1	collagen type XVI alpha 1	1.142580344	8.52E-05
COL6A3	collagen type VI alpha 3	1.235264085	0.008236356
CTSL	cathepsin L	-1.11586899	0.000520418
EFEMP1	EGF containing fibulin-like extracellular matrix protein 1	-1.107212363	1.45E-05

EMP1	epithelial membrane protein 1	1.066337757	0.00039777
FDFT1	farnesyl-diphosphate farnesyltransferase 1	-1.211101529	6.79E-05
GPER1	G protein-coupled estrogen receptor 1	-1.022377796	0.000849251
HCFC1R1	host cell factor C1 regulator 1 (XPO1 dependent)	1.135688289	0.010152687
HIST1H2BJ	histone cluster 1, H2bj	-1.109399047	0.000258967
HIST1H2BK	histone cluster 1, H2bk	-1.169444099	0.000936835
HIST2H2AA3	histone cluster 2, H2aa3	-1.088237014	0.000252319
IGFBP5	insulin-like growth factor binding protein 5	1.767032218	2.10E-05
KRT16	keratin 16	1.239019501	1.50E-05
KRT17	keratin 17	1.827551385	7.18E-07
LMCD1	LIM and cysteine rich domains 1	1.054704837	1.60E-05
LRRC17	leucine rich repeat containing 17	-1.042187645	0.002971122
MYEOV	myeloma overexpressed	1.129678114	0.000162586
NUDT14	nudix hydrolase 14	1.11382006	3.14E-08
P3H2	prolyl 3-hydroxylase 2	-1.087915425	0.002448284
PBK	PDZ binding kinase	-0.990579559	0.000168208
PDLIM7	PDZ and LIM domain 7	1.268311165	3.36E-07
PLAC8	placenta specific 8	-1.983913326	3.20E-05
PSG4	pregnancy specific beta-1-glycoprotein 4	-1.112249658	0.002361373
RAC2	ras-related C3 botulinum toxin substrate 2 (rho family, small GTP binding protein Rac2)	1.3751747	0.001845234

RNA28S5	RNA, 28S ribosomal 5	1.072756499	0.013713749
SERPINE2	serpin peptidase inhibitor, clade E (nexin, plasminogen activator inhibitor type 1), member 2	1.163933728	0.000261233
SERPINH1	serpin peptidase inhibitor, clade H (heat shock protein 47), member 1, (collagen binding protein 1)	0.993493696	1.30E-05
SLC2A1	solute carrier family 2 member 1	1.099496082	6.79E-06
SLC35A2	solute carrier family 35 member A2	1.007438091	2.26E-07
SNORA12	small nucleolar RNA, H/ACA box 12	-1.097060919	0.009487205
SNU13	SNU13 homolog, small nuclear ribonucleoprotein (U4/U6.U5)	2.371030645	3.61E-14
THBS1	thrombospondin 1	1.026307944	0.000223653
TIGAR	TP53 induced glycolysis regulatory phosphatase	0.988027775	6.02E-05
TIMP1	TIMP metallopeptidase inhibitor 1	1.556765865	1.60E-05
TNFAIP6	TNF alpha-induced protein 6	1.681452977	0.001883701
ZNF395	zinc finger protein 395	-1.265209721	0.000243198

8.5.2. Wild-type vs IGF-1R null 4

Gene Symbol	**Gene Name**	**Fold-change (log)**	**Adjusted p-value**
GAGE5	G antigen 5	-3.349654958	3.58E-12
GAGE12J	G antigen 12J	-3.286581919	8.53E-12
GAGE12I	G antigen 12I	-3.286448595	3.58E-12

GAGE12G	G antigen 12G	-3.25496079	3.58E-12
GAGE2B	G antigen 2B	-3.227291553	2.39E-11
GAGE4	G antigen 4	-3.205582701	5.36E-12
GAGE12H	G antigen 12H	-3.166301666	8.24E-11
GAGE6	G antigen 6	-3.142070935	5.40E-12
GAGE12C	G antigen 12C	-3.017728439	1.84E-10
GAGE12B	G antigen 12B	-2.814175977	6.74E-12
GAGE2E	G antigen 2E	-2.50186782	8.24E-11
GAGE2A	G antigen 2A	-2.46356864	2.55E-10
GAGE12F	G antigen 12F	-2.14190062	0.00170345
GAGE8	G antigen 8	-1.489976717	4.51E-09
CCL2	C-C motif chemokine ligand 2	-1.470276389	0.000444998
GAGE12E	G antigen 12E	-1.448185743	9.60E-09
LBH	limb bud and heart development	-1.384525099	0.018461553
FDFT1	farnesyl-diphosphate farnesyltransferase 1	-1.348917888	0.000225302
COL8A1	collagen type VIII alpha 1	-1.306160951	0.001859908
IL1RAPL1	interleukin 1 receptor accessory protein like 1	-1.223787896	6.52E-05
CAV1	caveolin 1	-1.050011024	0.005951319
SCARNA13	small Cajal body-specific RNA 13	-1.025257279	0.004312137
LRRN1	leucine rich repeat neuronal 1	-0.992071841	0.002739195
CGB5	chorionic gonadotropin beta subunit 5	1.016340486	0.033222328
CGB1	chorionic gonadotropin beta subunit 1	1.173115339	0.023024539
DDIT4	DNA damage inducible transcript 4	1.281382963	0.022493911
CT45A1	cancer/testis antigen family 45, member A1	1.617869838	0.038136126

8.5.3. Controls vs IGF-1R knockdown

Gene Symbol	Gene Name	Fold-change (log)	Adjusted p-value
MARCH4	membrane associated ring-CH-type finger 4	-1.687432585	0.00016944
ACKR3	atypical chemokine receptor 3	1.588041578	0.000615568
ADAMTS6	ADAM metallopeptidase with thrombospondin type 1 motif 6	-1.376124954	0.00011943
ALPL	alkaline phosphatase, liver/bone/kidney	-1.124010151	0.00530772
ANTXR2	anthrax toxin receptor 2	-1.428653889	1.42E-06
AOX1	aldehyde oxidase 1	-1.436375982	1.74E-06
ARHGDIB	Rho GDP dissociation inhibitor (GDI) beta	-1.498233952	0.000519603
ARL14	ADP ribosylation factor like GTPase 14	-1.279444534	1.42E-06
BMP5	bone morphogenetic protein 5	1.035568872	5.46E-06
C9orf84	chromosome 9 open reading frame 84	1.097857252	0.000833932
CACNA2D4	calcium voltage-gated channel auxiliary subunit alpha2delta 4	-1.109641117	1.42E-06
CCDC148	coiled-coil domain containing 148	-1.094756597	0.005911765
CCDC167	coiled-coil domain containing 167	1.005317549	2.76E-05
CD163L1	CD163 molecule like 1	-1.095209072	3.42E-05

CFAP58	cilia and flagella associated protein 58	-1.397813799	2.16E-05
CNTNAP2	contactin associated protein-like 2	1.03252358	2.63E-05
COL13A1	collagen type XIII alpha 1	-1.411167176	4.13E-06
COL17A1	collagen type XVII alpha 1	-1.308731815	3.60E-05
COL22A1	collagen type XXII alpha 1	-1.434253346	0.00043524
CPE	carboxypeptidase E	1.009027216	0.002480976
CXCL14	C-X-C motif chemokine ligand 14	1.267983765	0.013486129
CXCL8	C-X-C motif chemokine ligand 8	-2.000921503	0.004010569
CXXC5	CXXC finger protein 5	1.021240928	0.000602787
DBNDD1	dysbindin (dystrobrevin binding protein 1) domain containing 1	1.013820249	0.003369613
DCLK1	doublecortin like kinase 1	-1.378653191	2.12E-05
DDIT4	DNA damage inducible transcript 4	0.987944219	0.021718307
DEFB103A	defensin beta 103A	-1.714471356	3.32E-06
DIRC3	disrupted in renal carcinoma 3	-1.008464181	2.16E-05
EBI3	Epstein-Barr virus induced 3	-1.130264339	0.000532455
EDIL3	EGF like repeats and discoidin domains 3	1.027792139	0.000160081
EFR3B	EFR3 homolog B	-1.090977321	4.15E-05
EMP1	epithelial membrane protein 1	-1.252655085	0.001876315
EPHB1	EPH receptor B1	-1.152089638	5.21E-06
ESM1	endothelial cell specific molecule 1	-1.714926269	5.46E-06
FAM24B	family with sequence similarity 24 member B	-1.253357991	1.85E-06
FOXD1	forkhead box D1	-1.023006386	0.001397894
FOXS1	forkhead box S1	1.131024035	7.53E-05

GADD45A	growth arrest and DNA damage-inducible alpha	-1.020460253	4.39E-05
GLIPR1	GLI pathogenesis related 1	-1.306287331	0.001714567
HAPLN1	hyaluronan and proteoglycan link protein 1	1.444281244	0.002377852
IGFBP5	insulin-like growth factor binding protein 5	1.41879316	0.001979381
IL1RAPL1	interleukin 1 receptor accessory protein like 1	-1.193495665	0.000275075
IL24	interleukin 24	-1.178182839	1.62E-05
KCNK1	Potassium channel subfamily K member 1	1.147598419	0.001783334
KIAA1324	KIAA1324	-1.540710675	2.76E-05
KISS1	KiSS-1 metastasis-suppressor	-3.228795293	3.32E-05
KRT34	keratin 34	-2.229196718	5.65E-06
LAMA5	laminin subunit alpha 5	1.123835717	0.000907785
LBH	limb bud and heart development	1.52049602	0.003369613
LETM2	leucine zipper and EF-hand containing transmembrane protein 2	-1.123584303	2.28E-05
LPXN	Leupaxin	-2.191075631	1.42E-06
LY96	lymphocyte antigen 96	-1.356195744	4.14E-06
MAP3K7CL	MAP3K7 C-terminal like	-1.40717704	0.00357951
MMP3	matrix metallopeptidase 3	-2.717888716	2.38E-05
MN1	meningioma (disrupted in balanced translocation) 1	1.781006255	5.46E-06
MPP4	membrane protein, palmitoylated 4	-1.247176699	1.82E-06

NLRP3	NLR family, pyrin domain containing 3	-1.16936174	4.14E-06
NRG1	neuregulin 1	-1.288464386	0.002480976
NTNG1	netrin G1	-1.007818341	1.12E-06
P3H2	prolyl 3-hydroxylase 2	1.035864074	0.014951279
PDE1C	phosphodiesterase 1C	-1.029740062	0.000386037
PLAU	plasminogen activator, urokinase	-1.332754477	3.80E-05
PLEK2	pleckstrin 2	-1.037647317	9.30E-06
PRR36	proline rich 36	1.10097759	0.000408327
RGS4	regulator of G-protein signaling 4	-1.120473703	2.03E-05
RGS7	regulator of G-protein signaling 7	-1.096071393	1.80E-05
RHOBTB3	Rho related BTB domain containing 3	1.246656766	0.002987761
RNF150	ring finger protein 150	1.388982797	7.80E-05
SBK1	SH3 domain binding kinase 1	1.387243978	1.03E-05
SCARNA11	small Cajal body-specific RNA 11	1.038005746	0.000149529
SCARNA20	small Cajal body-specific RNA 20	1.164355418	0.003151742
SCG5	secretogranin V	-2.384395447	1.42E-06
SERPINB7	serpin peptidase inhibitor, clade B (ovalbumin), member 7	-1.35546633	1.80E-05
SLC2A12	solute carrier family 2 member 12	1.358993229	5.07E-06
SMAD6	SMAD family member 6	1.248095589	0.000406594
SMAGP	small cell adhesion glycoprotein	-1.041667902	1.78E-05
SNORA12	small nucleolar RNA, H/ACA box 12	1.210749646	0.001974586
STXBP6	syntaxin binding protein 6	-1.143571567	3.93E-07

SUGCT	succinyl-CoA:glutarate-CoA transferase	-1.237108677	0.000275075
SYTL3	synaptotagmin like 3	-2.141133397	7.57E-07
TGM2	transglutaminase 2	-1.42595354	0.029589474
THBS1	thrombospondin 1	-1.046189794	0.023343483
TM4SF1	transmembrane 4 L six family member 1	-1.009240239	1.39E-05
TMEM154	transmembrane protein 154	-1.266369915	0.015790195
TNFRSF11B	tumor necrosis factor receptor superfamily member 11b	-1.205088126	1.91E-05
TRIB1	tribbles pseudokinase 1	-1.182766524	1.65E-06
TRIML2	tripartite motif family like 2	-1.591298724	4.14E-05
TUBB3	tubulin beta 3 class III	1.105915042	1.42E-06
VSTM1	V-set and transmembrane domain containing 1	-1.342564117	2.55E-05
ZNF503	zinc finger protein 503	1.334808836	4.96E-05

8.6. RStudio Scripts for generating heatmaps

8.6.1. Launching the pheatmap package

```
library(pheatmap)
library (RColorBrewer)
```

8.6.2. Comparing wild-type vs IGF-1R null4

---

title: "crisprWTvs1E5"

author: "Wilfride P."

output: html_document

```{r heatmap}

setwd("C:/microarray_analysis/Heatmaps")

mydata <- read.table("KOexpressionmatrix.txt", header=T, sep= "\t", row.names=1)

mydata <- mydata[apply(mydata, MARGIN = 1, FUN = function(x) sd(x) != 0),]

set <- read.table("WTvs1E5crisprdrgGeneSet.txt", header=FALSE, sep="\t")

set <- as.character(set[, 1])

setgene <- c(set)

setgene <- unique(setgene)

Gene_for_heatmap <- mydata[setgene,]

head(Gene_for_heatmap, 10)

pheatmap(Gene_for_heatmap, scale="row", key=T, keysize=1.5, density.info="none", trace="none", cexCol=0.9, fontsize_row = 5, fontsize_col = 10, main='edgeR_BRN2_top1000', cluster_cols = TRUE, cluster_col=FALSE, color = colorRampPalette(rev(brewer.pal(n = 11, name ="RdBu")))(100))

```

8.6.3. Comparing wild-type vs IGF-1R null3

---

title: "Untitled"

output: html_document

```{r heatmap}

setwd("C:/microarray_analysis/Wilfride")

mydata <- read.table("KOexpressionmatrix.txt", header=T, sep= "\t", row.names=1)

mydata <- mydata[apply(mydata, MARGIN = 1, FUN = function(x) sd(x) != 0),]

set <- read.table("1D5geneset.txt", header=FALSE, sep="\t")

set <- as.character(set[, 1])

setgene <- c(set)

setgene <- unique(setgene)
```

Gene_for_heatmap <- mydata[setgene,]

head(Gene_for_heatmap, 10)

pheatmap(Gene_for_heatmap, scale="row", key=T, keysize=1.5, density.info="none", trace="none", cexCol=0.9, fontsize_row = 5, fontsize_col = 10, main='edgeR_BRN2_top1000', cluster_cols = TRUE, cluster_col=FALSE, color = colorRampPalette(rev(brewer.pal(n = 11, name ="RdBu")))(100))

```

### 8.6.4. Heatmap with metabolomics data

---

title: "Updated_MetabolomicsScript"

author: "Wilfride P."

output: html_document

---

```{r heatmap}

setwd("C:/microarray_analysis/Wilfride")

mydata <- read.table("SUPERIORdrgmetabolites.txt", header=T, sep= "\t", row.names=1)

mydata <- mydata[apply(mydata, MARGIN = 1, FUN = function(x) sd(x) != 0),]

set <- read.table("SUPERIORmetaboliteset.txt", header=FALSE, sep="\t")

set <- as.character(set[, 1])

setgene <- c(set)

setgene <- unique(setgene)

Gene_for_heatmap <- mydata[setgene,]

head(Gene_for_heatmap, 10)

pheatmap(Gene_for_heatmap, scale="row", key=T, keysize=1.5, density.info="none", trace="none", cexCol=0.9, fontsize_row = 5, fontsize_col = 10, main='edgeR_BRN2_top1000', cluster_cols = TRUE, cluster_col=FALSE, color = colorRampPalette(rev(brewer.pal(n = 11, name ="RdBu")))(100))

```
```

Bibliography

ABRAMOVITCH, S., GLASER, T., OUCHI, T. & WERNER, H. 2003. BRCA1–Sp1 interactions in transcriptional regulation of the IGF-IR gene. *FEBS Letters,* 541**,** 149-154.

ADACHI, Y., LI, R., YAMAMOTO, H., MIN, Y., PIAO, W., WANG, Y., IMSUMRAN, A., LI, H., ARIMURA, Y., LEE, C. T., IMAI, K., CARBONE, D. P. & SHINOMURA, Y. 2009. Insulin-like growth factor-I receptor blockade reduces the invasiveness of gastrointestinal cancers via blocking production of matrilysin. *Carcinogenesis,* 30**,** 1305-13.

ADAMS, T. E., EPA, V. C., GARRETT, T. P. & WARD, C. W. 2000. Structure and function of the type 1 insulin-like growth factor receptor. *Cell Mol Life Sci,* 57**,** 1050-93.

AGARWAL, M. L., AGARWAL, A., TAYLOR, W. R. & STARK, G. R. 1995. p53 controls both the G2/M and the G1 cell cycle checkpoints and mediates reversible growth arrest in human fibroblasts. *Proc Natl Acad Sci U S A,* 92**,** 8493-7.

AGUIRRE, G. A., DE ITA, J. R., DE LA GARZA, R. G. & CASTILLA-CORTAZAR, I. 2016. Insulin-like growth factor-1 deficiency and metabolic syndrome. *Journal of Translational Medicine,* 14**,** 3.

AHN, J.-Y., LI, X., DAVIS, H. L. & CANMAN, C. E. 2002. Phosphorylation of Threonine 68 Promotes Oligomerization and Autophosphorylation of the Chk2 Protein Kinase via the Forkhead-associated Domain. *Journal of Biological Chemistry,* 277**,** 19389-19395.

AHN, J. Y., SCHWARZ, J. K., PIWNICA-WORMS, H. & CANMAN, C. E. 2000. Threonine 68 phosphorylation by ataxia telangiectasia mutated is required for efficient activation of Chk2 in response to ionizing radiation. *Cancer Res,* 60**,** 5934-6.

AHNESORG, P., SMITH, P. & JACKSON, S. P. 2006. XLF Interacts with the XRCC4-DNA Ligase IV Complex to Promote DNA Nonhomologous End-Joining. *Cell,* 124**,** 301-313.

AHUJA, D., SAENZ-ROBLES, M. T. & PIPAS, J. M. 2005. SV40 large T antigen targets multiple cellular pathways to elicit cellular transformation. *Oncogene,* 24**,** 7729-45.

AKEN, B. L., AYLING, S., BARRELL, D., CLARKE, L., CURWEN, V., FAIRLEY, S., FERNANDEZ BANET, J., BILLIS, K., GARCÍA GIRÓN, C., HOURLIER, T., HOWE, K., KÄHÄRI, A., KOKOCINSKI, F., MARTIN, F. J., MURPHY, D. N., NAG, R., RUFFIER, M., SCHUSTER, M., TANG, Y. A., VOGEL, J.-H., WHITE, S., ZADISSA, A., FLICEK, P. & SEARLE, S. M. J. 2016. The Ensembl gene annotation system. *Database,* 2016**,** baw093-baw093.

ALEKSIC, T., CHITNIS, M. M., PERESTENKO, O. V., GAO, S., THOMAS, P. H., TURNER, G. D., PROTHEROE, A. S., HOWARTH, M. & MACAULAY, V. M. 2010. Type 1 insulin-like growth factor receptor translocates to the nucleus of human tumor cells. *Cancer Res,* 70**,** 6412-9.

ALESSI, D. R., ANDJELKOVIC, M., CAUDWELL, B., CRON, P., MORRICE, N., COHEN, P. & HEMMINGS, B. A. 1996. Mechanism of activation of protein kinase B by insulin and IGF-1. *Embo j,* 15**,** 6541-51.

ALL-ERICSSON, C., GIRNITA, L., SEREGARD, S., BARTOLAZZI, A., JAGER, M. J. & LARSSON, O. 2002. Insulin-like growth factor-1 receptor in uveal melanoma: a predictor for metastatic disease and a potential therapeutic target. *Invest Ophthalmol Vis Sci,* 43**,** 1-8.

AMENTE, S., ZHANG, J., LUBRANO LAVADERA, M., LANIA, L., AVVEDIMENTO, E. V. & MAJELLO, B. 2011. Myc and PI3K/AKT signaling cooperatively repress FOXO3a-dependent PUMA and GADD45a gene expression. *Nucleic Acids Research,* 39**,** 9498-9507.

AMERICAN CANCER SOCIETY. 2017. *Chemotherapy for Osteosarcoma* [Online]. Available: https://www.cancer.org/cancer/osteosarcoma/treating/chemotherapy.html [Accessed April 2016].

AMIN, S., KUMAR, A., NILCHI, L., WRIGHT, K. & KOZLOWSKI, M. 2011. Breast Cancer Cells Proliferation Is Regulated by Tyrosine Phosphatase SHP1 through c-jun N-Terminal

Kinase and Cooperative Induction of RFX-1 and AP-4 Transcription Factors. *Molecular Cancer Research,* 9**,** 1112-1125.

ASMANE, I., WATKIN, E., ALBERTI, L., DUC, A., MAREC-BERARD, P., RAY-COQUARD, I., CASSIER, P., DECOUVELAERE, A.-V., RANCHÈRE, D., KURTZ, J.-E., BERGERAT, J.-P. & BLAY, J.-Y. 2012. Insulin-like growth factor type 1 receptor (IGF-1R) exclusive nuclear staining: A predictive biomarker for IGF-1R monoclonal antibody (Ab) therapy in sarcomas. *European Journal of Cancer,* 48**,** 3027-3035.

ASUTHKAR, S., NALLA, A. K., GONDI, C. S., DINH, D. H., GUJRATI, M., MOHANAM, S. & RAO, J. S. 2011. Gadd45a sensitizes medulloblastoma cells to irradiation and suppresses MMP-9–mediated EMT. *Neuro-Oncology,* 13**,** 1059-1073.

BACHELDER, R. E., YOON, S. O., FRANCI, C., DE HERREROS, A. G. & MERCURIO, A. M. 2005. Glycogen synthase kinase-3 is an endogenous inhibitor of Snail transcription: implications for the epithelial-mesenchymal transition. *J Cell Biol,* 168**,** 29-33.

BAKER, J., LIU, J.-P., ROBERTSON, E. J. & EFSTRATIADIS, A. 1993. Role of insulin-like growth factors in embryonic and postnatal growth. *Cell,* 75**,** 73-82.

BAKKENIST, C. J. & KASTAN, M. B. 2003. DNA damage activates ATM through intermolecular autophosphorylation and dimer dissociation. *Nature,* 421**,** 499-506.

BANIN, S., MOYAL, L., SHIEH, S.-Y., TAYA, Y., ANDERSON, C. W., CHESSA, L., SMORODINSKY, N. I., PRIVES, C., REISS, Y., SHILOH, Y. & ZIV, Y. 1998. Enhanced Phosphorylation of p53 by ATM in Response to DNA Damage. *Science,* 281**,** 1674-1677.

BASERGA, R., HONGO, A., RUBINI, M., PRISCO, M. & VALENTINIS, B. 1997. The IGF-I receptor in cell growth, transformation and apoptosis. *Biochimica et Biophysica Acta (BBA) - Reviews on Cancer,* 1332**,** F105-F126.

BASKAR, R., LEE, K. A., YEO, R. & YEOH, K.-W. 2012. Cancer and Radiation Therapy: Current Advances and Future Directions. *International Journal of Medical Sciences,* 9**,** 193-199.

BAUMANN, M. U., SCHNEIDER, H., MALEK, A., PALTA, V., SURBEK, D. V., SAGER, R., ZAMUDIO, S. & ILLSLEY, N. P. 2014. Regulation of Human Trophoblast GLUT1 Glucose Transporter by Insulin-Like Growth Factor I (IGF-I). *PLOS ONE,* 9**,** e106037.

BAXTER, R. C. 2014. IGF binding proteins in cancer: mechanistic and clinical insights. *Nat Rev Cancer,* 14**,** 329-341.

BAYNE, M. L., APPLEBAUM, J., CHICCHI, G. G., MILLER, R. E. & CASCIERI, M. A. 1990. The roles of tyrosines 24, 31, and 60 in the high affinity binding of insulin-like growth factor-I to the type 1 insulin-like growth factor receptor. *J Biol Chem,* 265**,** 15648-52.

BEATTIE, J., MCINTOSH, L. & VAN DER WALLE, C. F. 2010. Cross-talk between the insulin-like growth factor (IGF) axis and membrane integrins to regulate cell physiology. *Journal of Cellular Physiology,* 224**,** 605-611.

BEHJATI, S., TARPEY, P. S., HAASE, K., YE, H., YOUNG, M. D., ALEXANDROV, L. B., FARNDON, S. J., COLLORD, G., WEDGE, D. C., MARTINCORENA, I., COOKE, S. L., DAVIES, H., MIFSUD, W., LIDGREN, M., MARTIN, S., LATIMER, C., MADDISON, M., BUTLER, A. P., TEAGUE, J. W., PILLAY, N., SHLIEN, A., MCDERMOTT, U., FUTREAL, P. A., BAUMHOER, D., ZAIKOVA, O., BJERKEHAGEN, B., MYKLEBOST, O., AMARY, M. F., TIRABOSCO, R., VAN LOO, P., STRATTON, M. R., FLANAGAN, A. M. & CAMPBELL, P. J. 2017. Recurrent mutation of IGF signalling genes and distinct patterns of genomic rearrangement in osteosarcoma. 8**,** 15936.

BELFIORE, A., FRASCA, F., PANDINI, G., SCIACCA, L. & VIGNERI, R. 2009. Insulin receptor isoforms and insulin receptor/insulin-like growth factor receptor hybrids in physiology and disease. *Endocr Rev,* 30**,** 586-623.

BENINI, S., MANARA, M. C., CERISANO, V., PERDICHIZZI, S., STRAMMIELLO, R., SERRA, M., PICCI, P. & SCOTLANDI, K. 2004. Contribution of MEK/MAPK and PI3-K signaling pathway to the malignant behavior of Ewing's sarcoma cells: therapeutic prospects. *Int J Cancer,* 108**,** 358-66.

BENTLEY, J., DIGGLE, C. P., HARNDEN, P., KNOWLES, M. A. & KILTIE, A. E. 2004. DNA double strand break repair in human bladder cancer is error prone and involves microhomology-associated end-joining. *Nucleic Acids Research,* 32**,** 5249-5259.

BERANEK, D. T. 1990. Distribution of methyl and ethyl adducts following alkylation with monofunctional alkylating agents. *Mutat Res,* 231**,** 11-30.

BERELOWITZ, M., SZABO, M., FROHMAN, L. A., FIRESTONE, S., CHU, L. & HINTZ, R. L. 1981. Somatomedin-C mediates growth hormone negative feedback by effects on both the hypothalamus and the pituitary. *Science,* 212**,** 1279-81.

BERNS, E. M., KLIJN, J. G., VAN STAVEREN, I. L., PORTENGEN, H. & FOEKENS, J. A. 1992. Sporadic amplification of the insulin-like growth factor 1 receptor gene in human breast tumors. *Cancer Res,* 52**,** 1036-9.

BINZ, S. K., SHEEHAN, A. M. & WOLD, M. S. 2004. Replication Protein A phosphorylation and the cellular response to DNA damage. *DNA Repair,* 3**,** 1015-1024.

BLACKFORD, A. N. & JACKSON, S. P. 2017. ATM, ATR, and DNA-PK: The Trinity at the Heart of the DNA Damage Response. *Molecular Cell,* 66**,** 801-817.

BLAKESLEY, V. A., KOVAL, A. P., STANNARD, B. S., SCRIMGEOUR, A. & LEROITH, D. 1998. Replacement of tyrosine 1251 in the carboxyl terminus of the insulin-like growth factor-I receptor disrupts the actin cytoskeleton and inhibits proliferation and anchorage-independent growth. *J Biol Chem,* 273**,** 18411-22.

BLANQUART, C., BOUTE, N., LACASA, D. & ISSAD, T. 2005. Monitoring the activation state of the insulin-like growth factor-1 receptor and its interaction with protein tyrosine phosphatase 1B using bioluminescence resonance energy transfer. *Mol Pharmacol,* 68**,** 885-94.

BOKOV, A. F., GARG, N., IKENO, Y., THAKUR, S., MUSI, N., DEFRONZO, R. A., ZHANG, N., ERICKSON, R. C., GELFOND, J., HUBBARD, G. B., ADAMO, M. L. & RICHARDSON, A. 2011. Does reduced IGF-1R signaling in Igf1r+/- mice alter aging? *PLoS One,* 6**,** e26891.

BONI-SCHNETZLER, M., SCHMID, C., MEIER, P. J. & FROESCH, E. R. 1991. Insulin regulates insulin-like growth factor I mRNA in rat hepatocytes. *Am J Physiol,* 260**,** E846-51.

BRADY, M., VLATKOVIĆ, N. & BOYD, M. T. 2005. Regulation of p53 and MDM2 Activity by MTBP. *Molecular and Cellular Biology,* 25**,** 545-553.

BRENNAND, J. & MARGISON, G. P. 1986. Reduction of the toxicity and mutagenicity of alkylating agents in mammalian cells harboring the Escherichia coli alkyltransferase gene. *Proceedings of the National Academy of Sciences of the United States of America,* 83**,** 6292-6296.

BROWN, J., DELAINE, C., ZACCHEO, O. J., SIEBOLD, C., GILBERT, R. J., VAN BOXEL, G., DENLEY, A., WALLACE, J. C., HASSAN, A. B., FORBES, B. E. & JONES, E. Y. 2008. Structure and functional analysis of the IGF-II/IGF2R interaction. *The EMBO Journal,* 27**,** 265-276.

BUCKLEY, D. A., CHENG, A., KIELY, P. A., TREMBLAY, M. L. & O'CONNOR, R. 2002. Regulation of Insulin-Like Growth Factor Type I (IGF-I) Receptor Kinase Activity by Protein Tyrosine Phosphatase 1B (PTP-1B) and Enhanced IGF-I-Mediated Suppression of Apoptosis and Motility in PTP-1B-Deficient Fibroblasts. *Molecular and Cellular Biology,* 22**,** 1998-2010.

BUISSON, R., DION-COTE, A.-M., COULOMBE, Y., LAUNAY, H., CAI, H., STASIAK, A. Z., STASIAK, A., XIA, B. & MASSON, J.-Y. 2010. Cooperation of breast cancer proteins PALB2 and piccolo BRCA2 in stimulating homologous recombination. *Nat Struct Mol Biol,* 17**,** 1247-1254.

BUNZ, F., DUTRIAUX, A., LENGAUER, C., WALDMAN, T., ZHOU, S., BROWN, J. P., SEDIVY, J. M., KINZLER, K. W. & VOGELSTEIN, B. 1998. Requirement for p53 and p21 to Sustain G2 Arrest After DNA Damage. *Science,* 282**,** 1497-1501.

BURKS, D. J., WANG, J., TOWERY, H., ISHIBASHI, O., LOWE, D., RIEDEL, H. & WHITE, M. F. 1998. IRS pleckstrin homology domains bind to acidic motifs in proteins. *J Biol Chem,* 273**,** 31061-7.

BURNIER, J. V., WANG, N., MICHEL, R. P., HASSANAIN, M., LI, S., LU, Y., METRAKOS, P., ANTECKA, E., BURNIER, M. N., PONTON, A., GALLINGER, S. & BRODT, P. 2011. Type IV collagen-initiated signals provide survival and growth cues required for liver metastasis. *Oncogene,* 30**,** 3766-83.

CADET, J., DOUKI, T. & RAVANAT, J. L. 2008. Oxidatively generated damage to the guanine moiety of DNA: mechanistic aspects and formation in cells. *Acc Chem Res,* 41**,** 1075-83.
CADET, J., SAGE, E. & DOUKI, T. 2005. Ultraviolet radiation-mediated damage to cellular DNA. *Mutat Res,* 571**,** 3-17.
CAGNOL, S. & CHAMBARD, J.-C. 2010. ERK and cell death: Mechanisms of ERK-induced cell death – apoptosis, autophagy and senescence. *FEBS Journal,* 277**,** 2-21.
CANMAN, C. E., LIM, D.-S., CIMPRICH, K. A., TAYA, Y., TAMAI, K., SAKAGUCHI, K., APPELLA, E., KASTAN, M. B. & SILICIANO, J. D. 1998. Activation of the ATM Kinase by Ionizing Radiation and Phosphorylation of p53. *Science,* 281**,** 1677-1679.
CAO, Y., ROTH, M., PIPERDI, S., MONTOYA, K., SOWERS, R., RAO, P., GELLER, D., HOUGHTON, P., KOLB, E. A. & GILL, J. 2014. Insulin-like growth factor 1 receptor and response to anti-IGF1R antibody therapy in osteosarcoma. *PLoS One,* 9.
CARRIER, F., GEORGEL, P. T., POURQUIER, P., BLAKE, M., KONTNY, H. U., ANTINORE, M. J., GARIBOLDI, M., MYERS, T. G., WEINSTEIN, J. N., POMMIER, Y. & FORNACE, A. J. 1999. Gadd45, a p53-Responsive Stress Protein, Modifies DNA Accessibility on Damaged Chromatin. *Molecular and Cellular Biology,* 19**,** 1673-1685.
CEJKA, P., PLANK, J. L., BACHRATI, C. Z., HICKSON, I. D. & KOWALCZYKOWSKI, S. C. 2010. Rmi1 stimulates decatenation of double Holliday junctions during dissolution by Sgs1-Top3. *Nat Struct Mol Biol,* 17**,** 1377-82.
CHANG, H. H., WATANABE, G., GERODIMOS, C. A., OCHI, T., BLUNDELL, T. L., JACKSON, S. P. & LIEBER, M. R. 2016. Different DNA End Configurations Dictate Which NHEJ Components Are Most Important for Joining Efficiency. *J Biol Chem,* 291**,** 24377-24389.
CHANG, H. H. Y., PANNUNZIO, N. R., ADACHI, N. & LIEBER, M. R. 2017. Non-homologous DNA end joining and alternative pathways to double-strand break repair. *Nat Rev Mol Cell Biol,* 18**,** 495-506.
CHAPMAN, J. R., BARRAL, P., VANNIER, J. B., BOREL, V., STEGER, M., TOMAS-LOBA, A., SARTORI, A. A., ADAMS, I. R., BATISTA, F. D. & BOULTON, S. J. 2013. RIF1 is essential for 53BP1-dependent nonhomologous end joining and suppression of DNA double-strand break resection. *Mol Cell,* 49**,** 858-71.
CHAUDHARY, A. K., NOKUBO, M., REDDY, G. R., YEOLA, S. N., MORROW, J. D., BLAIR, I. A. & MARNETT, L. J. 1994. Detection of endogenous malondialdehyde-deoxyguanosine adducts in human liver. *Science,* 265**,** 1580-2.
CHEN, C., SHIMIZU, S., TSUJIMOTO, Y. & MOTOYAMA, N. 2005. Chk2 regulates transcription-independent p53-mediated apoptosis in response to DNA damage. *Biochem Biophys Res Commun,* 333**,** 427-31.
CHEN, L., NIEVERA, C. J., LEE, A. Y.-L. & WU, X. 2008. Cell Cycle-dependent Complex Formation of BRCA1·CtIP·MRN Is Important for DNA Double-strand Break Repair. *Journal of Biological Chemistry,* 283**,** 7713-7720.
CHEN, Y.-J., TSAI, C.-H., WANG, P.-Y. & TENG, S.-C. 2017. SMYD3 Promotes Homologous Recombination via Regulation of H3K4-mediated Gene Expression. *Scientific Reports,* 7**,** 3842.
CHITNIS, M. M., LODHIA, K. A., ALEKSIC, T., GAO, S., PROTHEROE, A. S. & MACAULAY, V. M. 2014. IGF-1R inhibition enhances radiosensitivity and delays double-strand break repair by both non-homologous end-joining and homologous recombination. *Oncogene,* 33**,** 5262-73.
CHITNIS, M. M., YUEN, J. S. P., PROTHEROE, A. S., POLLAK, M. & MACAULAY, V. M. 2008. The Type 1 Insulin-Like Growth Factor Receptor Pathway. *Clinical Cancer Research,* 14**,** 6364-6370.
CHO, S. W., KIM, S., KIM, J. M. & KIM, J.-S. 2013. Targeted genome engineering in human cells with the Cas9 RNA-guided endonuclease. *Nat Biotech,* 31**,** 230-232.
CHRISTMANN, M. & KAINA, B. 2016. MGMT-a critical DNA repair gene target for chemotherapy resistance. *DNA Repair in Cancer Therapy: Molecular Targets and Clinical Applications: Second Edition.*

CLEMMONS, D. R. & MAILE, L. A. 2005. Interaction between insulin-like growth factor-I receptor and alphaVbeta3 integrin linked signaling pathways: cellular responses to changes in multiple signaling inputs. *Mol Endocrinol,* 19**,** 1-11.

COHEN, B. D., BAKER, D. A., SODERSTROM, C., TKALCEVIC, G., ROSSI, A. M., MILLER, P. E., TENGOWSKI, M. W., WANG, F., GUALBERTO, A., BEEBE, J. S. & MOYER, J. D. 2005. Combination therapy enhances the inhibition of tumor growth with the fully human anti-type 1 insulin-like growth factor receptor monoclonal antibody CP-751,871. *Clin Cancer Res,* 11**,** 2063-73.

CORTÉS-LEDESMA, F. & AGUILERA, A. 2006. Double-strand breaks arising by replication through a nick are repaired by cohesin-dependent sister-chromatid exchange. *EMBO Reports,* 7**,** 919-926.

COSACEANU, D., BUDIU, R., CARAPANCEA, M., CASTRO, J., LEWENSOHN, R. & DRICU, A. 2007. Ionizing radiation activates IGF-1R triggering a cytoprotective signaling by interfering with Ku-DNA binding and by modulating Ku86 expression via a p38 kinase-dependent mechanism. *Oncogene,* 26.

COSTANZO, V., PAULL, T., GOTTESMAN, M. & GAUTIER, J. 2004. Mre11 Assembles Linear DNA Fragments into DNA Damage Signaling Complexes. *PLOS Biology,* 2**,** e110.

COX, O. T., O'SHEA, S., TRESSE, E., BUSTAMANTE-GARRIDO, M., KIRAN-DEEVI, R. & O'CONNOR, R. 2015. IGF-1 Receptor and Adhesion Signaling: An Important Axis in Determining Cancer Cell Phenotype and Therapy Resistance. *Frontiers in Endocrinology,* 6.

CRADDOCK, B. P. & MILLER, W. T. 2012. Effects of Somatic Mutations in the C-Terminus of Insulin-Like Growth Factor 1 Receptor on Activity and Signaling. *Journal of Signal Transduction,* 2012**,** 7.

CRAPARO, A., O'NEILL, T. J. & GUSTAFSON, T. A. 1995. Non-SH2 domains within insulin receptor substrate-1 and SHC mediate their phosphotyrosine-dependent interaction with the NPEY motif of the insulin-like growth factor I receptor. *J Biol Chem,* 270**,** 15639-43.

CRIGHTON, D., WILKINSON, S., O'PREY, J., SYED, N., SMITH, P., HARRISON, P. R., GASCO, M., GARRONE, O., CROOK, T. & RYAN, K. M. 2006. DRAM, a p53-Induced Modulator of Autophagy, Is Critical for Apoptosis. *Cell,* 126**,** 121-134.

D'ERCOLE, A. J., STILES, A. D. & UNDERWOOD, L. E. 1984. Tissue concentrations of somatomedin C: further evidence for multiple sites of synthesis and paracrine or autocrine mechanisms of action. *Proc Natl Acad Sci U S A,* 81**,** 935-9.

DAI, C., TANG, Y., JUNG, S. Y., QIN, J., AARONSON, S. A. & GU, W. 2011. Differential effects on p53-mediated cell cycle arrest vs. apoptosis by p90. *Proceedings of the National Academy of Sciences,* 108**,** 18937-18942.

DALE, O. T., ALEKSIC, T., SHAH, K. A., HAN, C., MEHANNA, H., RAPOZO, D. C., SHEARD, J. D., GOODYEAR, P., UPILE, N. S., ROBINSON, M., JONES, T. M., WINTER, S. & MACAULAY, V. M. 2015. IGF-1R expression is associated with HPV-negative status and adverse survival in head and neck squamous cell cancer. *Carcinogenesis,* 36**,** 648-55.

DALLE, S., RICKETTS, W., IMAMURA, T., VOLLENWEIDER, P. & OLEFSKY, J. M. 2001. Insulin and insulin-like growth factor I receptors utilize different G protein signaling components. *J Biol Chem,* 276**,** 15688-95.

DE BONT, R. & VAN LAREBEKE, N. 2004. Endogenous DNA damage in humans: a review of quantitative data. *Mutagenesis,* 19**,** 169-85.

DE ITA, J. R., CASTILLA-CORTÁZAR, I., AGUIRRE, G. A., SÁNCHEZ-YAGO, C., SANTOS-RUIZ, M. O., GUERRA-MENÉNDEZ, L., MARTÍN-ESTAL, I., GARCÍA-MAGARIÑO, M., LARA-DÍAZ, V. J., PUCHE, J. E. & MUÑOZ, U. 2015. Altered liver expression of genes involved in lipid and glucose metabolism in mice with partial IGF-1 deficiency: an experimental approach to metabolic syndrome. *Journal of Translational Medicine,* 13**,** 326.

DEBERARDINIS, R. J., LUM, J. J., HATZIVASSILIOU, G. & THOMPSON, C. B. 2008. The biology of cancer: metabolic reprogramming fuels cell growth and proliferation. *Cell Metab,* 7**,** 11-20.

DENG, H., LIN, Y., BADIN, M., VASILCANU, D., STROMBERG, T., JERNBERG-WIKLUND, H., SEHAT, B. & LARSSON, O. 2011. Over-accumulation of nuclear IGF-1 receptor in tumor cells requires elevated expression of the receptor and the SUMO-conjugating enzyme Ubc9. *Biochem Biophys Res Commun,* 404**,** 667-71.

DEY, B. R., FRICK, K., LOPACZYNSKI, W., NISSLEY, S. P. & FURLANETTO, R. W. 1996. Evidence for the direct interaction of the insulin-like growth factor I receptor with IRS-1, Shc, and Grb10. *Mol Endocrinol,* 10**,** 631-41.

DEY, B. R., SPENCE, S. L., NISSLEY, P. & FURLANETTO, R. W. 1998. Interaction of human suppressor of cytokine signaling (SOCS)-2 with the insulin-like growth factor-I receptor. *J Biol Chem,* 273**,** 24095-101.

DIGIOVANNI, J., KIGUCHI, K., FRIJHOFF, A., WILKER, E., BOL, D. K., BELTRÁN, L., MOATS, S., RAMIREZ, A., JORCANO, J. & CONTI, C. 2000. Deregulated expression of insulin-like growth factor 1 in prostate epithelium leads to neoplasia in transgenic mice. *Proceedings of the National Academy of Sciences of the United States of America,* 97**,** 3455-3460.

DING, L., GETZ, G., WHEELER, D. A., MARDIS, E. R., MCLELLAN, M. D., CIBULSKIS, K., SOUGNEZ, C., GREULICH, H., MUZNY, D. M., MORGAN, M. B., FULTON, L., FULTON, R. S., ZHANG, Q., WENDL, M. C., LAWRENCE, M. S., LARSON, D. E., CHEN, K., DOOLING, D. J., SABO, A., HAWES, A. C., SHEN, H., JHANGIANI, S. N., LEWIS, L. R., HALL, O., ZHU, Y., MATHEW, T., REN, Y., YAO, J., SCHERER, S. E., CLERC, K., METCALF, G. A., NG, B., MILOSAVLJEVIC, A., GONZALEZ-GARAY, M. L., OSBORNE, J. R., MEYER, R., SHI, X., TANG, Y., KOBOLDT, D. C., LIN, L., ABBOTT, R., MINER, T. L., POHL, C., FEWELL, G., HAIPEK, C., SCHMIDT, H., DUNFORD-SHORE, B. H., KRAJA, A., CROSBY, S. D., SAWYER, C. S., VICKERY, T., SANDER, S., ROBINSON, J., WINCKLER, W., BALDWIN, J., CHIRIEAC, L. R., DUTT, A., FENNELL, T., HANNA, M., JOHNSON, B. E., ONOFRIO, R. C., THOMAS, R. K., TONON, G., WEIR, B. A., ZHAO, X., ZIAUGRA, L., ZODY, M. C., GIORDANO, T., ORRINGER, M. B., ROTH, J. A., SPITZ, M. R., WISTUBA, II, OZENBERGER, B., GOOD, P. J., CHANG, A. C., BEER, D. G., WATSON, M. A., LADANYI, M., BRODERICK, S., YOSHIZAWA, A., TRAVIS, W. D., PAO, W., PROVINCE, M. A., WEINSTOCK, G. M., VARMUS, H. E., GABRIEL, S. B., LANDER, E. S., GIBBS, R. A., MEYERSON, M. & WILSON, R. K. 2008. Somatic mutations affect key pathways in lung adenocarcinoma. *Nature,* 455**,** 1069-75.

DING, M., BRUICK, R. K. & YU, Y. 2016. Secreted IGFBP5 Mediates mTORC1-Dependent Feedback Inhibition of IGF-1 Signaling. *Nature cell biology,* 18**,** 319-327.

DIZDAROGLU, M. & JARUGA, P. 2012. Mechanisms of free radical-induced damage to DNA. *Free Radic Res,* 46**,** 382-419.

DOIL, C., MAILAND, N., BEKKER-JENSEN, S., MENARD, P., LARSEN, D. H., PEPPERKOK, R., ELLENBERG, J., PANIER, S., DUROCHER, D., BARTEK, J., LUKAS, J. & LUKAS, C. 2009. RNF168 binds and amplifies ubiquitin conjugates on damaged chromosomes to allow accumulation of repair proteins. *Cell,* 136**,** 435-46.

DOLBEARE, F., GRATZNER, H., PALLAVICINI, M. G. & GRAY, J. W. 1983. Flow cytometric measurement of total DNA content and incorporated bromodeoxyuridine. *Proc Natl Acad Sci U S A,* 80**,** 5573-7.

DOUDNA, J. A. & CHARPENTIER, E. 2014. The new frontier of genome engineering with CRISPR-Cas9. *Science,* 346.

DOWNS, J. A. & JACKSON, S. P. 2004. A means to a DNA end: the many roles of Ku. *Nat Rev Mol Cell Biol,* 5**,** 367-78.

DOWNWARD, J. 2003. Targeting RAS signalling pathways in cancer therapy. *Nat Rev Cancer,* 3**,** 11-22.

DUAN, Z., CHOY, E., HARMON, D., YANG, C., RYU, K., SCHWAB, J., MANKIN, H. & HORNICEK, F. J. 2009. Insulin-like growth factor-I receptor tyrosine kinase inhibitor cyclolignan picropodophyllin inhibits proliferation and induces apoptosis in multidrug resistant osteosarcoma cell lines. *Molecular Cancer Therapeutics,* 8**,** 2122-2130.

DUNN, S. E., KARI, F. W., FRENCH, J., LEININGER, J. R., TRAVLOS, G., WILSON, R. & BARRETT, J. C. 1997. Dietary Restriction Reduces Insulin-like Growth Factor I Levels, Which Modulates Apoptosis, Cell Proliferation, and Tumor Progression in p53-deficient Mice. *Cancer Research,* 57**,** 4667-4672.

DURFORT, T., TKACH, M., MESCHANINOVA, M. I., RIVAS, M. A., ELIZALDE, P. V., VENYAMINOVA, A. G., SCHILLACI, R. & FRANÇOIS, J.-C. 2012. Small Interfering RNA Targeted to IGF-IR Delays Tumor Growth and Induces Proinflammatory Cytokines in a Mouse Breast Cancer Model. *PLoS ONE,* 7**,** e29213.

EL-AWADY, R. A., DIKOMEY, E. & DAHM-DAPHI, J. 2003. Radiosensitivity of human tumour cells is correlated with the induction but not with the repair of DNA double-strand breaks. *Br J Cancer,* 89**,** 593-601.

ELIA, L., CONTU, R., QUINTAVALLE, M., VARRONE, F., CHIMENTI, C., RUSSO, M. A., CIMINO, V., DE MARINIS, L., FRUSTACI, A., CATALUCCI, D. & CONDORELLI, G. 2009. Reciprocal regulation of microRNA-1 and insulin-like growth factor-1 signal transduction cascade in cardiac and skeletal muscle in physiological and pathological conditions. *Circulation,* 120**,** 2377-85.

ELIEZER, Y., ARGAMAN, L., KORNOWSKI, M., RONIGER, M. & GOLDBERG, M. 2014. Interplay between the DNA Damage Proteins MDC1 and ATM in the Regulation of the Spindle Assembly Checkpoint. *Journal of Biological Chemistry,* 289**,** 8182-8193.

ESCRIBANO-DIAZ, C., ORTHWEIN, A., FRADET-TURCOTTE, A., XING, M., YOUNG, J. T., TKAC, J., COOK, M. A., ROSEBROCK, A. P., MUNRO, M., CANNY, M. D., XU, D. & DUROCHER, D. 2013. A cell cycle-dependent regulatory circuit composed of 53BP1-RIF1 and BRCA1-CtIP controls DNA repair pathway choice. *Mol Cell,* 49**,** 872-83.

EVERS, B., JASTRZEBSKI, K., HEIJMANS, J. P. M., GRERNRUM, W., BEIJERSBERGEN, R. L. & BERNARDS, R. 2016. CRISPR knockout screening outperforms shRNA and CRISPRi in identifying essential genes. *Nat Biotech,* 34**,** 631-633.

FAVELYUKIS, S., TILL, J. H., HUBBARD, S. R. & MILLER, W. T. 2001. Structure and autoregulation of the insulin-like growth factor 1 receptor kinase. *Nat Struct Biol,* 8**,** 1058-63.

FEI, P. & EL-DEIRY, W. S. 2003. P53 and radiation responses. *Oncogene,* 22**,** 5774-83.

FERNANDEZ, A. M., KIM, J. K., YAKAR, S., DUPONT, J., HERNANDEZ-SANCHEZ, C., CASTLE, A. L., FILMORE, J., SHULMAN, G. I. & LE ROITH, D. 2001. Functional inactivation of the IGF-I and insulin receptors in skeletal muscle causes type 2 diabetes. *Genes Dev,* 15**,** 1926-34.

FERNANDEZ, C. A., ROY, R., LEE, S., YANG, J., PANIGRAHY, D., VAN VLIET, K. J. & MOSES, M. A. 2010. The anti-angiogenic peptide, loop 6, binds insulin-like growth factor-1 receptor. *J Biol Chem,* 285**,** 41886-95.

FERTÉ, C., LORIOT, Y., CLÉMENSON, C., COMMO, F., GOMBOS, A., BIBAULT, J.-E., FUMAGALLI, I., HAMAMA, S., AUGER, N., LAHON, B., CHARGARI, C., CALDERARO, J., SORIA, J.-C. & DEUTSCH, E. 2013. IGF-1R Targeting Increases the Antitumor Effects of DNA-Damaging Agents in SCLC Model: An Opportunity to Increase the Efficacy of Standard Therapy. *Molecular Cancer Therapeutics,* 12**,** 1213-1222.

FLANIGAN, S. A., PITTS, T. M., ECKHARDT, S. G., TENTLER, J. J., TAN, A. C., THORBURN, A. & LEONG, S. 2010. The insulin-like growth factor I receptor/insulin receptor tyrosine kinase inhibitor PQIP exhibits enhanced antitumor effects in combination with chemotherapy against colorectal cancer models. *Clin Cancer Res,* 16**,** 5436-46.

FORNACE, A. J., NEBERT, D. W., HOLLANDER, M. C., LUETHY, J. D., PAPATHANASIOU, M., FARGNOLI, J. & HOLBROOK, N. J. 1989. Mammalian genes coordinately regulated by growth arrest signals and DNA-damaging agents. *Molecular and Cellular Biology,* 9**,** 4196-4203.

FRASER, M., HARDING, S. M., ZHAO, H., COACKLEY, C., DUROCHER, D. & BRISTOW, R. G. 2011. MRE11 promotes AKT phosphorylation in direct response to DNA double-strand breaks. *Cell Cycle,* 10**,** 2218-32.

FUGGER, K. & WEST, S. C. 2016. Keeping homologous recombination in check. *Cell Res,* 26**,** 397-398.

FURLING, D., MARETTE, A. & PUYMIRAT, J. 1999. Insulin-like growth factor I circumvents defective insulin action in human myotonic dystrophy skeletal muscle cells. *Endocrinology,* 140**,** 4244-50.

GARRETT, T. P., MCKERN, N. M., LOU, M., FRENKEL, M. J., BENTLEY, J. D., LOVRECZ, G. O., ELLEMAN, T. C., COSGROVE, L. J. & WARD, C. W. 1998. Crystal structure of the first three domains of the type-1 insulin-like growth factor receptor. *Nature,* 394**,** 395-9.

GEOERGER, B., BRASME, J. F., DAUDIGEOS-DUBUS, E., OPOLON, P., VENOT, C., DEBUSSCHE, L., VRIGNAUD, P. & VASSAL, G. 2010. Anti-insulin-like growth factor 1 receptor antibody EM164 (murine AVE1642) exhibits anti-tumour activity alone and in combination with temozolomide against neuroblastoma. *Eur J Cancer,* 46**,** 3251-62.

GINGRAS, A.-C., RAUGHT, B., GYGI, S. P., NIEDZWIECKA, A., MIRON, M., BURLEY, S. K., POLAKIEWICZ, R. D., WYSLOUCH-CIESZYNSKA, A., AEBERSOLD, R. & SONENBERG, N. 2001. Hierarchical phosphorylation of the translation inhibitor 4E-BP1. *Genes & Development,* 15**,** 2852-2864.

GIRNITA, L., SHENOY, S. K., SEHAT, B., VASILCANU, R., GIRNITA, A., LEFKOWITZ, R. J. & LARSSON, O. 2005. {beta}-Arrestin is crucial for ubiquitination and down-regulation of the insulin-like growth factor-1 receptor by acting as adaptor for the MDM2 E3 ligase. *J Biol Chem,* 280**,** 24412-9.

GLOTZER, M. 2001. Animal cell cytokinesis. *Annu Rev Cell Dev Biol,* 17**,** 351-86.

GOGINENI, V. R., NALLA, A. K., GUPTA, R., DINH, D. H., KLOPFENSTEIN, J. D. & RAO, J. S. 2011. Chk2-mediated G2/M Cell Cycle Arrest Maintains Radiation Resistance in Malignant Meningioma Cells. *Cancer letters,* 313**,** 64-75.

GOODARZI, A. A., NOON, A. T., DECKBAR, D., ZIV, Y., SHILOH, Y., LOBRICH, M. & JEGGO, P. A. 2008. ATM signaling facilitates repair of DNA double-strand breaks associated with heterochromatin. *Mol Cell,* 31**,** 167-77.

GOODARZI, A. A., YU, Y., RIBALLO, E., DOUGLAS, P., WALKER, S. A., YE, R., HÄRER, C., MARCHETTI, C., MORRICE, N., JEGGO, P. A. & LEES-MILLER, S. P. 2006. DNA-PK autophosphorylation facilitates Artemis endonuclease activity. *The EMBO Journal,* 25**,** 3880-3889.

GOODHEAD, D. T. 1994. Initial events in the cellular effects of ionizing radiations: clustered damage in DNA. *Int J Radiat Biol,* 65**,** 7-17.

GRAHAM, T. R., ZHAU, H. E., ODERO-MARAH, V. A., OSUNKOYA, A. O., KIMBRO, K. S., TIGHIOUART, M., LIU, T., SIMONS, J. W. & O'REGAN, R. M. 2008. Insulin-like growth factor-I-dependent up-regulation of ZEB1 drives epithelial-to-mesenchymal transition in human prostate cancer cells. *Cancer Res,* 68**,** 2479-88.

GRAWUNDER, U., ZIMMER, D. & LIEBER, M. R. 1998. DNA ligase IV binds to XRCC4 via a motif located between rather than within its BRCT domains. *Current Biology,* 8**,** 873-879.

GREENMAN, C., STEPHENS, P., SMITH, R., DALGLIESH, G. L., HUNTER, C., BIGNELL, G., DAVIES, H., TEAGUE, J., BUTLER, A., STEVENS, C., EDKINS, S., O/'MEARA, S., VASTRIK, I., SCHMIDT, E. E., AVIS, T., BARTHORPE, S., BHAMRA, G., BUCK, G., CHOUDHURY, B., CLEMENTS, J., COLE, J., DICKS, E., FORBES, S., GRAY, K., HALLIDAY, K., HARRISON, R., HILLS, K., HINTON, J., JENKINSON, A., JONES, D., MENZIES, A., MIRONENKO, T., PERRY, J., RAINE, K., RICHARDSON, D., SHEPHERD, R., SMALL, A., TOFTS, C., VARIAN, J., WEBB, T., WEST, S., WIDAA, S., YATES, A., CAHILL, D. P., LOUIS, D. N., GOLDSTRAW, P., NICHOLSON, A. G., BRASSEUR, F., LOOIJENGA, L., WEBER, B. L., CHIEW, Y.-E., DEFAZIO, A., GREAVES, M. F., GREEN, A. R., CAMPBELL, P., BIRNEY, E., EASTON, D. F., CHENEVIX-TRENCH, G., TAN, M.-H., KHOO, S. K., TEH, B. T., YUEN, S. T., LEUNG, S. Y., WOOSTER, R., FUTREAL, P. A. & STRATTON, M. R. 2007. Patterns of somatic mutation in human cancer genomes. *Nature,* 446**,** 153-158.

GUEVARA-AGUIRRE, J., BALASUBRAMANIAN, P., GUEVARA-AGUIRRE, M., WEI, M., MADIA, F., CHENG, C. W., HWANG, D., MARTIN-MONTALVO, A., SAAVEDRA, J., INGLES, S., DE CABO, R., COHEN, P. & LONGO, V. D. 2011. Growth hormone

receptor deficiency is associated with a major reduction in pro-aging signaling, cancer, and diabetes in humans. *Sci Transl Med,* 3**,** 70ra13.

GULSTON, M., FULFORD, J., JENNER, T., DE LARA, C. & O'NEILL, P. 2002. Clustered DNA damage induced by γ radiation in human fibroblasts (HF19), hamster (V79-4) cells and plasmid DNA is revealed as Fpg and Nth sensitive sites. *Nucleic Acids Research,* 30**,** 3464-3472.

GUPTA, A. K., MCKENNA, W. G., WEBER, C. N., MACHTAY, M., ROSENTHAL, D. I., BAKANAUSKAS, V. J., CERNIGLIA, G. J., BERNHARD, E. J., FELDMAN, M. D., GOLDSMITH, J. D., MUSCHEL, R. J., MICK, R. & WEBER, R. S. 2002. Local recurrence in head and neck cancer: Relationship to radiation resistance and signal transduction. *Clinical Cancer Research,* 8**,** 885-892.

GUPTA, M., GUPTA, S. K., HOFFMAN, B. & LIEBERMANN, D. A. 2006. Gadd45a and Gadd45b Protect Hematopoietic Cells from UV-induced Apoptosis via Distinct Signaling Pathways, including p38 Activation and JNK Inhibition. *Journal of Biological Chemistry,* 281**,** 17552-17558.

GUVAKOVA, M. A. & SURMACZ, E. 1999. The activated insulin-like growth factor I receptor induces depolarization in breast epithelial cells characterized by actin filament disassembly and tyrosine dephosphorylation of FAK, Cas, and paxillin. *Exp Cell Res,* 251**,** 244-55.

HABEL, N., HAMIDOUCHE, Z., GIRAULT, I., PATINO-GARCIA, A., LECANDA, F., MARIE, P. J. & FROMIGUE, O. 2013. Zinc chelation: a metallothionein 2A's mechanism of action involved in osteosarcoma cell death and chemotherapy resistance. *Cell Death Dis,* 4**,** e874.

HALLING-BROWN, M. D., BULUSU, K. C., PATEL, M., TYM, J. E. & AL-LAZIKANI, B. 2012. canSAR: an integrated cancer public translational research and drug discovery resource. *Nucleic Acids Res,* 40**,** D947-56.

HANAI, R., YAZU, M. & HIEDA, K. 1998. On the experimental distinction between ssbs and dsbs in circular DNA. *Int J Radiat Biol,* 73**,** 475-9.

HANKINSON, S. E., WILLETT, W. C., COLDITZ, G. A., HUNTER, D. J., MICHAUD, D. S., DEROO, B., ROSNER, B., SPEIZER, F. E. & POLLAK, M. 1998. Circulating concentrations of insulin-like growth factor-I and risk of breast cancer. *Lancet,* 351**,** 1393-6.

HEILMANN, A. M., PERERA, R. M., ECKER, V., NICOLAY, B. N., BARDEESY, N., BENES, C. H. & DYSON, N. J. 2014. CDK4/6 and IGF1 receptor inhibitors synergize to suppress the growth of p16INK4A-deficient pancreatic cancers. *Cancer Res,* 74**,** 3947-58.

HELLEDAY, T., ESHTAD, S. & NIK-ZAINAL, S. 2014. Mechanisms underlying mutational signatures in human cancers. *Nat Rev Genet,* 15**,** 585-598.

HELLSTRÖM, A., CARLSSON, B. R., NIKLASSON, A., SEGNESTAM, K., BOGUSZEWSKI, M., DE LACERDA, L., SAVAGE, M., SVENSSON, E., SMITH, L., WEINBERGER, D., ALBERTSSON WIKLAND, K. & LARON, Z. 2002. IGF-I Is Critical for Normal Vascularization of the Human Retina. *The Journal of Clinical Endocrinology & Metabolism,* 87**,** 3413-3416.

HEMMINGS, B. A. & RESTUCCIA, D. F. 2012. PI3K-PKB/Akt Pathway. *Cold Spring Harbor Perspectives in Biology,* 4.

HIGASHI, Y., SUKHANOV, S., PARTHASARATHY, S. & DELAFONTAINE, P. 2008. The ubiquitin ligase Nedd4 mediates oxidized low-density lipoprotein-induced downregulation of insulin-like growth factor-1 receptor. *Am J Physiol Heart Circ Physiol,* 295**,** H1684-9.

HIRAO, A., CHEUNG, A., DUNCAN, G., GIRARD, P. M., ELIA, A. J., WAKEHAM, A., OKADA, H., SARKISSIAN, T., WONG, J. A., SAKAI, T., DE STANCHINA, E., BRISTOW, R. G., SUDA, T., LOWE, S. W., JEGGO, P. A., ELLEDGE, S. J. & MAK, T. W. 2002. Chk2 is a tumor suppressor that regulates apoptosis in both an ataxia telangiectasia mutated (ATM)-dependent and an ATM-independent manner. *Mol Cell Biol,* 22**,** 6521-32.

HIRAO, A., KONG, Y. Y., MATSUOKA, S., WAKEHAM, A., RULAND, J., YOSHIDA, H., LIU, D., ELLEDGE, S. J. & MAK, T. W. 2000. DNA damage-induced activation of p53 by the checkpoint kinase Chk2. *Science,* 287**,** 1824-7.

HOA, N. N., KOBAYASHI, J., OMURA, M., HIRAKAWA, M., YANG, S. H., KOMATSU, K., PAULL, T. T., TAKEDA, S. & SASANUMA, H. 2015. BRCA1 and CtIP Are Both Required to Recruit Dna2 at Double-Strand Breaks in Homologous Recombination. *PLoS One,* 10**,** e0124495.

HOLLANDER, M. C., KOVALSKY, O., SALVADOR, J. M., KIM, K. E., PATTERSON, A. D., HAINES, D. C. & FORNACE, A. J. 2001. Dimethylbenzanthracene carcinogenesis in Gadd45a-null Mice is associated with decreased DNA Repair and increased mutation frequency. *Cancer Research,* 61**,** 2487-2491.

HOUSDEN, B. E. & PERRIMON, N. 2016. Comparing CRISPR and RNAi-based screening technologies. *Nat Biotech,* 34**,** 621-623.

HSU, D., KNUDSON, P. E., ZAPF, A., ROLBAND, G. C. & OLEFSKY, J. M. 1994. NPXY motif in the insulin-like growth factor-I receptor is required for efficient ligand-mediated receptor internalization and biological signaling. *Endocrinology,* 134**,** 744-50.

HSU, PATRICK D., LANDER, ERIC S. & ZHANG, F. 2014. Development and Applications of CRISPR-Cas9 for Genome Engineering. *Cell,* 157**,** 1262-1278.

HU, Y. K., WANG, X., LI, L., DU, Y. H., YE, H. T. & LI, C. Y. 2013. MicroRNA-98 induces an Alzheimer's disease-like disturbance by targeting insulin-like growth factor 1. *Neurosci Bull,* 29**,** 745-51.

HUBBARD, S. R. 1997. Crystal structure of the activated insulin receptor tyrosine kinase in complex with peptide substrate and ATP analog. *Embo j,* 16**,** 5572-81.

HUEN, M. S., GRANT, R., MANKE, I., MINN, K., YU, X., YAFFE, M. B. & CHEN, J. 2007. RNF8 transduces the DNA-damage signal via histone ubiquitylation and checkpoint protein assembly. *Cell,* 131**,** 901-14.

HUERTAS, P. & JACKSON, S. P. 2009. Human CtIP mediates cell cycle control of DNA end resection and double strand break repair. *J Biol Chem,* 284**,** 9558-65.

IM, J.-Y., LEE, K.-W., WON, K.-J., KIM, B.-K., BAN, H. S., YOON, S.-H., LEE, Y.-J., KIM, Y.-J., SONG, K.-B. & WON, M. 2016. DNA damage-induced apoptosis suppressor (DDIAS), a novel target of NFATc1, is associated with cisplatin resistance in lung cancer. *Biochimica et Biophysica Acta (BBA) - Molecular Cell Research,* 1863**,** 40-49.

INAMDAR, K. V., POULIOT, J. J., ZHOU, T., LEES-MILLER, S. P., RASOULI-NIA, A. & POVIRK, L. F. 2002. Conversion of phosphoglycolate to phosphate termini on 3' overhangs of DNA double strand breaks by the human tyrosyl-DNA phosphodiesterase hTdp1. *J Biol Chem,* 277**,** 27162-8.

ISEBAERT, S. F., SWINNEN, J. V., MCBRIDE, W. H. & HAUSTERMANS, K. M. 2011. Insulin-Like Growth Factor–Type 1 Receptor Inhibitor NVP-AEW541 Enhances Radiosensitivity of PTEN Wild-Type but Not PTEN-Deficient Human Prostate Cancer Cells. *International Journal of Radiation Oncology*Biology*Physics,* 81**,** 239-247.

IVASHKEVICH, A., REDON, C. E., NAKAMURA, A. J., MARTIN, R. F. & MARTIN, O. A. 2012. USE OF THE γ-H2AX ASSAY TO MONITOR DNA DAMAGE AND REPAIR IN TRANSLATIONAL CANCER RESEARCH. *Cancer letters,* 327**,** 123-133.

IWASA, T., OKAMOTO, I., SUZUKI, M., HATASHITA, E., YAMADA, Y., FUKUOKA, M., ONO, K. & NAKAGAWA, K. 2009. Inhibition of insulin-like growth factor 1 receptor by CP-751,871 radiosensitizes non–small cell lung cancer cells. *Clin Cancer Res,* 15.

JACK, M. T., WOO, R. A., HIRAO, A., CHEUNG, A., MAK, T. W. & LEE, P. W. 2002. Chk2 is dispensable for p53-mediated G1 arrest but is required for a latent p53-mediated apoptotic response. *Proc Natl Acad Sci U S A,* 99**,** 9825-9.

JACKSON, A. L., CHEN, R. & LOEB, L. A. 1998. Induction of microsatellite instability by oxidative DNA damage. *Proceedings of the National Academy of Sciences of the United States of America,* 95**,** 12468-12473.

JACKSON, S. P. & BARTEK, J. 2009. The DNA-damage response in human biology and disease. *Nature,* 461**,** 1071-1078.

JACOBS, S., KULL, F. C., JR. & CUATRECASAS, P. 1983. Monensin blocks the maturation of receptors for insulin and somatomedin C: identification of receptor precursors. *Proc Natl Acad Sci U S A,* 80**,** 1228-31.

JANSSEN, A. & MEDEMA, R. H. 2013. Genetic instability: tipping the balance. *Oncogene,* 32**,** 4459-4470.
JANSSON, M., UHLEN, M. & NILSSON, B. 1997. Structural changes in insulin-like growth factor (IGF) I mutant proteins affecting binding kinetic rates to IGF binding protein 1 and IGF-I receptor. *Biochemistry,* 36**,** 4108-17.
JASIN, M. & ROTHSTEIN, R. 2013. Repair of strand breaks by homologous recombination. *Cold Spring Harb Perspect Biol,* 5**,** a012740.
JEGGO, P. & LOBRICH, M. 2006. Radiation-induced DNA damage responses. *Radiat Prot Dosimetry,* 122**,** 124-7.
JIANG, H., SU, Z. Z., LIN, J. J., GOLDSTEIN, N. I., YOUNG, C. S. & FISHER, P. B. 1996. The melanoma differentiation associated gene mda-7 suppresses cancer cell growth. *Proc Natl Acad Sci U S A,* 93**,** 9160-5.
JIANG, Y., WANG, L., GONG, W., WEI, D., LE, X., YAO, J., AJANI, J., ABBRUZZESE, J. L., HUANG, S. & XIE, K. 2005. A high expression level of insulin-like growth factor I receptor is associated with increased expression of transcription factor Sp1 and regional lymph node metastasis of human gastric cancer. *Clinical & Experimental Metastasis,* 21**,** 755-764.
JIMÉNEZ, C., HERNÁNDEZ, C., PIMENTEL, B. & CARRERA, A. C. 2002. The p85 Regulatory Subunit Controls Sequential Activation of Phosphoinositide 3-Kinase by Tyr Kinases and Ras. *Journal of Biological Chemistry,* 277**,** 41556-41562.
JIN, S., ANTINORE, M. J., LUNG, F. D., DONG, X., ZHAO, H., FAN, F., COLCHAGIE, A. B., BLANCK, P., ROLLER, P. P., FORNACE, A. J., JR. & ZHAN, Q. 2000. The GADD45 inhibition of Cdc2 kinase correlates with GADD45-mediated growth suppression. *J Biol Chem,* 275**,** 16602-8.
JUNG, H. J. & SUH, Y. 2014. Regulation of IGF -1 signaling by microRNAs. *Front Genet,* 5.
JUNNILA, R. K., LIST, E. O., BERRYMAN, D. E., MURREY, J. W. & KOPCHICK, J. J. 2013. The GH/IGF-1 axis in ageing and longevity. *Nat Rev Endocrinol,* 9**,** 366-376.
KAINA, B., CHRISTMANN, M., NAUMANN, S. & ROOS, W. P. 2007. MGMT: Key node in the battle against genotoxicity, carcinogenicity and apoptosis induced by alkylating agents. *DNA Repair,* 6**,** 1079-1099.
KAVRAN, J. M., MCCABE, J. M., BYRNE, P. O., CONNACHER, M. K., WANG, Z., RAMEK, A., SARABIPOUR, S., SHAN, Y., SHAW, D. E., HRISTOVA, K., COLE, P. A. & LEAHY, D. J. 2014. How IGF-1 activates its receptor. *eLife,* 3**,** e03772.
KAWASHIMA, Y., KANZAKI, S., YANG, F., KINOSHITA, T., HANAKI, K., NAGAISHI, J., OHTSUKA, Y., HISATOME, I., NINOMOYA, H., NANBA, E., FUKUSHIMA, T. & TAKAHASHI, S. 2005. Mutation at cleavage site of insulin-like growth factor receptor in a short-stature child born with intrauterine growth retardation. *J Clin Endocrinol Metab,* 90**,** 4679-87.
KEARSEY, J. M., COATES, P. J., PRESCOTT, A. R., WARBRICK, E. & HALL, P. A. 1995. Gadd45 is a nuclear cell cycle regulated protein which interacts with p21Cip1. *Oncogene,* 11**,** 1675-83.
KEIR, S. T., MARIS, J. M., REYNOLDS, C. P., KANG, M. H., KOLB, E. A., GORLICK, R., LOCK, R., CAROL, H., MORTON, C. L., WU, J., KURMASHEVA, R. T., HOUGHTON, P. J. & SMITH, M. A. 2013. Initial testing (stage 1) of temozolomide by the pediatric preclinical testing program. *Pediatric Blood & Cancer,* 60**,** 783-790.
KELLY, G. M., BUCKLEY, D. A., KIELY, P. A., ADAMS, D. R. & O'CONNOR, R. 2012. Serine Phosphorylation of the Insulin-like Growth Factor I (IGF-1) Receptor C-terminal Tail Restrains Kinase Activity and Cell Growth. *Journal of Biological Chemistry,* 287**,** 28180-28194.
KIELY, P. A., BAILLIE, G. S., BARRETT, R., BUCKLEY, D. A., ADAMS, D. R., HOUSLAY, M. D. & O'CONNOR, R. 2009. Phosphorylation of RACK1 on tyrosine 52 by c-Abl is required for insulin-like growth factor I-mediated regulation of focal adhesion kinase. *J Biol Chem,* 284**,** 20263-74.
KIELY, P. A., BAILLIE, G. S., LYNCH, M. J., HOUSLAY, M. D. & O'CONNOR, R. 2008. Tyrosine 302 in RACK1 is essential for insulin-like growth factor-I-mediated competitive

binding of PP2A and beta1 integrin and for tumor cell proliferation and migration. *J Biol Chem,* 283**,** 22952-61.

KIELY, P. A., LEAHY, M., O'GORMAN, D. & O'CONNOR, R. 2005. RACK1-mediated Integration of Adhesion and Insulin-like Growth Factor I (IGF-I) Signaling and Cell Migration Are Defective in Cells Expressing an IGF-I Receptor Mutated at Tyrosines 1250 and 1251. *Journal of Biological Chemistry,* 280**,** 7624-7633.

KIM, H.-J., LITZENBURGER, B. C., CUI, X., DELGADO, D. A., GRABINER, B. C., LIN, X., LEWIS, M. T., GOTTARDIS, M. M., WONG, T. W., ATTAR, R. M., CARBONI, J. M. & LEE, A. V. 2007. Constitutively Active Type I Insulin-Like Growth Factor Receptor Causes Transformation and Xenograft Growth of Immortalized Mammary Epithelial Cells and Is Accompanied by an Epithelial-to-Mesenchymal Transition Mediated by NF-κB and Snail. *Molecular and Cellular Biology,* 27**,** 3165-3175.

KIM, J.-S., KRASIEVA, T. B., KURUMIZAKA, H., CHEN, D. J., TAYLOR, A. M. R. & YOKOMORI, K. 2005. Independent and sequential recruitment of NHEJ and HR factors to DNA damage sites in mammalian cells. *The Journal of Cell Biology,* 170**,** 341-347.

KIM, T. J., LEE, J. W., SONG, S. Y., CHOI, J. J., CHOI, C. H., KIM, B. G., LEE, J. H. & BAE, D. S. 2006. Increased expression of pAKT is associated with radiation resistance in cervical cancer. *British Journal Of Cancer,* 94**,** 1678.

KIM, T. K. & EBERWINE, J. H. 2010. Mammalian cell transfection: the present and the future. *Analytical and Bioanalytical Chemistry,* 397**,** 3173-3178.

KOLAS, N. K., CHAPMAN, J. R., NAKADA, S., YLANKO, J., CHAHWAN, R., SWEENEY, F. D., PANIER, S., MENDEZ, M., WILDENHAIN, J., THOMSON, T. M., PELLETIER, L., JACKSON, S. P. & DUROCHER, D. 2007. Orchestration of the DNA-damage response by the RNF8 ubiquitin ligase. *Science,* 318**,** 1637-40.

KONDO, N., TAKAHASHI, A., MORI, E., NODA, T., ZDZIENICKA, M. Z., THOMPSON, L. H., HELLEDAY, T., SUZUKI, M., KINASHI, Y., MASUNAGA, S., ONO, K., HASEGAWA, M. & OHNISHI, T. 2011. FANCD1/BRCA2 plays predominant role in the repair of DNA damage induced by ACNU or TMZ. *PLoS One,* 6**,** e19659.

KONDO, N., TAKAHASHI, A., ONO, K. & OHNISHI, T. 2010. DNA Damage Induced by Alkylating Agents and Repair Pathways. *Journal of Nucleic Acids,* 2010.

KRUECKL, S. L., SIKES, R. A., EDLUND, N. M., BELL, R. H., HURTADO-COLL, A., FAZLI, L., GLEAVE, M. E. & COX, M. E. 2004. Increased insulin-like growth factor I receptor expression and signaling are components of androgen-independent progression in a lineage-derived prostate cancer progression model. *Cancer Res,* 64**,** 8620-9.

KUEMMERLE, J. F. 2006. Occupation of alphavbeta3-integrin by endogenous ligands modulates IGF-I receptor activation and proliferation of human intestinal smooth muscle. *Am J Physiol Gastrointest Liver Physiol,* 290**,** G1194-202.

KUIJJER, M. L., PETERSE, E. F., VAN DEN AKKER, B. E., BRIAIRE-DE BRUIJN, I. H., SERRA, M., MEZA-ZEPEDA, L. A., MYKLEBOST, O., HASSAN, A. B., HOGENDOORN, P. C. & CLETON-JANSEN, A.-M. 2013. IR/IGF1R signaling as potential target for treatment of high-grade osteosarcoma. *BMC Cancer,* 13**,** 245.

KULIK, G., KLIPPEL, A. & WEBER, M. J. 1997. Antiapoptotic signalling by the insulin-like growth factor I receptor, phosphatidylinositol 3-kinase, and Akt. *Molecular and Cellular Biology,* 17**,** 1595-606.

KUO, L. J. & YANG, L. X. 2008. Gamma-H2AX - a novel biomarker for DNA double-strand breaks. *In Vivo,* 22**,** 305-9.

LAVOIE, H. & THERRIEN, M. 2015. Regulation of RAF protein kinases in ERK signalling. *Nat Rev Mol Cell Biol,* 16**,** 281-298.

LEE, J.-H., PARK, S.-J., KIM, S. W., HARIHARASUDHAN, G., JUNG, S.-M., JUN, S., YONG, J. & YOU, H. J. 2017. c-Fos-dependent miR-22 targets MDC1 and regulates DNA repair in terminally differentiated cells. *Oncotarget,* 8**,** 48204-48221.

LEE, J. & ZHOU, P. 2007. DCAFs, the Missing Link of the CUL4-DDB1 Ubiquitin Ligase. *Molecular Cell,* 26**,** 775-780.

LEHMANN, M., ANDRE, F., BELLAN, C., REMACLE-BONNET, M., GARROUSTE, F., PARAT, F., LISSITSKY, J. C., MARVALDI, J. & POMMIER, G. 1998. Deficient

processing and activity of type I insulin-like growth factor receptor in the furin-deficient LoVo-C5 cells. *Endocrinology,* 139**,** 3763-71.
LEVITZKI, A. & GAZIT, A. 1995. Tyrosine kinase inhibition: an approach to drug development. *Science,* 267**,** 1782-8.
LI, H.-F., KIM, J.-S. & WALDMAN, T. 2009. Radiation-induced Akt activation modulates radioresistance in human glioblastoma cells. *Radiation Oncology,* 4**,** 43.
LI, Z., SHAO, C., KONG, Y., CARLOCK, C., AHMAD, N. & LIU, X. 2017. DNA Damage Response-Independent Role for MDC1 in Maintaining Genomic Stability. *Molecular and Cellular Biology,* 37**,** e00595-16.
LIANG, Z., DIEPSTRA, A., XU, C., VAN IMHOFF, G., PLATTEL, W., VAN DEN BERG, A. & VISSER, L. 2014. Insulin-like growth factor 1 receptor is a prognostic factor in classical Hodgkin lymphoma. *PLoS One,* 9**,** e87474.
LINDAHL, T. 1993. Instability and decay of the primary structure of DNA. *Nature,* 362**,** 709-15.
LIU, J., DOTY, T., GIBSON, B. & HEYER, W.-D. 2010. Human BRCA2 protein promotes RAD51 filament formation on RPA-covered single-stranded DNA. *Nat Struct Mol Biol,* 17**,** 1260-1262.
LIU, P., GAN, W., GUO, C., XIE, A., GAO, D., GUO, J., ZHANG, J., WILLIS, N., SU, A., ASARA, JOHN M., SCULLY, R. & WEI, W. 2015. Akt-Mediated Phosphorylation of XLF Impairs Non-Homologous End-Joining DNA Repair. *Molecular Cell,* 57**,** 648-661.
LIU, Q., GUNTUKU, S., CUI, X. S., MATSUOKA, S., CORTEZ, D., TAMAI, K., LUO, G., CARATTINI-RIVERA, S., DEMAYO, F., BRADLEY, A., DONEHOWER, L. A. & ELLEDGE, S. J. 2000. Chk1 is an essential kinase that is regulated by Atr and required for the G(2)/M DNA damage checkpoint. *Genes Dev,* 14**,** 1448-59.
LIVAK, K. J. & SCHMITTGEN, T. D. 2001. Analysis of relative gene expression data using real-time quantitative PCR and the 2(-Delta Delta C(T)) Method. *Methods,* 25**,** 402-8.
LLORET, M., LARA, P. C., BORDÓN, E., PINAR, B., REY, A., FALCÓN, O., MOLANO, F. & HERNÁNDEZ, M. A. 2007. IGF-1R expression in localized cervical carcinoma patients treated by radiochemotherapy. *Gynecologic Oncology,* 106**,** 8-11.
LOCASALE, J. W. 2013. Serine, glycine and one-carbon units: cancer metabolism in full circle. *Nat Rev Cancer,* 13**,** 572-583.
LOMAX, M. E., FOLKES, L. K. & O'NEILL, P. 2013. Biological consequences of radiation-induced DNA damage: relevance to radiotherapy. *Clin Oncol (R Coll Radiol),* 25**,** 578-85.
LOMAX, M. E., GULSTON, M. K. & O'NEILL, P. 2002. Chemical aspects of clustered DNA damage induction by ionising radiation. *Radiat Prot Dosimetry,* 99**,** 63-8.
LOUGHERY, J., COX, M., SMITH, L. M. & MEEK, D. W. 2014. Critical role for p53-serine 15 phosphorylation in stimulating transactivation at p53-responsive promoters. *Nucleic Acids Research,* 42**,** 7666-7680.
LOVEJOY, C. A., LOCK, K., YENAMANDRA, A. & CORTEZ, D. 2006. DDB1 maintains genome integrity through regulation of Cdt1. *Mol Cell Biol,* 26**,** 7977-90.
LUKANOVA, A., LUNDIN, E., TONIOLO, P., MICHELI, A., AKHMEDKHANOV, A., RINALDI, S., MUTI, P., LENNER, P., BIESSY, C., KROGH, V., ZELENIUCH-JACQUOTTE, A., BERRINO, F., HALLMANS, G., RIBOLI, E. & KAAKS, R. 2002. Circulating levels of insulin-like growth factor-I and risk of ovarian cancer. *Int J Cancer,* 101**,** 549-54.
LUTTRELL, L. M., VAN BIESEN, T., HAWES, B. E., KOCH, W. J., TOUHARA, K. & LEFKOWITZ, R. J. 1995. G beta gamma subunits mediate mitogen-activated protein kinase activation by the tyrosine kinase insulin-like growth factor 1 receptor. *J Biol Chem,* 270**,** 16495-8.
MACAULAY, V. M., SALISBURY, A. J., BOHULA, E. A., PLAYFORD, M. P., SMORODINSKY, N. I. & SHILOH, Y. 2001. Downregulation of the type 1 insulin-like growth factor receptor in mouse melanoma cells is associated with enhanced radiosensitivity and impaired activation of Atm kinase. *Oncogene,* 20**,** 4029-40.
MAHANEY, B. L., MEEK, K. & LEES-MILLER, S. P. 2009. Repair of ionizing radiation-induced DNA double strand breaks by non-homologous end-joining. *The Biochemical journal,* 417**,** 639-650.

MAK, S. K. & KÜLTZ, D. 2004. Gadd45 Proteins Induce G2/M Arrest and Modulate Apoptosis in Kidney Cells Exposed to Hyperosmotic Stress. *Journal of Biological Chemistry,* 279**,** 39075-39084.

MALI, P., YANG, L., ESVELT, K. M., AACH, J., GUELL, M., DICARLO, J. E., NORVILLE, J. E. & CHURCH, G. M. 2013. RNA-Guided Human Genome Engineering via Cas9. *Science,* 339**,** 823-826.

MAO, Z., BOZZELLA, M., SELUANOV, A. & GORBUNOVA, V. 2008. DNA repair by nonhomologous end joining and homologous recombination during cell cycle in human cells. *Cell cycle (Georgetown, Tex.),* 7**,** 2902-2906.

MARECHAL, A. & ZOU, L. 2015. RPA-coated single-stranded DNA as a platform for post-translational modifications in the DNA damage response. *Cell Res,* 25**,** 9-23.

MARÉCHAL, A. & ZOU, L. 2013. DNA Damage Sensing by the ATM and ATR Kinases. *Cold Spring Harbor Perspectives in Biology,* 5.

MARGISON, G. P. & SANTIBANEZ-KOREF, M. F. 2002. O6-alkylguanine-DNA alkyltransferase: role in carcinogenesis and chemotherapy. *Bioessays,* 24**,** 255-66.

MARUMOTO, T., ZHANG, D. & SAYA, H. 2005. Aurora-A - a guardian of poles. *Nat Rev Cancer,* 5**,** 42-50.

MATSUOKA, S., ROTMAN, G., OGAWA, A., SHILOH, Y., TAMAI, K. & ELLEDGE, S. J. 2000. Ataxia telangiectasia-mutated phosphorylates Chk2 in vivo and in vitro. *Proc Natl Acad Sci U S A,* 97**,** 10389-94.

MAY, W. A., GRIGORYAN, R. S., KESHELAVA, N., CABRAL, D. J., CHRISTENSEN, L. L., JENABI, J., JI, L., TRICHE, T. J., LAWLOR, E. R. & REYNOLDS, C. P. 2013. Characterization and Drug Resistance Patterns of Ewing's Sarcoma Family Tumor Cell Lines. *PLoS ONE,* 8**,** e80060.

MAYO, L. D. & DONNER, D. B. 2001. A phosphatidylinositol 3-kinase/Akt pathway promotes translocation of Mdm2 from the cytoplasm to the nucleus. *Proc Natl Acad Sci U S A,* 98**,** 11598-603.

MEACHAM, C. E. & MORRISON, S. J. 2013. Tumor heterogeneity and cancer cell plasticity. *Nature,* 501**,** 328-337.

MEGYESI, K., KAHN, C. R., ROTH, J., NEVILLE, D. M., JR., NISSLEY, S. P., HUMBEL, R. E. & FROESCH, E. R. 1975. The NSILA-s receptor in liver plasma membranes. Characterization and comparison with the insulin receptor. *J Biol Chem,* 250**,** 8990-6.

MEINDL, A., HELLEBRAND, H., WIEK, C., ERVEN, V., WAPPENSCHMIDT, B., NIEDERACHER, D., FREUND, M., LICHTNER, P., HARTMANN, L., SCHAAL, H., RAMSER, J., HONISCH, E., KUBISCH, C., WICHMANN, H. E., KAST, K., DEISSLER, H., ENGEL, C., MULLER-MYHSOK, B., NEVELING, K., KIECHLE, M., MATHEW, C. G., SCHINDLER, D., SCHMUTZLER, R. K. & HANENBERG, H. 2010. Germline mutations in breast and ovarian cancer pedigrees establish RAD51C as a human cancer susceptibility gene. *Nat Genet,* 42**,** 410-4.

METALLI, D., LOVAT, F., TRIPODI, F., GENUA, M., XU, S. Q., SPINELLI, M., ALBERGHINA, L., VANONI, M., BAFFA, R., GOMELLA, L. G., IOZZO, R. V. & MORRIONE, A. 2010. The insulin-like growth factor receptor I promotes motility and invasion of bladder cancer cells through Akt- and mitogen-activated protein kinase-dependent activation of paxillin. *Am J Pathol,* 176**,** 2997-3006.

MIN, Y., ADACHI, Y., YAMAMOTO, H., ITO, H., ITOH, F., LEE, C. T., NADAF, S., CARBONE, D. P. & IMAI, K. 2003. Genetic blockade of the insulin-like growth factor-I receptor: a promising strategy for human pancreatic cancer. *Cancer Res,* 63**,** 6432-41.

MIRA, E., MAÑES, S., LACALLE, R. A., MÁRQUEZ, G. & MARTÍNEZ-A, C. 1999. Insulin-Like Growth Factor I-Triggered Cell Migration and Invasion Are Mediated by Matrix Metalloproteinase-9*. *Endocrinology,* 140**,** 1657-1664.

MIURA, M. & BASERGA, R. 1997. The tyrosine residue at 1250 of the insulin-like growth factor I receptor is required for ligand-mediated internalization. *Biochem Biophys Res Commun,* 239**,** 182-5.

MOHSENY, A. B., MACHADO, I., CAI, Y., SCHAEFER, K. L., SERRA, M., HOGENDOORN, P. C., LLOMBART-BOSCH, A. & CLETON-JANSEN, A. M. 2011. Functional

characterization of osteosarcoma cell lines provides representative models to study the human disease. *Lab Invest,* 91**,** 1195-205.

MOJAS, N., LOPES, M. & JIRICNY, J. 2007. Mismatch repair-dependent processing of methylation damage gives rise to persistent single-stranded gaps in newly replicated DNA. *Genes Dev,* 21**,** 3342-55.

MONAMI, G., EMILIOZZI, V. & MORRIONE, A. 2008. Grb10/Nedd4-mediated multiubiquitination of the insulin-like growth factor receptor regulates receptor internalization. *J Cell Physiol,* 216**,** 426-37.

MORRIONE, A., PLANT, P., VALENTINIS, B., STAUB, O., KUMAR, S., ROTIN, D. & BASERGA, R. 1999. mGrb10 Interacts with Nedd4. *Journal of Biological Chemistry,* 274**,** 24094-24099.

MORRISON, K. B., TOGNON, C. E., GARNETT, M. J., DEAL, C. & SORENSEN, P. H. 2002. ETV6-NTRK3 transformation requires insulin-like growth factor 1 receptor signaling and is associated with constitutive IRS-1 tyrosine phosphorylation. *Oncogene,* 21**,** 5684-95.

MOUDI, M., GO, R., YIEN, C. Y. S. & NAZRE, M. 2013. Vinca Alkaloids. *International Journal of Preventive Medicine,* 4**,** 1231-1235.

MOUNTZIOS, G., KOSTOPOULOS, I., KOTOULA, V., SFAKIANAKI, I., FOUNTZILAS, E., MARKOU, K., KARASMANIS, I., LEVA, S., ANGOURIDAKIS, N., VLACHTSIS, K., NIKOLAOU, A., KONSTANTINIDIS, I. & FOUNTZILAS, G. 2013. Insulin-Like Growth Factor 1 Receptor (IGF1R) Expression and Survival in Operable Squamous-Cell Laryngeal Cancer. *PLOS ONE,* 8**,** e54048.

MUNSHI, A., HOBBS, M. & MEYN, R. E. 2005. Clonogenic cell survival assay. *Methods Mol Med,* 110**,** 21-8.

MURRAY-ZMIJEWSKI, F., SLEE, E. A. & LU, X. 2008. A complex barcode underlies the heterogeneous response of p53 to stress. *Nat Rev Mol Cell Biol,* 9**,** 702-12.

MYERS, M. G., JR., BACKER, J. M., SUN, X. J., SHOELSON, S., HU, P., SCHLESSINGER, J., YOAKIM, M., SCHAFFHAUSEN, B. & WHITE, M. F. 1992. IRS-1 activates phosphatidylinositol 3'-kinase by associating with src homology 2 domains of p85. *Proc Natl Acad Sci U S A,* 89**,** 10350-4.

MYNARCIK, D. C., WILLIAMS, P. F., SCHAFFER, L., YU, G. Q. & WHITTAKER, J. 1997. Identification of common ligand binding determinants of the insulin and insulin-like growth factor 1 receptors. Insights into mechanisms of ligand binding. *J Biol Chem,* 272**,** 18650-5.

NASCIMENTO, E. B., SNEL, M., GUIGAS, B., VAN DER ZON, G. C., KRIEK, J., MAASSEN, J. A., JAZET, I. M., DIAMANT, M. & OUWENS, D. M. 2010. Phosphorylation of PRAS40 on Thr246 by PKB/AKT facilitates efficient phosphorylation of Ser183 by mTORC1. *Cell Signal,* 22**,** 961-7.

NICKERSON, T., CHANG, F., LORIMER, D., SMEEKENS, S. P., SAWYERS, C. L. & POLLAK, M. 2001. In vivo progression of LAPC-9 and LNCaP prostate cancer models to androgen independence is associated with increased expression of insulin-like growth factor I (IGF-I) and IGF-I receptor (IGF-IR). *Cancer Res,* 61**,** 6276-80.

NIEMINUSZCZY, J., SCHWAB, R. A. & NIEDZWIEDZ, W. 2016. The DNA fibre technique – tracking helicases at work. *Methods,* 108**,** 92-98.

NIETO, M. A., HUANG, R. Y.-J., JACKSON, R. A. & THIERY, J. P. 2016. EMT: 2016. *Cell,* 166.

NIEWOLIK, D., PANNICKE, U., LU, H., MA, Y., WANG, L.-C. V., KULESZA, P., ZANDI, E., LIEBER, M. R. & SCHWARZ, K. 2006. DNA-PKcs Dependence of Artemis Endonucleolytic Activity, Differences between Hairpins and 5′ or 3′ Overhangs. *Journal of Biological Chemistry,* 281**,** 33900-33909.

NIKJOO, H., O'NEILL, P., TERRISSOL, M. & GOODHEAD, D. T. 1994. Modelling of radiation-induced DNA damage: the early physical and chemical event. *Int J Radiat Biol,* 66**,** 453-7.

NIMONKAR, A. V., GENSCHEL, J., KINOSHITA, E., POLACZEK, P., CAMPBELL, J. L., WYMAN, C., MODRICH, P. & KOWALCZYKOWSKI, S. C. 2011. BLM-DNA2-RPA-MRN and EXO1-BLM-RPA-MRN constitute two DNA end resection machineries for human DNA break repair. *Genes Dev,* 25**,** 350-62.

O'CONNOR, M. J. 2015. Targeting the DNA Damage Response in Cancer. *Mol Cell,* 60**,** 547-60.
O'CONNOR, R. 2003. Regulation of IGF-I receptor signaling in tumor cells. *Horm Metab Res,* 35**,** 771-7.
O'CONNOR, R., FENNELLY, C. & KRAUSE, D. 2000. Regulation of survival signals from the insulin-like growth factor-I receptor. *Biochem Soc Trans,* 28**,** 47-51.
OCHI, T., BLACKFORD, A. N., COATES, J., JHUJH, S., MEHMOOD, S., TAMURA, N., TRAVERS, J., WU, Q., DRAVIAM, V. M., ROBINSON, C. V., BLUNDELL, T. L. & JACKSON, S. P. 2015. PAXX, a paralog of XRCC4 and XLF, interacts with Ku to promote DNA double-strand break repair. *Science (New York, N.Y.),* 347**,** 185-188.
OECK, S., AL-REFAE, K., RIFFKIN, H., WIEL, G., HANDRICK, R., KLEIN, D., ILIAKIS, G. & JENDROSSEK, V. 2017. Activating Akt1 mutations alter DNA double strand break repair and radiosensitivity. *Scientific Reports,* 7**,** 42700.
OHTANI, N., YAMAKOSHI, K., TAKAHASHI, A. & HARA, E. 2004. The p16INK4a-RB pathway: molecular link between cellular senescence and tumor suppression. *J Med Invest,* 51**,** 146-53.
OKAICHI, K., NOSE, K., KOTAKE, T., IZUMI, N. & KUDO, T. 2011. Phosphorylation of p53 Modifies Sensitivity to Ionizing Radiation. *Anticancer Research,* 31**,** 2255-2258.
OLIVE, P. L. 1998. The role of DNA single- and double-strand breaks in cell killing by ionizing radiation. *Radiat Res,* 150**,** S42-51.
OLIVE, P. L. & BANATH, J. P. 2006. The comet assay: a method to measure DNA damage in individual cells. *Nat. Protocols,* 1**,** 23-29.
OLMOS, D., POSTEL-VINAY, S., MOLIFE, L. R., OKUNO, S. H., SCHUETZE, S. M., PACCAGNELLA, M. L., BATZEL, G. N., YIN, D., PRITCHARD-JONES, K., JUDSON, I., WORDEN, F. P., GUALBERTO, A., SCURR, M., DE BONO, J. S. & HALUSKA, P. 2010. Safety, pharmacokinetics, and preliminary activity of the anti-IGF-1R antibody figitumumab (CP-751,871) in patients with sarcoma and Ewing's sarcoma: a phase 1 expansion cohort study. *Lancet Oncol,* 11**,** 129-35.
OSHIMA, A., NOLAN, C. M., KYLE, J. W., GRUBB, J. H. & SLY, W. S. 1988. The human cation-independent mannose 6-phosphate receptor. Cloning and sequence of the full-length cDNA and expression of functional receptor in COS cells. *Journal of Biological Chemistry,* 263**,** 2553-2562.
OSUKA, S., SAMPETREAN, O., SHIMIZU, T., SAGA, I., ONISHI, N., SUGIHARA, E., OKUBO, J., FUJITA, S., TAKANO, S., MATSUMURA, A. & SAYA, H. 2013. IGF1 Receptor Signaling Regulates Adaptive Radioprotection in Glioma Stem Cells. *STEM CELLS,* 31**,** 627-640.
OTTAVIANO, L., SCHAEFER, K. L., GAJEWSKI, M., HUCKENBECK, W., BALDUS, S., ROGEL, U., MACKINTOSH, C., DE ALAVA, E., MYKLEBOST, O., KRESSE, S. H., MEZA-ZEPEDA, L. A., SERRA, M., CLETON-JANSEN, A. M., HOGENDOORN, P. C., BUERGER, H., AIGNER, T., GABBERT, H. E. & POREMBA, C. 2010. Molecular characterization of commonly used cell lines for bone tumor research: a trans-European EuroBoNet effort. *Genes Chromosomes Cancer,* 49**,** 40-51.
PARKER, A., CHEVILLE, J. C., LOHSE, C., CERHAN, J. R. & BLUTE, M. L. 2003. Expression of insulin-like growth factor I receptor and survival in patients with clear cell renal cell carcinoma. *J Urol,* 170**,** 420-4.
PASQUINELLI, A. E. 2012. MicroRNAs and their targets: recognition, regulation and an emerging reciprocal relationship. *Nat Rev Genet,* 13**,** 271-282.
PAUTSCH, A., ZOEPHEL, A., AHORN, H., SPEVAK, W., HAUPTMANN, R. & NAR, H. 2001. Crystal Structure of Bisphosphorylated IGF-1 Receptor Kinase: Insight into Domain Movements upon Kinase Activation. *Structure,* 9**,** 955-965.
PAYET, L. D., WANG, X. H., BAXTER, R. C. & FIRTH, S. M. 2003. Amino- and carboxyl-terminal fragments of insulin-like growth factor (IGF) binding protein-3 cooperate to bind IGFs with high affinity and inhibit IGF receptor interactions. *Endocrinology,* 144**,** 2797-806.
PEINADO, H., OLMEDA, D. & CANO, A. 2007. Snail, Zeb and bHLH factors in tumour progression: an alliance against the epithelial phenotype? *Nat Rev Cancer,* 7**,** 415-28.

PEIRÓ, G., BENLLOCH, S., SÁNCHEZ-TEJADA, L., ADROVER, E., LERMA, E., PEIRÓ, F. M., SÁNCHEZ-PAYÁ, J. & ARANDA, F. I. 2009. Low activation of Insulin-like Growth Factor 1-Receptor (IGF1R) is associated with local recurrence in early breast carcinoma. *Breast Cancer Research and Treatment,* 117**,** 433-441.

PENG, Y., DAI, Y., HITCHCOCK, C., YANG, X., KASSIS, E. S., LIU, L., LUO, Z., SUN, H. L., CUI, R., WEI, H., KIM, T., LEE, T. J., JEON, Y. J., NUOVO, G. J., VOLINIA, S., HE, Q., YU, J., NANA-SINKAM, P. & CROCE, C. M. 2013. Insulin growth factor signaling is regulated by microRNA-486, an underexpressed microRNA in lung cancer. *Proc Natl Acad Sci U S A,* 110**,** 15043-8.

PERETZ, S., JENSEN, R., BASERGA, R. & GLAZER, P. M. 2001. ATM-dependent expression of the insulin-like growth factor-I receptor in a pathway regulating radiation response. *Proceedings of the National Academy of Sciences,* 98**,** 1676-1681.

PERUZZI, F., PRISCO, M., DEWS, M., SALOMONI, P., GRASSILLI, E., ROMANO, G., CALABRETTA, B. & BASERGA, R. 1999. Multiple Signaling Pathways of the Insulin-Like Growth Factor 1 Receptor in Protection from Apoptosis. *Molecular and Cellular Biology,* 19**,** 7203-7215.

PLAYFORD, M. P., BICKNELL, D., BODMER, W. F. & MACAULAY, V. M. 2000. Insulin-like growth factor 1 regulates the location, stability, and transcriptional activity of beta-catenin. *Proc Natl Acad Sci U S A,* 97**,** 12103-8.

POLLACK, I. F., HAMILTON, R. L., SOBOL, R. W., BURNHAM, J., YATES, A. J., HOLMES, E. J., ZHOU, T. & FINLAY, J. L. 2006. O6-Methylguanine-DNA methyltransferase expression strongly correlates with outcome in childhood malignant gliomas: Results from the CCG-945 cohort. *Journal of Clinical Oncology,* 24**,** 3431-3437.

POLO, S. E. & JACKSON, S. P. 2011. Dynamics of DNA damage response proteins at DNA breaks: a focus on protein modifications. *Genes Dev,* 25**,** 409-33.

POUGET, J. P., FRELON, S., RAVANAT, J. L., TESTARD, I., ODIN, F. & CADET, J. 2002. Formation of modified DNA bases in cells exposed either to gamma radiation or to high-LET particles. *Radiat Res,* 157**,** 589-95.

PRAGER, D., LI, H. L., YAMASAKI, H. & MELMED, S. 1994. Human insulin-like growth factor I receptor internalization. Role of the juxtamembrane domain. *J Biol Chem,* 269**,** 11934-7.

QIU, P., SHANDILYA, H., D'ALESSIO, J. M., O'CONNOR, K., DUROCHER, J. & GERARD, G. F. 2004. Mutation detection using Surveyor nuclease. *Biotechniques,* 36**,** 702-7.

QIU, W., LEIBOWITZ, B., ZHANG, L. & YU, J. 2010. Growth factors protect intestinal stem cells from radiation-induced apoptosis by suppressing PUMA through the PI3K/AKT/p53 axis. *Oncogene,* 29**,** 1622-1632.

QUIROS, S., ROOS, W. P. & KAINA, B. 2010. Processing of O6-methylguanine into DNA double-strand breaks requires two rounds of replication whereas apoptosis is also induced in subsequent cell cycles. *Cell Cycle,* 9**,** 168-78.

RAILO, M. J., VON SMITTEN, K. & PEKONEN, F. 1994. The prognostic value of insulin-like growth factor-I in breast cancer patients. Results of a follow-up study on 126 patients. *Eur J Cancer,* 30a**,** 307-11.

RAMCHARAN, R. 2014. *DPhil Thesis: Investigation of the effects if IGF-1 receptor blockade on chemoresistance of advanced melanoma.* DPhil, University of Oxford.

RAMCHARAN, R., ALEKSIC, T., KAMDOUM, W. P., GAO, S., PFISTER, S. X., TANNER, J., BRIDGES, E., ASHER, R., WATSON, A. J., MARGISON, G. P., WOODCOCK, M., REPAPI, E., LI, J.-L., MIDDLETON, M. R. & MACAULAY, V. M. 2015. IGF-1R inhibition induces schedule-dependent sensitization of human melanoma to temozolomide. *Oncotarget,* 6**,** 39877-39890.

RAN, F. A., HSU, P. D., WRIGHT, J., AGARWALA, V., SCOTT, D. A. & ZHANG, F. 2013. Genome engineering using the CRISPR-Cas9 system. *Nature protocols,* 8**,** 2281-2308.

RAO, D. D., VORHIES, J. S., SENZER, N. & NEMUNAITIS, J. 2009. siRNA vs. shRNA: Similarities and differences. *Advanced Drug Delivery Reviews,* 61**,** 746-759.

RAVEROT, G., STURM, N., DE FRAIPONT, F., MULLER, M., SALENAVE, S., CARON, P., CHABRE, O., CHANSON, P., CORTET-RUDELLI, C., ASSAKER, R., DUFOUR, H., GAILLARD, S., FRANÇOIS, P., JOUANNEAU, E., PASSAGIA, J. G., BERNIER, M.,

CORNÉLIUS, A., FIGARELLA-BRANGER, D., TROUILLAS, J., BORSON-CHAZOT, F. & BRUE, T. 2010. Temozolomide treatment in aggressive pituitary tumors and pituitary carcinomas: A French multicenter experience. *Journal of Clinical Endocrinology and Metabolism,* 95**,** 4592-4599.

RAVICHANDRAN, K. S. 2001. Signaling via Shc family adapter proteins. *Oncogene,* 20**,** 6322-30.

RAY CHAUDHURI, A. & NUSSENZWEIG, A. 2017. The multifaceted roles of PARP1 in DNA repair and chromatin remodelling. *Nat Rev Mol Cell Biol*.

RAYNARD, S., BUSSEN, W. & SUNG, P. 2006. A double Holliday junction dissolvasome comprising BLM, topoisomerase IIIalpha, and BLAP75. *J Biol Chem,* 281**,** 13861-4.

REINHARDT, H. C., ASLANIAN, A. S., LEES, J. A. & YAFFE, M. B. 2007. p53 deficient cells rely on ATM and ATR-mediated checkpoint signaling through the p38 MAPK/MK2pathway for survival after DNA damage. *Cancer cell,* 11**,** 175-189.

REN, J.-G., SETH, P., YE, H., GUO, K., HANAI, J.-I., HUSAIN, Z. & SUKHATME, V. P. 2017. Citrate Suppresses Tumor Growth in Multiple Models through Inhibition of Glycolysis, the Tricarboxylic Acid Cycle and the IGF-1R Pathway. *Scientific Reports,* 7**,** 4537.

RENEHAN, A. G., ZWAHLEN, M., MINDER, C., O'DWYER, S. T., SHALET, S. M. & EGGER, M. 2004. Insulin-like growth factor (IGF)-I, IGF binding protein-3, and cancer risk: systematic review and meta-regression analysis. *The Lancet,* 363**,** 1346-1353.

RICHESON, C. E., MULDER, P., BOWRY, V. W. & INGOLD, K. U. 1998. The Complex Chemistry of Peroxynitrite Decomposition: New Insights1. *Journal of the American Chemical Society,* 120**,** 7211-7219.

RIEDEMANN, J., TAKIGUCHI, M., SOHAIL, M. & MACAULAY, V. M. 2007. The EGF receptor interacts with the type 1 IGF receptor and regulates its stability. *Biochem Biophys Res Commun,* 355**,** 707-14.

RIESTERER, O., YANG, Q., RAJU, U., TORRES, M., MOLKENTINE, D., PATEL, N., VALDECANAS, D., MILAS, L. & ANG, K. K. 2011. Combination of anti-IGF-1R antibody A12 and ionizing radiation in upper respiratory tract cancers. *Int J Radiat Oncol Biol Phys,* 79**,** 1179-87.

RIPPS, H. & SHEN, W. 2012. Review: taurine: a "very essential" amino acid. *Mol Vis,* 18**,** 2673-86.

RISS, T. L., MORAVEC, R. A., NILES, A. L., BENINK, H. A., WORZELLA, T. J. & MINOR, L. 2004. Cell Viability Assays. *In:* SITTAMPALAM, G. S., GAL-EDD, N., ARKIN, M., AULD, D., AUSTIN, C., BEJCEK, B., GLICKSMAN, M., INGLESE, J., LEMMON, V., LI, Z., MCGEE, J., MCMANUS, O., MINOR, L., NAPPER, A., RISS, T., TRASK, O. J. & WEIDNER, J. (eds.) *Assay Guidance Manual.* Bethesda (MD): Eli Lilly & Company and the National Center for Advancing Translational Sciences.

ROCHESTER, M. A., RIEDEMANN, J., HELLAWELL, G. O., BREWSTER, S. F. & MACAULAY, V. M. 2005. Silencing of the IGF1R gene enhances sensitivity to DNA-damaging agents in both PTEN wild-type and mutant human prostate cancer. *Cancer Gene Ther,* 12**,** 90-100.

RODGERS, K. & MCVEY, M. 2016. Error-Prone Repair of DNA Double-Strand Breaks. *Journal of Cellular Physiology,* 231**,** 15-24.

ROMANELLI, R. J., LEBEAU, A. P., FULMER, C. G., LAZZARINO, D. A., HOCHBERG, A. & WOOD, T. L. 2007. Insulin-like growth factor type-I receptor internalization and recycling mediate the sustained phosphorylation of Akt. *J Biol Chem,* 282**,** 22513-24.

ROOS, W. P., NIKOLOVA, T., QUIROS, S., NAUMANN, S. C., KIEDRON, O., ZDZIENICKA, M. Z. & KAINA, B. 2009. Brca2/Xrcc2 dependent HR, but not NHEJ, is required for protection against O(6)-methylguanine triggered apoptosis, DSBs and chromosomal aberrations by a process leading to SCEs. *DNA Repair (Amst),* 8**,** 72-86.

ROSKOSKI, R., JR. 2012. ERK1/2 MAP kinases: structure, function, and regulation. *Pharmacol Res,* 66**,** 105-43.

ROSSI, J. J. 2008. Expression Strategies for Short Hairpin RNA Interference Triggers. *Human gene therapy,* 19**,** 313-317.

RSTUDIO TEAM 2016. RStudio: Integrated Development for R.: RStudio, Inc.

RYDBERG, B. & LINDAHL, T. 1982. Nonenzymatic methylation of DNA by the intracellular methyl group donor S-adenosyl-L-methionine is a potentially mutagenic reaction. *Embo j,* 1**,** 211-6.

SACHDEV, D., LI, S.-L., HARTELL, J. S., FUJITA-YAMAGUCHI, Y., MILLER, J. S. & YEE, D. 2003. A Chimeric Humanized Single-Chain Antibody against the Type I Insulin-like Growth Factor (IGF) Receptor Renders Breast Cancer Cells Refractory to the Mitogenic Effects of IGF-I. *Cancer Research,* 63**,** 627-635.

SAFRAN, M., DALAH, I., ALEXANDER, J., ROSEN, N., INY STEIN, T., SHMOISH, M., NATIV, N., BAHIR, I., DONIGER, T., KRUG, H., SIROTA-MADI, A., OLENDER, T., GOLAN, Y., STELZER, G., HAREL, A. & LANCET, D. 2010. GeneCards Version 3: the human gene integrator. *Database: The Journal of Biological Databases and Curation,* 2010**,** baq020.

SAKAGUCHI, K., HERRERA, J. E., SAITO, S. I., MIKI, T., BUSTIN, M., VASSILEV, A., ANDERSON, C. W. & APPELLA, E. 1998. DNA damage activates p53 through a phosphorylation–acetylation cascade. *Genes & Development,* 12**,** 2831-2841.

SAKAI, K., LOWMAN, H. B. & CLEMMONS, D. R. 2002. Increases in free, unbound insulin-like growth factor I enhance insulin responsiveness in human hepatoma G2 cells in culture. *J Biol Chem,* 277**,** 13620-7.

SALVADOR, J. M., BROWN-CLAY, J. D. & FORNACE, A. J. 2013. Gadd45 in Stress Signaling, Cell Cycle Control, and Apoptosis. *In:* LIEBERMANN, D. A. & HOFFMAN, B. (eds.) *Gadd45 Stress Sensor Genes.* New York, NY: Springer New York.

SANDER, J. D. & JOUNG, J. K. 2014. CRISPR-Cas systems for editing, regulating and targeting genomes. *Nat Biotech,* 32**,** 347-355.

SANDERS, M. R., LU, H., WALKER, F., SORBA, S. & DAINIAK, N. 1998. The Raf-1 protein mediates insulin-like growth factor-induced proliferation of erythroid progenitor cells. *Stem Cells,* 16**,** 200-7.

SANDHU, M. S., HEALD, A. H., GIBSON, J. M., CRUICKSHANK, J. K., DUNGER, D. B. & WAREHAM, N. J. 2002. Circulating concentrations of insulin-like growth factor-I and development of glucose intolerance: a prospective observational study. *Lancet,* 359**,** 1740-5.

SARBASSOV, D. D., ALI, S. M. & SABATINI, D. M. 2005. Growing roles for the mTOR pathway. *Curr Opin Cell Biol,* 17**,** 596-603.

SARFSTEIN, R., PASMANIK-CHOR, M., YEHESKEL, A., EDRY, L., SHOMRON, N., WARMAN, N., WERTHEIMER, E., MAOR, S., SHOCHAT, L. & WERNER, H. 2012. Insulin-like growth factor-I receptor (IGF-IR) translocates to nucleus and autoregulates IGF-IR gene expression in breast cancer cells. *J Biol Chem,* 287**,** 2766-76.

SARTORI, A. A., LUKAS, C., COATES, J., MISTRIK, M., FU, S., BARTEK, J., BAER, R., LUKAS, J. & JACKSON, S. P. 2007. Human CtIP promotes DNA end resection. *Nature,* 450**,** 509-14.

SAYEED, A., ALAM, N., TREROTOLA, M. & LANGUINO, L. R. 2012. Insulin-Like Growth Factor 1 Stimulation of Androgen Receptor Activity Requires β(1A) Integrins. *Journal of cellular physiology,* 227**,** 751-758.

SCHWARTZ, J. L., ROTMENSCH, J., GIOVANAZZI, S., COHEN, M. B. & WEICHSELBAUM, R. R. 1988. Faster repair of DNA double-strand breaks in radioresistant human tumor cells. *International Journal of Radiation Oncology*Biology*Physics,* 15**,** 907-912.

SEHAT, B., ANDERSSON, S., GIRNITA, L. & LARSSON, O. 2008. Identification of c-Cbl as a new ligase for insulin-like growth factor-I receptor with distinct roles from Mdm2 in receptor ubiquitination and endocytosis. *Cancer Res,* 68**,** 5669-77.

SEHAT, B., ANDERSSON, S., VASILCANU, R., GIRNITA, L. & LARSSON, O. 2007. Role of Ubiquitination in IGF-1 Receptor Signaling and Degradation. *PLOS ONE,* 2**,** e340.

SEHAT, B., TOFIGH, A., LIN, Y., TROCME, E., LILJEDAHL, U., LAGERGREN, J. & LARSSON, O. 2010. SUMOylation mediates the nuclear translocation and signaling of the IGF-1 receptor. *Sci Signal,* 3**,** ra10.

SEKI, M., NAKAGAWA, T., SEKI, T., KATO, G., TADA, S., TAKAHASHI, Y., YOSHIMURA, A., KOBAYASHI, T., AOKI, A., OTSUKI, M., HABERMANN, F. A., TANABE, H.,

ISHII, Y. & ENOMOTO, T. 2006. Bloom Helicase and DNA Topoisomerase IIIα Are Involved in the Dissolution of Sister Chromatids. *Molecular and Cellular Biology,* 26**,** 6299-6307.

SELL, C., RUBINI, M., RUBIN, R., LIU, J. P., EFSTRATIADIS, A. & BASERGA, R. 1993. Simian virus 40 large tumor antigen is unable to transform mouse embryonic fibroblasts lacking type 1 insulin-like growth factor receptor. *Proc Natl Acad Sci U S A,* 90**,** 11217-21.

SELUANOV, A., MAO, Z. & GORBUNOVA, V. 2010. Analysis of DNA Double-strand Break (DSB) Repair in Mammalian Cells. *Journal of Visualized Experiments : JoVE,* 2002.

SEMENENKO, V. A. & STEWART, R. D. 2004. A Fast Monte Carlo Algorithm to Simulate the Spectrum of DNA Damages Formed by Ionizing Radiation. *Radiation Research,* 161**,** 451-457.

SESTI, G., SCIACQUA, A., CARDELLINI, M., MARINI, M. A., MAIO, R., VATRANO, M., SUCCURRO, E., LAURO, R., FEDERICI, M. & PERTICONE, F. 2005. Plasma concentration of IGF-I is independently associated with insulin sensitivity in subjects with different degrees of glucose tolerance. *Diabetes Care,* 28**,** 120-5.

SHIBATA, A., CONRAD, S., BIRRAUX, J., GEUTING, V., BARTON, O., ISMAIL, A., KAKAROUGKAS, A., MEEK, K., TAUCHER-SCHOLZ, G., LÖBRICH, M. & JEGGO, P. A. 2011. Factors determining DNA double-strand break repair pathway choice in G2 phase. *The EMBO Journal,* 30**,** 1079-1092.

SHIEH, S.-Y., IKEDA, M., TAYA, Y. & PRIVES, C. 1997. DNA Damage-Induced Phosphorylation of p53 Alleviates Inhibition by MDM2. *Cell,* 91**,** 325-334.

SIBANDA, B. L., CRITCHLOW, S. E., BEGUN, J., PEI, X. Y., JACKSON, S. P., BLUNDELL, T. L. & PELLEGRINI, L. 2001. Crystal structure of an Xrcc4-DNA ligase IV complex. *Nat Struct Biol,* 8**,** 1015-9.

SIMPSON, A., PETNGA, W., MACAULAY, V. M., WEYER-CZERNILOFSKY, U. & BOGENRIEDER, T. 2017. Insulin-Like Growth Factor (IGF) Pathway Targeting in Cancer: Role of the IGF Axis and Opportunities for Future Combination Studies. *Targeted Oncology,* 12**,** 571-597.

SINGH, R. K., GAIKWAD, S. M., JINAGER, A., CHAUDHURY, S., MAHESHWARI, A. & RAY, P. 2014. IGF-1R inhibition potentiates cytotoxic effects of chemotherapeutic agents in early stages of chemoresistant ovarian cancer cells. *Cancer Lett,* 354**,** 254-62.

SMEENK, L., VAN HEERINGEN, S. J., KOEPPEL, M., GILBERT, B., JANSSEN-MEGENS, E., STUNNENBERG, H. G. & LOHRUM, M. 2011. Role of p53 serine 46 in p53 target gene regulation. *PLoS One,* 6**,** e17574.

SMITH, M. L., FORD, J. M., HOLLANDER, M. C., BORTNICK, R. A., AMUNDSON, S. A., SEO, Y. R., DENG, C.-X., HANAWALT, P. C. & FORNACE, A. J. 2000. p53-Mediated DNA Repair Responses to UV Radiation: Studies of Mouse Cells Lacking p53, p21, and/orgadd45 Genes. *Molecular and Cellular Biology,* 20**,** 3705-3714.

SMITH, T. J. 2010. Insulin-Like Growth Factor-I Regulation of Immune Function: A Potential Therapeutic Target in Autoimmune Diseases? *Pharmacological Reviews,* 62**,** 199-236.

SORENSEN, C. S., SYLJUASEN, R. G., FALCK, J., SCHROEDER, T., RONNSTRAND, L., KHANNA, K. K., ZHOU, B. B., BARTEK, J. & LUKAS, J. 2003. Chk1 regulates the S phase checkpoint by coupling the physiological turnover and ionizing radiation-induced accelerated proteolysis of Cdc25A. *Cancer Cell,* 3**,** 247-58.

SPENTZOS, D., CANNISTRA, S. A., GRALL, F., LEVINE, D. A., PILLAY, K., LIBERMANN, T. A. & MANTZOROS, C. S. 2007. IGF axis gene expression patterns are prognostic of survival in epithelial ovarian cancer. *Endocr Relat Cancer,* 14**,** 781-90.

SPITZ, M. R., BARNETT, M. J., GOODMAN, G. E., THORNQUIST, M. D., WU, X. & POLLAK, M. 2002. Serum insulin-like growth factor (IGF) and IGF-binding protein levels and risk of lung cancer: a case-control study nested in the beta-Carotene and Retinol Efficacy Trial Cohort. *Cancer Epidemiol Biomarkers Prev,* 11**,** 1413-8.

STEUERMAN, R., SHEVAH, O. & LARON, Z. 2011. Congenital IGF1 deficiency tends to confer protection against post-natal development of malignancies. *European Journal of Endocrinology,* 164**,** 485-489.

STEWART, G. S., WANG, B., BIGNELL, C. R., TAYLOR, A. M. & ELLEDGE, S. J. 2003. MDC1 is a mediator of the mammalian DNA damage checkpoint. *Nature,* 421**,** 961-6.

STRÖMBERG, T., EKMAN, S., GIRNITA, L., DIMBERG, L. Y., LARSSON, O., AXELSON, M., LENNARTSSON, J., HELLMAN, U., CARLSON, K., ÖSTERBORG, A., VANDERKERKEN, K., NILSSON, K. & JERNBERG-WIKLUND, H. 2006. IGF-1 receptor tyrosine kinase inhibition by the cyclolignan PPP induces G₂/M-phase accumulation and apoptosis in multiple myeloma cells. *Blood,* 107**,** 669-678.

SU, Z. Z., LEBEDEVA, I. V., SARKAR, D., GOPALKRISHNAN, R. V., SAUANE, M., SIGMON, C., YACOUB, A., VALERIE, K., DENT, P. & FISHER, P. B. 2003. Melanoma differentiation associated gene-7, mda-7/IL-24, selectively induces growth suppression, apoptosis and radiosensitization in malignant gliomas in a p53-independent manner. *Oncogene,* 22**,** 1164-80.

SUTHERLAND, B. M., BENNETT, P. V., SIDORKINA, O. & LAVAL, J. 2000. Clustered DNA damages induced in isolated DNA and in human cells by low doses of ionizing radiation. *Proceedings of the National Academy of Sciences,* 97**,** 103-108.

TADI, S. K., TELLIER-LEBEGUE, C., NEMOZ, C., DREVET, P., AUDEBERT, S., ROY, S., MEEK, K., CHARBONNIER, J. B. & MODESTI, M. 2016. PAXX Is an Accessory c-NHEJ Factor that Associates with Ku70 and Has Overlapping Functions with XLF. *Cell Rep,* 17**,** 541-555.

TAKAHARI, D., YAMADA, Y., OKITA, N. T., HONDA, T., HIRASHIMA, Y., MATSUBARA, J., TAKASHIMA, A., KATO, K., HAMAGUCHI, T., SHIRAO, K., SHIMADA, Y. & SHIMODA, T. 2009. Relationships of insulin-like growth factor-1 receptor and epidermal growth factor receptor expression to clinical outcomes in patients with colorectal cancer. *Oncology,* 76**,** 42-8.

TAKAI, H., NAKA, K., OKADA, Y., WATANABE, M., HARADA, N., SAITO, S., ANDERSON, C. W., APPELLA, E., NAKANISHI, M., SUZUKI, H., NAGASHIMA, K., SAWA, H., IKEDA, K. & MOTOYAMA, N. 2002. Chk2-deficient mice exhibit radioresistance and defective p53-mediated transcription. *Embo j,* 21**,** 5195-205.

TEZUKA, M., WATANABE, H., NAKAMURA, S., YU, D., AUNG, W., SASAKI, T., SHIBUYA, H. & MIURA, M. 2001. Antiapoptotic activity is dispensable for insulin-like growth factor I receptor-mediated clonogenic radioresistance after gamma-irradiation. *Clin Cancer Res,* 7**,** 3206-14.

THIERY, J. P., ACLOQUE, H., HUANG, R. Y. & NIETO, M. A. 2009. Epithelial-mesenchymal transitions in development and disease. *Cell,* 139**,** 871-90.

THOMPSON, L. H. 2012. Recognition, signaling, and repair of DNA double-strand breaks produced by ionizing radiation in mammalian cells: The molecular choreography. *Mutation Research/Reviews in Mutation Research,* 751**,** 158-246.

TILL, B. J., BURTNER, C., COMAI, L. & HENIKOFF, S. 2004. Mismatch cleavage by single-strand specific nucleases. *Nucleic Acids Research,* 32**,** 2632-2641.

TOMINAGA, Y., TSUZUKI, T., SHIRAISHI, A., KAWATE, H. & SEKIGUCHI, M. 1997. Alkylation-induced apoptosis of embryonic stem cells in which the gene for DNA-repair, methyltransferase, had been disrupted by gene targeting. *Carcinogenesis,* 18**,** 889-96.

TOULANY, M., KEHLBACH, R., FLORCZAK, U., SAK, A., WANG, S., CHEN, J., LOBRICH, M. & RODEMANN, H. P. 2008. Targeting of AKT1 enhances radiation toxicity of human tumor cells by inhibiting DNA-PKcs-dependent DNA double-strand break repair. *Mol Cancer Ther,* 7**,** 1772-81.

TOULANY, M., LEE, K. J., FATTAH, K. R., LIN, Y. F., FEHRENBACHER, B., SCHALLER, M., CHEN, B. P., CHEN, D. J. & RODEMANN, H. P. 2012. Akt promotes post-irradiation survival of human tumor cells through initiation, progression, and termination of DNA-PKcs-dependent DNA double-strand break repair. *Mol Cancer Res,* 10**,** 945-57.

TOULANY, M. & RODEMANN, H. P. 2015. Phosphatidylinositol 3-kinase/Akt signaling as a key mediator of tumor cell responsiveness to radiation. *Seminars in Cancer Biology,* 35**,** 180-190.

TRAVIS, R. C., APPLEBY, P. N., MARTIN, R. M., HOLLY, J. M. P., ALBANES, D., BLACK, A., BUENO-DE-MESQUITA, H. B. A., CHAN, J. M., CHEN, C., CHIRLAQUE, M. D.,

COOK, M. B., DESCHASAUX, M., DONOVAN, J. L., FERRUCCI, L., GALAN, P., GILES, G. G., GIOVANNUCCI, E. L., GUNTER, M. J., HABEL, L. A., HAMDY, F. C., HELZLSOUER, K. J., HERCBERG, S., HOOVER, R. N., JANSSEN, J., KAAKS, R., KUBO, T., LE MARCHAND, L., METTER, E. J., MIKAMI, K., MORRIS, J. K., NEAL, D. E., NEUHOUSER, M. L., OZASA, K., PALLI, D., PLATZ, E. A., POLLAK, M., PRICE, A. J., ROOBOL, M. J., SCHAEFER, C., SCHENK, J. M., SEVERI, G., STAMPFER, M. J., STATTIN, P., TAMAKOSHI, A., TANGEN, C. M., TOUVIER, M., WALD, N. J., WEISS, N. S., ZIEGLER, R. G., KEY, T. J. & ALLEN, N. E. 2016. A Meta-analysis of Individual Participant Data Reveals an Association between Circulating Levels of IGF-I and Prostate Cancer Risk. *Cancer Res,* 76**,** 2288-2300.

TROJANEK, J., CROUL, S., HO, T., WANG, J. Y., DARBINYAN, A., NOWICKI, M., VALLE, L. D., SKORSKI, T., KHALILI, K. & REISS, K. 2006. T-antigen of the human polyomavirus JC attenuates faithful DNA repair by forcing nuclear interaction between IRS-1 and Rad51. *Journal of Cellular Physiology,* 206**,** 35-46.

TROJANEK, J., HO, T., DEL VALLE, L., NOWICKI, M., WANG, J. Y., LASSAK, A., PERUZZI, F., KHALILI, K., SKORSKI, T. & REISS, K. 2003. Role of the Insulin-Like Growth Factor I/Insulin Receptor Substrate 1 Axis in Rad51 Trafficking and DNA Repair by Homologous Recombination. *Molecular and Cellular Biology,* 23**,** 7510-7524.

TRONT, J. S., HOFFMAN, B. & LIEBERMANN, D. A. 2006. Gadd45a Suppresses Ras-Driven Mammary Tumorigenesis by Activation of c-Jun NH2-Terminal Kinase and p38 Stress Signaling Resulting in Apoptosis and Senescence. *Cancer Research,* 66**,** 8448-8454.

TURNER, B. C., HAFFTY, B. G., NARAYANAN, L., YUAN, J., HAVRE, P. A., GUMBS, A. A., KAPLAN, L., BURGAUD, J.-L., CARTER, D., BASERGA, R. & GLAZER, P. M. 1997. Insulin-like Growth Factor-I Receptor Overexpression Mediates Cellular Radioresistance and Local Breast Cancer Recurrence after Lumpectomy and Radiation. *Cancer Research,* 57**,** 3079-3083.

TURNEY, B. W., KERR, M., CHITNIS, M. M., LODHIA, K., WANG, Y., RIEDEMANN, J., ROCHESTER, M., PROTHEROE, A. S., BREWSTER, S. F. & MACAULAY, V. M. 2012. Depletion of the type 1 IGF receptor delays repair of radiation-induced DNA double strand breaks. *Radiother Oncol,* 103**,** 402-9.

TWIGG, S. M. & BAXTER, R. C. 1998. Insulin-like growth factor (IGF)-binding protein 5 forms an alternative ternary complex with IGFs and the acid-labile subunit. *J Biol Chem,* 273**,** 6074-9.

TZIVION, G., DOBSON, M. & RAMAKRISHNAN, G. 2011. FoxO transcription factors; Regulation by AKT and 14-3-3 proteins. *Biochimica et Biophysica Acta (BBA) - Molecular Cell Research,* 1813**,** 1938-1945.

UEMATSU, N., WETERINGS, E., YANO, K.-I., MOROTOMI-YANO, K., JAKOB, B., TAUCHER-SCHOLZ, G., MARI, P.-O., VAN GENT, D. C., CHEN, B. P. C. & CHEN, D. J. 2007. Autophosphorylation of DNA-PK(CS) regulates its dynamics at DNA double-strand breaks. *The Journal of Cell Biology,* 177**,** 219-229.

ULLRICH, A., GRAY, A., TAM, A. W., YANG-FENG, T., TSUBOKAWA, M., COLLINS, C., HENZEL, W., LE BON, T., KATHURIA, S., CHEN, E. & ET AL. 1986. Insulin-like growth factor I receptor primary structure: comparison with insulin receptor suggests structural determinants that define functional specificity. *Embo j,* 5**,** 2503-12.

UZIEL, T., LERENTHAL, Y., MOYAL, L., ANDEGEKO, Y., MITTELMAN, L. & SHILOH, Y. 2003. Requirement of the MRN complex for ATM activation by DNA damage. *The EMBO Journal,* 22**,** 5612-5621.

VAESSEN, N., HEUTINK, P., JANSSEN, J. A., WITTEMAN, J. C. M., TESTERS, L., HOFMAN, A., LAMBERTS, S. W. J., OOSTRA, B. A., POLS, H. A. P. & VAN DUIJN, C. M. 2001. A Polymorphism in the Gene for IGF-I. *Functional Properties and Risk for Type 2 Diabetes and Myocardial Infarction,* 50**,** 637-642.

VALVERDE, A. M., MUR, C., PONS, S., ALVAREZ, A. M., WHITE, M. F., KAHN, C. R. & BENITO, M. 2001. Association of insulin receptor substrate 1 (IRS-1) y895 with Grb-2 mediates the insulin signaling involved in IRS-1-deficient brown adipocyte mitogenesis. *Mol Cell Biol,* 21**,** 2269-80.

VAMVAKAS, S., VOCK, E. H. & LUTZ, W. K. 1997. On the role of DNA double-strand breaks in toxicity and carcinogenesis. *Crit Rev Toxicol,* 27**,** 155-74.

VAN DER SCHANS, G. P. 1978. Gamma-ray induced double-strand breaks in DNA resulting from randomly-inflicted single-strand breaks: temporal local denaturation, a new radiation phenomenon? *Int J Radiat Biol Relat Stud Phys Chem Med,* 33**,** 105-20.

VAN VALEN, F., HARRER, H., HOTFILDER, M., DIRKSEN, U., PAP, T., GOSHEGER, G., HUMPF, H.-U. & JÜRGENS, H. 2012. A Novel Role of IGF1 in Apo2L/TRAIL-Mediated Apoptosis of Ewing Tumor Cells. *Sarcoma,* 2012**,** 782970.

VECCHIONE, A., MARCHESE, A., HENRY, P., ROTIN, D. & MORRIONE, A. 2003. The Grb10/Nedd4 complex regulates ligand-induced ubiquitination and stability of the insulin-like growth factor I receptor. *Mol Cell Biol,* 23**,** 3363-72.

VIGNARD, J., MIREY, G. & SALLES, B. 2013. Ionizing-radiation induced DNA double-strand breaks: a direct and indirect lighting up. *Radiother Oncol,* 108**,** 362-9.

VILLANO, J. L., SEERY, T. E. & BRESSLER, L. R. 2009. Temozolomide in malignant gliomas: current use and future targets. *Cancer Chemother Pharmacol,* 64**,** 647-55.

WALSH, L. A. & DAMJANOVSKI, S. 2011. IGF-1 increases invasive potential of MCF 7 breast cancer cells and induces activation of latent TGF-β1 resulting in epithelial to mesenchymal transition. *Cell Communication and Signaling : CCS,* 9**,** 10-10.

WANG, C., SUN, H., ZOU, R., ZHOU, T., WANG, S., SUN, S., TONG, C., LUO, H., LI, Y., LI, Z., WANG, E., CHEN, Y., CAO, L., LI, F. & ZHAO, Y. 2015. MDC1 functionally identified as an androgen receptor co-activator participates in suppression of prostate cancer. *Nucleic Acids Research,* 43**,** 4893-4908.

WANG, H., RUSSA, M. L. & QI, L. S. 2016. CRISPR/Cas9 in Genome Editing and Beyond. *Annual Review of Biochemistry,* 85**,** 227-264.

WANG, H., SHI, L. Z., WONG, C. C., HAN, X., HWANG, P. Y., TRUONG, L. N., ZHU, Q., SHAO, Z., CHEN, D. J., BERNS, M. W., YATES, J. R., 3RD, CHEN, L. & WU, X. 2013. The interaction of CtIP and Nbs1 connects CDK and ATM to regulate HR-mediated double-strand break repair. *PLoS Genet,* 9**,** e1003277.

WANG, X. W., ZHAN, Q., COURSEN, J. D., KHAN, M. A., KONTNY, H. U., YU, L., HOLLANDER, M. C., O'CONNOR, P. M., FORNACE, A. J. & HARRIS, C. C. 1999. GADD45 induction of a G2/M cell cycle checkpoint. *Proceedings of the National Academy of Sciences,* 96**,** 3706-3711.

WANG, Y. H., WANG, Z. X., QIU, Y., XIONG, J., CHEN, Y. X., MIAO, D. S. & DE, W. 2009. Lentivirus-mediated RNAi knockdown of insulin-like growth factor-1 receptor inhibits growth, reduces invasion, and enhances radiosensitivity in human osteosarcoma cells. *Mol Cell Biochem,* 327**,** 257-66.

WANG, Y. H., XIONG, J., WANG, S. F., YU, Y., WANG, B., CHEN, Y. X., SHI, H. F. & QIU, Y. 2010. Lentivirus-mediated shRNA targeting insulin-like growth factor-1 receptor (IGF-1R) enhances chemosensitivity of osteosarcoma cells in vitro and in vivo. *Mol Cell Biochem,* 341**,** 225-33.

WANG, Z., LI, Y., BANERJEE, S. & SARKAR, F. H. 2008. Exploitation of the Notch signaling pathway as a novel target for cancer therapy. *Anticancer Res,* 28.

WANG, Z., WADE, P., MANDELL, K. J., AKYILDIZ, A., PARKOS, C. A., MRSNY, R. J. & NUSRAT, A. 2007. Raf 1 represses expression of the tight junction protein occludin via activation of the zinc-finger transcription factor slug. *Oncogene,* 26**,** 1222-30.

WEISS, W. A., TAYLOR, S. S. & SHOKAT, K. M. 2007. Recognizing and exploiting differences between RNAi and small-molecule inhibitors. *Nat Chem Biol,* 3**,** 739-744.

WERNER, H., KARNIELI, E., RAUSCHER, F. J. & LEROITH, D. 1996. Wild-type and mutant p53 differentially regulate transcription of the insulin-like growth factor I receptor gene. *Proc Natl Acad Sci U S A,* 93**,** 8318-23.

WHITTAKER, J., GROTH, A. V., MYNARCIK, D. C., PLUZEK, L., GADSBOLL, V. L. & WHITTAKER, L. J. 2001. Alanine scanning mutagenesis of a type 1 insulin-like growth factor receptor ligand binding site. *J Biol Chem,* 276**,** 43980-6.

WICK, M. J., DONG, L. Q., RIOJAS, R. A., RAMOS, F. J. & LIU, F. 2000. Mechanism of Phosphorylation of Protein Kinase B/Akt by a Constitutively Active 3-Phosphoinositide-dependent Protein Kinase-1. *Journal of Biological Chemistry,* 275**,** 40400-40406.

WILKINS, H. R., OHNEDA, K., KEKU, T. O., D'ERCOLE, A. J., FULLER, C. R., WILLIAMS, K. L. & LUND, P. K. 2002. Reduction of spontaneous and irradiation-induced apoptosis in small intestine of IGF-I transgenic mice. *Am J Physiol Gastrointest Liver Physiol,* 283**,** G457-64.

WINDHOFER, F., KRAUSE, S., HADER, C., SCHULZ, W. A. & FLORL, A. R. 2008. Distinctive differences in DNA double-strand break repair between normal urothelial and urothelial carcinoma cells. *Mutation Research/Fundamental and Molecular Mechanisms of Mutagenesis,* 638**,** 56-65.

WISHART, D. S., JEWISON, T., GUO, A. C., WILSON, M., KNOX, C., LIU, Y., DJOUMBOU, Y., MANDAL, R., AZIAT, F., DONG, E., BOUATRA, S., SINELNIKOV, I., ARNDT, D., XIA, J., LIU, P., YALLOU, F., BJORNDAHL, T., PEREZ-PINEIRO, R., EISNER, R., ALLEN, F., NEVEU, V., GREINER, R. & SCALBERT, A. 2013. HMDB 3.0--The Human Metabolome Database in 2013. *Nucleic Acids Res,* 41**,** D801-7.

WOODSON, K., TANGREA, J. A., POLLAK, M., COPELAND, T. D., TAYLOR, P. R., VIRTAMO, J. & ALBANES, D. 2003. Serum insulin-like growth factor I: tumor marker or etiologic factor? A prospective study of prostate cancer among Finnish men. *Cancer Res,* 63**,** 3991-4.

WU, L., BACHRATI, C. Z., OU, J., XU, C., YIN, J., CHANG, M., WANG, W., LI, L., BROWN, G. W. & HICKSON, I. D. 2006. BLAP75/RMI1 promotes the BLM-dependent dissolution of homologous recombination intermediates. *Proc Natl Acad Sci U S A,* 103**,** 4068-73.

WU, X., TORTOLERO-LUNA, G., ZHAO, H., PHATAK, D., SPITZ, M. R. & FOLLEN, M. 2003a. Serum levels of insulin-like growth factor I and risk of squamous intraepithelial lesions of the cervix. *Clin Cancer Res,* 9**,** 3356-61.

WU, Y., CUI, K., MIYOSHI, K., HENNIGHAUSEN, L., GREEN, J. E., SETSER, J., LEROITH, D. & YAKAR, S. 2003b. Reduced circulating insulin-like growth factor I levels delay the onset of chemically and genetically induced mammary tumors. *Cancer Res,* 63**,** 4384-8.

XIAO, G., CHICAS, A., OLIVIER, M., TAYA, Y., TYAGI, S., KRAMER, F. R. & BARGONETTI, J. 2000. A DNA damage signal is required for p53 to activate gadd45. *Cancer Res,* 60**,** 1711-9.

YAGI, T., BAROJA-FERNANDEZ, E., YAMAMOTO, R., MUNOZ, F. J., AKAZAWA, T., HONG, K. S. & POZUETA-ROMERO, J. 2003. Cloning, expression and characterization of a mammalian Nudix hydrolase-like enzyme that cleaves the pyrophosphate bond of UDP-glucose. *Biochem J,* 370**,** 409-15.

YAKAR, S., LIU, J. L., FERNANDEZ, A. M., WU, Y., SCHALLY, A. V., FRYSTYK, J., CHERNAUSEK, S. D., MEJIA, W. & LE ROITH, D. 2001. Liver-specific igf-1 gene deletion leads to muscle insulin insensitivity. *Diabetes,* 50**,** 1110-8.

YAMAMOTO, T., OSHIMA, T., YOSHIHARA, K., NISHI, T., ARAI, H., INUI, K., KANEKO, T., NOZAWA, A., ADACHI, H., RINO, Y., MASUDA, M. & IMADA, T. 2012. Clinical significance of immunohistochemical expression of insulin-like growth factor-1 receptor and matrix metalloproteinase-7 in resected non-small cell lung cancer. *Exp Ther Med,* 3**,** 797-802.

YAVARI, K., TAGHIKHANI, M., MARAGHEH, M. G., MESBAH-NAMIN, S. A., BABAEI, M. H., ARFAEE, A. J., MADANI, H. & MIRZAEI, H. R. 2010. SiRNA-mediated IGF-1R inhibition sensitizes human colon cancer SW480 cells to radiation. *Acta Oncol,* 49**,** 70-5.

YEELES, J. T., POLI, J., MARIANS, K. J. & PASERO, P. 2013. Rescuing stalled or damaged replication forks. *Cold Spring Harb Perspect Biol,* 5**,** a012815.

YEH, A. H., BOHULA, E. A. & MACAULAY, V. M. 2006. Human melanoma cells expressing V600E B-RAF are susceptible to IGF1R targeting by small interfering RNAs. *Oncogene,* 25**,** 6574-6581.

YOO, E., KIM, B. U., LEE, S. Y., CHO, C. H., CHUNG, J. H. & LEE, C. H. 2005. 53BP1 is associated with replication protein A and is required for RPA2 hyperphosphorylation following DNA damage. *Oncogene,* 24**,** 5423-30.

YU, D., WATANABE, H., SHIBUYA, H. & MIURA, M. 2003. Redundancy of Radioresistant Signaling Pathways Originating from Insulin-like Growth Factor I Receptor. *Journal of Biological Chemistry,* 278**,** 6702-6709.

YUEN, J. S., COCKMAN, M. E., SULLIVAN, M., PROTHEROE, A., TURNER, G. D., ROBERTS, I. S., PUGH, C. W., WERNER, H. & MACAULAY, V. M. 2007. The VHL tumor suppressor inhibits expression of the IGF1R and its loss induces IGF1R upregulation in human clear cell renal carcinoma. *Oncogene,* 26**,** 6499-508.

ZAFFARONI, N., ORLANDI, L., VILLA, R., BEARZATTO, A., ROFSTAD, E. K. & SILVESTRINI, R. 1994. DNA double-strand break repair and radiation response in human tumour primary cultures. *Int J Radiat Biol,* 66**,** 279-85.

ZERBINI, L. F., CZIBERE, A., WANG, Y., CORREA, R. G., OTU, H., JOSEPH, M., TAKAYASU, Y., SILVER, M., GU, X., RUCHUSATSAWAT, K., LI, L., SARKAR, D., ZHOU, J.-R., FISHER, P. B. & LIBERMANN, T. A. 2006. A Novel Pathway Involving Melanoma Differentiation Associated Gene-7/Interleukin-24 Mediates Nonsteroidal Anti-inflammatory Drug–Induced Apoptosis and Growth Arrest of Cancer Cells. *Cancer Research,* 66**,** 11922-11931.

ZHAN, Q., ANTINORE, M. J., WANG, X. W., CARRIER, F., SMITH, M. L., HARRIS, C. C. & FORNACE, A. J., JR. 1999. Association with Cdc2 and inhibition of Cdc2/Cyclin B1 kinase activity by the p53-regulated protein Gadd45. *Oncogene,* 18**,** 2892-900.

ZHANG, D., BAR-ELI, M., MELOCHE, S. & BRODT, P. 2004. Dual regulation of MMP-2 expression by the type 1 insulin-like growth factor receptor: the phosphatidylinositol 3-kinase/Akt and Raf/ERK pathways transmit opposing signals. *J Biol Chem,* 279**,** 19683-90.

ZHANG, X.-P., LIU, F. & WANG, W. 2011. Two-phase dynamics of p53 in the DNA damage response. *Proceedings of the National Academy of Sciences of the United States of America,* 108**,** 8990-8995.

ZHANG, Y., GAO, X., SAUCEDO, L. J., RU, B., EDGAR, B. A. & PAN, D. 2003. Rheb is a direct target of the tuberous sclerosis tumour suppressor proteins. *Nat Cell Biol,* 5**,** 578-581.

ZHENG, H., WORRALL, C., SHEN, H., ISSAD, T., SEREGARD, S., GIRNITA, A. & GIRNITA, L. 2012. Selective recruitment of G protein-coupled receptor kinases (GRKs) controls signaling of the insulin-like growth factor 1 receptor. *Proc Natl Acad Sci U S A,* 109**,** 7055-60.

ZHOU, D., DEOLIVEIRA, D., KANG, Y., CHOI, S. S., LI, Z., CHAO, N. J. & CHEN, B. J. 2013. Insulin-Like Growth Factor 1 Mitigates Hematopoietic Toxicity after Lethal Total Body Irradiation. *International journal of radiation oncology, biology, physics,* 85**,** 1141-1148.

ZHOU, H., RAO, J., LIN, J., YIN, B., SHENG, H., LIN, F., ZHANG, N. & YANG, L. 2011. The insulin-like growth factor-I receptor kinase inhibitor NVP-ADW742 sensitizes medulloblastoma to the effects of chemotherapy. *Oncol Rep,* 25**,** 1565-71.

ZIELINSKA, H. A., BAHL, A., HOLLY, J. M. P. & PERKS, C. M. 2015. Epithelial-to-mesenchymal transition in breast cancer: a role for insulin-like growth factor I and insulin-like growth factor–binding protein 3? *Breast Cancer : Targets and Therapy,* 7**,** 9-19.

ZIV, Y., BIELOPOLSKI, D., GALANTY, Y., LUKAS, C., TAYA, Y., SCHULTZ, D. C., LUKAS, J., BEKKER-JENSEN, S., BARTEK, J. & SHILOH, Y. 2006. Chromatin relaxation in response to DNA double-strand breaks is modulated by a novel ATM- and KAP-1 dependent pathway. *Nat Cell Biol,* 8**,** 870-6.

ZONCU, R., EFEYAN, A. & SABATINI, D. M. 2011. mTOR: from growth signal integration to cancer, diabetes and ageing. *Nat Rev Mol Cell Biol,* 12**,** 21-35.